Tar Destruction in a Coandă Tar Cracker
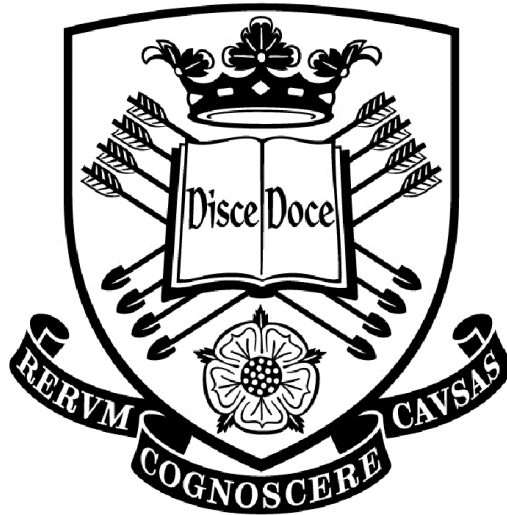
Peter Weston, MEng (Hons), AMIChemE, GradEI

Supervisors: Prof. Vida Sharifi & Prof. Jim Swithenbank

Thesis submitted to the Department of Chemical and Biological Engineering,
the University of Sheffield, for the Degree of Doctor of Philosophy (PhD)

Department of Chemical and Biological Engineering

The University of Sheffield

September 2014

Summary

Increasing the utilisation of bioenergy systems has the potential to become a vital component in the struggle to maintain and fulfil global energy demands. In particular, biomass gasification can offer a solution to the '*Energy Trilemma*', and provide an affordable, reliable and carbon neutral technology. The limiting factor hampering the progression of biomass gasification power plants is tar. Tars formed during the thermal breakdown of biomass, condense and foul downstream equipment, causing reliability issues and damaging energy conversion equipment, such as engines and turbines. Treating tar through partial oxidation offers tar destruction without waste and soot, as well as maintaining the heating value of the tar in the producer gas. Coandă burners which are fuelled by more conventional fuels have been proven to operate close to, and below, stoichiometric conditions; as such, these devices were prime for further investigation.

The main objective of this research project was to develop a small-scale system which utilises a novel Coandă burner for tar destruction. An experimental rig consisting of a wood pellet pyrolyser, which produced a gas loaded with tar, and a Coandă tar cracker, was designed, constructed and operated in order to determine the effectiveness of the process, with respect to tar reduction.

The principal experimental program was divided into two phases, so that comparisons of the tar composition, before and after treatment, could be formed. In the first experimental phase, wood pellets were pyrolysed at a range of temperatures between 500 and 800ºC. The pyrolysis products (gas, tar and char) were analysed. As the pyrolysis temperature increased from 500 to 800ºC there was a decrease in the yield of gravimetric tar in the sampled gas from 78.59 to 16.55 g/Nm^3.

In the second phase the tarry gas was treated by the Coandă tar cracker. The Coandă tar cracker was shown to be effective at significantly reducing the tar content in the product gas. The yield of key tar components in the treated gas was reduced for all tested pyrolysis temperatures. For example; when the pyrolysis temperature was 800ºC; the yields of benzene, toluene and naphthalene were reduced by over 90% and the gravimetric tar yield by 88%. The success of the tar cracker can be attributed to the high flame temperature (>1000ºC) and the addition of oxygen which leads to the production of a greater proportion of radicals in the flame which initiate tar destruction reactions.

Acknowledgements

I would like to express great thanks to my supervisors; Professor Vida Sharifi and Professor Jim Swithenbank for their guidance, support and help throughout the duration of this research. They have been invaluable.

I would like to thank the technical staff of the Chemical and Biological Engineering: Mike O'Meara, David Palmer, Oz McFarlane, Keith Penny and Mark Jones for their assistance. Mike and David were, in particular, extremely helpful in providing their technical support and experience.

Finally, I would like to thank the EPSRC for providing the funding for this project and my family and friends for their support and encouragement.

"God help us, we're in the hands of engineers." [Dr Ian Malcolm, Jurassic Park]

Table of Contents

List of Figures

List of Tables

List of Abbreviations

AFR	Air Fuel Ratio
AOAC	Association of Official Analytical Chemists
ASTM	American Society for Testing Materials
BSP	British Standard Pipe
CFB	Circulating Fluidised Bed
CFD	Computation Fluid Dynamics
CHN	Carbon Hydrogen Nitrogen
CHP	Combined Heat and Power
CTC	Coandă Tar Cracker
DECC	Department of Energy and Climate Change
DTG	Differential Thermogravimetry
EFB	Empty Fruit Bunch
EU	European Union
GC	Gas Chromatograph
GCV	Gross Calorific Value
GCMS	Gas Chromatography-Mass Spectrometer
HACA	Hydrogen Abstraction Acetylene Addition
IEA	International Energy Agency
IGCC	Integrated Gasification Combined Cycle
PIV	Particle Image Velocimetry
P&ID	Piping & Instrumentation Diagram
PAH	Polycyclic Aromatic Hydrocarbons
PTFE	Polytetrafluoroethylene
RNG	Re-normalisation Group
RSR	Resonantly Stabilised Radical
SST	Shear Stress Transport
TC	Thermocouple
TCD	Thermal Conductivity
TG	Thermogravimetric
TGA	Thermogravimetric Analysis

Nomenclature

Symbol	Description	Unit
A	Area	m^2
D	Diameter	mm
e	Coandă throat gap	mm
I.D	Inside diameter	mm
LHV	Lower heating value	MJ/Nm^3
m	Mass	g
NL	Nozzle length	mm
o	Ejector outlet plane	-
ṁ	Mass flow rate	kg/s
Q	Net calorific value	J/kg
LPM	Litres per minute	l/m
CV	Gross heat of combustion	J/kg
P	Pressure	$kg/m.s^2$
R	Radius	°
u	Velocity	m/s
T	Temperature	°C
W	Energy equivalent	J/s

Greek Symbols

φ	Entrainment Ratio	-
Ø	Stoichiometric Ratio	-
λ	Excess Air Ratio	-
ρ	Density	kg/m^3

1. Introduction

1.1 Background

1.1.1 Future Global Energy Demands

The importance of biomass as a key source for energy production has intensified over the past decade. There have been strong endorsements both globally and nationally to replace traditional fuels with sustainable, renewable fuels. Supplies of oil, coal and natural gas are expected to deplete over the next hundred years, strengthening the need for alternative energy sources. In addition to the depletion of fossil fuels it is predicted that by the year 2040 total global energy consumption will have increased by 56% when compared to 2010 levels (U.S. Energy Information Administration, 2013). The combination of decreasing fossil fuel supplies and increasing energy demand poses a challenging and demanding problem for the international community.

The link between human activities and climate change is well established. Evidence indicates that human activity has caused an increase in the temperature of the Earth's atmosphere over the last fifty years (The Royal Society, 2010). The concentration of carbon dioxide in the atmosphere is now almost 40% greater when compared with pre-industrial revolution levels, as a result, the average global temperature has increased and continues to rise (DECC, 2011). Climate change has, and will continue to have, a negative impact on an array of essential systems and sectors; creating problems with food supplies, ecological systems and the supply and sanitation of water (IPCC, 2007).

1.1.2 UK Energy and Environmental Targets

The 2008 Climate Change act made a number of ambitious targets to respond to and manage climate change in the UK. The two key objectives of the act are to facilitate the conversion towards a low-carbon economy and for the UK to demonstrate international leadership, by actively engaging with the issue and taking responsibility for reducing emissions. The crucial specification of the act is a legally binding target to reduce greenhouse gas emissions by 80% by 2050, against a 1990 baseline; included in this target is a 34% cut by 2020 (DECC, 2011).

The current renewable energy strategy is to deliver energy security and promote the transformation to a low carbon economy. As part of this plan the UK signed up to the EU Renewable Energy Directive in 2009 which set a target to have 15 percent of energy from renewable sources by 2020 (DECC, 2009). Therefore, by 2020, the UK plans to increase the

application of renewable energy sources seven fold from 2009 levels. This ambitious goal is proposed to be met by applying renewable sources for the following:

- More than 30% of total electricity generated

- 12% of heat

- 10% of transport energy

These recommended solutions are represented in Figure 1.1, which specifies the increase of renewable energy sources required to meet the targets.
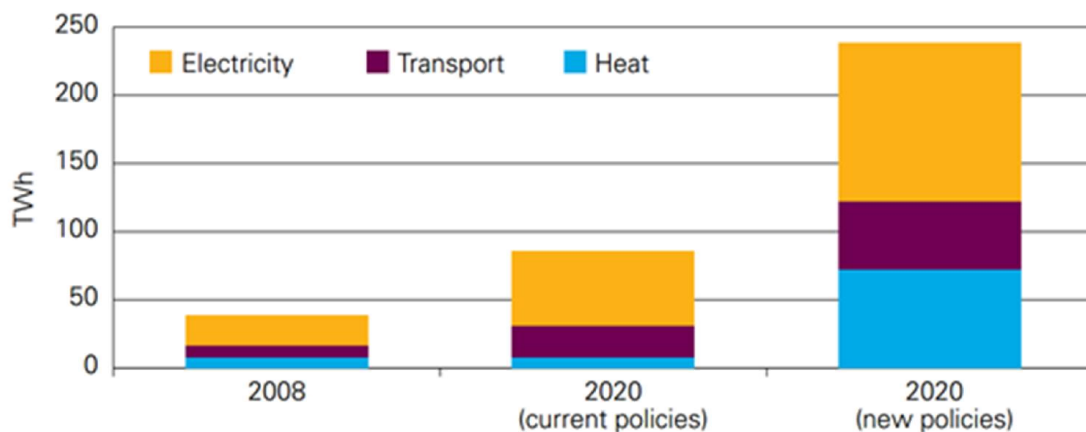
Figure 1.1 – A potential scenario to utilise renewable energy sources for 15% of total UK energy demand by 2020 (DECC, 2009)

1.1.3 Biomass in the UK

Biomass has an important role to play in the UK to reduce net emissions of carbon dioxide and also to provide a sustainable energy source. Biomass can be defined as *'any biological mass derived recently from plant or animal matter'* (Taylor, 2008). This definition covers a broad range of materials from forests cuttings and residues to wastes (municipal, food and industrial) to dedicated energy crops. It is estimated that the UK has 20 million tonnes of biomass available to produce energy; however, the use of biomass only currently contributes to 4.1% of total heat and electricity production. There are four principles that will act as the future framework for government policy on bioenergy; three of the key points are outlined below:

- Policies that support bioenergy should deliver carbon reductions that help meet the 2050 UK target to reduce CO_2 emissions

- Bioenergy should provide a cost effective contribution to the UK's carbon emission objectives

- Support for bioenergy should aim to minimise costs and maximum the overall benefits for the UK economy (DECC, 2012)

It is predicted in 2020 that UK biomass feed-stocks could provide between 8% and 11% of the UK's primary energy demand, this figure is expected to rise to between 10% and 14% by the year 2030 (Figure 1.2)(DECC, 2012). It is expected that the utilisation of UK biomass will change depending on a number of factors, ranging from government legislation to advances in biomass thermal conversion systems. Perhaps more significant will be the associated costs and whether the UK bioenergy market can compete with biomass supplies from international markets.
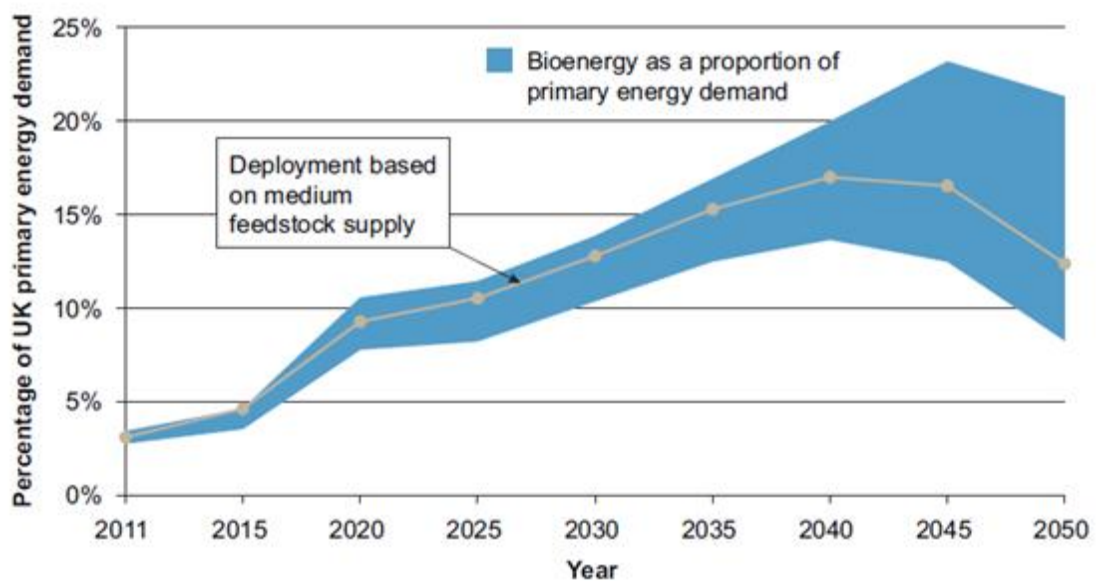
Figure 1.2 – Potential bioenergy contribution to primary energy input in the UK (DECC, 2012)

1.1.4 Biomass Thermal Conversion Technologies

There are three main routes for biomass conversion; combustion, pyrolysis and gasification. Biomass combustion offers the most direct and simplest method but it has the lowest efficiency (Kumar et al., 2009). The net efficiency of converting biomass to electricity through combustion is between 20-40% (Caputo et al., 2005). Gasification of biomass can reach conversion values of up to 50% when combined with a gas steam cycle (Caputo et al., 2005). Gasification is considered a clean and efficient process which is capable of utilising a wide range of different biomass materials. The produced gas can be used in a number of applications. Biomass gasification is considered a potential solution to provide clean, sustainable energy in both developed countries using advanced techniques and in developing countries to provide rural electrification (Kirkels & Verbong, 2011).

The technological advantages of biomass gasification are summarised by Rezaiyan & Cheremisinoff (2005): the process is considered to be clean because of the overall reduction in CO_2 emissions; the thermal efficiency is high and there is good operational control; when biomass is locally available gasifier systems offer economic advantages. Gasification of biomass, when using air as the gasifying agent, produces a gas with a low calorific value, normally between 4.0 and 6.0 MJ/Nm^3 (Stassen & Knoef, 1993).

Small-scale gasifiers (>1 MWth) are predominantly fixed bed in design (Stassen & Knoef, 1993). Fixed bed gasifiers are setup to have two stages. In the first stage biomass is heated in a pyrolysis regime in the absence, or with small quantities, of air. The pyrolysis stage is described as slow or fast depending on the heating rate. For slow pyrolysis, the heating rate is typically between 0.1 – 1.0 K/s (Babu, 2008). Products of pyrolysis are permanent gases, a tar vapour and a solid char product.

Feedstock and pre-treatment • Wood • Waste • Crop Residues	**Gasifiers** • Fixed Bed • Fluidised Bed • Entrained Flow
Gas Cleaning • Primary Methods • Secondary Methods	**Applications** • Heat • Electricity • Chemical
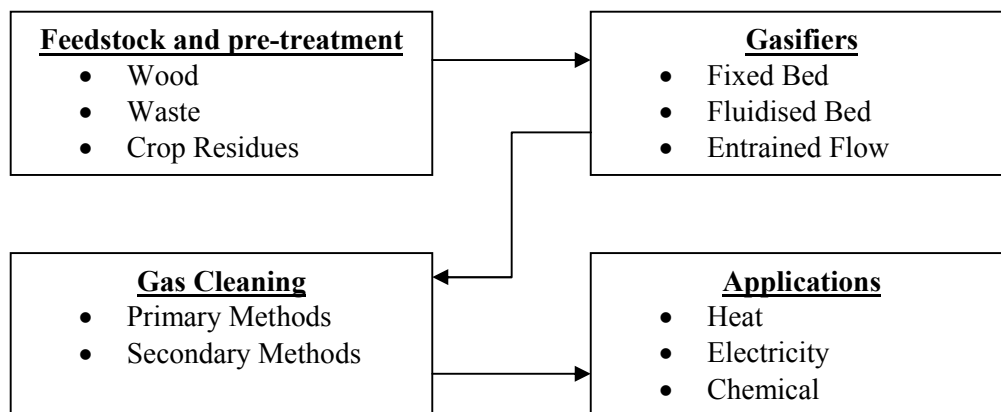
Figure 1.3 – Gasification technology (Adapted from: Kirkels & Verbong, 2011)

1.1.5 The Tar Problem

Tars are formed when biomass is pyrolysed. Tar is a complicated mixture of single to five ringed hydrocarbon compounds, as well as polycyclic aromatic hydrocarbons (PAH) and hydrocarbons containing oxygen (Devi et al., 2003). The most common description for tar is defined by Milne et al., (1998) as *'the organics produced under thermal or partial-oxidation regimes (gasification) of any organic material are called "tar" and are generally assumed to be largely aromatic'.* A similar definition was agreed upon by a number of experts at an EU/IEA/IS-DOE meeting on the measurement protocol of tar in Brussels in 1998, tar was defined as all contaminating organic compounds with a larger molecular weight than benzene (Devi et al., 2003).

Tar formation is unavoidable, they are formed when biomass is heated, causing molecular bonds to break. In this mechanism small molecules normally in the form of permanent gas species and larger molecules called primary tars are created (Houben, 2004). Primary tars in the gaseous phase can be converted to secondary tars and tertiary tars at higher temperatures (Li & Suzuki, 2009).

The main issue with tar production is that they condense at lower temperatures causing fouling, blocking and plugging in equipment downstream from the gasifier, thus causing reliability issues with filters, engines and turbines (Li & Suzuki, 2009; Han & Kim, 2008; Houben et al., 2005). Milne et al. (1998) detailed a general rule for the level of production of tars for various types of gasifiers; updraft – 100 g/Nm^3, downdraft – 1 g/Nm^3 and fluidised beds - 10 g/Nm^3. For syngas applications the tar content is required to be 0.05 g/Nm^3 (Han & Kim, 2008) thus the requirement for effective tar removal methods becomes imminent and obvious.

1.1.6 Tar Removal Methods

Existing tar removal methods can be classified as either primary or secondary. Primary methods refer to operations within the thermal conversion unit; secondary methods cover technologies that are external to the process (Figure 1.4). The key primary measures are to select the most efficient operating parameters, use bed additives or catalysts and to modify the design (Devi et al., 2003). Secondary methods are downstream of the process and treat the produced gas, examples include: mechanical methods (filters and scrubbers), catalysts, thermal cracking and partial oxidative treatment (Han & Kim, 2008; van der Hoeven, 2007). The discussed secondary methods are efficient at removing tar but are often not cost effective, especially for small-scale operations (van der Hoeven, 2007). Thermal treatment or tar reduction through partial oxidation is attractive because the process is normally cheaper than existing methods and is relatively waste-free potentially offering a long-term solution. These attributes are attractive for small-scale installations where there are strict financial limits which prevent the application of expensive tar removal systems.
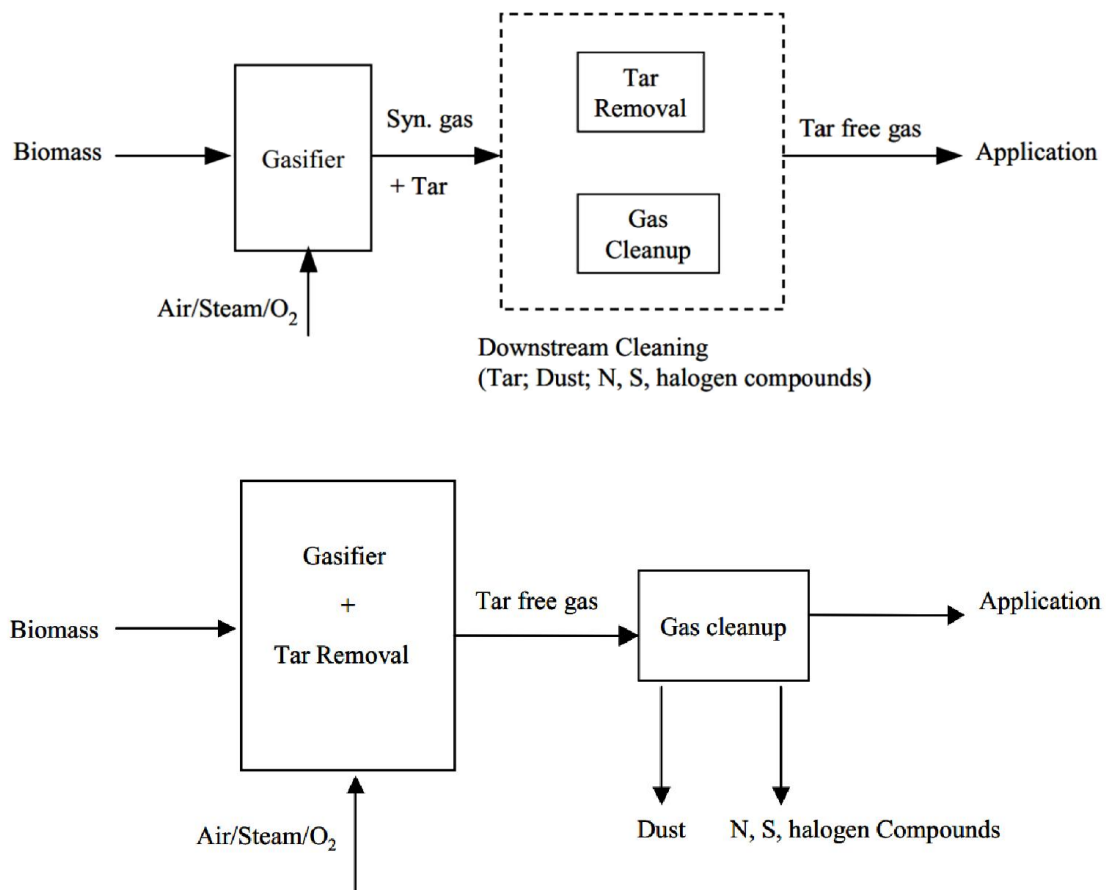
Figure 1.4 – Secondary (top) & Primary (bottom) removal methods (Devi et al., 2003)

1.1.7 Thermal Cracking and Partial Oxidation

Thermal cracking is the breakdown of tar molecules into lighter gases caused by high temperature. High temperatures influence tar stability allowing for the conversion into other species (Anis & Zainal, 2011). Anis & Zainal (2011) determined that the temperate range for thermal tar cracking is between 700 and 1250°C. For effective decomposition additional means are required such as increasing the gas residence time, directly contacting the gas with an independently heated surface or adding air or oxygen.

Partial oxidation offers tar reduction without waste or soot with the added benefit of maintaining the heating value of the tars in the produced gas. However, this comes at a loss of a proportion of the heating value of the treated gas, which is partially combusted. There are a number of previous studies that have used two-staged systems to analyse the effectiveness of partial oxidation for tar reduction (Ahrenfeldt et al., 2013a; Su et al., 2011; Wu et al., 2011; Chen et al., 2009; Fassinou et al., 2009). In these studies, various biomass fuels were pyrolysed in the first stage. In the second stage the pyrolysed gas, which contained the vaporised tar is treated in different thermal and oxidative environments. The majority of these

studies control the equivalence ratio (ER) in the second stage; however, the addition of oxygen was not used for combustion in a burner set-up, instead oxygen or air was supplied to react with the pyrolysis vapours.

Partial oxidation burners have been previously tested for tar cracking as shown by Houben (2004) and van der Hoeven (2007). Houben (2004) used a micro-scale swirl burner (Figure 1.5) to crack tar through partial oxidation. An artificial producer gas containing known amounts of naphthalene was used. It was shown that the excess-air ratio has a major influence on the cracking of naphthalene; up to 92.5% of the added naphthalene could be converted into smaller molecular species.
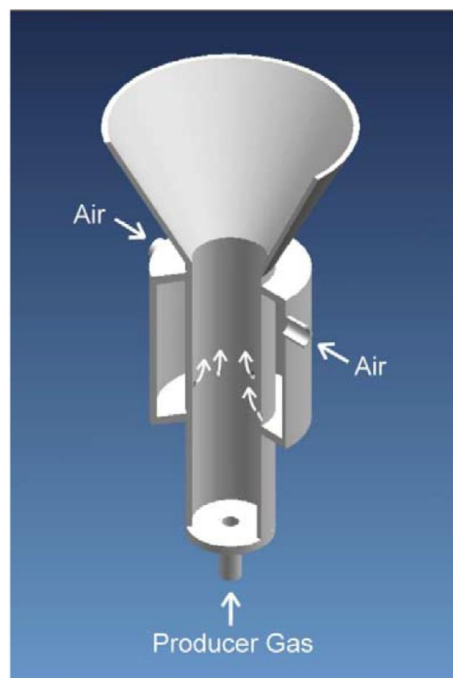
Figure 1.5 – Micro-swirl burner (Houben, 2004)

1.1.8 Coandă burners

The Coandă effect was one of the principle discoveries of Romanian inventor Henri Coandă. The Coandă effect is used to describe the phenomenon in which a fluid that is passed at high velocity over a curved surface attaches to the wall (O'Nions, 1997). This principle is used for the design of aeroplane wings and also for ejector devices. Coandă ejector devices can be modified to become efficient burners (O'Nions, 1997; Prior, 1977).

In the setup of a Coandă burner the flame products are recycled and mixed in a pre-chamber within the burner body. The mixed products are entrained through the burner by an oxidant which is fed through an annular slit adjacent to the curved throat of the burner. The primary feed attaches itself to the curved throat surface because of the Coandă effect and is in the form of a jet layer (Prior, 1977). The jet on the surface entrains surrounding fluids through viscous

forces which, if properly designed, causes recirculation of combustion products. The key benefit of the Coandă burner is that blue flames can be produced on the rich side of stoichiometric. These unique features are ideal for partial combustion of tarry pyrolysis gases.

1.2 Defining the problem

This study aims to determine whether a Coandă burner could be used to partially combust a biomass pyrolysis gas to destroy tar. It is suggested that tarry gases produced in a pyrolysis stage would be treated in a second stage, a Coandă burner. Fresh pyrolysis gas and recirculated, hot exhaust products from the burner are mixed before entering the combustion zone. The mixed gas is entrained through the burner and into the flame zone by an oxidant, most likely air, which enters the ejector through an annular slit and attaches to the curved surface of the Coandă throat. The Coandă burner could potentially partially combust the pyrolysis gas in a fuel rich environment, thus destroying tar species in a high temperature and low soot blue flame. The novel features of the Coandă burner make it an ideal device to be considered to be fitted between the output of a pyrolysis stage and a downdraft char gasification stage in a complete gasifier.
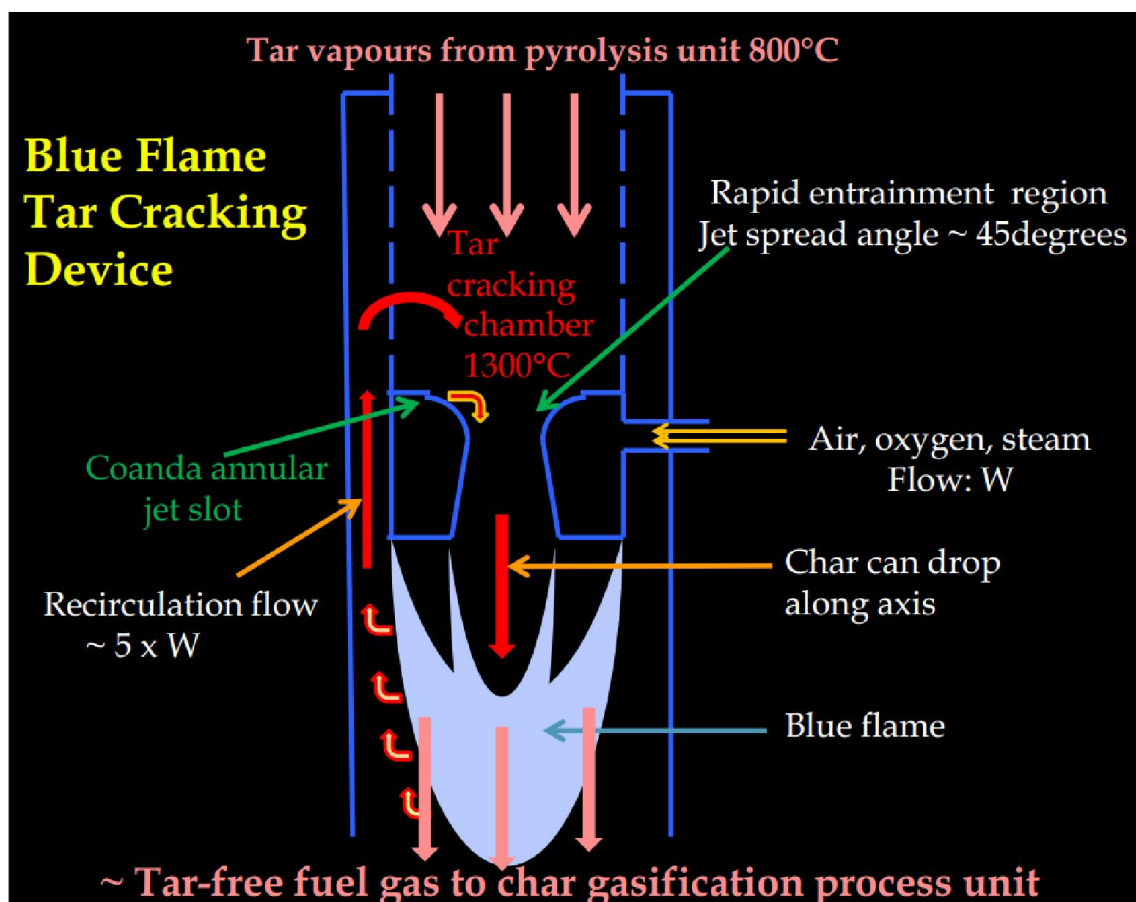
Figure 1.6 – Pyrolysis tar vapour cracking using a blue flame Coandă burner (Swithenbank et al., 2012)

1.3 Aims and Objectives

The main aim of this research is to determine whether a Coandă burner can be modified and used to partially oxidise tarry vapours produced when biomass is pyrolysed. Depending on the success of the tar cracking system will determine whether a three-stage system which implements the tar cracker between an initial pyrolysis stage and a final char gasification stage is worth pursuing (see Figure 1.6). The objectives and aims of the study are presented below:

1. **Complete an extensive literature search to review:**

    -   Biomass gasification systems

    -   Existing tar removal technologies

    -   The design principles of Coandă burners

2. **Design and develop a Coandă tar cracker (CTC):**

    -   Investigate a Coandă burner fuelled by propane

    -   Construct a two stage (pyrolysis-CTC) system

    -   Analyse the destruction of key tar components by thermal destruction and partial oxidation

3. **Computational fluid dynamics (CFD) modelling of the Coandă**

    -   Use of CFD to model the CTC

    -   Determine how key parameters affect the mixing performance

1.4 Outline of the thesis

This thesis consists of nine chapters. Chapter 1, The Introduction, presents the justification for the research and a background of the associated topics. Chapter 2 contains a review of relevant literature. Chapter 3 explore the scientific theory behind Coandă burners and describes some of the key tar cracking pathways for partial oxidation and thermal destruction of key tar species.

The experimental programme is separated into three chapters. Chapter 4 details the material characterisation tests, the preliminary experiments on a Coandă burner fuelled using propane gas, preliminary pyrolysis tests and the combined experiment where the pyrolysis unit and CTC are combined. Chapter 5 details the design modifications and improvements made to improve the operation of the overall system. The key modifications were made to extend the

run-time of the system by altering the feeding system and re-design the CTC to enhance combustion performance.

CFD modelling of the Coandă ejector is described in Chapter 7. Key parameters, including the size of the Coandă gap width and inlet pressure, were altered to determine their effect on the performance of the ejector. Chapter 8 details an overall discussion to summarise the impact of the study and highlight potential industrial applications of the CTC. The final chapter outlines the conclusions of the study and prescribes future work that is required for the enhancement of the field.

2. Literature Review

2.1 Gasification

2.1.1 General Description

Gasification covers the term used to describe the process of converting a carbon-based fuel into a gaseous fuel with a beneficial heating value (Higman and van der Burgt, 2008). Gasification of a solid fuel utilises the technology of partial oxidation, pyrolysis and hydrogenation, of these three the governing factor is the former. When carbonaceous fuel undergoes partial oxidation a synthesis gas or syngas is formed. This gaseous product contains hydrogen and carbon monoxide in varying proportions and can be used to manufacture hydrogen, transport fuels or chemicals or alternatively for electricity production (Stiegel and Maxwell, 2001). Low valued feed stocks can be converted through gasification to create products and which are of greater economic value and use (Breault, 2010).

2.1.2 Historical Development

The majority of modern gasification systems have evolved from scientific developments in the early part of the 20th century. Carl von Linde successfully commercialised the cryogenic process to separate air which prompted the design of continuous gasification units which used blasts of oxygen to produce syngas and hydrogen (Higman and van der Burgt, 2008). Also; this time period saw the discovery of devices which are predecessors to modern devices including Lurgi's pressurised moving bed gasifier (1931), Winkler's fluidised bed gasifier (1926) and the Koppers-Totzek entrained flow process (1940) (Kolb, 2011). With these techniques established the capacities and throughputs of such devices increased over the succeeding forty years.

The last thirty years of the 20th century saw a revival in coal gasification. The oil crisis of the 1970's coincided with anxieties over natural gas supplies which kick started this interest (Higman and van der Burgt, 2008). Investment went into developing new technologies capable of producing liquid and gas fuels through the gasification of coal in order to find alternative energy supplies. One major aim of this development was to create a substitute for natural gas by the hydrogenation of coal to methane, however this was ultimately deemed to be commercially unviable. Other developments in gasification in this period led to improvements of existing methods. Such improvements were often fronted by major energy companies, for example, Shell and Koppers developed a pressurised version of the Koppers-Totzek gasifier, and, through the partnership of Lurgi and British Gas a slagging version of Lurgi's previous design was produced (Higman and van der Burgt, 2008).

The interest and following development of gasification is closely linked with the availability and price of oil in developed countries, further associated factors include environmental awareness, the commercial success of integrated gasification combined cycle (IGCC) units and the deregulation of domestic electricity markets.

2.1.3 Current Applications and Trends

There has been a recent revival in gasification due the emergence of China as a global economic and energy power, unstable fuel prices and the strengthening concerns regarding carbon dioxide and climate change (Kirkels and Verbong, 2011). In 2010 the U.S Department of Energy (DOE) published the Worldwide Gasification Database.

The 2010 report showed a recent surge in the total capacity of syngas produced from the 144 plants that are currently in operation. There are currently plans for a further 37 plants to be built as well as 11 plants currently being constructed (U.S. DoE and NETL, 2010). If this growth goes ahead as planned it is expected that in 2016 the worldwide capacity of syngas produced from the existing and proposed 192 plants will be roughly 122,000 thermal megawatts (MWth).
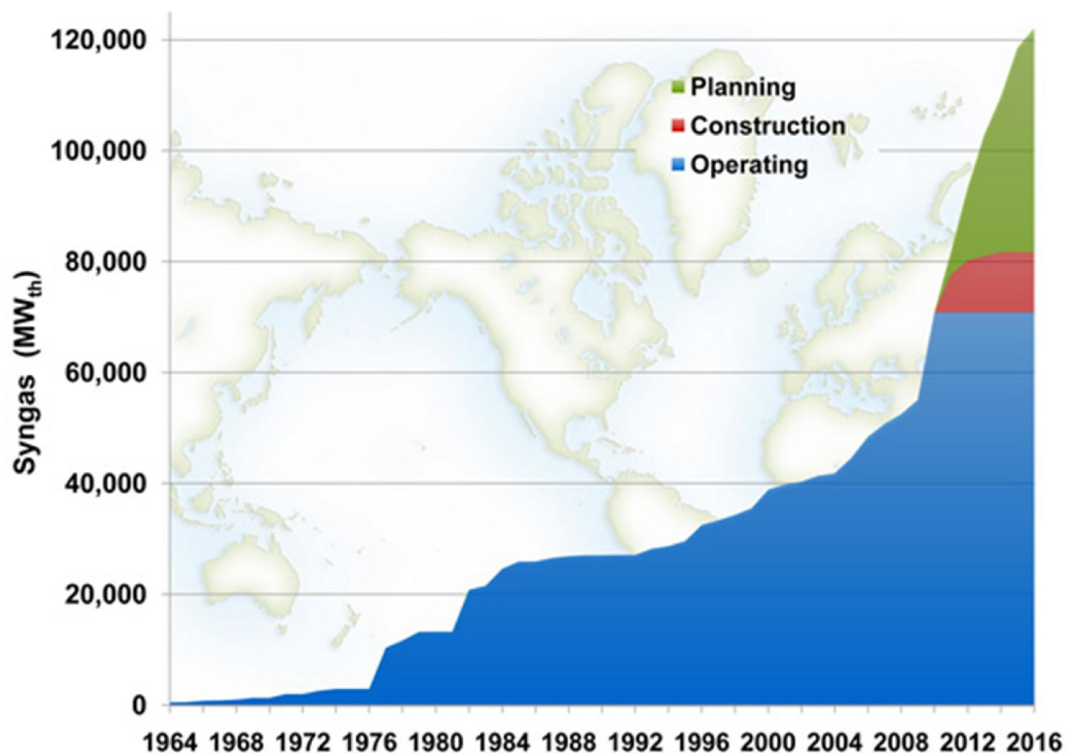
Figure 2.1 – Current and planned gasification capacity (U.S. DoE and NETL, 2010)

There are approximately fifteen different gasification technologies in operation worldwide, the three most popular technologies are Shell, GE Energy and Sasol Lurgi. Currently 37% of gasification plants are situated in Asia and Australia. This region plans to expand the number

of total plants, 65% of worldwide plants presently under-construction will be situated in either Asia or Australia, the majority of these plants will be in China (U.S. DoE and NETL, 2010). The U.S plans on drastically increasing the total amount of gasification plants in future years and are likely to compete with China in terms of operating gasification plants over the next ten years; however this may change due to the increased production of gas using fracking.

Fossil fuels are predominately used as the feed material for gasification units. Currently coal accounts for 51% of all worldwide feedstock and this figure is likely to increase in the future due to the large coal reserves of both the U.S and China. Of the gasification plants that are scheduled to be operational within the next 5 years 70% will utilise coal (U.S. DoE and NETL, 2010). Biomass contributes to less than one percent of total gasifier feedstock.

There are four main products created using syngas: chemicals, power, liquid fuels and gaseous fuels. Currently 45% is attributed to chemical production. Of the proposed plants to be finished before 2016 it is expected that 38% will apply syngas for power generation.
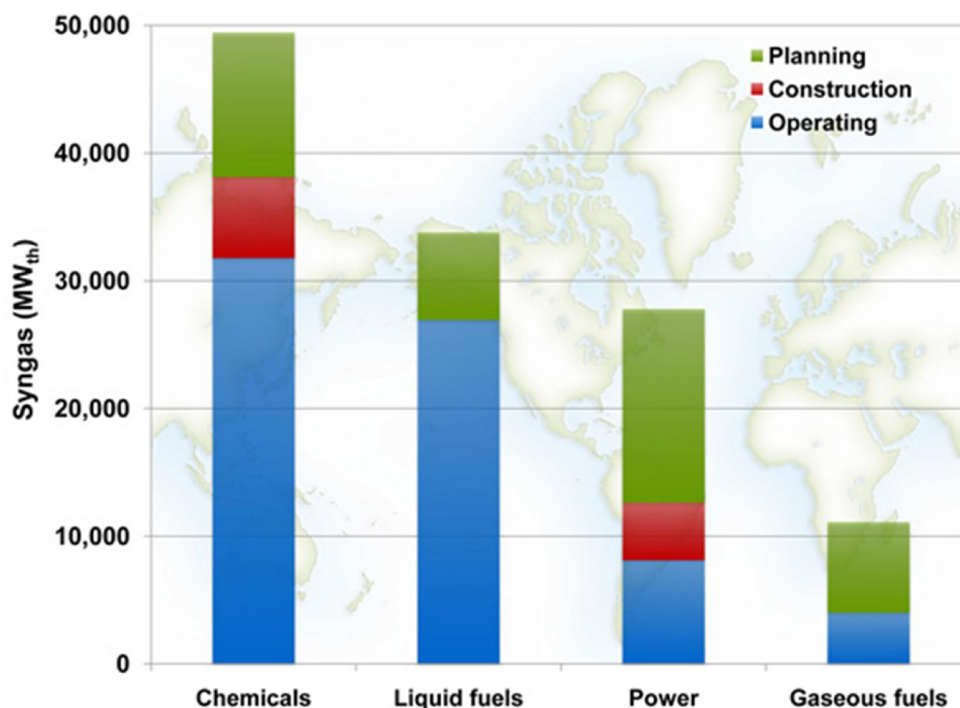
Figure 2.2 – Current and planned growth of gasification applications (U.S. DoE and NETL, 2010)

2.1.4 Theory of Gasification

The feed material for gasification usually contains a mixture of carbon, oxygen and hydrogen. The fuel may also contain sulphur, nitrogen and other trace elements, these species will be ignored for the following analysis due to the small quantities at which they are present. The following reactions explain the principle reactions involved in gasification:

Combustion reactions;

$C + \frac{1}{2}O_2 = CO$ -111 MJ/Kmol   (Eqn. 2.1)

$CO + \frac{1}{2}O_2 = CO_2$ -283 MJ/Kmol   (Eqn. 2.2)

$H_2 + \frac{1}{2}O_2 = H_2O$ -242 MJ/Kmol   (Eqn. 2.3)

Boudouard reaction;

$C + CO_2 \leftrightarrow 2CO$ +172 MJ/Kmol   (Eqn. 2.4)

Water gas reaction;

$C + H_2O \leftrightarrow CO + H_2$ +131 MJ/Kmol   (Eqn. 2.5)

Methanation reaction;

$C + 2H_2 \leftrightarrow CH_4$ -75MJ/Kmol   (Eqn. 2.6)

(Higman and van der Burgt, 2008)

To determine the equilibrium syngas composition the combustion reactions (with free oxygen) need not be considered as these reactions are effectively complete under gasification conditions. Therefore the Boudouard, water gas and methanation reactions, which are heterogeneous, are used. For further analysis it is assumed that carbon conversion is virtually complete. These circumstances allow for the following gas homogeneous reactions by reducing the Boudouard, water gas and methanation reactions:

CO shift reaction;

$CO + H_2O \leftrightarrow CO_2 + H_2$ -41 MJ/Kmol   (Eqn. 2.7)

Steam Methane reforming reaction;

$CH_4 + H_2O \leftrightarrow CO + 3H_2$ +206 MJ/Kmol   (Eqn. 2.8)

(Higman and van der Burgt, 2008)

The CO shift reaction is obtained by deducting the heat value and moles of equation (2.4) from (2.5); similarly the steam methane reforming reaction is formed by deducting equation (2.6) from (2.5).

The gasification process of a carbon based fuel or hydrocarbon is illustrated by equations (2.1), (2.4), (2.5) and (2.6). The Boudouard reaction (2.4) plays an important role as it allows for the production of pure carbon monoxide. The production of syngas by gasification relies heavily on equations (2.1) and (2.5).

2.1.5 Gasification Compared with Combustion

Gasification is a process that turns a carbonaceous material into a more valuable product. The key difference between gasification and combustion is that combustion uses an excess of oxygen whereas the oxygen supply for gasification is limited as shown in Table 2.1 (Rezaiyan and Cheremisinoff, 2005). The primary goal of combustion is to thermally destruct the feed material to produce heat.

	Combustion	**Gasification**
Purpose	Heat generation	Fuel upgrading
Chemical Process	Full oxidation	Partial oxidation
Primary Product	Heat	Syngas
Downstream Products	Electric power	Liquid fuels, chemicals, pure hydrogen, electric power
Efficiency	35-37% (GCV)	39-42% (GCV)
Raw Gas Composition	H_2O, CO_2, NO_x, SO_2 and particulates	H_2, CO, H_2S, NH_3 and particulates

Table 2.1 – Key features of gasification and combustion, Adapted from (Breault, 2010; Rezaiyan and Cheremisinoff, 2005)

GCV – Gross Calorific Value

2.2 Pyrolysis

2.2.1 General Description

Pyrolysis is a term used to describe the thermal decomposition of materials in such conditions where there is limited or no oxygen so that there can be no complete combustion (Mohan et al., 2006). The key difference between pyrolysing and gasifying a fuel is that gasification decomposes the material to syngas in an environment where oxygen is controlled, whereas oil and char are the preferred products from pyrolysis. The products of pyrolysis, as mentioned, are a solid char, a liquid and gases. The gases and liquid come from volatile fractions of the pyrolysed material and the remaining char is from fixed carbon (Cheng, 2010). The pyrolysis conditions determine the yield fraction of the products. Longer residence times and lower temperatures promote char production, short residence times and moderate temperatures favours liquid; high temperatures and longer residence time supports gas production (Bridgwater, 2004). The six steps that occur during pyrolysis are outlined below:

1. Supplied heat is transferred to the fuel material increasing its internal temperature

2. The increased temperature of the fuel leads to the release of volatiles and char production

3. As the volatiles exit the fuel particle heat transfer is active between hot volatiles and the remaining unpyrolysed fuel

4. Volatiles condense in cooler parts of the fuel particle resulting in tar production

5. Autocatalytic secondary pyrolysis caused by the preceding interactions

6. Additional thermal decomposition, water gas shift reactions, reformation and dehydrations can occur depending on the residence time, temperature of pressure of the procedure

(Babu, 2008; Mohan et al., 2006)

Neves et al. (2011) separates the pyrolysis of biomass into three parts. The first occurs when the solid fuel is introduced into a high temperature environment initially causing the release of moisture and leading into the primary pyrolysis stage which results in the release of pyrolytic volatiles. These pyrolytic volatiles are released from the thermal breaking of chemical bonds contained within biomass and consist of gas species (CO_2, CH_4, CO) and species which condense at ambient conditions (Neves et al., 2011). The secondary stage of pyrolysis involves previously released species participating in further reactions (outlined in part six of the six steps of pyrolysis). Primary pyrolysis can be referred to as inter-fuel reactions and secondary as extra-fuel; although this division is not flawless as secondary pyrolysis can occur in pores within the fuel and in the gas phase. Thus, both primary and secondary reactions can occur in parallel in different parts of the fuel. Figure 2.3 below offers a graphical interpretation of the three different stages of pyrolysis.
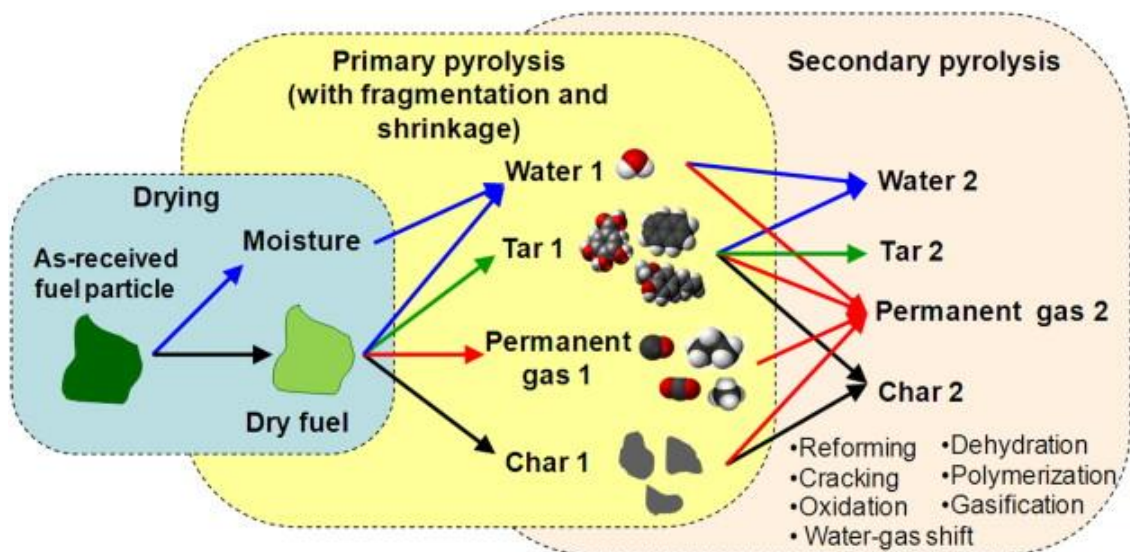
Figure 2.3 – Graphical interpretation of pyrolysis (Neves et al., 2011)

2.2.2 Types of Pyrolysis

Pyrolysis can be defined into different categories depending on the speed at which the process is performed. Slow pyrolysis, often referred to as conventional pyrolysis refers to the heating of the source material to around 500°C. Fast pyrolysis has much shorter heating rates, often between 0.5 and 5 seconds (Cheng, 2010) the resulting short residence time results in fewer interactions between the hot volatiles and the cooler char resulting in a higher liquid and gas yield. Table 2.2 outlines the different pyrolysis methods and the ensuing products when pyrolysing biomass.

Technology	Residence Time	Heating Rate	Temperature	Products
Carbonisation	Days	Very Low	400	Charcoal
Conventional	5 – 30 min	Low - 0.1-1 (°C/s)	300-700	Oil, gas, char
Fast	0.5 – 5 s	High - 10 - 200 (°C/s)	650 – 1000	Bio-oil
Flash-Liquid	< 1 s	Very High - >1000 (°C/s)	< 650	Bio-oil
Flash-Gas	< 1 s	High	< 650	Chemicals, gas
Ultra	< 0.5 s	Very High	1000	Chemicals, gas
Vacuum	2 – 30 s	Medium	400	Bio-oil

Table 2.2 – Types of pyrolysis (Maschio et al., 1992; Mohan et al., 2006)

2.2.3 Fast Pyrolysis

As shown in Table 2.2 the primary product from fast pyrolysis is a bio-oil. Bridgwater et al. (1999) highlights the essential characteristics of fast pyrolysis as:

- High heating and rapid rates of heat transfer which normally require the biomass feed material to be finely ground

- Controlling the reaction temperature for pyrolysis in the vapour phase at a temperature of around 500°C

- Short vapour residence times normally less than two seconds

- Rapid cooling of the pyrolysis vapours to produce bio-oil

When biomass undergoes fast pyrolysis treatment the resulting products are mostly vapours and aerosols with a small amount of charcoal. In order to increase the yield of liquid product it is important to minimise secondary reactions which is done by having minimal residence times (Bridgwater et al., 1999). Heating rates for fast pyrolysis have been reported at anywhere between 1000 and 10000 °C/second (Mohan et al., 2006). After the vapours have been cooled and condensed a dark brown liquid which has half the heating value, when

compared with conventional oil, is formed. The created bio-oil is a miscible mixture which contains roughly 75-80 mass.% of polar organics and the rest is made up from water. The properties of bio-oil are shown in Table 2.3.

Property	Value	Notes
Moisture Content	25%	Water comes from moisture contained within the fuel and cannot be separated. Values range from 15 – 35%.
pH	2.5	Low pH caused by organic acids.
Density	1.2 kg/l	Very high when compared with light fuel oil (0.85 kg/l). When compared with energy content of fuel oil, bio-oil has about 40% of the energy content on a weight basis and around 60% on a volumetric basis.
Elemental Analysis	-	Carbon: 57%, Hydrogen: 6%, Oxygen: 37%, N: trace
Higher Heating Value	18 MJ/kg	This is bio-oil that also contains 25 mass% of water which cannot be removed.
Solids/Char	0.2%	Can be between 0.1% and 1%.
Appearance	-	A dark brown free flowing liquid.
Odour	-	Smoky smell

Table 2.3 – Typical properties of wood derived bio-oil (Bridgwater, 2004)

2.2.4 Slow Pyrolysis

Conventional or slow pyrolysis has historically been used to produce charcoal (Mohan et al., 2006). For the pyrolysis of wood the raw material is heated to about 500°C with vapour residence times between 5 and 30 minutes which is considerably longer when compared with fast pyrolysis. The longer residence time means species in the vapour phase continually react with each other before they are removed.

2.2.5 Effect of Temperature and Heating Rate on Pyrolysis

Williams & Besler (1996) performed studies to determine how the heating rate and temperature influence the slow pyrolysis of biomass. Their results indicate that as the temperature at which pyrolysis is performed is increased, the product yields of gas and oil increased, and the yield of char decreased. In this study, wood samples were pyrolysed at a number of heating rates (5, 20, 40, 80 K/min) and final temperatures (300, 420, 600, 720°C); the results from this study are shown in Table 2.4.

	Char Yield (mass.%)	Oil Yield (mass.%)	Aqueous Yield (mass.%)	Gas Yield (mass.%)
5 °C/min				
300°C	53.8	10.6	21.0	14.6
420°C	29.7	12.4	35.9	21.5
600°C	24.4	12.4	36.6	26.4
720°C	23.2	13.0	37.0	26.8
20 °C/min				
300°C	55.6	10.1	20.5	14.0
420°C	27.2	12.2	37.4	23.0
600°C	22.6	12.8	37.6	27.0
720°C	19.6	14.1	37.5	28.8
40 °C/min				
300°C	58.0	6.7	21.7	13.6
420°C	26.4	11.8	34.2	27.6
600°C	20.4	13.2	37.6	28.8
720°C	18.4	14.3	37.7	29.6
80 °C/min				
300°C	60.8	6.4	21.6	11.2
420°C	25.2	11.9	36.9	26.0
600°C	18.7	14.6	37.8	29.1
720°C	16.2	15.9	37.7	30.2

Table 2.4 – Product yields from the slow pyrolysis of wood at different heating rates and temperature (Williams and Besler, 1996)

Table 2.4 indicates that the yield of char reduces as the final pyrolysis temperature increases which is the case for each of the four heating rates. The opposite occurs for yields of gas and oil; the higher the final temperature the higher the yield of gas and oil. At final temperatures above 420°C the aqueous yield remains relatively constant at weight percents of 36-38% (Williams and Besler, 1996). The gas composition of the produced gas was also analysed at different temperatures and heating rates. When the heating rate was at 5 K/min and final temperature 720°C it was found that the gas evolution of CO and CO_2 was prominent at lower temperatures generally between 200 and 400°C. At higher temperatures H_2 and CH_4 were found at higher concentrations with lower levels of CO and CO_2 (Williams and Besler, 1996). It was found that when the pyrolysis heating rate was increased the peaks for gas evolutions became less apparent. Increasing the rate also led to an increase in the yields of CO, CO_2, H_2, CH_4 and C_2H_2 and lower yields of propane and butane consequently the calculated calorific

value of the gas was higher. When the final temperature was 720°C and the heating rate was 5 K/min the calorific value was 13.6 MJ/m^3 for the same final temperature, but with a heating rate of 80 K/min the calorific value was 15.8 MJ/m^3.

A similar experiment into how increasing the final reactor temperature affects the production yields was performed by Chen et al. (2003). In these experiments the fuels tested were rice straw and sawdust. The results were similar to those reported by (Williams and Besler, 1996); increasing the temperature leads to an increase in gas production and decrease in char. Chen et al. (2003) reports that the liquid fraction hits a maximum at about 500°C and suggests that gas formation is more prominent from this point due to the liquid fraction being cracked at temperatures above 500°C.
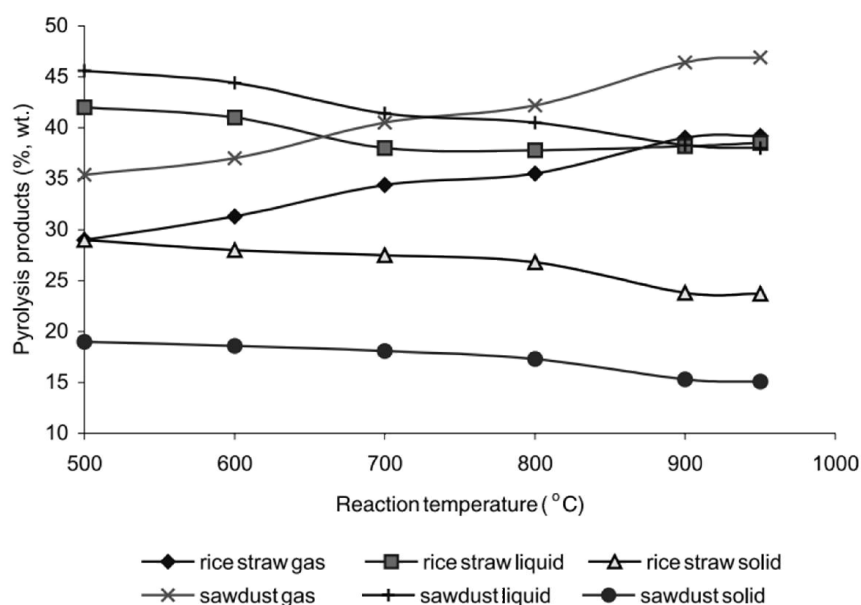
Figure 2.4 – Effect of reactor temperature on pyrolysis product yield (Chen et al., 2003)

Dufour et al. (2009) performed an extensive study into the composition of synthesis gas formed from biomass and how the gas composition is affected by the temperature. The experimental apparatus used for wood pyrolysis is shown in Figure 2.5.
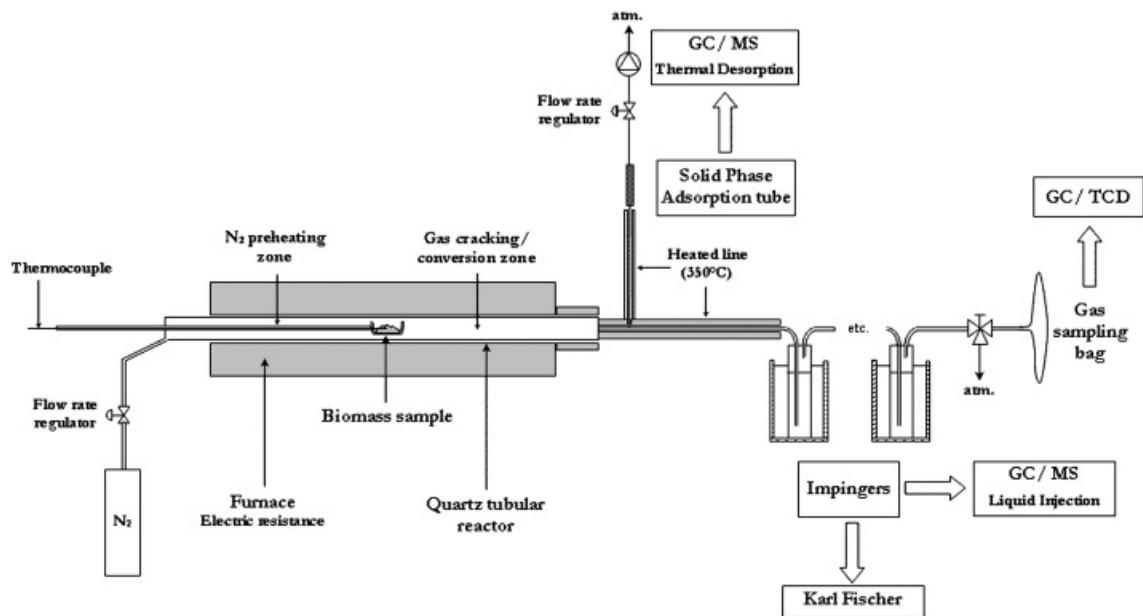
Figure 2.5 – Pyrolysis apparatus (Dufour et al., 2009)

Spruce wood chips were heated at rates between 20 and 40 °C/second in a quartz tube with an internal diameter of 35mm and a heated length of 600 mm. Nitrogen was used as the carrier gas. All the permanent gases were collected in a collapsible plastic bag before being injected into a gas chromatograph. The product gases are analysed the results of which are shown in Figure 2.6.
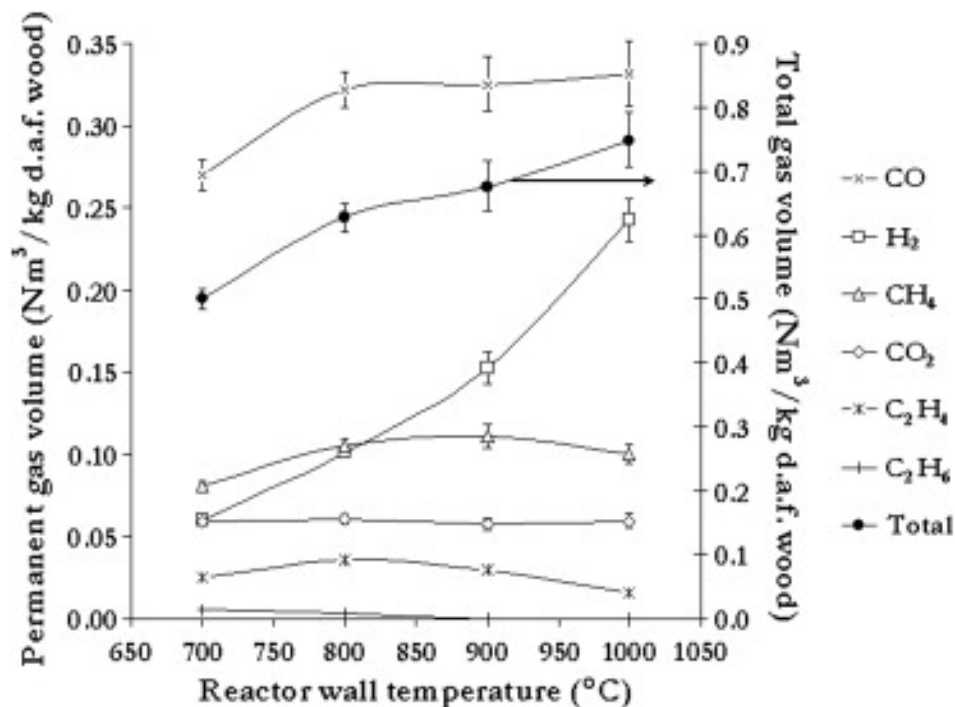
Figure 2.6 – Gas volume as a function of reactor wall temperature (Dufour et al., 2009)

The results indicate that as the temperature increased from 700 to 1000°C the total amount of gas produced also increased from 0.5 to 0.75 Nm^3/kg of wood (Dufour et al., 2009). This is

attributed to the increase of H_2 production which increases from 0.06 to 0.24 Nm^3/kg when the temperature was increased from 700 to 1000°C. Carbon monoxide production increased slightly between 700 to 800°C and then remained relatively constant as the reactor wall temperature reaches 1000°C (Dufour et al., 2009). Therefore the ratio between H_2 and CO increased from 22% to 73%, caused mainly by the increase in hydrogen production. Yields of methane and ethylene reach a maximum yield at 800°C.

The study also investigated the production of aromatic tar during pyrolysis. The compounds that were quantified in the study were benzene, toluene, o-xylene, phenol, o-cresol, indene, naphthalene, 1, 2-methyl-napthalene and phenanthrene (Dufour et al., 2009). The author states that between 700 and 800°C o-cresol is converted into toluene and phenol whilst simultaneously being decomposed into indene, benzene and naphthalene. Between 800 and 900°C there was almost complete conversion of indene, phenol and toluene into benzene and PAHs. Benzene is the most common and stable tar produced and makes up for more than 80% mol of the total quantified tar from the study at 900 and 1000°C.

An overall mass balance was carried out at each reactor temperatures (700, 800, 900 and 1000°C) Figure 2.7 shows how the reactor temperature affects the yields from pyrolysis.
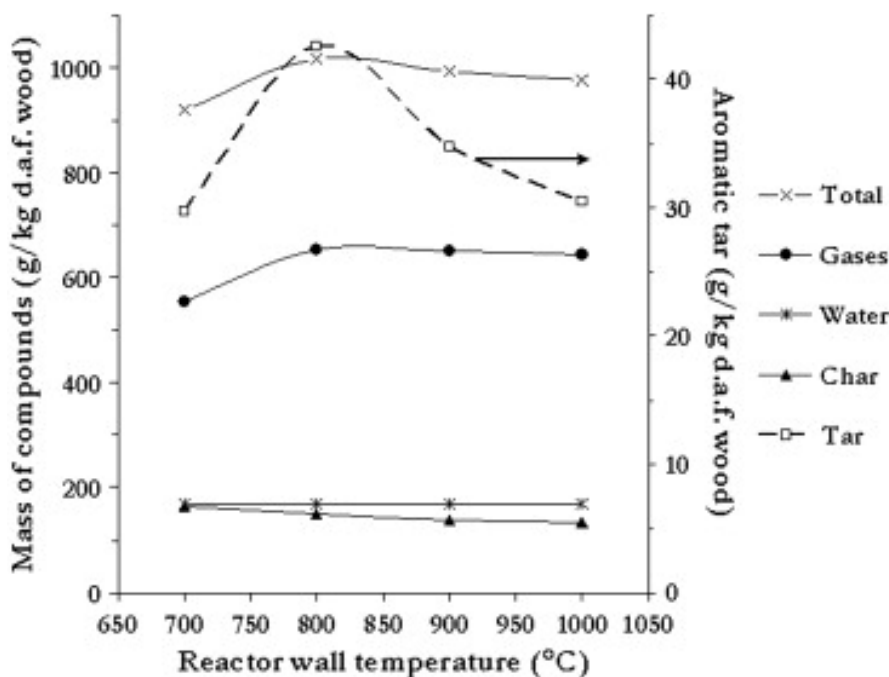
Figure 2.7 – Total yields of gases, water and char at different reactor wall temperatures (Dufour et al., 2009)

Gas yield reaches a maximum at 800°C and then remains relatively constant despite an increase in reactor temperature. Char yield decreases from 16.5 mass% to 13.3 mass% from 700 to 1000°C. The amount of quantified tar reached a maximum at 800°C.

2.2.6 Effect of Biomass Particle Size on Pyrolysis

The size of the biomass fuel plays an important role in the pyrolysis process. Particle size affects the heating rate of the solids and therefore controls the rate at which the fuel decomposes. Fine particles have a uniform heating rate due to negligible resistance from intraparticle and extraparticle heat transfer (Neves et al., 2011). Smaller particles allow for moisture and primary volatiles to exit without interacting with each other and the formed char; limiting the amount of internal secondary reactions.

Increasing the particle size results in a decrease in the overall rate of drying and primary pyrolysis (Neves et al., 2011). This creates a non-uniform process meaning that both processes occur at the same time in different parts of the particle. This dual process moves in sequence from the outer surface towards the centre of the particle creating different layers as the particle undergoes decomposition. The outer layer becomes char and contains no moisture and volatiles. There is also an intermediate zone where the dried fuel produces primary pyrolysis products, finally the particle centre which consists of the raw material and undergoes drying (Neves et al., 2011). There is an increase in the number of intraparticle reactions thus secondary reactions involving water and volatiles are increased. Species produced within the particle have to pass through the outer char layer to exit meaning the transport time of these species leaving the particle is increased as they exit through the porous char layer resulting in more homogeneous and heterogeneous reactions. Over time the char layer will increase so heterogeneous reactions between volatiles and char that occurs in this layer may become more effective (Neves et al., 2011).

Demirbas (2004) performed studies to discover the link between the particle size and the yield of char on a number of biomass products. It was found that increasing the particle size led to an increase in the char yield, see Figure 2.8. In experiments using olive husks pyrolysed to a final temperature of 950K it was found that when the particle size was reduced from 2.2 to 0.5 mm, the char yield decreased by 45.5%.
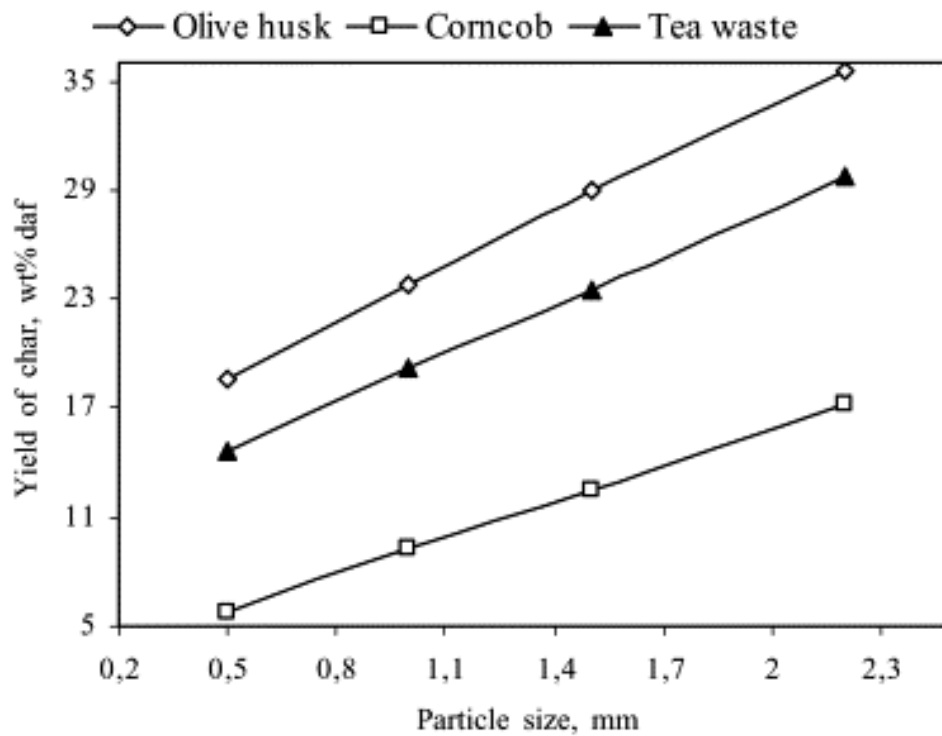
Figure 2.8 – Relationship between particle size and char yield (Demirbas, 2004)

2.3 Biomass Gasification: Introduction and Background

The use of biomass as a fuel for gasification is a logical choice. Fears over climate, energy supply and cost should allow for biomass to play an important role in solving these issues. Biomass gasification appears relatively simple in theory; a solid carbon based fuel that can undergo gasification to produce high amounts of gaseous products with low char and ash quantities (Balat et al., 2009). For complete thermal biomass gasification the minimum temperature required is between 800 to 900ºC, a value which is similar to coal (≈900ºC) (Higman and van der Burgt, 2008). The three foremost variations in which biomass gasification differs from coal include; the higher reactivity of biomass, high tar production rates and the difference in the quality of ash produced. Of these three variations it is problems regarding tar formation that have created the biggest setbacks in regards to making biomass a technically and commercially viable option.

The application of biomass gasification units is most prominent in North America (U.S.A and Canada) and Northern Europe (Finland, Sweden and Denmark) (Kirkels and Verbong, 2011). This can be explained because of the large woody biomass and peat resources of the mentioned countries. The USA, in particular, played an important role in the research and development of biomass gasification due to anxieties sparked by the supply and cost of oil in the 1970's.

The beginning of the 1980's coincided with an increase in the progression of small-scale gasifiers (up to 250kW$_{el}$). The fuel for these units was normally wood or charcoal and the majority of units were installed in developing countries (Quaak et al., 1999). The 1990's brought heightened awareness with respect to climate change and global warming resulting in fresh interest in biomass gasification.

As discussed earlier biomass contributes to less than one percent of the total feedstock for gasification, this leaves room for expansion and development into this area. Of this 1% of biomass feedstock the majority is made up from wood products, although other sources have been used for gasification including rice husk, peat and black liquor (a by-product from the paper industry) (Kirkels and Verbong, 2011). The total usage of biomass in gasifiers is fractional when compared to coal fed gasifiers but the similar conditions required for gasification would allow for such plants to potentially be retrofitted and converted to use biomass instead (Klass, 1998).

2.3.1 Applications for Biomass Gasification

The utilisation of the syngas product after biomass gasification is almost identical to the applications for any fuel which has been gasified. Figure 2.9 below shows the products and potential applications of biomass gasification.
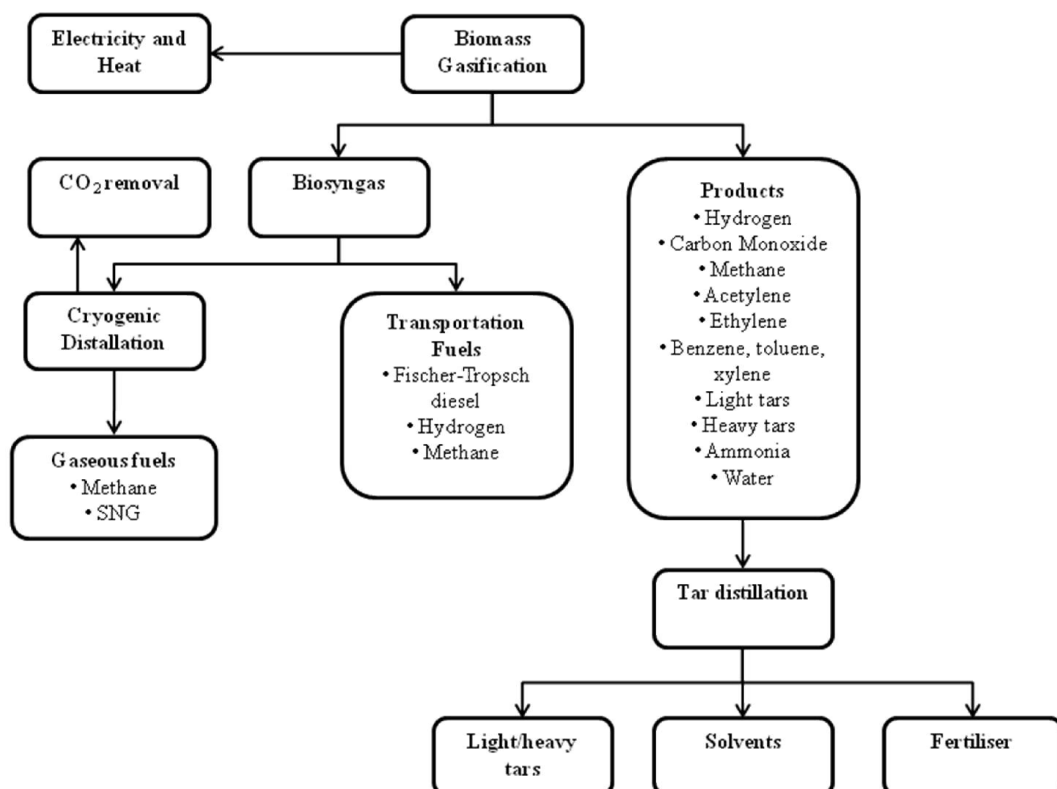
Figure 2.9 – Products from the gasification of biomass (Adapted from Balat et al., 2009)

Biomass is primarily turned into energy through combustion with gasification being used on a smaller scale. Currently combustion accounts for 90% of total electricity and heat production from biomass. The application of biomass is increasing with time, in particular for CHP (Kirkels and Verbong, 2011). Biomass gasification systems have been put into action at coal power stations. The products from biomass gasification are fed into the system and combusted together with coal; this reduces the potential damage to the boilers. However direct co-combustion where biomass and coal are combusted together is still the preferred option (Kirkels and Verbong, 2011).

2.3.2 Biomass Gasification Technologies

Biomass gasifiers can be divided into three categories; updraft, downdraft and fluidised bed. The simplest method for biomass gasification is updraft or counter-current gasifiers (Quaak et al., 1999). Biomass is fed into the top of the reactor and air is fed from the bottom moving upwards through interstitial spaces in the solid fuel (Neathery, 2010). Biomass moves downwards through the gasifier. The product gas leaves through the top at a lower temperature when compared with downdraft gasifiers but is often contaminated with tars and oil as tar vapours from pyrolysis are forced upwards by the gases (Rezaiyan and Cheremisinoff, 2005). As the biomass moves through the gasifier it moves through four different stages; drying, pyrolysis, reduction and finally combustion see Figure 2.10.
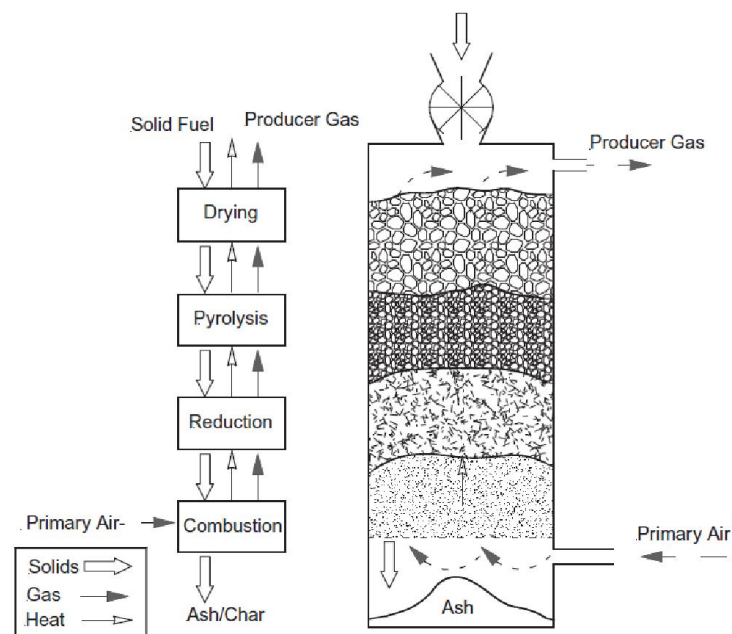
Figure 2.10 – Updraft gasification (Neathery, 2010)

In downdraft gasifiers fuel is fed into the top of the reactor and air is added either with the fuel or at a lower level. Biomass can be added at ambient pressure and temperatures making the feeding process simple. The product gas is withdrawn through the bottom of the reactor by

applying a slight vacuum (Neathery, 2010). Downdraft gasifiers have the same four zones (drying, pyrolysis, reduction, combustion) as updraft systems but the solid fuels pass through each zone in a different order; the combustion and reduction sections are reversed see Figure 2.11. The key advantage downdraft has over updraft is that the tar content from the product gas is lower (Quaak et al., 1999). The 'tars' are cracked by thermal processes as the product gases are drawn through the hot reaction zone (Rezaiyan and Cheremisinoff, 2005).
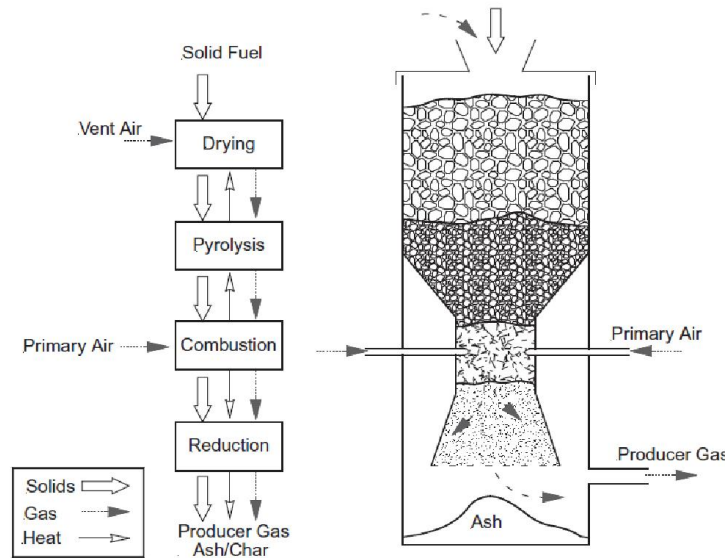
Figure 2.11 – Downdraft gasification (Neathery, 2010)

Stassen (1995) analysed the typical gas composition of updraft and downdrafts, the results of which are in Table 2.5.

Gasifier Type: Fuel	Updraft: Wood	Downdraft: Wood
Moisture in feed (% wet basis)	10 - 20	10 - 20
Hydrogen (%)	8 - 14	12 – 20
Carbon Monoxide (%)	20 - 30	15 - 22
Methane (%)	2 - 3	1 - 3
Carbon Dioxide (%)	5 - 10	8 - 15
Nitrogen (%)	45 - 55	45 - 55
Oxygen (%)	1 - 3	1 - 3
Moisture in gas (Nm^3 H$_2$O/Nm^3)	0.2 – 0.3	0.06 – 0.12
Tar in gas (g/Nm^3)	2 - 10	0.1 - 3
Lower heating value (MJ/Nm^3)	5.3 – 6	4.5 – 5.5

Table 2.5 – Gas composition for different fuels and reactor types (Stassen, 1995)

Fluidised bed gasifiers use an inner material often sand to mix with the biomass fuel and create a moving bed. Air is injected at the bottom of the unit through a distribution device in the form of nozzle or a perforated plate suspending the bed in a fluid like state (Neathery, 2010). The fuel is fed into the lower region of the bed; the feeding system is normally under pressure so a rotary seal valve or lock hoppers are required to isolate the feeding mechanism. When the particles enter the bed they are rapidly heated thus the four zones (drying, pyrolysis, reduction, combustion) run in parallel with one another. Bubbles from the distributor rise upwards and increase in size due to a decrease in hydrostatic pressure. The air bubbles exchange with gases produced through combustion and pyrolysis and are converted into the product gas. As bubbles are ejected; char, fly ash and inert bed material are removed. Fluidised bed gasifiers are designed so that larger particles are returned to the bed.

The turbulent nature of the bed promotes high rates of heat transfer causing the maximum temperature, between 800 and 900°C, of the bed to be lower when compared with fixed bed designs. The residence times for the gases are low which with the comparatively low internal temperature results in yields of tar and oil higher than that of downdraft reactors (Neathery, 2010).
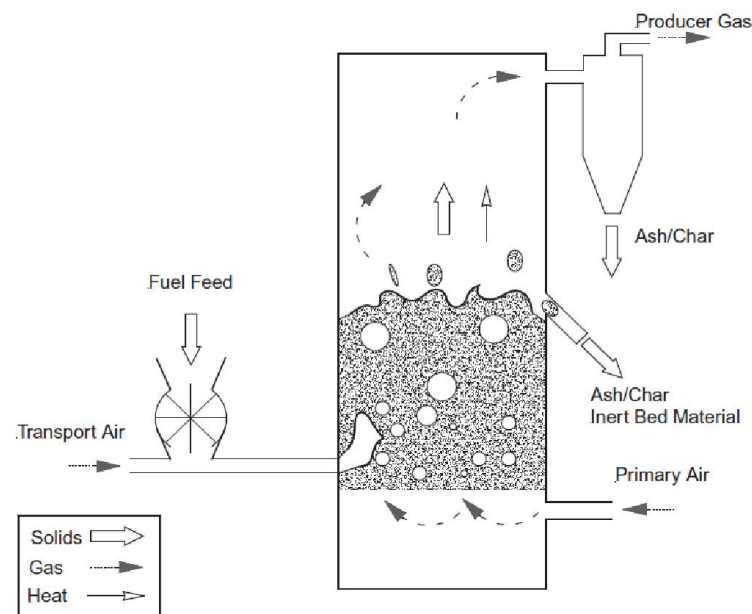
Figure 2.12 – Fluidised bed gasifier (Neathery, 2010)

2.3.3 Small-Scale Biomass Gasification

The use of small-scale gasifiers in rural areas has the potential to be an attractive strategy to provide rural areas with a sustainable supply of electricity (Larson, 1998). Setting up a biomass power system could benefit and help develop the area by creating potential employment to run the plant. Kirkels and Verbong (2011) documented the leading small-scale

manufacturers and technologies in developed countries. Maniatis and Millich (1998) also analysed some utility scale biomass gasification projects in the UK which are mainly IGCC. Akin to most biomass gasification; cleaning the produced tarry gas is the major difficulty. For complete tar clean-up an extensive, complicated and expensive system is required. Using advanced power cycles increases conversion efficiency thus reducing the required feedstock resulting in lower operating costs. A selection of existing and operational small-scale gasification units are analysed in section 2.3.4, 2.3.5 and 2.3.6.

2.3.4 Updraft Biomass Gasifiers Review

The *Bioneer gasifier* produces a tarry low calorific value fuel by using an updraft fixed bed gasifier (OPET Finland, 2002). The gasifier unit consists of rotating cone-shaped grate and a refractory lined vessel. The fuel is fed into the top of the unit and passes through the four stages discussed in section in 2.3.2. Ash is removed from the rotating grate at the bottom of the unit. The gasification medium is steam and air which are fed through the grate. The high amounts of tar in the product gas means that it cannot be transported over long distances or used in internal combustion engines as the tar would foul the equipment and pipelines. Figure 2.13 shows a schematic diagram of the *Bioneer gasifier*.
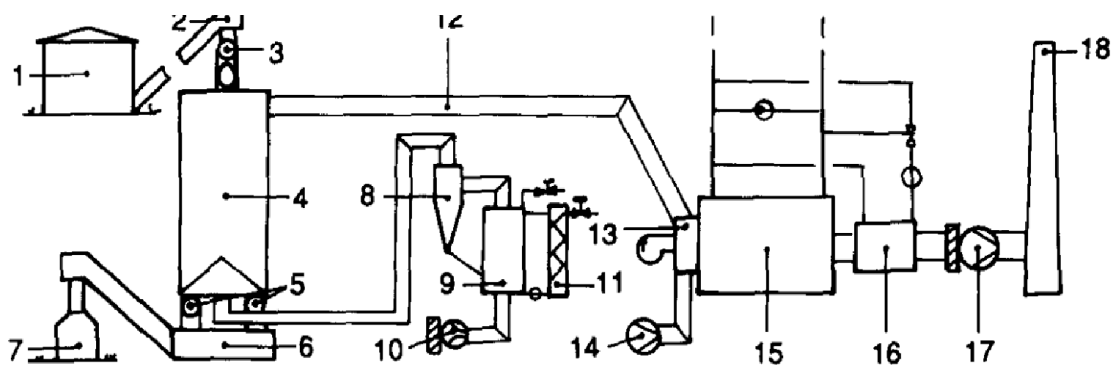
Figure 2.13 – Schematic diagram of the *Bioneer Gasifier* (Kurkela et al., 1989)

Where; 1, Fuel storage; 2, fuel conveyor; 3, fuel feeder; 4, gas generator; 5, ash removers; 6, ash conveyor; 7, ash pallete; 8, drop separator; 9, humidifier; 10, gasification air fan; 11, plate heat exchanger; 12, gas pipe; 13, gas burner; 14, combustion air fan; 15, gas boiler; 16, economiser; 17, flue gas fan; 18, flue. (Kurkela et al., 1989)

The technology for the *Bioneer gasifier* is well proven. Nine commercial plants have been in operation in Sweden and Finland since 1986 and there is also a 5 MW district heating system in Finland. The *Bioneer* technology can be used for district heating (1 – 15 MWth), for small-scale combined heat and power (1 – 3 MWe) and also for drying kilns and process ovens (OPET Finland, 2002).

Extensive tests were carried out in the 1980's on a pilot scale 1.5 MW test gasifier. The results for the product gas composition when using wood chips with a 41% moisture content was found to contain 30% carbon monoxide, 11% hydrogen, 3% methane, 7% carbon dioxide and 49% nitrogen. The higher heating value of the gas was 6.2 MJ/m^3 (OPET Finland, 2002). The tar content was estimated to be between 50 – 100 g/m^3.

Plis and Wilk (2011) designed and tested an updraft fixed bed gasifier and performed experiments to determine how the excess air ratio and parameters of biomass affected the composition of produced gas. The experimental rig was setup so that the produced gas would be co-combusted with coal in a water boiler. Wood pellets and oats husk pellets were used as the biomass fuel; both fuels are cylindrical in shape, between 10 – 30mm long and have a diameter of 6 mm. Figure 2.14 indicates the experimental setup and Figure 2.15 shows a schematic of the gasifier.
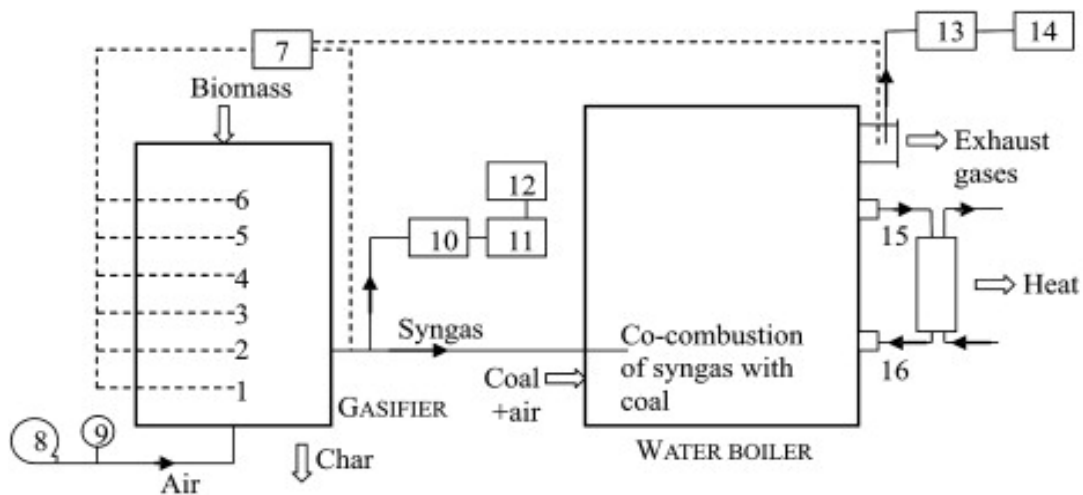
Where; 1-6 – Points of temperature measurement, 7 – Data recording system; 8 – Air blower, 9 – Flow meter, 10 – Cleaning and cooling system, 11 – Syngas composition analyser, 12 – Gas sample, 13 – Cleaning and cooling system, 14 – Exhaust gases analyser, 15 – Hot water, 16 - Feedwater

Figure 2.14 – Experimental setup (Plis and Wilk, 2011)
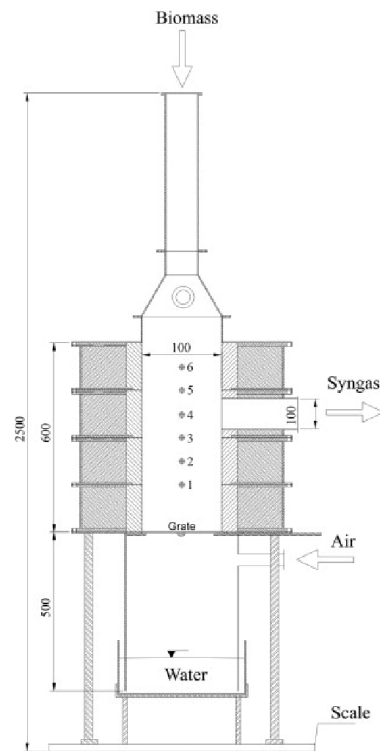
Figure 2.15 – Schematic of the gasifier (Plis and Wilk, 2011)

Six temperature probes were used to monitor the temperature within the gasifier. Temperatures within the gasifier ranged from 130°C in the drying zone to 1000°C in the combustion zone.

2.3.5 Downdraft Biomass Gasifiers Review

Zainal et al. (2002) presented an experimental investigation into a downdraft biomass gasifier shown in Figure 2.16.
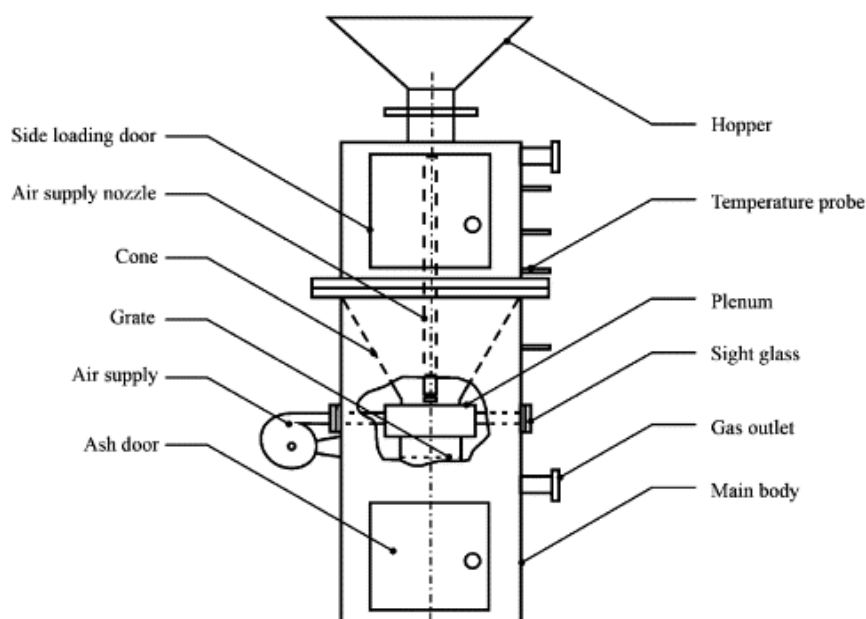
Figure 2.16 – Gasifier experimental setup (Zainal et al., 2002)

The gasifier contains a cone structure and is a blow-type downdraft gasifier. The height of the gasifier is 2.5m and the main body is made from 600 mm diameter mild steel pipe. The internal cone is inclined at a 60° angle to the horizontal, the diameter at the top of the cone is 600 mm and 200 mm at the bottom. Biomass is fed into the gasifier through a slide loading door. The biomass fuel used was wood chips and furniture wood which were cut into 50 mm cubes. Air was supplied into the gasifier through a 40 mm diameter pipe which contained eight 10 mm diameter nozzles (Zainal et al., 2002). The air pipe is positioned horizontally and the 8 nozzles placed 150 mm from the throat.

The temperature in the gasifier is measured by 5 k-type thermocouples, an additional thermocouple is situated at the gas outlet to record the temperature of the produced gas. Gas was sampled using a probe, condensation unit, polytetrafluoroethylene filter, dryer, a sampling bag and a suction pump (Zainal et al., 2002). The product gas is collected in Teflon sampling bags and the gas composition is analysed using a TCD (thermal conductivity) gas chromatograph.

Figure 2.17 indicates the temperatures that were recorded in the different zones in the gasifier. The fluctuation caused in the combustion zone is caused by a phenomenon called bridging. When a piece of glowing wood falls on a thermocouple the recorded temperature is high but if there is a void around the thermocouple then a lower value is recorded. The temperature in the combustion zone is high (1000°C) which cracks tar contained within the producer gas reducing the tar content (Zainal et al., 2002).
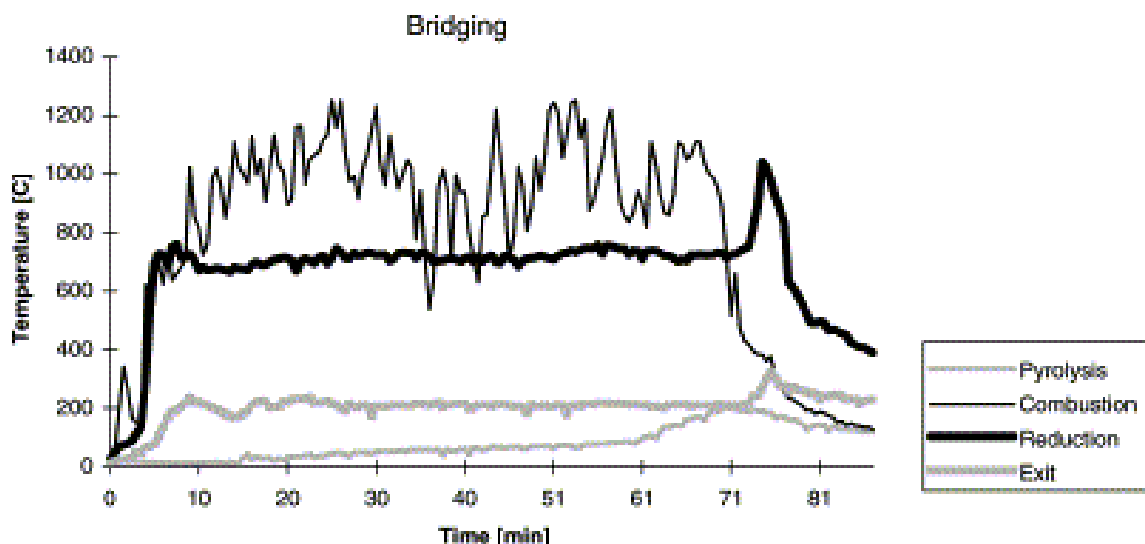
Figure 2.17 – Temperature profiles (Zainal et al., 2002)

The average gas composition of the product gas was found to be; 1.69% oxygen, 43.62% nitrogen, 24.04% hydrogen, 14.66% carbon dioxide, 24.04% carbon monoxide and 2.02%

methane (Zainal et al., 2002). The composition of the constituents in the producer gas varied when the equivalence ratio (see equation 2.9) changed.

$$Equivalence\ ratio\ \emptyset = \frac{(Flow\ rate\ of\ air) \times (Duration\ of\ run)}{(Mass\ input\ of\ wood) \times (\frac{Air}{Fuel}\ for\ \emptyset = 1\ )}$$

<div align="right">Eqn 2.9</div>

The air/fuel ratio when $\emptyset = 1$ is 5.22 Nm^3 of air/kg of wood. Carbon monoxide makes the most influential contribution to the calorific value of the producer gas. The effect of the equivalence ratio on the percentage composition of carbon monoxide is shown in Figure 2.18. The average calorific value of the producer gas was found to be 5.34 MJ/Nm^3. At an equivalence ratio of 0.38 the gasifier performed at its best.
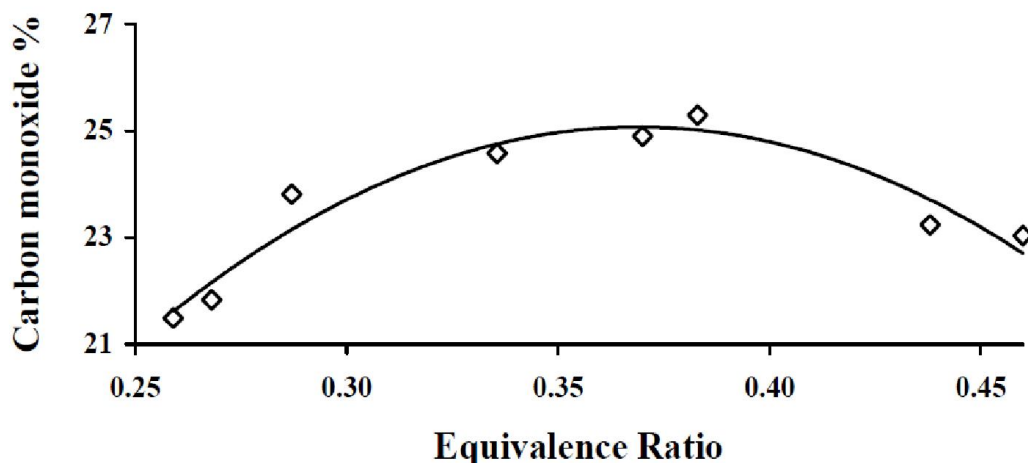
Figure 2.18 - Variation of carbon monoxide with equivalence ratio (Zainal et al., 2002)

Olgun et al. (2011) carried out a study into a small-scale gasifier with a fixed bed downdraft system. The biomass fuel used was agricultural and forestry residues, these are defined as wood chips which range between 10 and 30 mm in size and hazel nut shells which are between 5 and 10 mm. The experimental set up used is shown in Figure 2.19 and consists of a gasifier, ignition unit, cyclone, gas cleaning system, a flare and measurement, control system and data controlling units. As the produced gas enters the cyclone it is directed into two different streams, the first goes to the gas cleaning system and on to a gas analyser, the second is directed to a flare.

The gasifier has been designed to have 10 kg of biomass fed into the system. The gasifier has a throat design which offers lower tar production because temperatures in the throat region are above 900°C. The gasifier uses a pilot burner that is used to ignite the biomass fuel. Air is supplied into the unit by an electrical motor which can supply air at a rate of 120 m^3/hr (Olgun et al., 2011).
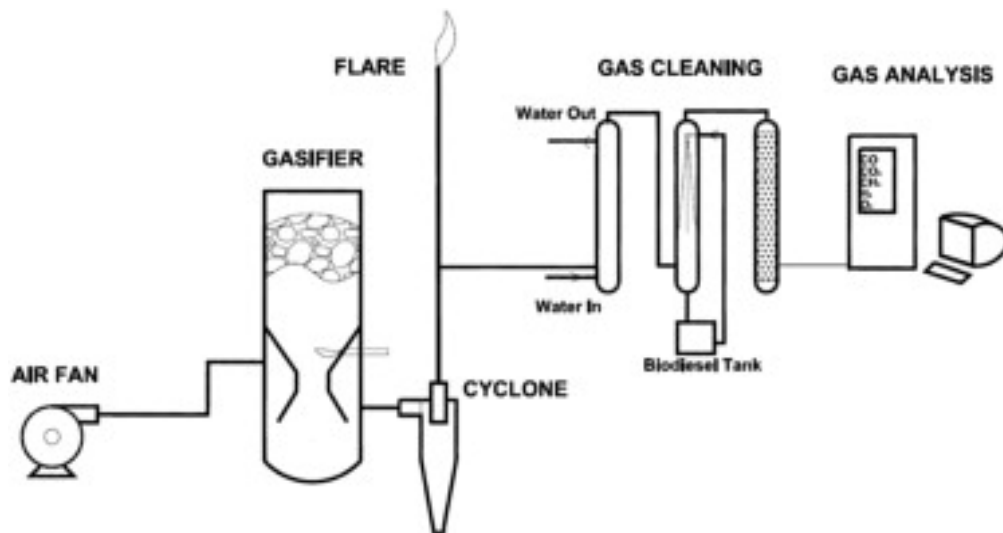
Figure 2.19 – Schematic setup (Olgun et al., 2011)

The gasifier is made from 3 mm thick stainless steel. The diameter of the gasifier at the top is 300 mm, the 'throat' is 100 mm, the gasifier is 1095 mm high (see Figure 2.20); five thermocouples are placed in the gasifier to monitor the temperature in the different reaction zones.
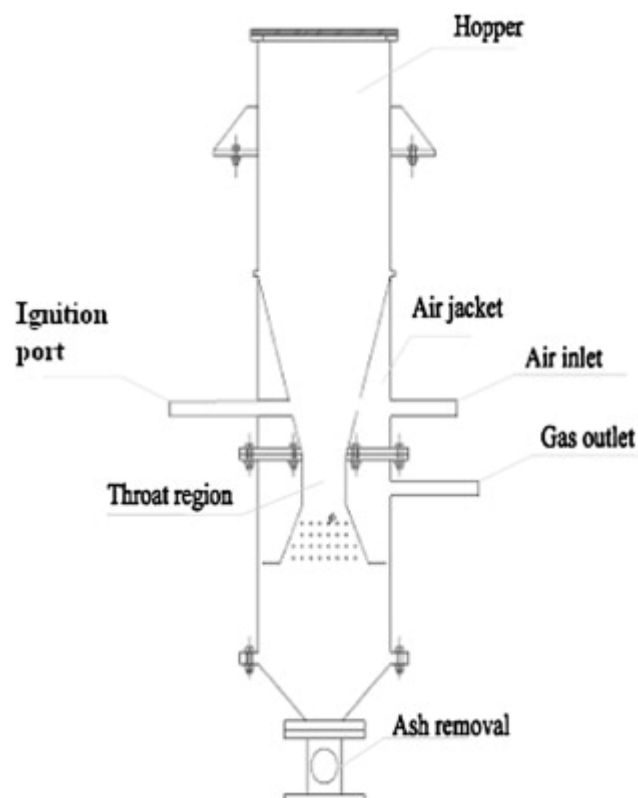
Figure 2.20 – Schematic of the fixed bed gasifier (Olgun et al., 2011)

The gasifier is fed with 10 kg of biomass and the lid is closed. The air blower is then turned on and the flow rate is adjusted so that the desired level of combustion is reached. Initially, the fuel is ignited and then the ignition is stopped once the gasifier can produce enough heat

to maintain the gasification process, this is normally when the oxidation zone temperature is between 600 and 700°C. The gasifier was run at different equivalence ratios (ER) between 0.2 and 0.5. The equivalence ratio is calculated as the 'actual air to fuel ratio divided by the air to fuel ratio calculated for complete combustion under stoichiometric conditions' (Olgun et al., 2011).

The highest heating rate of the produced gas was 5.5 MJ/Nm^3 when the ER was 0.35. Decreasing the ER below 0.35 leads to lower heating values as conditions are more suited for pyrolysis.

A separate study was performed to look into the how different types of biomass pellets effect performance in a downdraft gasifier (Erlich and Fransson, 2011). Pellets of identical diameter made from wood, sugar cane bagasse and empty fruit bunch (EFB) from the palm-oil production industry were gasified. Of the three fuels used; wood pellets have the lowest ash content and the highest lower heating value. The EFB pellets have a much higher ash and sulphur content. The downdraft gasifier used is shown in Figure 2.21.
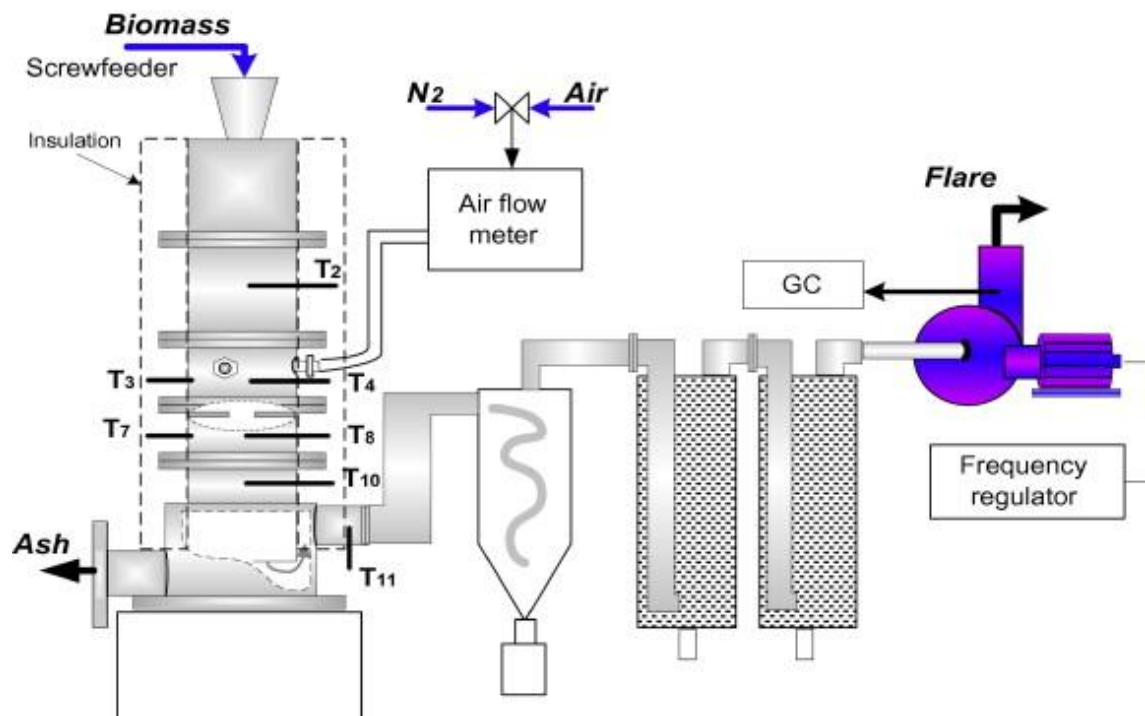
Figure 2.21 – The downdraft gasifier system (Erlich and Fransson, 2011)

A frequency regulated centrifugal blower creates suction which enables air to enter the gasifier from the air flow meter and into the gasifier through three equally placed nozzles. Tar cracking is promoted by forcing the gases through a constriction to the char zone, forcing the gases through a high temperature region. No grate is used in the gasifier because of the high ash content in the fuels. Instead there is a porous bed at the base of the gasifier.

Three steps are used to clean the produced gas. The gas is firstly run through a cyclone before passing through two packed bed filters before it is finally flared. The gas is sampled and analysed by a gas chromatograph.

2.3.6 Fluidised Bed Biomass Gasifiers

A pilot scale CFB biomass gasifier was tested and analysed. The gasifier was 6.5 m high and had a diameter of 0.1 m. Figure 2.22 shows a diagram of the experimental setup.
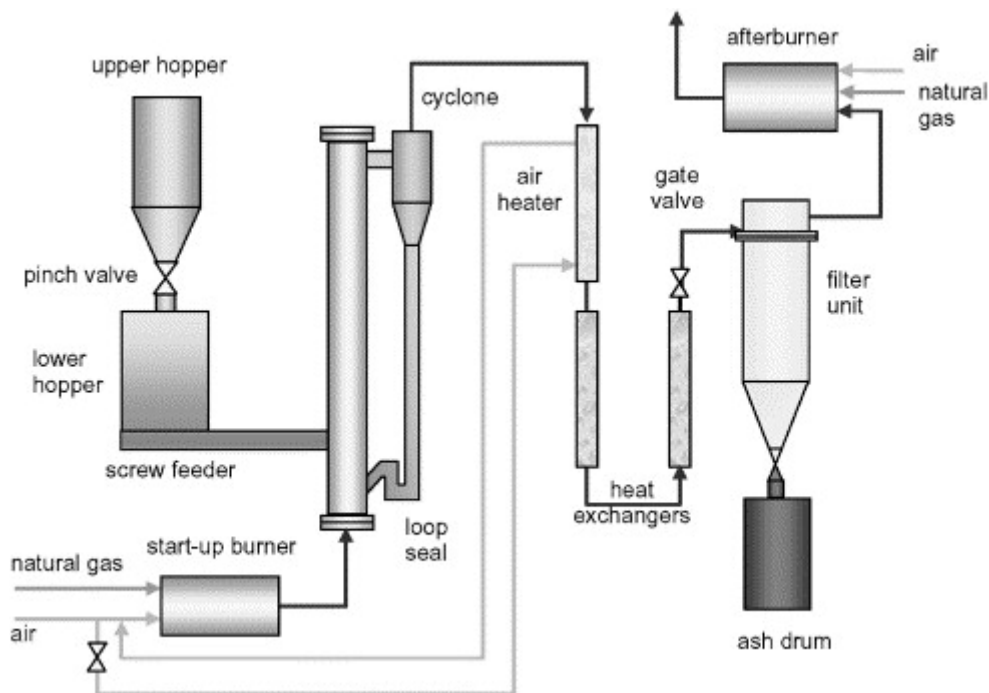
Figure 2.22 – Schematic diagram of CFB Gasifier (Li et al., 2004)

The cyclone that is attached to the gasifier re-circulates solids back to the gasifier. Air, acting as an oxidant and fluidising agent, and natural gas is passed through a start-up burner to preheat the bed and maintain the suspension temperature at the required level. Sawdust from six different species of wood were fed into the gasifier at a rate of 16-45 kg/h. Coarser particles were collected in the cyclone and fed back into the gasification unit through an air-driven loop seal. The hot product gas that leaves the cyclone is cooled by a two-stage water-jacketed heater and single stage air preheater, after this step the hot gas passes into a filter unit. Gas samples are taken every 20 minutes from the inlet near the heat exchanger and analysed using a gas chromatograph.

2.4 Tars from Biomass Gasification

One of the major concerns when biomass is gasified is the production of tars (Devi et al., 2003; Han and Kim, 2008). Tars formed within the thermal conversion process, cool, condense and foul process equipment downstream from the gasification unit. This can cause

serious operational issues if fuel lines, filters and engines become blocked (Han and Kim, 2008; Li and Suzuki, 2009). For the product gas from biomass gasification to be applied viably to conversion technologies there are strict specifications in place; for gas engines the limit is 50 mg/Nm^3, gas turbines – 5 mg/Nm^3, for fuel cells – 1 mg/Nm^3 and for methanol production 0.1 mg/Nm^3 (Iversen and Gøbel, 2005). Given that most current gasifiers produce a gas with a tar yield between 0.5 and 100 g/m^3 (Han and Kim, 2008), the effective removal of tar becomes a pressing subject. Finding an efficient method of removing tar from the gases produced is a key technical challenge currently preventing the commercialisation of biomass gasification technology (Kumar et al., 2009).

2.4.1 Tar Definition

The definition of what constitutes a "tar" from biomass gasification has been an issue in previous research. One of the most comprehensive reports on tars from gasification was written by (Milne et al., 1998) a starting definition of tar was used; "*The organics produced under thermal or partial-oxidation regimes (gasification) of any organic material are called tars and are generally assumed to be largely aromatic*". However, tars are also defined as organic contaminants that have a larger molecular weight than benzene (Devi et al., 2003; Li and Suzuki, 2009). This definition was first detailed after an EU meeting in 1998 by members of the IEA Bioenergy Gasification Task (Maniatis and Beenackers, 2000). In the main part tars are classified as organic products in the condensable fraction of the product gas and are primarily aromatic hydrocarbons (Li and Suzuki, 2009).

2.4.2 Tar Formation

Tars are formed during gasification through a number of complex reactions and the types of tar are affected by the conditions in the reactor. Increasing the reaction temperature increases the amount of secondary reactions in the gaseous phase, this promotes the conversion of oxygenated tar compounds to light hydrocarbons, oxygenates and aromatics with can later form larger polycyclic aromatic hydrocarbons (PAH) and higher hydrocarbons (Li and Suzuki, 2009). A scheme for tar formation was described by Elliott (1988) in Figure 2.23.

Mixed Oxygenate 400 °C	Phenolic Ethers 500 °C	Alkyl Phenolics 600 °C	Heterocyclic Esters 700 °C	PAH 800 °C	Larger PAH 900 °C
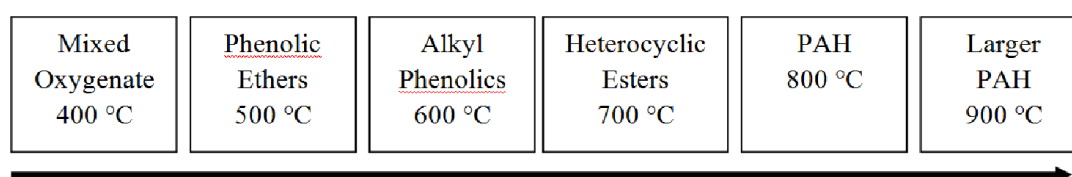
Figure 2.23 – Tar formation scheme (Elliott, 1988)

Figure 2.23 indicates how increasing the operational temperature affects the formation of different tars. At lower temperature the primary tar products are mixed oxygenates, and larger PAH are more likely at temperatures nearing 1000°C. Increasing the temperature prompts more secondary reactions in the gas phase thus larger tar molecules are formed. In another study into the characterisation of tars from gasification by Baker et al., (1988) it was concluded that tar yields are highest when biomass is gasified in a fixed bed updraft gasifier, this is due to the formed tar not passing through a hot zone in the reactor. In fixed bed downdraft gasifiers the product gases go through a hot zone, roughly 900°C, thus reducing the tar yield. In fluidised bed gasifiers the tar yield depends on the temperature of the bed and the utilised gas. Figure 2.24 indicates how the tar yield is effected by the maximum temperature gases are subjected to.
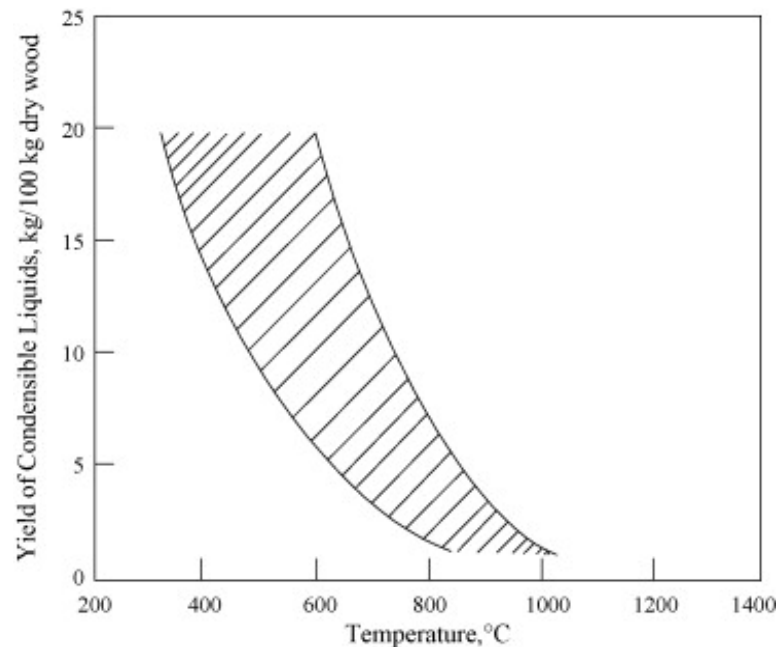
Figure 2.24 – Yield of tar vs. maximum temperature (Baker et al., 1988)

Evans and Milne, (1987) summarised the pathways in which species are formed when biomass is pyrolysed in both high and low pressure systems. The direct production of liquids requires pressure higher than atmospheric. Figure 2.25 shows how the products from pyrolysis are distributed across the different phases and are a function of certain process variables including; pressure, time, temperature and oxygen level.
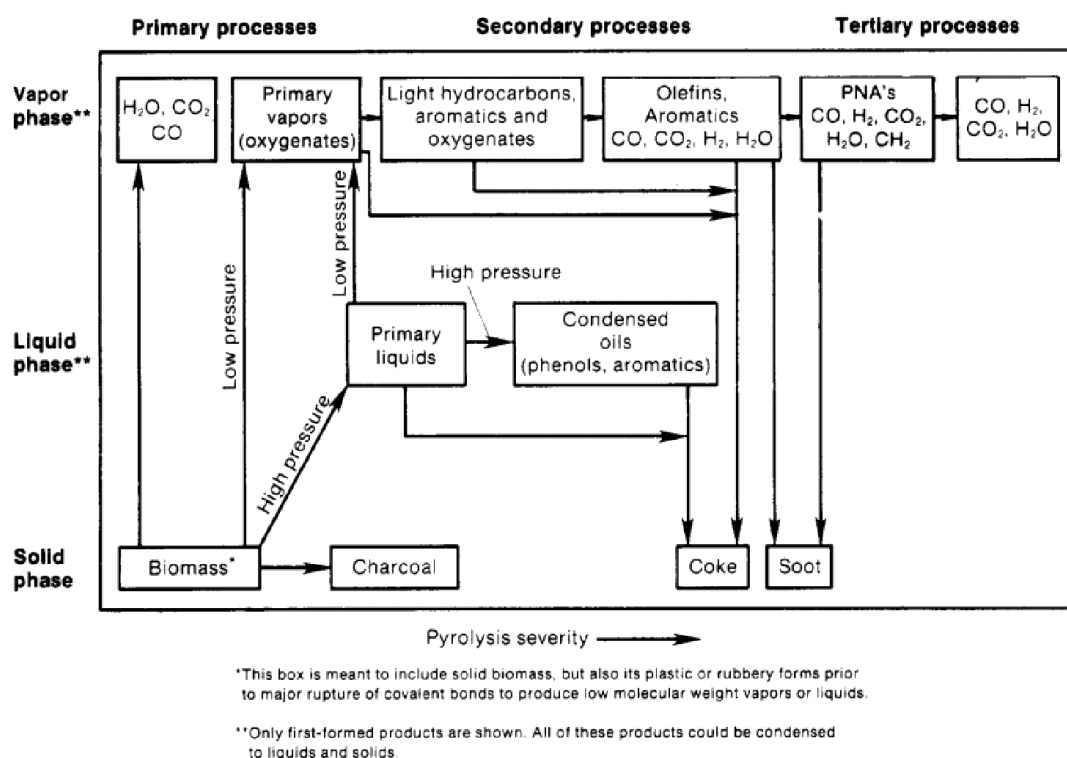
Figure 2.25 – Pyrolysis pathways (Evans and Milne, 1987)

2.4.3 Tar Classification

Tars can be divided into different classes depending on their molecular weight. There are five classes which are shown in Table 2.6.

Tar Class	Class Name	Properties	Compounds
1	GC-undetectable	Very heavy tars	Determined by subtracting GC-detectable tar fraction from the total gravimetric tar
2	Heterocyclic aromatics	Tars containing hetero atoms; highly soluble in water	Phenol, pyridine, cresols, quinoline
3	Light aromatics (1 ring)	Light hydrocarbons with single rings	Toluene, xylenes, styrene
4	Light PAH compounds	2 and 3 rings, condense at low temperature	Indene, naphthalene, biphenyl, fluorene, phenanthrene
5	Heavy PAH compounds	3 rings or larger, condense at high temperatures at low concentrations	Fluoranthene, pyrene, chrysene, perylene, coronene

Table 2.6 – Tar classes and compounds (Li and Suzuki, 2009; Zwart, 2009)

Tars foul once the product gas becomes over saturated causing deposits inside downstream process equipment. If tar is in its gas phase then there will be no fouling therefore it is thought that it is the composition of the tar rather than the quantity that causes fouling problems

(Bergman et al., 2002). Over saturation in the product occurs when the tar vapour pressure surpasses the pressure of the tar which ultimately leads to the tars condensing (Bergman et al., 2002; Li and Suzuki, 2009). The dewpoint of the tar is the temperature when the total partial pressure and saturation pressure of tar are equal. Knowing the tar dewpoint plays an integral role in evaluating the success of cleaning systems. It is expected that fouling issues relating to condensation and aerosol formation can be solved by reducing the tar dewpoint to below the lowest expected temperature (Bergman et al., 2002).

Using condensation curves for the individual tar classes described in Table 2.6 the dewpoint of the corresponding tars at different concentrations are shown in Figure 2.26. Class 1 is not included as its components are unknown.
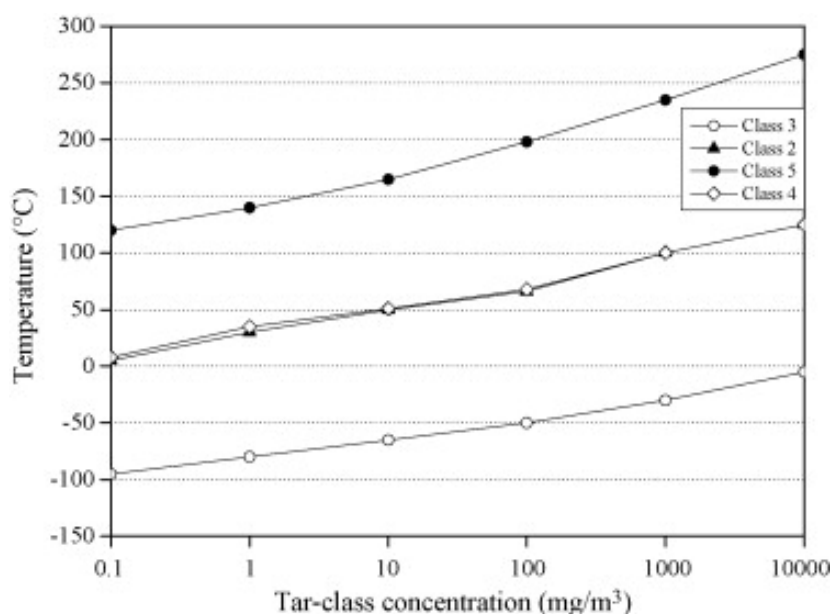
Figure 2.26 – The tar dewpoint of the different tar classes in relation to their concentration (Li and Suzuki, 2009)

Figure 2.26 indicates that the tars in *class 5* play a dominant role in the dewpoint of tar, at low concentrations (< 1 mg/m^3) a dew point below 100°C cannot be achieved. Tars in class 3 play an unimportant role in tar fouling problems due to sub minus temperatures at which they would foul even at large concentrations (>1000 mg/m^3).

An alternative tar classification system was developed by (Milne et al., 1998). In this approach tars are classed as primary, secondary or tertiary as a result of research performed on thermal cracking reactions in the gas phase. Primary tars are characterised by cellulose derived products (levoglucosan and furfurals), lignen derived methoxyphenols and analogous hemicellulose derived products. Phenolic and olefins are typically representing secondary tars. Tertiary tars are distributed into two further classes; alkyl tertiary products which include

methyl derivatives of aromatics (toluene, indene and methylnapthalene) and condensed tertiary products (benzene, naphthalene and pyrene).

2.4.4 Primary Tar Removal Methods

Tar removal methods can be split into two sections: primary and secondary methods. Primary methods are used internally within gasifiers to prevent tar formation or convert tar into useful products. In theory primary methods should eliminate the requirement for secondary methods. Devi et al., (2003) evaluated three primary issues that require almost complete optimisation of the gasifier; (1) operating conditions, (2) using additives or internal catalysts and (3) gasifier design. The goal of primary methods is to optimise the performance of the gasifier so that the quality of the gas produced is of the highest standard, thus removing the requirement for secondary measures. The majority of primary tar removal methods have yet to be utilised commercially and the functionality is not fully understood (Devi et al., 2003).

Gasification conditions play an important role in gasification performance with respect to the composition of the product gas, the carbon conversion of the biomass material and tar formation and destruction. The key parameters are the temperature, pressure, residence times, equivalence ratio, the use of catalysts or additives and the gasifying agent used. The design and configuration of the selected gasifier affects the choice and the effectiveness of these parameters.

2.4.5 Secondary Tar Removal Methods

Secondary methods treat the hot product gas chemically or physically. Physical methods include methods such as cyclones, filters (fabric, ceramic and electrostatic) and scrubbers. Chemical methods crack tar thermally or with a catalyst. Secondary methods are often expensive, not completely effective or shift the tar removal to wastewater utilised in the procedure.

Bergman et al., (2002) suggests that primary methods have the capability of reducing tar formation in gasifiers but for complete removal secondary functions are required. Primary measures also create disadvantages due to limits in scaling up equipment, flexibility in the feedstock and complex gasifier construction. However such disadvantages can be counteracted by the reduction or complete removal of expensive gas clean up systems (Bergman et al., 2002). The relationship between primary and secondary methods is outlined in Figure 2.27.
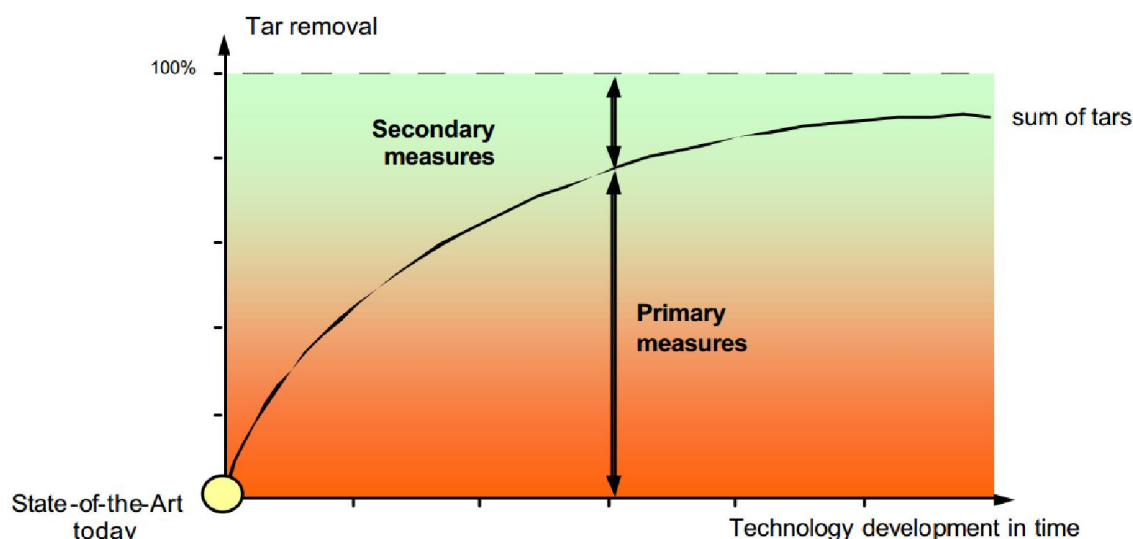
Figure 2.27 – Illustration of the relationship between primary and secondary tar removal methods against technology development in time (Bergman et al., 2002)

Han and Kim (2008) divided tar removal technologies into five broad groups; mechanical methods, catalytic crackers, thermal crackers, plasma methods and finally self-modification by selecting optimum conditions.

2.4.6 Mechanical/Physical Methods

The main goal of using mechanical methods is to capture and remove tars and particulates from product gases. Such devices include scrubbers, cyclones, filters and electrostatic precipitators. Milne et al. (1998) separated the physical removal of tar into two categories, wet and dry technologies. Wet methods are normally used at temperatures between 20-60°C, after the gases have been cooled. Dry methods can be used prior to cooling at temperatures greater than 500°C or after cooling at gas temperatures below 200°C (Anis and Zainal, 2011). The cleaning systems for both wet and dry types are shown in Table 2.7.

Tar Removal Type	Equipment
Dry	Cyclone, electrostatic precipitators (ESP), baffle filters, bag filters, ceramic filters, fabric filters, sand bed filters, rotating particle separators (RPS)
Wet	Packed column scrubber (wash tower), venturi scrubbers, wet electrostatic precipitators, wet cyclones, spray towers.

Table 2.7 – Wet and dry mechanical/physical gas cleaning systems (Anis and Zainal, 2011)

Wet gas cleaning systems have a key shortcoming in that all the systems generate wastewater. The wastewater is contaminated by organic and inorganic pollutants so the tar problem is exchanged from the gaseous phase to another phase which then has to be properly disposed at considerable cost (Milne et al., 1998).

In a comprehensive study by Hasler and Nussbaumer, (1999) the effectiveness of a number of different types of physical tar reduction methods were appraised, outlined in Table 2.8.

Tar Removal Equipment	Temperature (°C)	Tar Reduction (%)	Particle Reduction (%)
Sand bed filter	10-20	50-97	70-99
Wash tower	50-60	10-25	60-98
Venturi scrubber	n/a	50-90	n/a
Wet electrostatic precicpitator	40-50	0-60	>99
Fabric filter	130	0-50	70-95
Rotational particle separator	130	30-70	85-90
Fixed bed tar adsorber	80	50	n/a

Table 2.8 – Comparison of physical reduction methods (Hasler and Nussbaumer, 1999)

2.4.7 Catalytic Cracking

Sutton et al. (2001) summarised the main features and criteria needed for a successful catalyst used to reduce tar from biomass gasification. The seven requirements are as follows;

1. The catalyst must be effective at removing tars.

2. If syngas is the desired product the catalyst must be able to reform methane.

3. A suitable syngas ratio should be provided.

4. The catalyst should be strong enough for the process.

5. The catalyst should be inexpensive.

6. Regeneration of the catalyst should be easy.

7. The catalysts should be resistant to deactivation if sintering and carbon fouling are apparent.

Catalysts used for tar removal can be classified into six categories; (1) nickel based, (2) non-nickel metal, (3) alkali metal, (4) basic, (5) acid and (6) activated carbon (Anis and Zainal, 2011). One advantage of using catalysts instead of thermal methods is that catalysts operate at a lower temperature (600 – 800°C) when compared with using thermal cracking methods (above 1000°C) (Zhang et al., 2004). This reduces the requirement for expensive alloys needed for thermal cracking reactors. Using a catalyst destroys tar solving disposal problems which are apparent in mechanical/physical methods where the tar is merely removed from the

gas stream where it is then disposed of. Xu et al, (2010) summarised typical catalysts, their tar cracking performance and their operational temperature.

Catalysts	Chemical Composition	Temperature (°C)	Feed Gas Origins	Tar Conversion
Various Dolomites	18-21 mass.% MgO 30-32 mass.% CaO 0-3 mass.% SiO_2 0-0.8 mass.% Fe_2O_2 0-1 mass.% Al_2O_3	795 - 925	Product gas from air-blown gasifiers	70 – 96%
Chinese Dolomite	20 mass.% MgO 31 mass.% CaO 0.7 mass.% SiO_2 0.5 mass.% Al_2O_3	650 - 850	Nitrogen bubbled through melted biomass tar	43 - 95
ICI-46-1*	24 mass.% NiO 13 mass.% MgO 13 mass.% CaO 14 mass.% SiO_2 29 mass.% Al_2O_3	n/a	Nitrogen bubbled through melted biomass tar	87 - 99

Table 2.9 – Catalysts used for decomposition/reforming of biomass tar (Adapted from Xu et al., 2010)

Ni-supported commercial steam reforming catalyst

The tar cracking mechanism involved in tar cracking can be explained and illustrated as follows: Firstly the tar molecule absorbs on the catalyst surface forming radicals and immediate compounds which can be active or inert. Oxygen, carbon dioxide and water vapour are also absorbed on the surface and dissociate into carbon monoxide and free radicals of oxygen, hydroxide and hydrogen, this is followed by the desorption of the free radicals. The free radicals then react to form methane, carbon dioxide, hydrogen and small amounts of benzene (Xu et al., 2010). Figure 2.28 illustrates the mechanism.
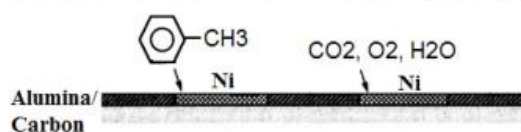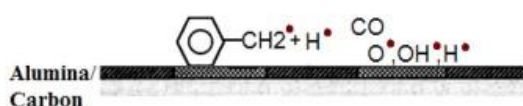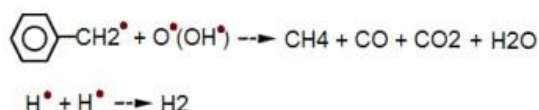
Figure 2.28 – Illustration of tar (toluene) cracking (Xu et al., 2010)

Catalytic conversion of tars can be enhanced by adding oxygen and/or steam. Steam promotes the water/gas shift reaction thus the concentration of hydrogen and carbon dioxide are increased whereas carbon monoxide formation is reduced. When oxygen is added at temperatures between 600 - 700°C the destruction of primary products is accelerated and aromatic formation is prevented (Zhang et al., 2004).

Nickel based catalysts can be used for both tar reduction and ammonia removal in both tar and coal gasification system (Anis and Zainal, 2011). Nickel based tars can remove almost all of the tar in the product gas but deposits of coke cause gradual deactivation. Nickel based catalysts usually have three components. A nickel element is the active site, a promoter increases stability and/or activity, finally a support gives coking resistance and a high surface area.

2.4.8 Thermal Cracking and Partial Oxidation

The thermal cracking of tar refers to heating the tar at certain temperatures and residence times so that the tar is converted into lighter gases (Anis and Zainal, 2011). Bridgwater, (1995) suggests that there are three suitable key areas in which tars can be cracked: increasing residence times, contacting tars with an independently heated surface or by adding oxygen to partially oxidise tars. By thermally decomposing tars not only is the tar quantity in the final gas product minimised but the yield of producer gas is increased as tars are converted into smaller molecular products. The temperature at which tars are cracked is reported to be between 700 and 1250°C (Anis and Zainal, 2011).

One study was performed by Fassinou et al. (2009) into the thermal cracking of tar in the pyrolysis stage of a two stage gasifier and specifically how the temperature, residence time and flow rate of biomass affect the cracking of tars throughout this stage. The biomass used was pinus pinaster which is a maritime pine which grows in conditions around the Mediterranean Sea. The equipment used for pyrolysis is shown in Figure 2.29.
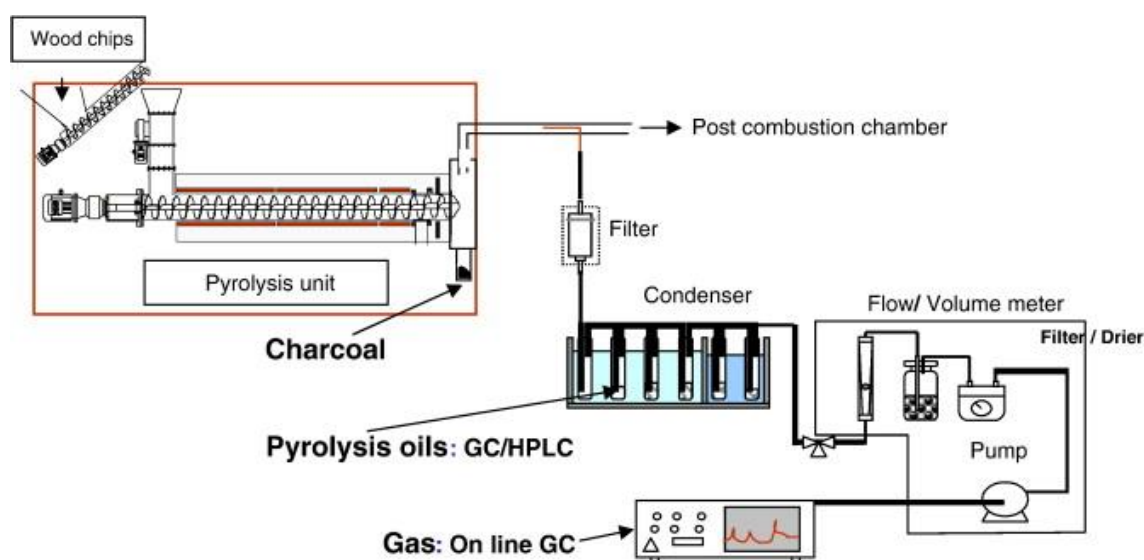
Figure 2.29 – Experimental setup (Fassinou et al., 2009)

Wood chips are fed into the pyrolysis unit and heated by a series of heating units. A screw feeder carries the wood chips through the pyrolysis unit at a set speed. Samples of the product gas are taken continuously. The non-condensable fractions are analysed by a gas chromatograph. Liquid and char samples are collected, measured and analysed.

Results from research by Fassinou et al. (2009) showed that increasing the temperature increased the yield of gas produced and decreased the char and liquid fraction. Table 2.10 highlights how the temperature affects the yield of gas, liquid and char.

Temperature (°C)	Biomass Flow rate (kg/h) – Residence Time (min)								
	15 – 15			15 - 30			15 - 60		
	Char (mass. %)	Liquid (mass. %)	Gas (mass. %)	Char (mass. %)	Liquid (mass. %)	Gas (mass. %)	Char (mass. %)	Liquid (mass. %)	Gas (mass. %)
450	35.30	50.34	14.36	30.55	51.28	18.17	32.56	45.82	21.62
550	23.46	51.63	24.91	26.22	50.56	23.22	-	-	-
650	18.77	43.80	37.43	19.76	42.32	37.93	-	-	-
750	16.77	30.38	52.85	17.87	22.91	59.22	20.35	31.73	47.92

Table 2.10 – Yield of pyrolysis products (Fassinou et al., 2009)

The gases formed during pyrolysis are low molecular weight hydrocarbons, hydrogen, carbon monoxide, carbon dioxide and methane. In this study by Fassinou et al. (2009) it was shown that increasing the temperature at which the wood chips were pyrolysed increased the yield of hydrogen, carbon monoxide, carbon dioxide and methane, see Table 2.11.

Temperature (°C)	Biomass Flow rate (kg/h) – Residence Time (min)					
	10 - 30					
	H_2	CO	CH_4	CO_2	C_2H_4	C_2H_6
450	0.31	54.74	7.15	82.21	0.90	1.39
550	1.93	115.41	20.15	96.12	2.85	4.68
650	650	203.27	43.07	132.15	9.32	10.38
750	750	245.33	62.51	172.09	13.31	6.58

Table 2.11 – Gas production (kg of gas/kg of pine wood chips)*10^3 (Fassinou et al., 2009)

In summary results from Fassinou et al. (2009) show that by increasing the temperature at which wood undergoes pyrolysis there is an increase into the amount of useful gases that are produced. Pyrolysing at higher temperatures 650 and 750°C promotes the production of stable heavy tars, group 3 and 4 in the tar classification (Table 2.6) whereas the lower temperatures causes the formation of tars in class 1 and 2.

Houben et al. (2005) performed a study into reducing tars through partial combustion of product gases. One of the key questions regarding tars is whether they expire through polymerisation or by thermal cracking. If tars are polymerised they form into soot which can potentially be removed by a filter. However the preferred method is to crack the tar into smaller more useful molecules. Houben et al. (2005) choose to use naphthalene as a model for the tar component. This was chosen as it is less harmful when compared with other tars, such as benzene, which can be carcinogenic. Naphthalene is a two ringed aromatic hydrocarbon so it would be able to show whether its removal is through cracking or polymerisation.

Figure 2.30 shows the experimental setup of the design. Naphthalene is saturated in nitrogen gas in a saturator which is set at a steady state temperature of 200°C. The nitrogen/naphthalene is mixed with a fuel gas mixture, the flow of which is controlled by flow meters. The fuel gas has the following composition; H_2: 22.4%, CH_4: 5%, N_2: 72.6%. After leaving the mixing unit the gases are fed into a burner where primary air is added. The fuel and tar mixture enters the burner through the central channel; air enters through two outer channels (Figure 2.31) and is injected into the inner part of the burner through one of seven nozzles. This causes a cross flow which creates swirling jets which generates a uniform distribution of air as well as a number of recirculation zones at the edges of the walls.

Figure 2.30 – Schematic diagram of equipment (Houben et al., 2005)

Figure 2.31 – Burner design (Houben et al., 2005)

Houben et al. (2005) determined that with respect to reducing the concentration of tar there is an optimum at which oxygen should be added. Having no or too much oxygen leads to the formation of soot and polyaromatic hydrocarbons. It was found that using low primary rates of air ($\lambda = 0.2$) in the partial combustion system over 90% of the total tar content could be

reduced. λ is defined in equation 2.10, where *exp* is the experimental conditions and *stoi* is flow ratio in the stoichiometric case.

$$\lambda \equiv \frac{\dot{m}_{fuel}}{\dot{m}_{air}}\bigg|_{exp}\frac{\dot{m}_{air}}{\dot{m}_{fuel}}\bigg|_{stoi}$$

(Eqn 2.10)

Su et al., (2011) developed a continuous reactor where tar was removed in a partial oxidation environment. The experiment was setup in two parts. The first was a pyrolysis unit where briquetted rice straw was supplied through the reactor and pyrolysed at 500°C. The second unit was a tube reactor which was heated at temperatures up to 1500°C. The temperature of the tube reactor used in the experiments was 900°C. Before the tube reactor an air mixer was installed so that the gaseous pyrolysis products could be mixed with air. The experimental setup is shown in Figure 2.32 where; *A: carrier gas, B: emergency flush, C: hopper, D: screw conveyor, E: ash bin, F: gas pre-mixer, G: tube reactor, J and K: gas sampling ports.*
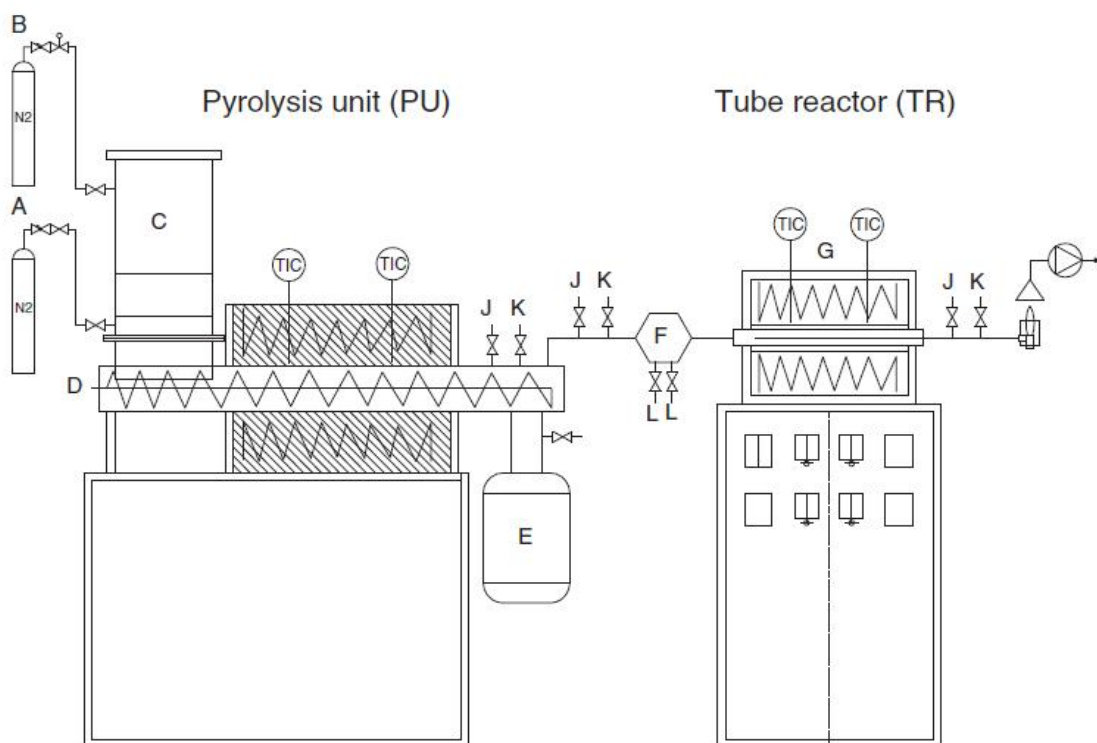
Figure 2.32 – Experimental apparatus (Su et al., 2011)

The gas composition was continuously measured and the produced gas was cleaned using a combined tar and gas sampling system. Tar was collected in a series of impinger bottles and analysed using a GCMS. Air was supplied at a range of equivalence ratios which were calculated using equation 2.11.

$$ER = \frac{V_{real}(Nm^3/kg)}{V_{theory}(Nm^3/kg)} \times 100\%$$

(Eqn. 2.11)

Where V_{theory} is the oxygen volume required for the complete oxidation of 1 kg of the biomass feed stock and V_{real} is the volume that was consumed in the partial oxidation regime. Su et al., (2011) showed how increasing the equivalence ratio from 0 (thermal cracking) to 0.34 reduced the level of total tar production. In the thermal regime where no air was added the mass yield of gravimetric tar was 10.15% of the original biomass stock this reduced to 0.26% for the increased equivalence ratio. An equivalence ratio of 0.34 was suggested by the author to be a crucial point at which the tar and soot levels are reduced to minimum values of 0.26% and 4.07% respectively and gas levels of carbon monoxide, hydrogen and methane increase to their maximum levels.

2.5 The Coandă Effect

2.5.1 Historical Background

The Coandă effect was one of the principal discoveries of Henri Coandă, a Romanian inventor who designed and built the first jet powered aircraft in the early 1900's (Circiu and Dinea, 2010). The phenomenon works by creating a depression zone in air along a wall which allows for the fluid to project itself forward along the direction of the wall (Circiu and Dinea, 2010).

The first patents that related to the Coandă effect were to generate a fluid jet over the upper surface of a fuselage. Henri Coandă obtained a patent in 1935 which suggested using the effect as a centrifugal fan to supply air. The Coandă effect has been utilised in the aviation industry for controlling wing flow on planes, for example on the original Boeing 387-80 which uses flaps driven by the effect (Circiu and Dinea, 2010).

The Coandă effect is also used for ejectors; for such applications as the moving of gases and air, because Coandă ejectors have no moving parts their performance is reliable, therefore they are used to eject toxic gases without the risk of the ejection unit becoming faulty. Further applications for Coandă ejectors include removing suspended solids. Finally the Coandă effect has been utilised in a number of unmanned aerial vehicles (Circiu and Dinea, 2010).

2.5.2 Theoretical Features

The Coandă effect can be described as a phenomenon in which a jet blown over a surface, that has a convex curvature, adheres to the surface (Gregory-Smith and Gilchrist, 1987). There are

three main features of the effect that have been identified by (Gregory-Smith and Gilchrist, 1987)

1. "an inviscid effect whereby a curved flow will remain attached to a curved surface"

2. "a viscous effect whereby a jet placed close to a curved surface will tend to be drawn towards the surface because of the low pressure created by the jet entrainment"

3. "the higher entrainment by a curved wall jet compared with a plane wall jet; this is caused by the destabilising effect of the curvature on the turbulence in the outer part of the jet"

2.5.3 Coandă Flares

Coandă flares are used in the petroleum industry to burn off waste gases. A Coandă flare works by having a high pressure combustible gas enter through a slot at the bottom of a axisymmetric tulip shaped mass (see Figure 2.33) (Gregory-Smith and Gilchrist, 1987). The jet from the slot adheres to the curved surface entraining the surrounding ambient air at a high rate which promotes mixing and effective combustion resulting in low smoke pollution and low radiation (Gregory-Smith and Gilchrist, 1987).

Combustion is normally commenced at the top of the flare body so that the gaseous flow at the base of the unit is not affected by combustion (Morrison and Gregory-Smith, 1984). At the base of the Coandă flare there is divergence, in such that gas flows radially outwards. The divergence reduces as the flow goes around the curved surface until there is finally convergence towards the top part of the flare where the mass becomes conical (Morrison and Gregory-Smith, 1984).
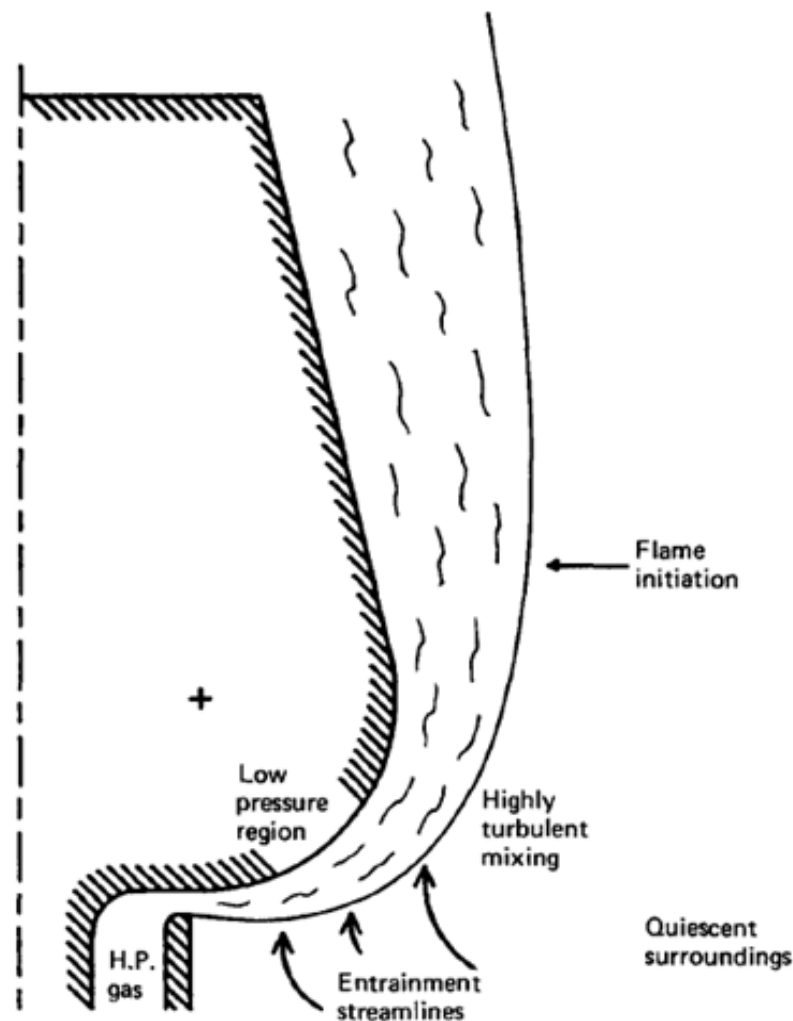
Figure 2.33 – Coandă flare (Gregory-Smith and Gilchrist, 1987)

2.5.4 Coandă Ejectors

A Coandă ejector utilises the primary flow from a high pressure reservoir which enters the main body of the unit through a slit. As the flow enters the ejector it follows the curved walls. The primary flow creates a mixing zone at the outlet due to its high velocity and expansion (Kim et al., 2006). Primary flow mixes turbulently with surrounding ambient air at the ejector inlet transferring the momentum from the primary flow to the stagnant air thus inducing 'secondary flow'. This induced secondary flow is dragged along the ejector by viscous effects as well as the turbulent shear stress, during this both flows are mixed due to the high turbulence in the ejector (Kim et al., 2006). Coandă ejectors are designed to create a high ratio of rate of induced mass flow to the rate of primary flow. There are a number of parameters that can be changed in the Coandă ejector. For example if the inlet nozzle for primary air is widened there will be an increase in the average velocity in the ejector thus resulting in an increase in the flow rate of induced air (Kim et al., 2006). A typical schematic of a Coandă ejector is shown below in Figure 2.34.
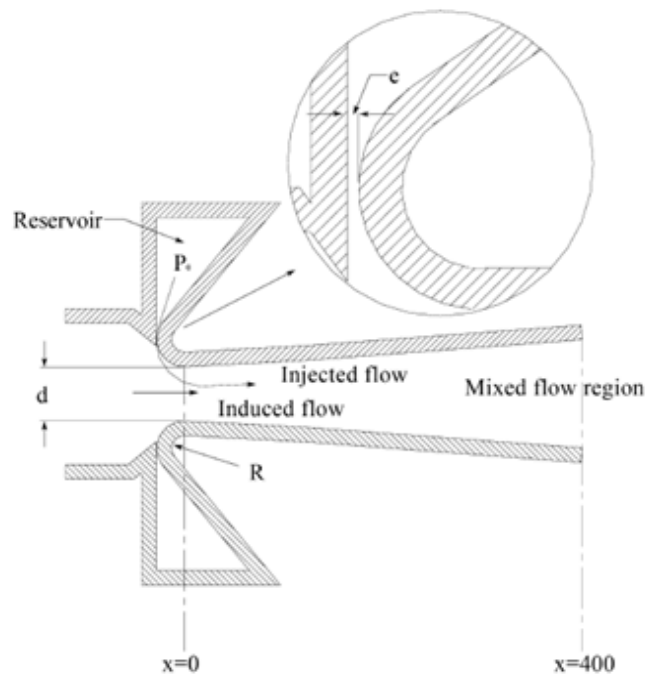
Figure 2.34 – Typical schematic of a Coandă ejector (Kim et al., 2006).

2.5.5 Coandă Burners

As discussed Coandă ejectors allow for surrounding air or flow to become entrained as primary air is injected radially into the ejector. Coandă ejectors do not entrain more induced flow when compared with a well-designed burner that inducts primary flow in the axial direction however the mixing potential in a Coandă ejector is greater due to the increased contact between the primary and secondary flow in the initial contact area (O'Nions, 1997). This allows for the possibility for Coandă ejectors to be modified so that they become efficient burners.

O'Nions, (1997) developed a low NOx burner using the Coandă effect with a maximum thermal rating of 30kW. Propane was the gaseous fuel used in the burner design. Four design parameters were assumed to be variables; air mass flow for combustion, air supply pressure, Coandă gap area and Coandă gap width. O'Nions, (1997) built an experimental rig with the aim to develop a burner to emit low concentrations of NOx and CO. Being able to easily modify the burner allowed for certain design parameters to be changed to determine how these affect the performance. The burner was designed so that it could be separated into five parts; the Coandă ejector, the fuel injection system, the ignition system, the outer casing and diffusing section. Figure 2.35 shows a diagram of the Coandă burner and its parts.
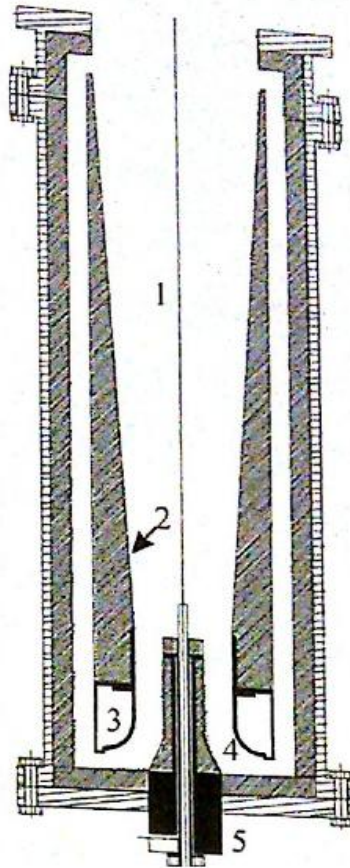
Figure 2.35 – Coandă burner diagram (O'Nions, 1997)

1. Combustion chamber 2. Diffusing section 3. Coandă ejector cavity   4. Coandă surface 5. Fuel injector

The burner was able to operate at near stoichiometric conditions and achieve low NOx emissions and flame stability. NOx emissions were found to be lowest (16 ppm) when the Coandă gap width was 0.2 mm and the air to fuel ratio was 1.5. At an air fuel ratio of 1.1 NOx emissions were found to be 23 ppm.

A similar Coandă burner was developed by the John Zink Company LLC. The burner was designed for use in a cracking furnace and was designed to meet certain considerations and challenges that exist when designing such burners (Poe et al., 2007). These considerations include; controlling the heat flux distribution from the burner to the process tubes, having burners that operate at a wide turndown range, improving the flame quality with regards to shape and size and improve emissions performance. The key emissions that are intended to be reduced are NO_x and CO (Poe et al., 2007).

The designed burner used the Coandă principle for mixing, controlling fluid flow and stability. The tile shape of the burner has both inner and outer Coandă devices integrated into its design to improve mixing and stability.

54
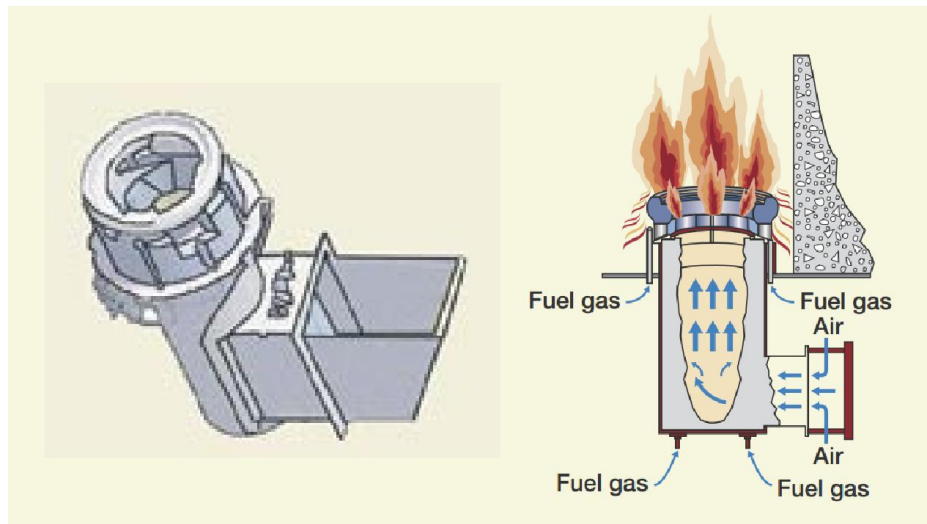
Figure 2.36 – Process schematic of the designed burner (Poe et al., 2007)

2.6 Summary of Literature Review

The application of small-scale biomass gasification systems for electricity and power generation could play an important role in the green economy, and provide a solution to global climate issues and energy supply. The main problem hampering the installation and commercial success of such projects is the formation of tar. The presence of tar in the producer gas is the main cause of damage to downstream equipment which prevents, and limits, long-term operation of biomass gasifiers. Small-scale installations do not benefit from heavy investment which effectively rules out the utilisation of expensive gas clean-up equipment such as scrubbers and catalysts, which can be commercially viable in large-scale processes. Primary tar measures, to improve the operation and functionality of the gasifier, can severely reduce the tar content in the producer meaning that secondary measures are not required, thus decreasing investment and operational costs.

Partial combustion of the tarry gas, produced from the pyrolysis stage of gasification, could be used to destroy the contained tars by converting them to smaller permanent species. Burners that can operate at sub-stoichiometric conditions are ideal and could provide a cost effective and permanent solution to the tar problem. Coandă burners have been proven to operate at high temperature, blue flame conditions at close to stoichiometric conditions therefore making them an interesting candidate for further investigation presented in this thesis.

3. Theoretical Background

This section of the thesis examines the chemical mechanisms involved when tar species are treated by thermal cracking and partial oxidation. The mechanisms and chemistry of tar conversion when tars are converted through partial combustion are not completely understood, although there has been an increase in the research carried out in this area in recent years. The complex composition of tar makes the process of generating a kinetic model difficult, added to this are the numerous parameters (temperature, pressure and reactor design) which affect tar formation and destruction in biomass thermal conversion systems furthers the complications. The majority of research concentrates on the mechanism for key tar species: benzene, toluene, phenol and naphthalene, are most commonly examined. In section 3.1 thermal tar treatment is discussed; looking specifically at the mentioned key tar species. In section 3.2 oxidative tar treatment is examined.

3.1 Thermal Tar Conversion

Tars produced from biomass can be broken down or cracked at high temperatures. The thermal treatment of tar refers to the conversion and breakdown at temperatures above 1000°C and at certain residence times (van der Hoeven, 2007). In a review paper by Anis and Zainal (2011) the tar cracking temperature range was concluded to be between 700 and 1250°C. It was shown by Miura et al. (2003) that increasing the temperature at which tar is treated leads to an increase in tar conversion. There are two types of products when tars are thermally converted; organic cracking products and species formed through polymerisation, which later form into 'soot'. There is a linear relationship between the amount of cracked and polymerisation products produced and the amount of tar converted into such products (van der Hoeven, 2007).

When tar is pyrolysed in an inert environment both cracked products and polymerised products will form. Formation of polymerisation products is due to tars having a low hydrogen content; thus when tar is cracked it is not possible to produce a smaller cracked product with a high hydrogen content without the formation of long chain hydrocarbons with a lower hydrogen content when compared with the original tar (van der Hoeven, 2007). This can be shown graphically in Figure 3.1. The formation of soot and soot-precursors are affected by the treatment temperature and gas residence times, as these parameters increase: the soot fraction increases and the level of soot pre-cursors decrease.

When tar undergoes cracking the maximum yields of gas and heavy tars depend heavily on the hydrogen content of the tar. The large amount of hydrogen contained within tar causes an

increase in released hydrogen as polymerisation products are formed (van der Hoeven, 2007) causing a higher gas/heavy tar yield ratio, this is referred to as the hydrogen shift see Figure 3.1.
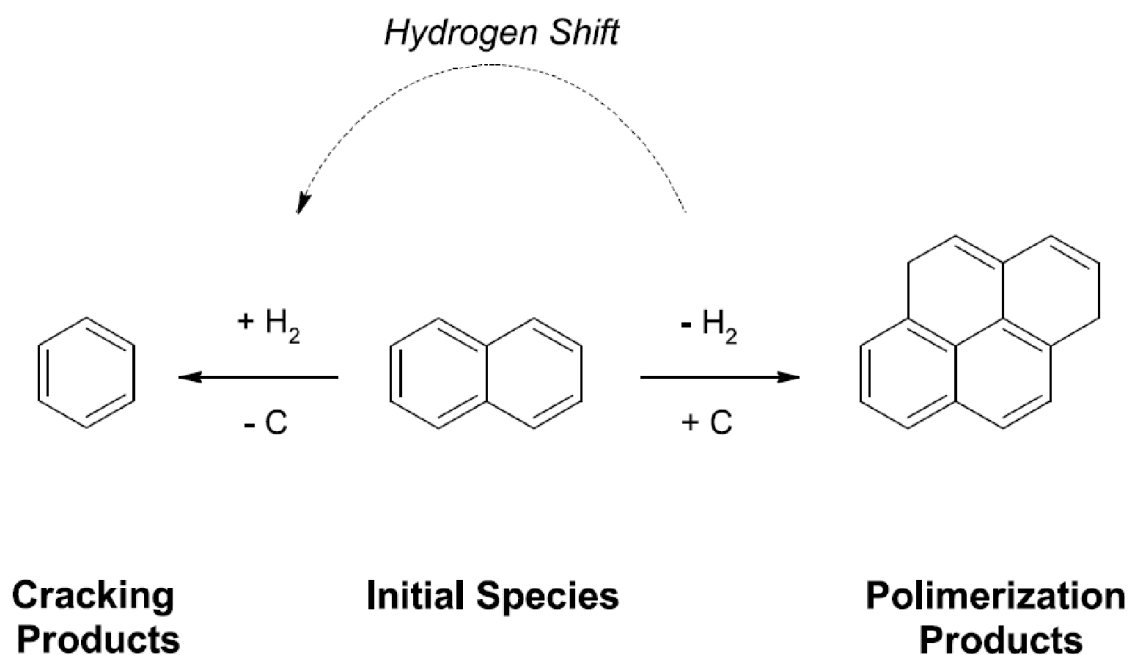
Figure 3.1 – The hydrogen shift in thermal tar conversion causing cracking and polymerisation products (van der Hoeven, 2007)

Cracking products are normally formed when hydrogen is added to aromatic compounds. The addition of hydrogen leads to the breaking of ring structures. Van der Hoeven (2007) states that methane, ethane, ethylene, and benzene are the most important cracking products. Each of these species are produced when they are released as tar species are broken down. These species are normally removed from tar structures in the form of radicals, they are then stabilised with the addition of atomic hydrogen.

Benzene and naphthalene are considered to be two of the key components of tar when biomass is thermally treated either by pyrolysis or gasification. The cracking system for benzene is shown below in Figure 3.2 and for naphthalene in Figure 3.3.
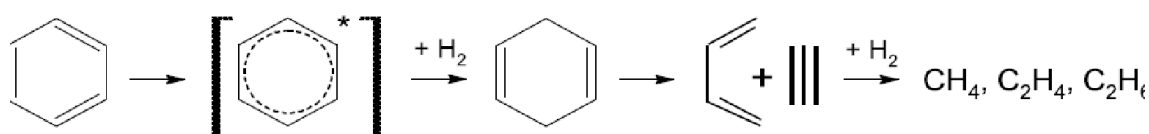
Figure 3.2 – Cracking scheme for benzene (van der Hoeven, 2007)

Figure 3.3 – Cracking scheme for naphthalene (van der Hoeven, 2007)

Both cracking cases show how hydration, the addition of water or one of the elements of water to a species, plays an important role in their destruction. For benzene, the ring is broken and the hydration reaction results in the production of mainly methane, ethane and ethylene (van der Hoeven, 2007). Whilst for naphthalene, the reaction is started with a first hydration step, where naphthalene is converted to dihydronaphthalene, and the continued addition of hydrogen leads to the production of methane, ethylene and finally benzene.

Nair et al. (2004) presented an alternative reaction path for the decomposition of naphthalene, see Figure 3.4. This scheme was proposed when looking into tar removal from biomass fuel gas using pulsed corona discharges. The decomposition scheme was proposed from experimental results, the by-products from the reactions are mainly formed by an oxidation mechanism (Li & Suzuki, 2009).

Figure 3.4 – Naphthalene decomposition scheme (Nair et al., 2004)

Norinaga et al. (2011) performed work into the thermal conversion of aromatic hydrocarbons in the presence of hydrogen and steam. The reaction pathway analysis is shown in Figure 3.5.

Figure 3.5 – Pathway analysis for the thermal conversion of naphthalene in the presence of steam and hydrogen at 1473K and a reaction time of 0.5 seconds (Norinaga et al., 2011)

Figures 3.5 show the key pathways applied when naphthalene is thermally converted at 1473K in the presence of steam and hydrogen. The arrows indicate how the particular compound is likely to be affected, the thicker the arrow the more of that compound is consumed in that direction (Norinaga et al., 2011).

There are two main directions in which naphthalene is converted. In the leftwards direction there is a synthesis reaction creating larger PAH particles. In the rightwards direction there is decomposition of the original particle into smaller species. For the decomposition the first reaction is a substitution with an OH radical forming napthhol which is then converted into to a naphthoxy radical which after the release of carbon monoxide forms a 9-carbon indenyl. Indene formed through this route is subsequently converted to a benzyl radical which can then go through two paths to form either vinylacetylene and a propargyl radical or benzene (Norinaga et al., 2011). In the opposing direction, the reaction between naphthalene and naphthyl radical to form perylene this then forms coronene. Jess (1996) suggested a thermal cracking scheme for naphthalene, shown in Figure 3.6. This scheme points at the formation of polymerisation products through the merging of aromatics as hydrogen is released.
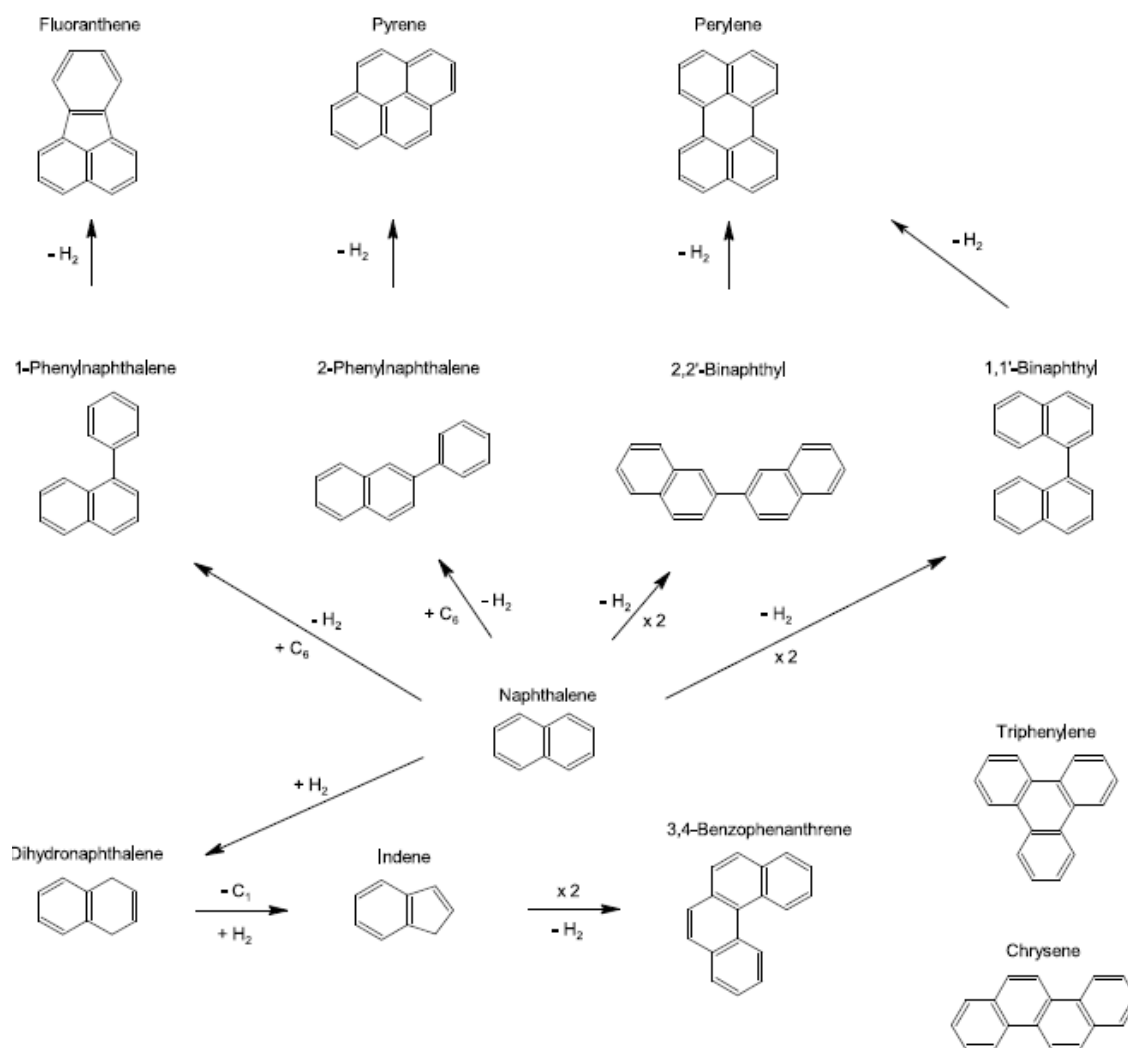
Figure 3.6 – Polymerisation scheme for naphthalene (Jess, 1996)

A reaction path for benzene was also mapped out; see Figure 3.7, using the same conditions as used for naphthalene. 38% of benzene is converted to phenol via either a direct route or indirectly through conversion to a phenoxy radical to cyclopentadiene, also releasing CO (Norinaga et al., 2011). Conversion from benzene to molecules with higher molecular mass are very minor, which is not the case for naphthalene as explained above. The author suggests that 66% of CO is produced through the decomposition of phenol and the majority of CO_2 is produced from CO.
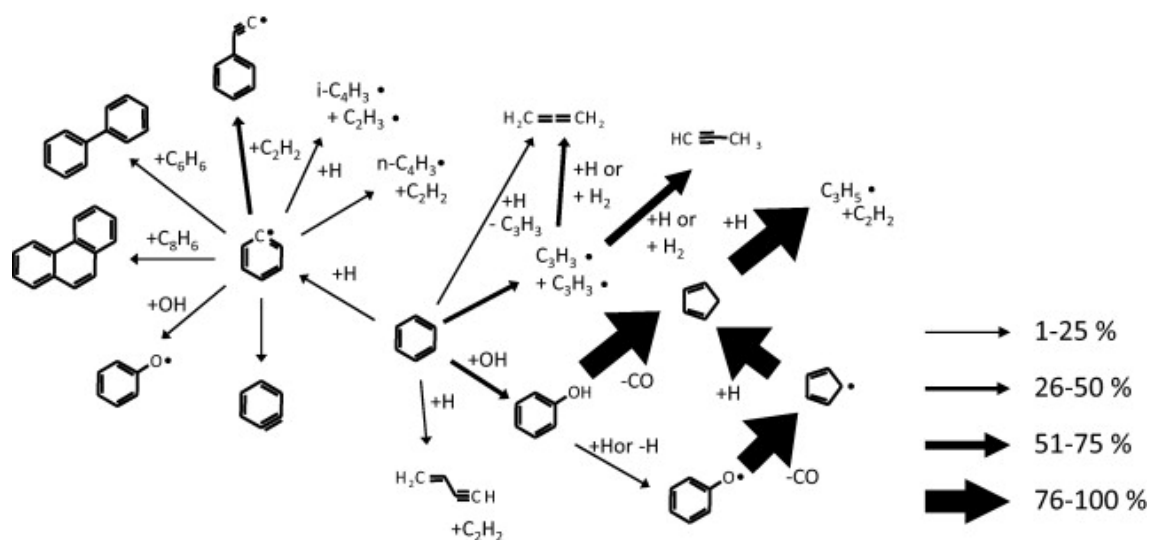
Figure 3.7 – Pathway analysis for the thermal conversion of benzene in the presence of steam and hydrogen at 1473K and a reaction time of 0.5 seconds (Norinaga et al., 2011)

Another possible model scheme in which benzene is polymerised into larger species developed by Jess (1996) is shown in Figure 3.8.
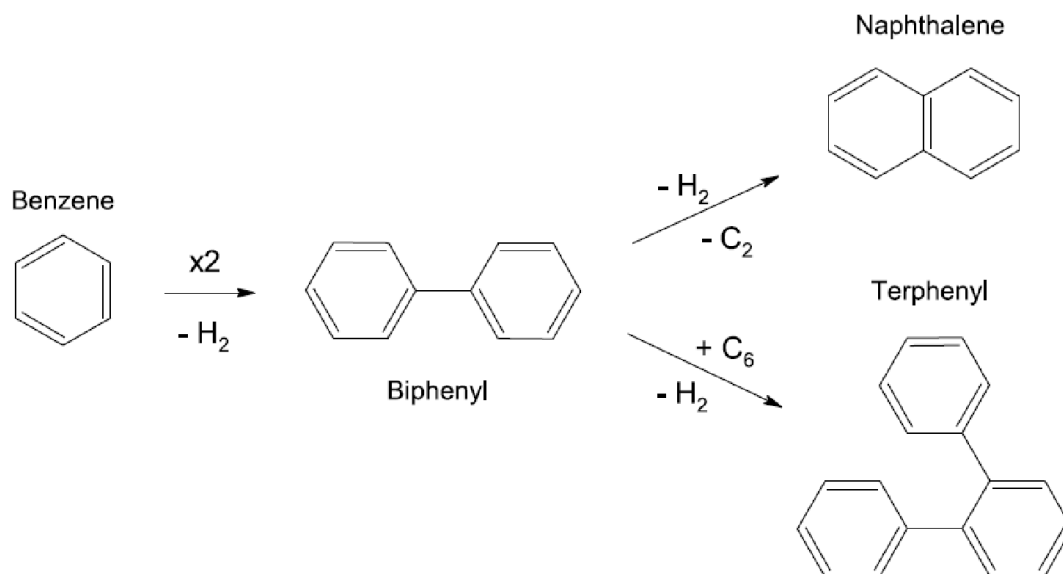
Figure 3.8 – Benzene polymerisation scheme (Jess, 1996)

Alkylated benzenes are the easiest tar molecules to crack due to their low decomposition energy meaning that they can be cracked at temperatures as low as 700°C. Of the tars mentioned in this section the relative thermal reactivity can be ranked as follows; alkylated benzenes > naphthalene > benzene (van der Hoeven, 2007). Jess (1996) found a similar ranking system when testing toluene, benzene and naphthalene conversion in a tubular reactor at various temperatures and in different reaction environments, see Figure 3.9, the residence

times for the experiments was set at 0.5 seconds. Jess (1996) notes that the conversion products for each of the three species are different.

Jess (1996) presented a simplified reaction model for the breakdown of toluene, benzene and naphthalene in the presence of steam and hydrogen, shown in Figure 3.10. It was concluded from this study that benzene is the crucial component in the thermal decomposition of hydrocarbons and soot is primarily formed from the destruction of naphthalene. The temperature for effective thermal conversion of aromatic hydrocarbons was deemed to be around 1200°C at residence times of technical relevance (< 10 s). To convert soot to carbon monoxide and hydrogen higher temperatures of around 1400°C are required.
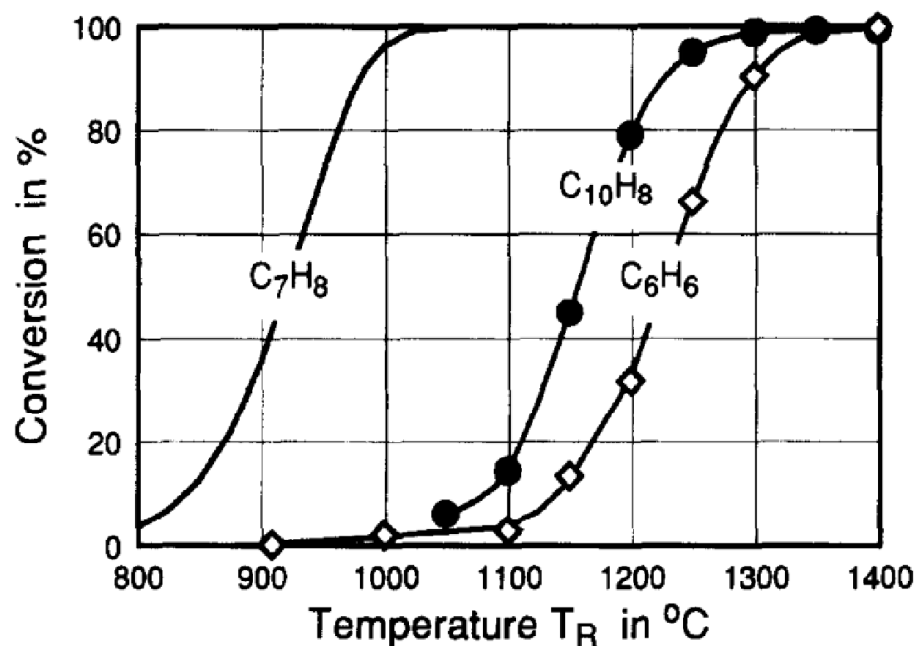
Figure 3.9 – Reactivity of toluene, benzene and naphthalene under thermal conditions (Jess, 1996)
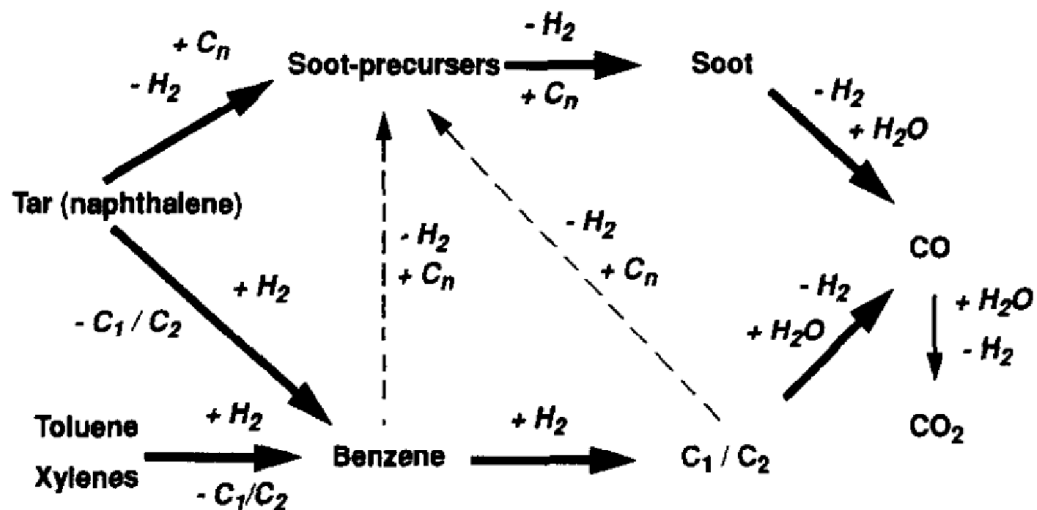
Figure 3.10 – Simplified reaction scheme for the thermal conversion of aromatic hydrocarbon in the presence of hydrogen and steam (Jess, 1996)

The cracking scheme for a simple alkylated benzene, toluene, is shown in Figure 3.11. The main difference between alkylated and non-alkylated aromatics is that the side chains of the tar molecules are transformed first forming products.
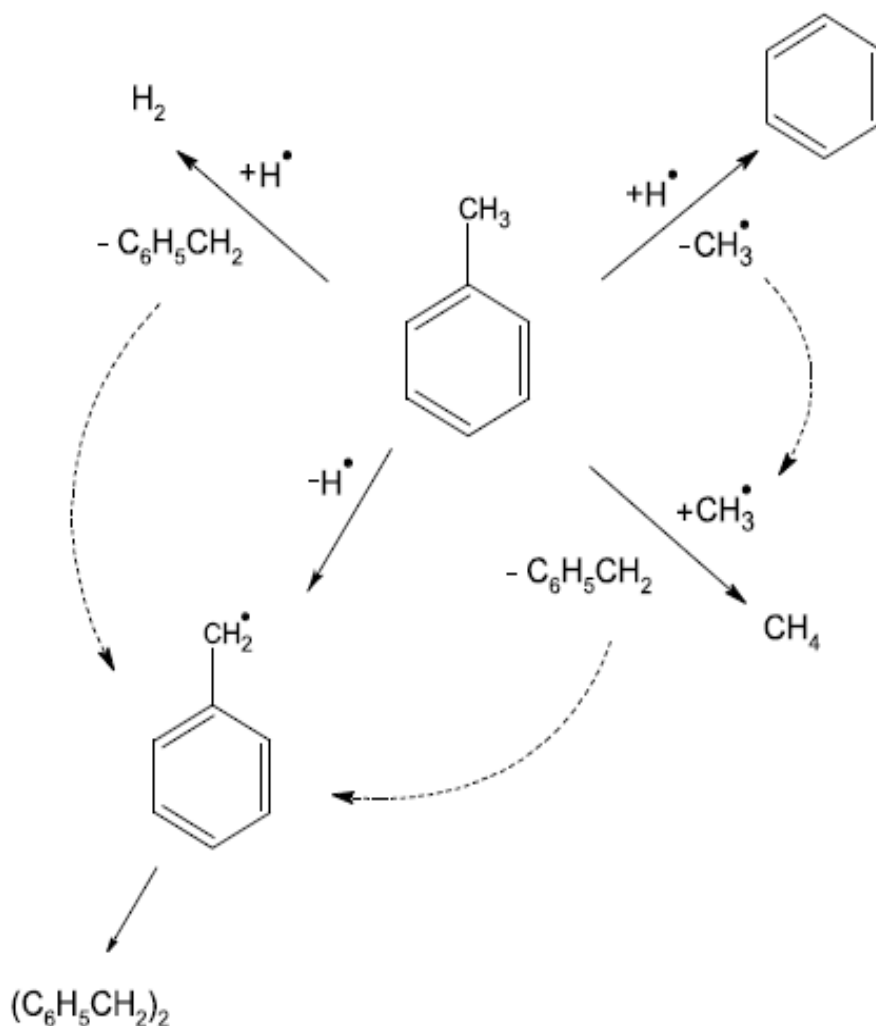
Figure 3.11 – Cracking scheme for toluene (van der Hoeven, 2007)

3.2 Partial Oxidation and Combustion of Tar Species

Houben (2004) and van der Hoeven (2007) performed experiments on a micro-swirl burner to remove a model tar, naphthalene, from a replicated biomass product gas. Figure 3.12 shows a model of how partial combustion in the micro-swirl burner causes the breakdown of naphthalene.
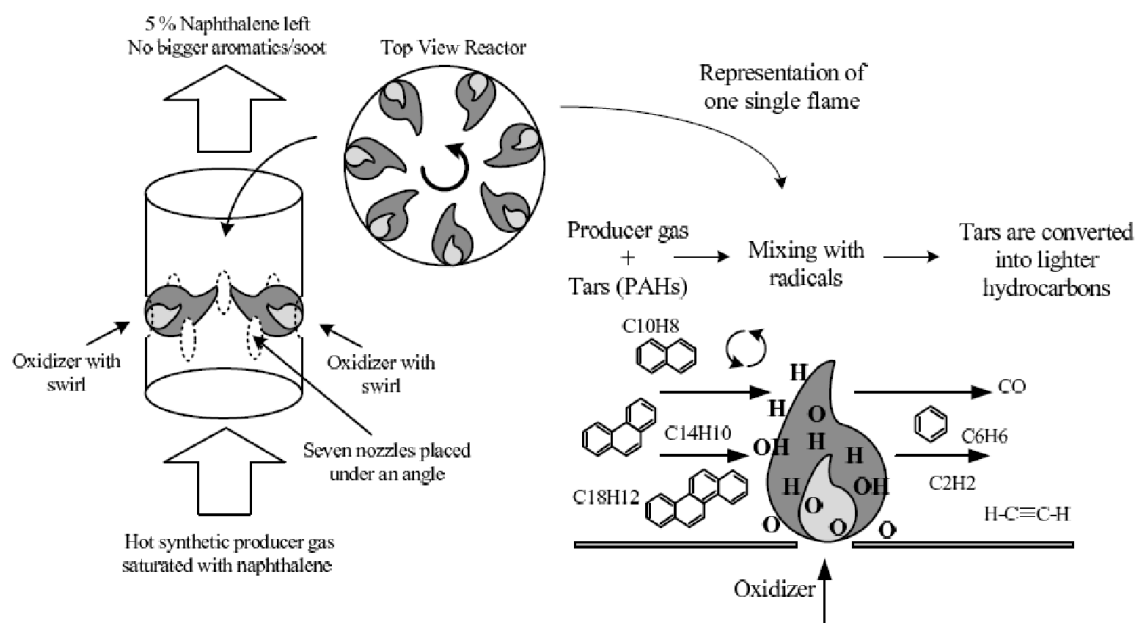
Figure 3.12 – Tar conversion in a micro-swirl burner (Verhoeven, 2011)

Figure 3.12 shows the seven air nozzles and resulting diffusion flames which prompt the partial oxidation of the tar saturated producer gas. The diffusion flames create localised regions of free radicals as well as an increase in temperature (Verhoeven, 2011). The free radicals then mix with the naphthalene contained within the producer gas causing the conversion into lighter hydrocarbons.

In the oxidative treatment of tar oxygen is used to combust product gas containing tar. The addition of oxygen increases reaction rates and reduces residence times when compared with thermal treatment (van der Hoeven, 2007). It is thought that oxidative treatment offers higher reactivity and lower activation energy than thermal treatment (van der Hoeven, 2007). The key difference is that both thermal and oxidative regimes rely on reactivity of different active radicals. For reactions when oxygen in present: oxygen, hydrogen, hydroperoxy and hydroxyl radicals are active. When thermal treatment is used: only hydrogen and methyl radicals are present. The active radicals for oxidative treatment increase hydrogen abstraction from hydrocarbons creating faster decomposition. The addition of oxygen also causes hydrocarbons to become oxidised forming carbon monoxide and water exothermically releasing heat for propagation reactions of the remaining hydrocarbons (van der Hoeven, 2007).

Su et al. (2011) determined that under fuel rich conditions the key reasons for ring fracture and side-chain separation are reactions between ring structures and O, HO_2 and O_2. The sequence for ring rupture is shown in Figure 3.13.
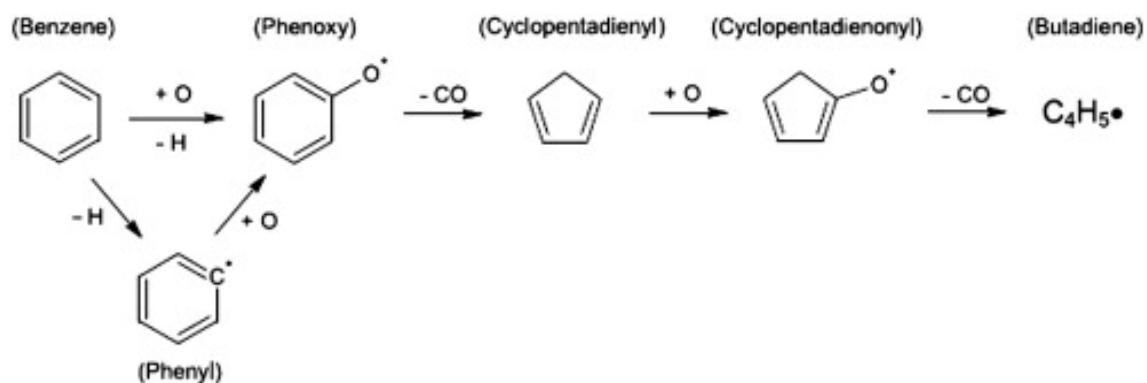
Figure 3.13 – General pathway for ring rupture at high temperature (Su et al., 2011)

Tars can also undergo polymerisation to become larger PAH and 'soot'. There are two methods which are used to describe the formation of these larger species. The first is the resonantly stabilised radical (RSR) mechanism and the second is hydrogen abstraction acetylene addition (HACA). Figure 3.14 shows the sequence involved in HACA of benzene to form larger species. Figure 3.15 indicates three RSR mechanisms. The top reaction shows the combination of a benzyl and propargyl to form naphthalene, the middle reaction shows the self-combination of cyclopentadienyl radical again to form naphthalene. The bottom reaction indicates the addition of a cyclopentadienyl radical to an idenyl radical, forming phenanthrene (Violi et al., 1999). The HACA method is dominant in fuel rich environments or pyrolysis conditions. In reverse conditions, when oxygen is rich, RSR mechanisms are prevailing in soot forming reactions (Su et al., 2011). Hence the HACA mechanism is often only considered for partial oxidation due to the low amounts of oxygen present.
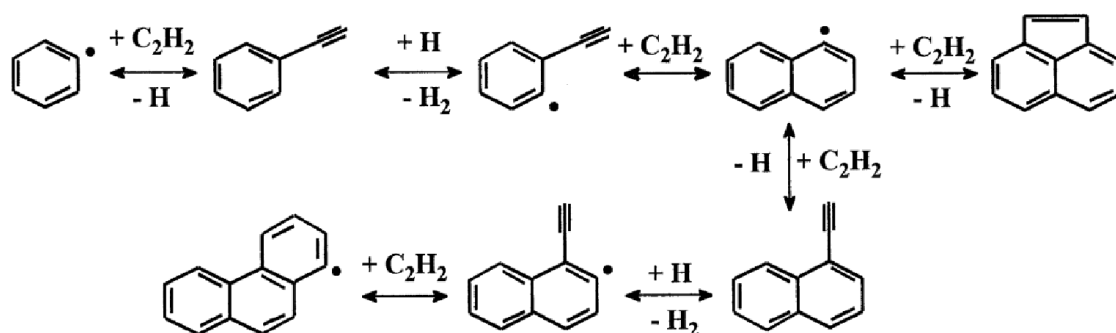
Figure 3.14 – HACA reaction mechanism to form larger PAH (Violi et al., 1999)
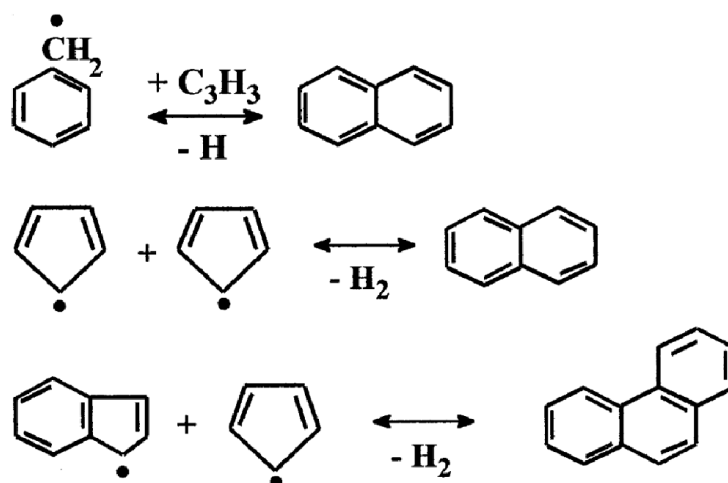
Figure 3.15 – RSR reaction mechanism to form larger PAH (Violi et al., 1999)

3.3 Summary

Chapter three examined the key theoretical features that are needed to be considered when designing a tar cracking device. Tar destruction by thermal treatment and through partial oxidation is examined.

The thermal cracking of tar into smaller permanent species is possible however such cracking reactions are likely to be accompanied by polymerisation into larger species. The hydrogen shift (Figure 3.1) demonstrates that hydrogen released through the formation of products through polymerisation is also used to stabilise cracked products (van der Hoeven, 2007). The hydrogen content of tar plays an important role. The greater the hydrogen content of tar the greater the concentration of hydrogen is required to be released for polymerisation products to form. When oxygen is added to the system and tars are treated by means of partial oxidation tar destruction is enhanced due to the higher number of oxygen containing radicals, when compared with thermal treatment. Key tar components (benzene, toluene and naphthalene) are discussed and tar destruction pathways for these species are examined.

4. Experimental: Preliminary Setup & Results

The description and analysis of the experimental work is separated into three chapters. Chapter 4 discusses; the analysis of the fuel properties of wood pellets used for the experimental programme; the initial setup and results from the preliminary experiments on the CTC and pyrolysis unit as individual experiments, before reporting on the experimental issues encountered from both experiments.

Chapter 5 describes how the set-up and design of the system was modified to improve the performance of the experimental rig. The two key features for improved operation were to alter the feeding system, to extend the run-time of each experiment and to re-design the CTC unit. Chapter 6 presents and discusses results obtained from experiments using the final setup of the system.

4.1 Material Characterisation

Wood pellets were used as the biomass fuel in this study, shown in Figure 4.1. Wood pellets were chosen because they provide a fair representation of a typical biomass material in terms of their chemical and thermal properties but also offer preferential fuel qualities. These qualities include; stability, robustness and the ability to be readily stored and handled.

Figure 4.1 – Wood pellets

The wood pellets were purchased from CPL Distribution Limited and are classified as ENPlus–A1, which is the highest grade of the three quality classes defined by the European Pellet Council. It is important to note that these standards are accredited for wood pellets to be used for non-industrial purposes. The ENPlus classification system was setup to ensure consistent quality but also to set certain requirements and controls for production, quality assurance, storage and delivery. Table 4.1 indicates the key properties of the wood pellets as

specified by the supplier. Although some key information is provided, the wood pellets were analysed to check and corroborate the data.

Property	Unit	Value
Diameter	mm	6 (±1)
Length	mm	$3.15 \leq L \leq 40$
Bulk Density	kg/m^3	≥ 600
Net Calorific Value	MJ/kg	$16.5 \leq Q \leq 19$
Moisture Content	mass.%	≤ 10
Ash Content	mass.%	≤ 0.7
Ash Melting Temp	°C	> 1200
Material		Stem wood and chemically untreated wood residues

Table 4.1 – Properties of wood pellets (CPL Distribution LTD, 2014)

4.1.1 Sample Preparation

The wood pellets were prepared for the material characterisation tests; gross calorific value, thermogravimetric analysis and ultimate analysis. The pellets were ground using a Retsch planetary ball mill PM100. Once ground, the wood pellet powder was passed through a sieve with an aperture of 212 μm, and stored in air-tight plastic containers. All material characterisation tests were carried out on an as-received basis; the samples were not dried to remove moisture.

4.1.2 Gross Calorific Value

The wood pellets were tested using a Parr 6200 oxygen bomb calorimeter. This unit had a removable bucket and bomb (Parr Instrument Company, 2010). The make and model of the removable bomb was a Parr 1108P oxygen bomb which was made from high strength stainless steel.

One gram of wood pellet powder was weighed out and placed inside a ceramic crucible and mounted in the calorimeter. Ignition wire, to combust the wood pellet powder, was placed so that it was just above the fuel sample. The ignition wire used was measured and cut to 80 mm. To adjust for the heat produced by the wire a correction factor of 0.963 J/mm was factored into the final calculation; this amendment had a minimal impact on the final result. The bomb was filled with pure oxygen at a pressure of 30 bar, as recommend by the equipment

instructions (Parr Instrument Company, 2010) and the appropriate European Standard (EN 14918, 2009). The gross calorific value was calculated using Equation 4.1;

$$CV = \frac{W\Delta T - e_1 - e_2 - e_3}{m}$$

(Eqn. 4.1)

Where;

CV	$=$	gross heat of combustion
W	$=$	energy equivalent of the bomb calorimeter
ΔT	$=$	temperature difference in (°C)
e_1	$=$	heat produced by the formation of nitric acid from trapped nitrogen
e_2	$=$	heat produced by the formation of sulphur dioxide
e_3	$=$	heat produced by the heating wire
m	$=$	mass of the sample (g)

(Parr Instrument Company, 2010)

The heat produced through the formation of nitric acid was assumed to be negligible. The heat produced by sulphur dioxide was also assumed to be nil due to the low amounts of sulphur present in the wood pellet sample.

The energy equivalent of the bomb calorimeter (W) was found by performing a number of tests which follow the same procedure for analysing a fuel sample. The standardisation procedure involves using a pellet of calorific grade benzoic acid which weighed between 0.9 and 1.1 grams. The energy equivalent can then be calculated using Equation 4.2.

$$W = \frac{Hm + c_1 + c_2 + c_3}{\Delta T}$$

(Eqn. 4.2)

Where;

W	$=$	energy equivalent of the bomb calorimeter
H	$=$	heat of combustion of the standardised benzoic acid sample
m	$=$	mass of the sample
ΔT	$=$	temperature rise (°C)
c_1	$=$	correction factor for heat of formation of nitric acid from nitrogen
c_2	$=$	correction factor for sulphur in the fuel, normally $= 0$
c_3	$=$	correction factor for heat produced by the heating wire

(Parr Instrument Company, 2010)

4.1.3 Gross Calorific Value Results and Analysis

	Wood Pellets
Mass (g)	1.02
Temperature Rise (°C)	1.87
Joules Released (J)	18480
Calorific Value (MJ/kg)	18.0

Table 4.2 – Gross calorific value

Table 4.2 shows the results of the calorific bomb experiment. The calorific value of wood pellets was compared to the average calorific value (MJ/kg) of a large sample of biomass fuels in a comprehensive study performed by Neves et al. (2011). The study analysed more than 60 samples of different biomass fuels and determined an average calorific value of 18.90 MJ/kg, which is slightly greater than the observed value of the analysed wood pellets. Obernberger and Thek (2010) determined the average gross calorific value from a sample of 21 different types of wood pellets to be 20.3 MJ/kg, higher than the result in this study.

4.1.4 Thermogravimetric Analysis

Thermogravimetric analysis (TGA) is a method used to characterise materials according to their inherent physical properties. The principle of TGA is relatively simple and is defined by PerkinElmer (2010) as "*TGA measures a sample's weight as it is heated or cooled in a furnace*". Monitoring the mass of the sample in a controlled and known environment reveals information regarding the moisture, volatile matter, fixed carbon and ash content of the tested material. In most cases the mass of the sample is monitored against increasing temperature within inert or oxidative environments.

The use of TGA or thermogravimetry (TG) as a method for determining the proximate analysis of a fuel has become increasingly popular because it is less time consuming and requires a smaller sample size when compared with more traditional analytical techniques (Mayoral et al., 2001). TGA results are comparable to methods used for British Standards (Muñoz-Guillena et al., 1992). A PerkinElmer TGA 4000 was used for the analysis, the key specifications of which are shown in Table 4.3.

A wood pellet sample was weighed and then loaded into a ceramic crucible; the desired sample weight, as recommended by the manufacturer (PerkinElmer, 2010), was between 2 and 50 mg. The crucible, containing the sample, was then placed inside a sensitive top loading balance inside the TGA 4000.

Technical Description	TGA 4000 Specification
TGA Balance Type	Top-loading balance
Balance Capacity	1500mg
Temperature Range	Ambient to 1000°C
Temperature Accuracy	± 1°C
Temperature Precision	± 0.8°C
Balance Sensitivity	1 μg
Balance Accuracy	± 0.02%
Balance Precision	± 0.01%

Table 4.3 – Key features of the PerkinElmer TGA 4000 (PerkinElmer, 2009)

The operating procedure used to determine the desired fuel properties (moisture content, volatile content, fixed carbon and ash) is described in points 1 to 4 below. The same operating procedure was used to determine the fuel properties of the wood pellet char, as detailed in section 6.5.2.

1. The fuel sample was loaded into the analyser and heated from ambient to 35°C where it was held for four minutes. At the same time the furnace is purged with nitrogen gas to remove any oxygen and create an inert atmosphere.

2. The sample was then heated at a rate of 75 °C/min to 110°C and held at this temperature for 6 minutes; during this stage any moisture contained within the fuel samples was lost causing a decrease in the sample mass.

3. The fuel sample was then heated at a rate of 80 °C/min to 900°C and held for one minute. Heating during this stage causes any volatile matter contained within the fuel to be released. The material was held at 900°C for four minutes.

4. Finally the furnace was heated from 900 to 950°C at a rate of 50 °C/min. Lastly oxygen was added into the furnace so the remaining fixed carbon was burnt leaving behind an ash residue (Muñoz-Guillena et al., 1992).

The TGA results were interpreted and analysed to determine the weight fractions of moisture, volatiles, fixed carbon and ash and the results are shown in Table 4.4.

Material	Wood Pellets
Sample Mass (mg)	14.0
Moisture (mass.%)	7.7
Volatiles (mass.%)	73.8
Fixed Carbon (mass.%)	17.7
Ash (mass.%)	0.4

Table 4.4 – TGA results

4.1.5 Thermogravimetric Analysis - Discussion

Wood consists of various constituents; cellulose, lignin, hemicellulose, water and minerals in different compositions depending on the species, age and location of the tree (Orfão et al., 1999). The thermogravimetric analysis of wood pellets indicated a loss of weight at 110°C which accounts for the contained moisture content. The moisture content of the analysed sample was calculated to be 7.7% (Table 4.4), which is within the range as set by the supplier.

The weight of the sample remained constant between 100 and 210°C. At this point the weight of the wood pellets began to decrease, initially at a comparatively slow rate up to a temperature of 350°C, at this point the weight of the sample decreased rapidly until the temperature in the furnace reached 475°C. From 475 to 875°C the weight of the sample decreased steadily. A study by Bilbao et al. (1989) concluded that the loss of weight is caused by the decomposition of hemicelluloses at temperatures below 230°C, then both cellulose and hemicelluloses at temperatures between 230 and 260°C, finally at temperatures above 290°C the decomposition of lignin and cellulose becomes the primary cause for weight loss. Heikkinen et al. (2004) performed a study that used thermogravimetry as a means to classify waste material. The rate of weight change of pine against temperature was analysed, results concluded that the rate of weight change (%/min) was greatest at 380°C which compares favourably to the presented results.

The fixed carbon content of the wood pellets was calculated to be 17.7% which was expected when compared with results from Telmo et al. (2010), who analysed various samples of wood. The majority of the results were found to contain between 14 – 18% of fixed carbon. The amount of ash left in the sample was measured to be 0.4% of the original sample which is well within the range set from the standards specified by the supplier.

4.1.6 Ultimate Analysis of Wood Pellets

A flash 2000 organic elemental analyser manufactured by Thermo Scientific was used to perform the ultimate analysis tests. The samples were weighed to between 2 and 5 mg and inserted into a tin capsule and placed in the analyser. The sample was heated to 900-1000°C. Oxygen was added to burn organic or inorganic material which resulted in the conversion of the sample into elemental gases. These gases then went through a separation column and a thermal conductivity detector which determined the elemental concentration (Thermo Fisher Scientific, 2008). Dedicated software used in conjunction with the analyser then allowed for the determination of the contained elements. This method of analysis is endorsed by institutes including the AOAC (Association of Official Analytical Chemists) and the ASTM (American Society for Testing Materials). Three samples were analysed and the results are presented in Table 4.5.

	A	B	C	Average
Carbon (mass.%)	45.56	45.49	45.72	45.59±0.12
Hydrogen (mass.%)	5.72	6.11	6.03	5.95±0.21
Nitrogen (mass.%)	0.15	0.14	0.17	0.15 ±0.02
Oxygen* (mass.%)	48.57	48.16	48.08	48.31

Table 4.5 – Ultimate analysis of wood pellets

The determined results compare well with Obernberger and Thek (2004) who performed studies on the properties of wood pellets in Europe. Obernberger and Thek (2004) found the average level of carbon, nitrogen and hydrogen from a sample of 21 wood pellets to be 50.7%, 0.22% and 5.7% respectively. The carbon level of the wood pellets analysed was slightly less, at 45.59%. The values for nitrogen and hydrogen also compare well with the results from Obernberger and Thek (2004).

The remaining concentration of the fuel is mainly made up from oxygen with small amounts of sulphur and chlorine. The quantity of sulphur and chlorine is normally less than that of nitrogen. The value of oxygen can be calculated by subtracting the values of the other elements (carbon, hydrogen and nitrogen) from the total (Obernberger & Thek, 2010; Erlich et al., 2006). For the analysis presented here the mass.% of oxygen would be around 48% which is towards the upper limit of oxygen content when compared to a review of biomass fuels performed by Neves et al. (2011).

4.2 Introduction to Experimental Work

The preliminary experimental programme was divided into three experimental sections. In the first section a Coandă burner was developed and tested using propane as the gaseous fuel; in the second section pyrolysis of wood pellets at a range of temperatures is performed; lastly initial experiments on the combined system where the gaseous products from wood pellet pyrolysis are combusted in the Coandă burner. In the combined experiment the Coandă burner acts as a CTC.

4.2.1 Experimental Setup - Coandă Burner

Figure 4.2 shows the initial setup of the Coandă burner/CTC. There are four major components; the Coandă ejector; the pre-mixing vessel; a pre-combustion chamber and finally the burner and flame stabiliser (see Figure 4.2). The burner was firstly run using propane and air to ensure the burner is safe and usable. This section explains the set-up of the burner for the propane combustion experiments.
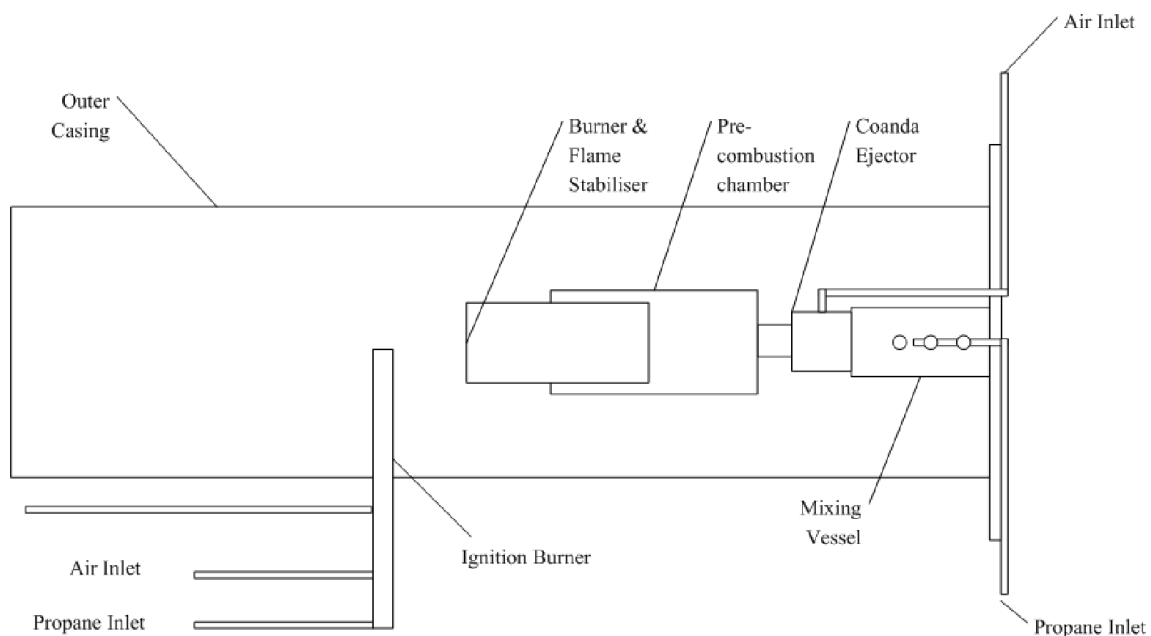
Figure 4.2 – Schematic of the tar cracking unit

Coandă Ejector

The Coandă ejector is the key component used in the system. The ejector was purchased from Beck-Air Ltd. The ejector is a motorless and bladeless ejector which is normally used to extract gases and other materials by using a small volume of compressed air and the Coandă effect to entrain large volumes of surrounding gases.

The total length of the ejector was 85 mm, the diameter at the inlet was 50 mm and it was made from stainless steel 304. The manufacturers recommend that air is supplied at 4 bar and

at a flow rate of 397 SLPM (standard litres per minute) which produces a flow-rate at the outlet of 5500 SLPM (Beck-Air, 2012), the Coandă air inlet was a ¼" BSP (British Standard Pipe) connector. The ejector was modified so that it could be attached to other units in the tar cracking system. Screw threads were threaded onto either end to allow for the primary mixing vessel and the pre-combustion chamber to be connected. Screw threads were used as they allowed for quick and easy assembly and disassembly. This feature allowed for the unit to be removed and, if required, cleaned or modified. See Figure 4.3 for a technical drawing of the Coandă ejector and Figure 4.4 for a 3D drawing.
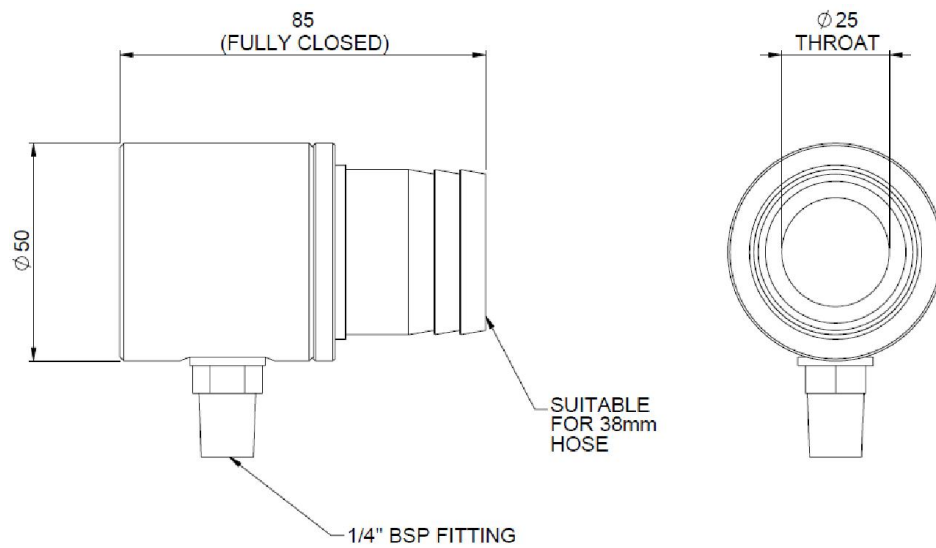
Figure 4.3 – Side view of the Coandă ejector (All values in mm)
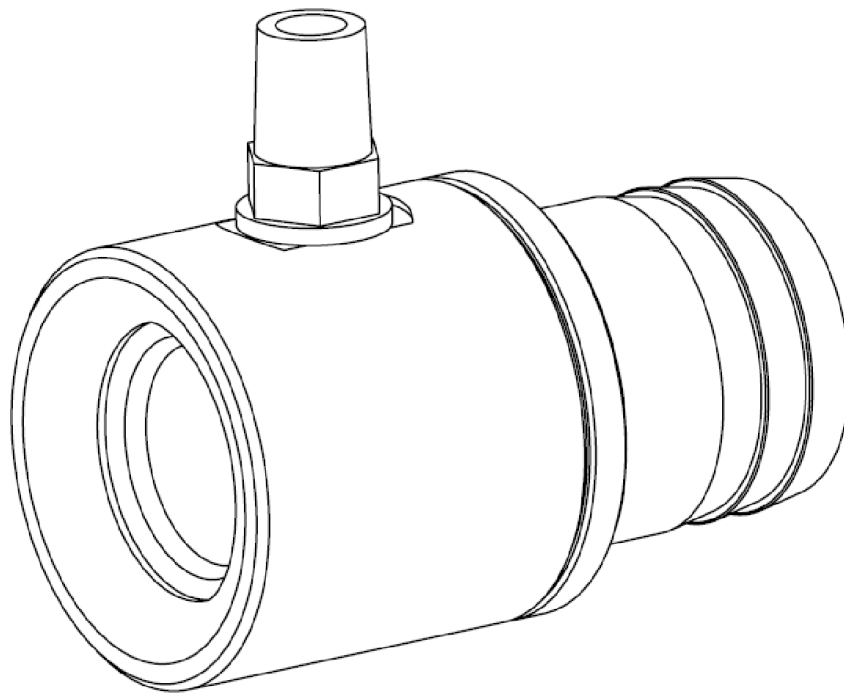
Figure 4.4 – 3D drawing of the Coandă ejector

Burner and Flame Stabiliser

The burner was the final part of the system. In a similar manner to the Coandă ejector the burner was designed so that it could be removed from the setup therefore a screw thread was inserted at the midway point to allow for removability and maintenance. The screw thread was 10 mm in length and connected the post Coandă chamber and the burner together. The dimensions of the burner are shown in Figure 4.5 and the unit is shown in Figure 4.6.
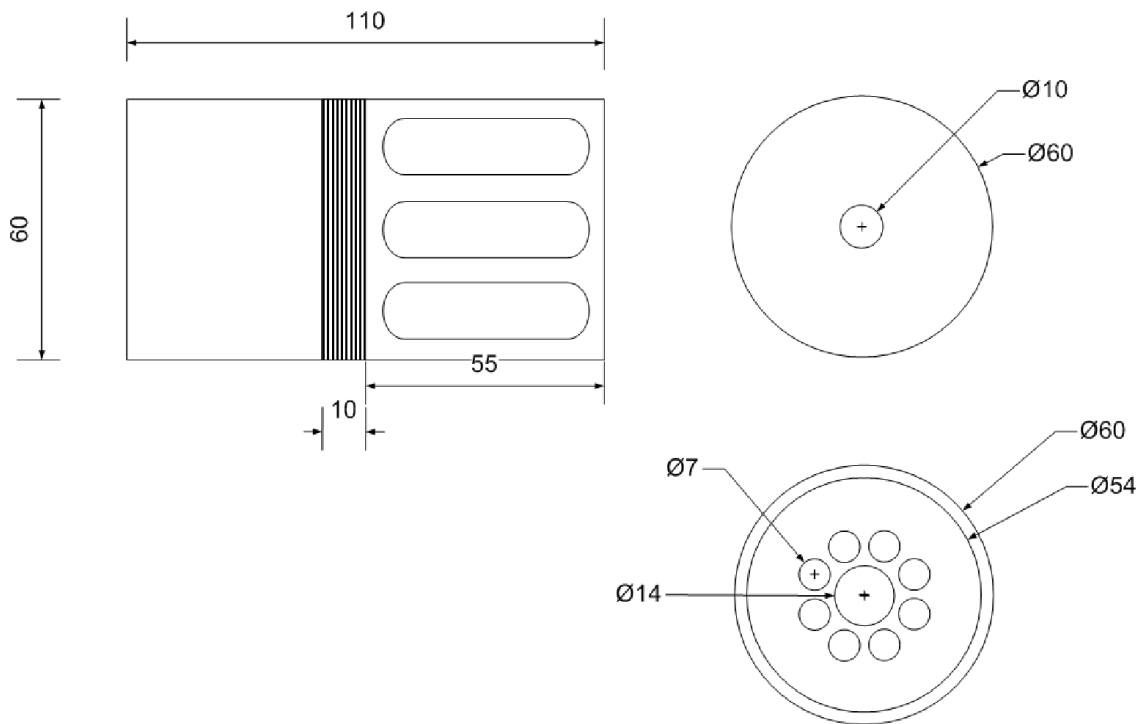
Figure 4.5 – Technical drawing of burner (All values in mm)
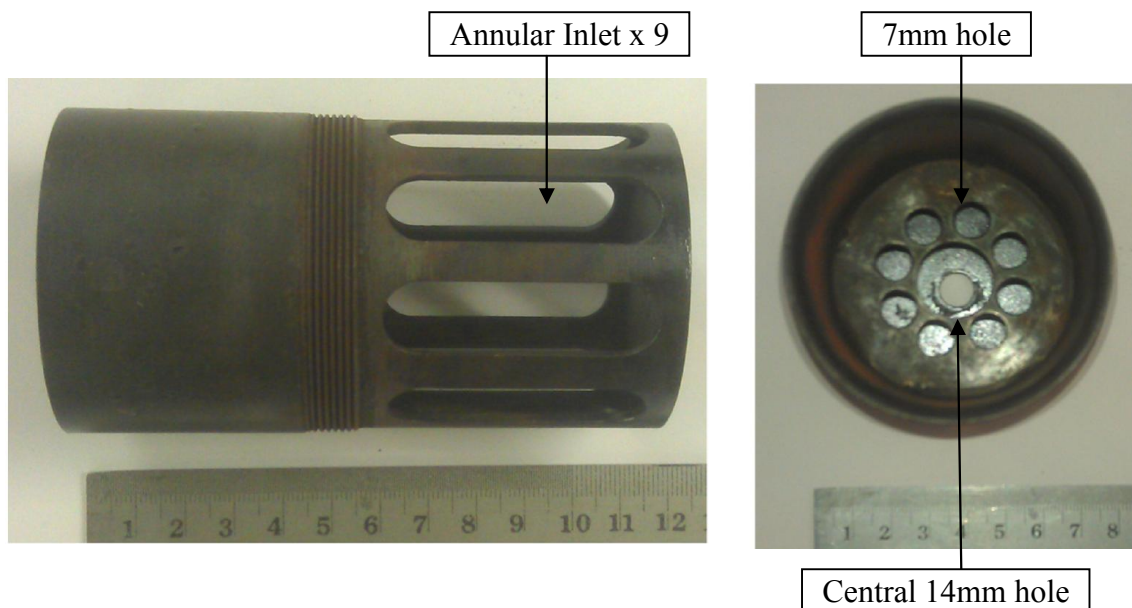
Figure 4.6 – Burner and flame stabiliser

The burner has a 10 mm inlet on the front plate of the unit. The burner also contains a flame stabiliser 55 mm from the front face. At the back of the burner there are nine annular inlets which promote mixing of the fuel and oxidant. The stabiliser has a central hole 14 mm in diameter and is surrounded by eight 7 mm in diameter holes. The burner was manufactured from mild steel EN3A which was chosen due to its ability to be easily machined and stability at high temperatures.

Post Coandă Chamber

The post Coandă chamber connected the Coandă ejector and the burner together. The unit was made from mild steel EN3A. The chamber was cylindrical in shape and had a wall thickness of 6 mm. The chamber was 148 mm in length and has an outside diameter of 90 mm. At either end 'shoulders' were inserted to allow the chamber to connect to the Coandă ejector and the end burner. Using Figure 4.7 as a reference; on the right hand side the inserted threaded shoulder created an internal diameter of 38 mm this allowed the chamber to be connected to the Coandă ejector; on the opposite end the shoulder created an internal diameter of 60 mm. The chamber ensured that all of the flow that is entrained by the Coandă ejector entered the burner. The chamber enclosed the gases and also allowed for the gases to mix before they entered the burner.
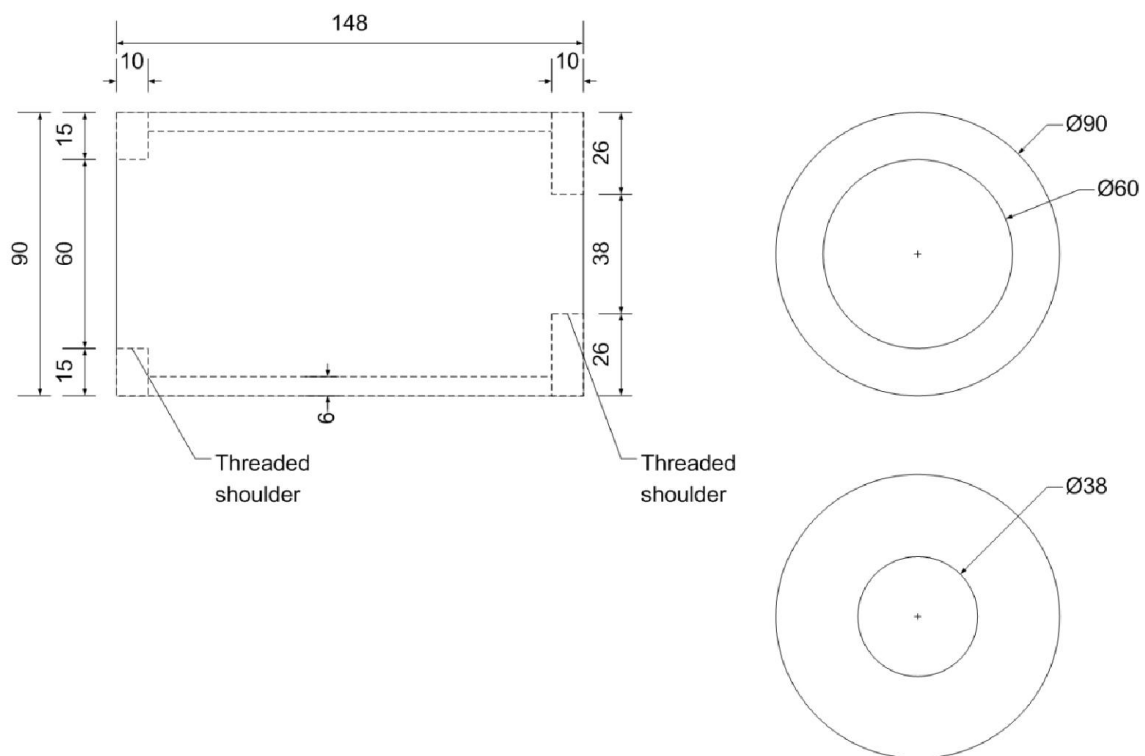
Figure 4.7 – Technical drawing post Coandă chamber (All values in mm)

Mixing Vessel

The mixing vessel was situated at the front of the tar cracking unit. The purpose of the vessel was to allow for recirculation of the hot gas produced from the burner. The mixing vessel had six 20 mm holes and was designed to create mixing from gases that recirculate after going through the burner with fresh fuel gas. The mixing vessel was designed so that the outer mixing holes could be closed to prevent any recirculation, if required. The vessel consisted of two cases that fit concentrically. The outer case rotated around the inner cases allowing for the recirculation holes to be opened and closed. The mixing vessel was made from mild steel EN3A and like the other components of the tar cracker was designed so that it can be removed for maintenance and modification. The inner case has a threaded shoulder built in to allow it to be connected to the Coandă ejector and also has an outside thread allowing for connection to the pyrolyser. A technical drawing and a picture of the inner and outer cases of the mixing vessel are shown in Figures 4.8 and 4.9.
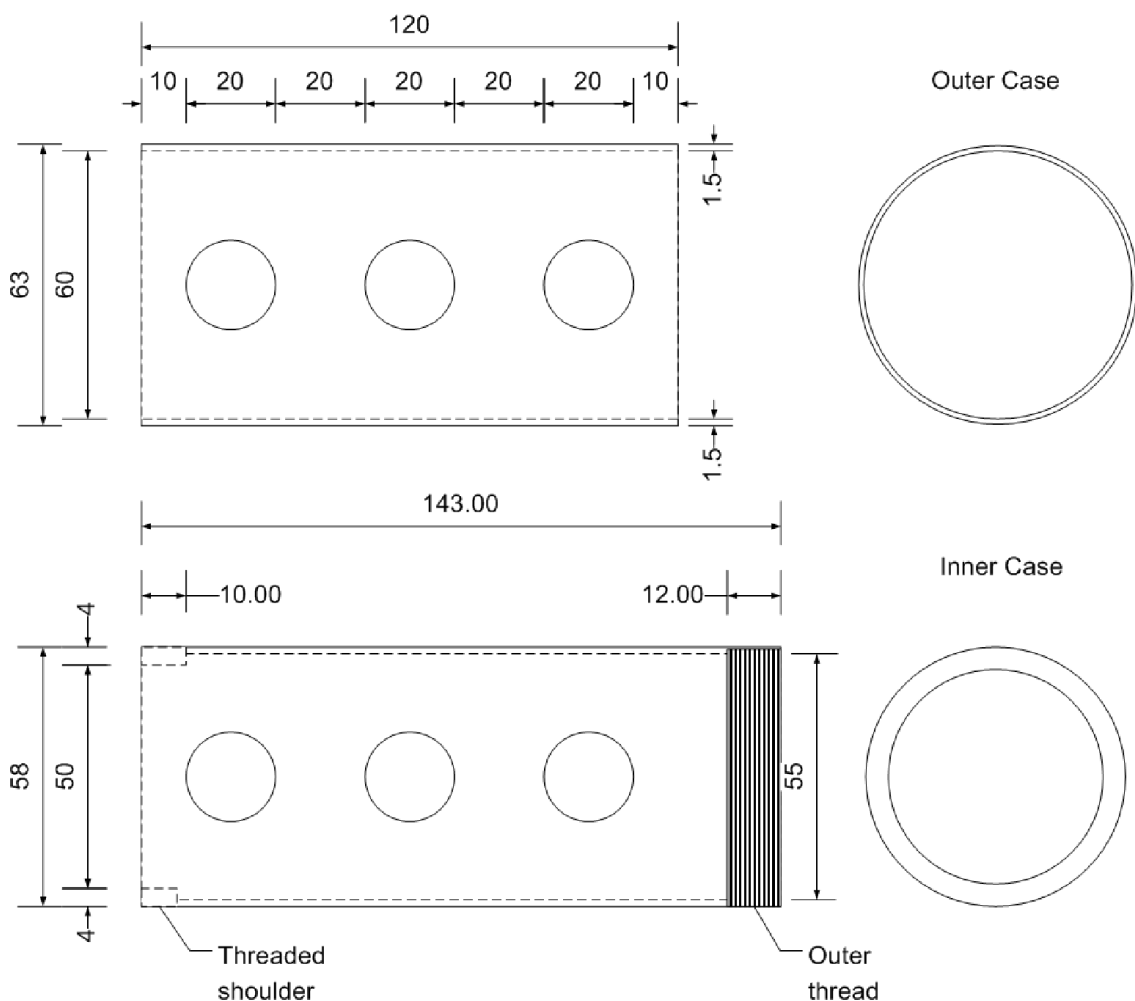
Figure 4.8 – Inner case of the mixing vessel technical drawing (All values in mm)
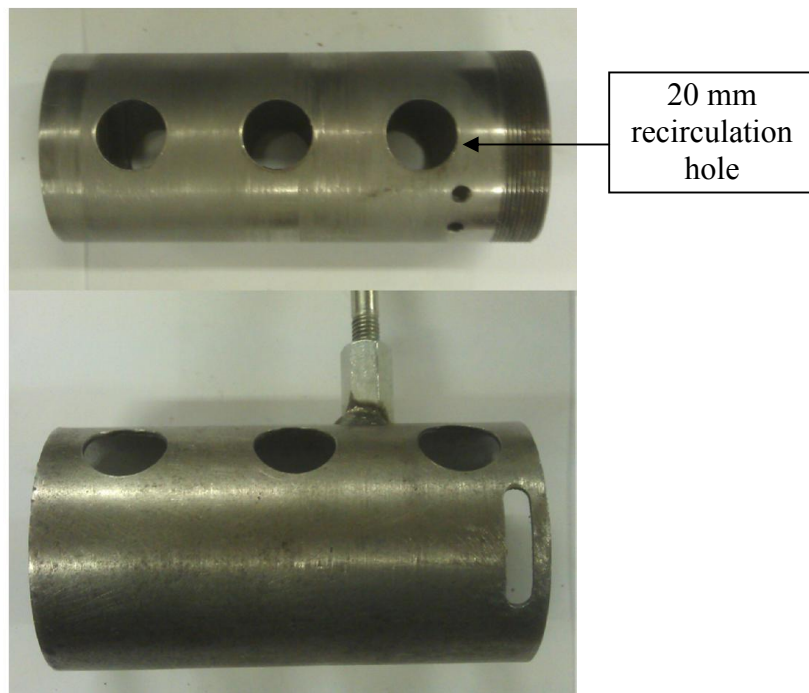
Figure 4.9 – Mixing vessel (top – inner section; bottom – outer section)

Outer Casing

The system was situated in an outer case. This was used to control the direction of the flame and to allow for measurement of the flame temperature. The outer casing was made from mild steel EN3A. The outer casing was cylindrical and hollow with a wall thickness of 2 mm. The total length of the unit was 1000 mm and the external diameter was 254 mm. The casing was designed so that it can be attached to a flange using 6 butterfly nuts. Seven sampling ports were placed on the outer casing at a number of points that allowed for thermocouples to be inserted to monitor the temperature in the system at various points.
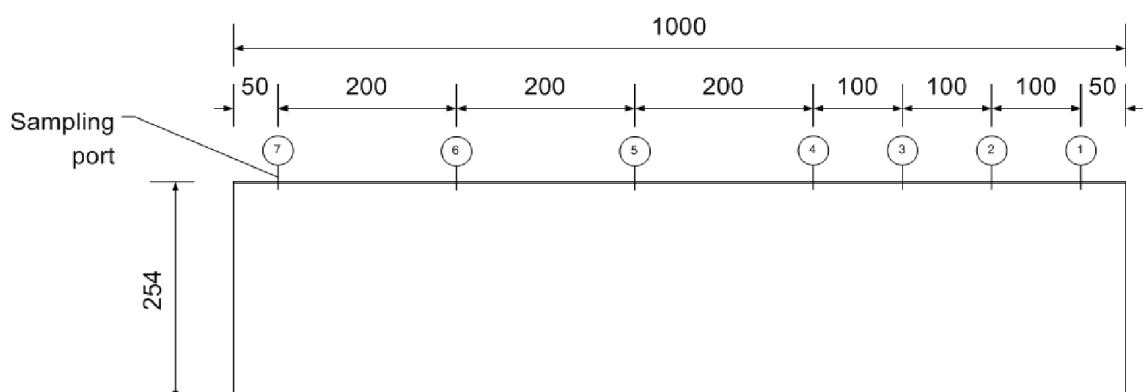
Figure 4.10 – Technical drawing outer casing (All values in mm)

Completed Coandă Burner - Version 1

As discussed the four main components of the tar cracking unit all have screw threads in-built. Figure 4.11 shows how the individual pieces connected together.

| Burner and flame stabiliser | Post Coandă Chamber | Coandâ Ejector | Mixing Vessel |
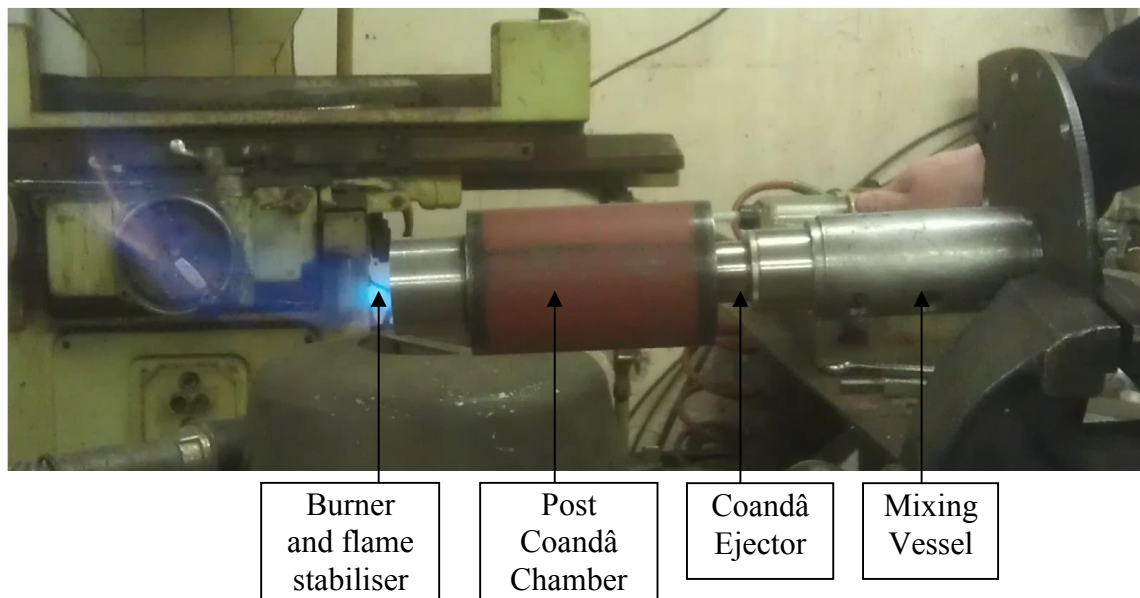
Figure 4.11 – Complete Coandă burner: Version 1

Gas Flow-meters

As previously discussed; for the primary experiments the Coandă burner was operated using only propane gas. The flow rate of both propane and air was controlled by manual valves and volume flow rates were measured and controlled by a FL-2014 series acrylic flow-meter purchased from Omega Engineering LTD. The limit of the propane flow-meter was 0-10 LPM. The accuracy at full scale was ±5%. Air supplied to the Coandă ejector was again controlled by manual valves and volume flow rates were measured and controlled by a FL-2016 series acrylic flow-meter. The range of the flow meter was 4-50 LPM, with an accuracy of ±5%. In the initial experiments, propane gas was fed into the mixing vessel through a 6mm internal diameter stainless steel pipe. The original proposal was to feed propane into the inlet of the outer burner but this would negate the mixing potential of the Coandă ejector.

Ignition Burner

An ignition burner was installed and fitted in the outer casing. The ignition burner produced a stable flame which is used to ignite the gases that come out of the Coandă burner. The ignition burner was manufactured by the North American NFB Company in Cleveland Ohio. Propane and air were supplied into the premixed burner. The name of the ignition burner was the 'pilot mixer 4-8131'; the component can be seen in Figure 4.12. The burner is attached to the outer casing of the unit at the midway point, 500 mm from either end of the outer case.
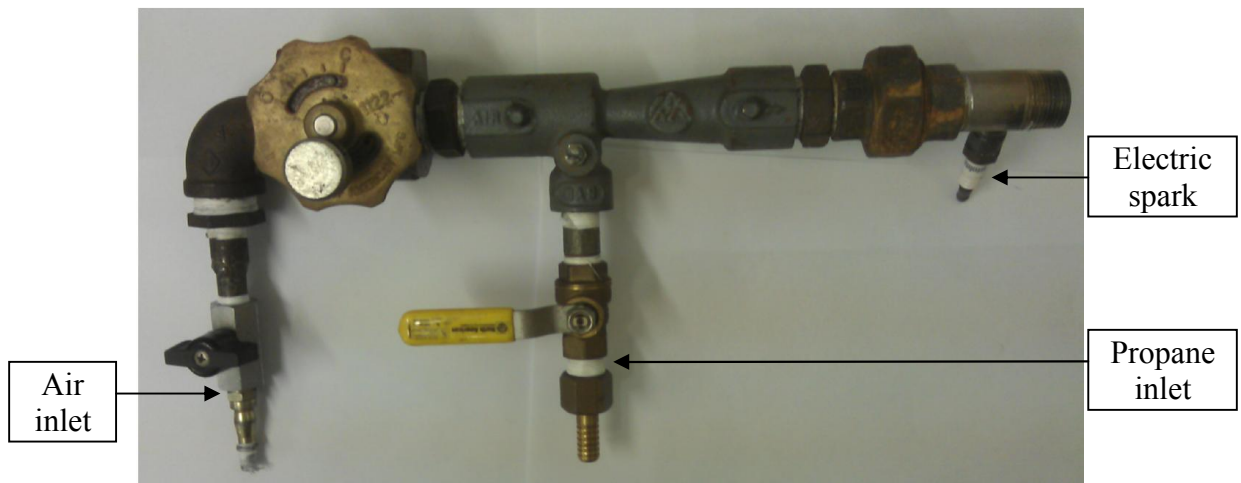
Figure 4.12 – Propane fuelled ignition burner

Temperature Measurement

The temperature of the flame produced by the burner and the internal temperature of the gases in the burner was monitored. Three Ni/Cr- thermocouples (K-type) were used to measure the gas temperature in the outer casing. The thermocouples are insulated with a 310 stainless steel sheath and have a temperature range between -40°C and +1100°C, making them adequate for measuring higher temperature gaseous environments. The accuracy of the thermocouples is ±2.2°C or ±0.75% depending on which value is greater.

Three K-type thermocouples were placed at sample points 1, 3 and 6 (see Figure 4.10). The thermocouples were placed at these points so that the temperatures within the whole unit could be investigated which may give an indication of whether the Coandă ejector caused hot gases to circulate through the holes in the mixing vessel.

A platinum based thermocouple (R-type) in a protective ceramic sheath was used to measure the flame temperature. The R-type thermocouple has a temperature range between 0 to 1450°C with an error limit of ±1.5°C or ±0.25%. The R-type thermocouple was placed into sample point 5. All the thermocouples were connected to a Graphtec GL220 midi logger so that the temperatures could be recorded. Temperature recordings from the thermocouples were taken at a rate of one per second.

4.2.2 Experimental Procedures

Figure 4.13 shows the piping and instrumentation diagram (P&ID) used to describe the procedure used to run the propane only burner experiments. In each of the burner experiments the flow rate of propane was set and kept constant throughout the experiment.
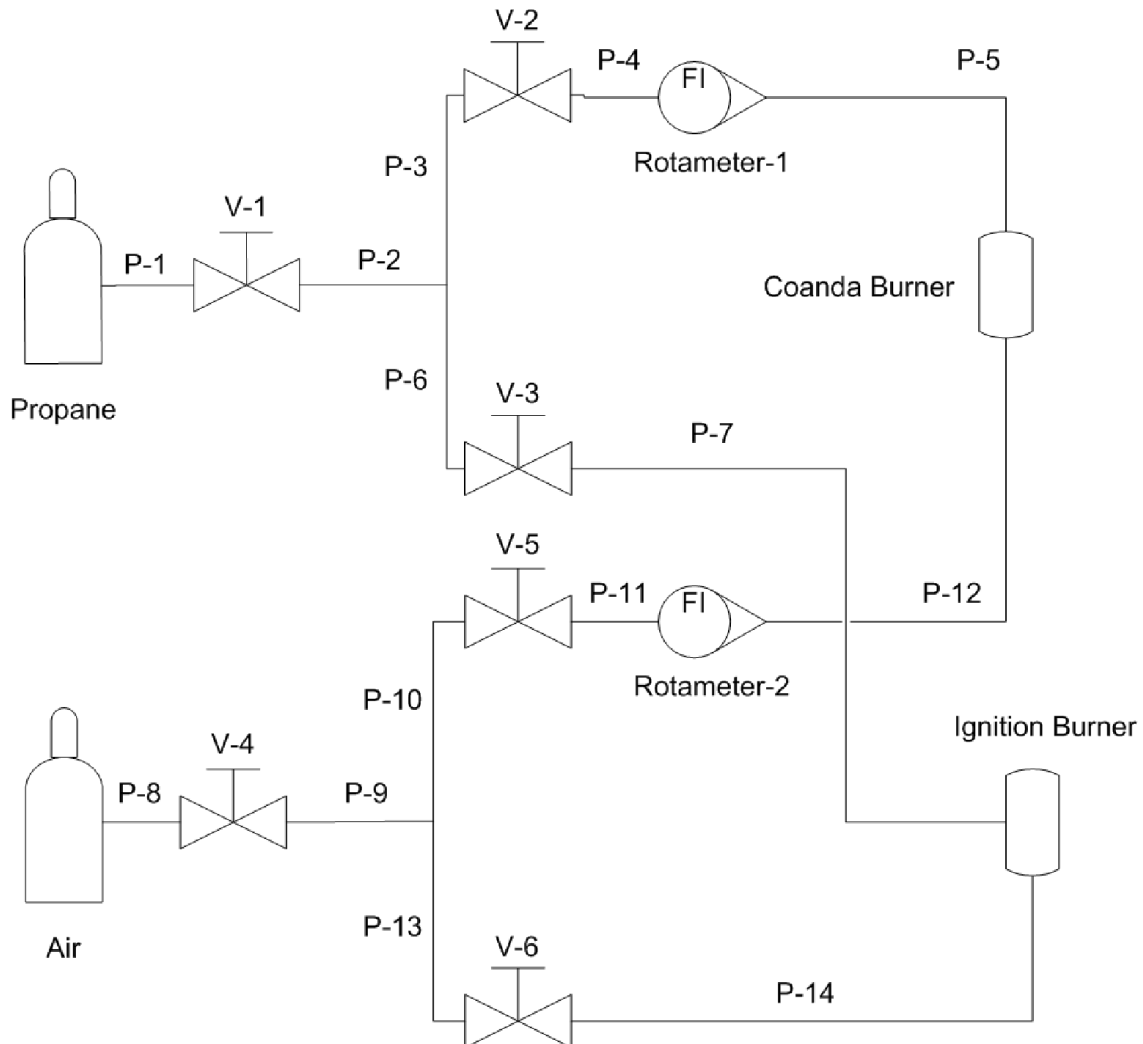
Figure 4.13 – Burner Experiment P&I.D

Start-up Procedure

1. The data logger was switched on and the temperature readings for the thermocouples were checked

2. Memory recording of the data logger was started and the time when the experiment was started recorded

3. The propane ignition burner was turned on first. Turned on air supply (OPENED V-4)

4. Turned on air to ignition burner (OPENED V-6)

5. Turned on propane supply (OPENED V-1)

6. Turned on propane supply to ignition burner (OPENED V-3)

7. Ignite ignition burner with electrical spark

8. Once the ignition burner has a steady flame the Coandă burner can be started. Turned on air to Coandă burner (OPENED V-5)

9. Set initial air flow rate using Rotameter-2

10. Turned on propane to Coandă burner (OPENED V-2)

11. Set fixed propane flow rate using Rotameter-1

12. Ensure flame from the Coandă burner has ignited

13. Once the flame from the Coandă burner is steady the ignition burner can be turned off. Turned off propane to the ignition burner (CLOSED V-3)

14. Turned off air to the ignition burner (CLOSED V-6)

15. The final stage was to ensure that the flame from the Coandă burner was steady

16. At three minute intervals the flow rate of air was increased using Rotameter-2 by increments of 2 LPM. The colour, shape, size and stability of the flame was recorded by hand as well as a photograph taken

Shut-down Procedure

1. Once the flow rate of air through the Coandă was increased to levels that extinguished the flame the experiment was shut down

2. Propane supply shut down. Turned off propane flow to Coandă burner (CLOSE V-3)

3. Turned off propane flow (CLOSE V-1)

4. Turned off air flow to Coandă burner (CLOSE V-5)

5. Turned off air flow (CLOSE V-4)

6. Turned off propane at the cylinder

7. The memory recording of the data logger was turned off and the equipment left to cool

4.2.3 Burner Results

The initial burner tests were run solely using propane as the fuel. This was done to understand firstly if the burner would work with its current setup and also to determine what changes could be made to make the burner more efficient. A secondary effect of operating the burner was that it would increase the temperature of the four internal parts that make up the burner.

The higher the temperature of the burner parts the less likely it is for tar to condense in this region which would reduce the need for cleaning of the equipment as tar is likely to cause blockages. Thus in the combined experiment propane could be combusted in the unit to heat the surroundings before pyrolysis gases entered the tar cracking region.

Propane was used because it is a cheap, available gas and also it is easy to ignite. There were two available setups for the burner; the mixing vessel can either be opened or closed.

Flow-rates for propane were kept the same during every experiment but the flow-rate of air was increased using the rotameter by 2 litres per minute at 3 minute intervals.

Propane Combustion

$$C_3H_8 + 5(O_2 + 3.76N_2) = 3CO_2 + 4H_2O + 18.8N_2$$
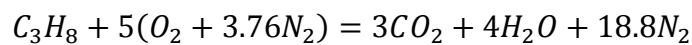
(Eqn. 4.3)

Equation 4.3 shows the stoichiometric chemical reaction for propane with air. The ratio by volume of air to propane is 23.8:1. The ratio in mass of air to propane is 15.7:1.

Case A: Propane flow rate 2.6 (LPM), Air mover closed

Propane was run when the air mixer was closed. At the initial flow rate there was an air-fuel ratio (AFR) of 2.9 and λ which was calculated using Equation 4.4 was 0.19.

$$\lambda = \frac{AFR}{AFR_{stoich}}$$

(Eqn. 4.4)

The initial flame was a large flickering orange flame, the gas mixture was fuel rich. The flame colour remained orange until λ increased to 0.40 after 21 minutes (1260 seconds); at this point the flame became blue in colour with slight flickers of orange. The temperature of the flame region measured by the R-type thermocouple remained relatively constant at around 200°C until λ increased to 0.56 at 36 minutes, at this point the temperature increased rapidly (Figure 4.14).

After 42 minutes (2520 seconds) λ was 0.62 at this point the flame reduced in size and became a stable but small dark blue flame. As the flow of air into the Coandă was increased so that λ was 0.77 the flame started to come away from the burner plate and the flame became less stable it and eventually extinguished, the flame was at its highest temperature, 588°C, just before it extinguished. The temperatures in the front section of the burner which was monitored by thermocouples 1 and 2 remained relatively constant throughout the run time of

the experiment. At the outlet of the burner there was a gradual increase in the temperature as the air flow rate increased.
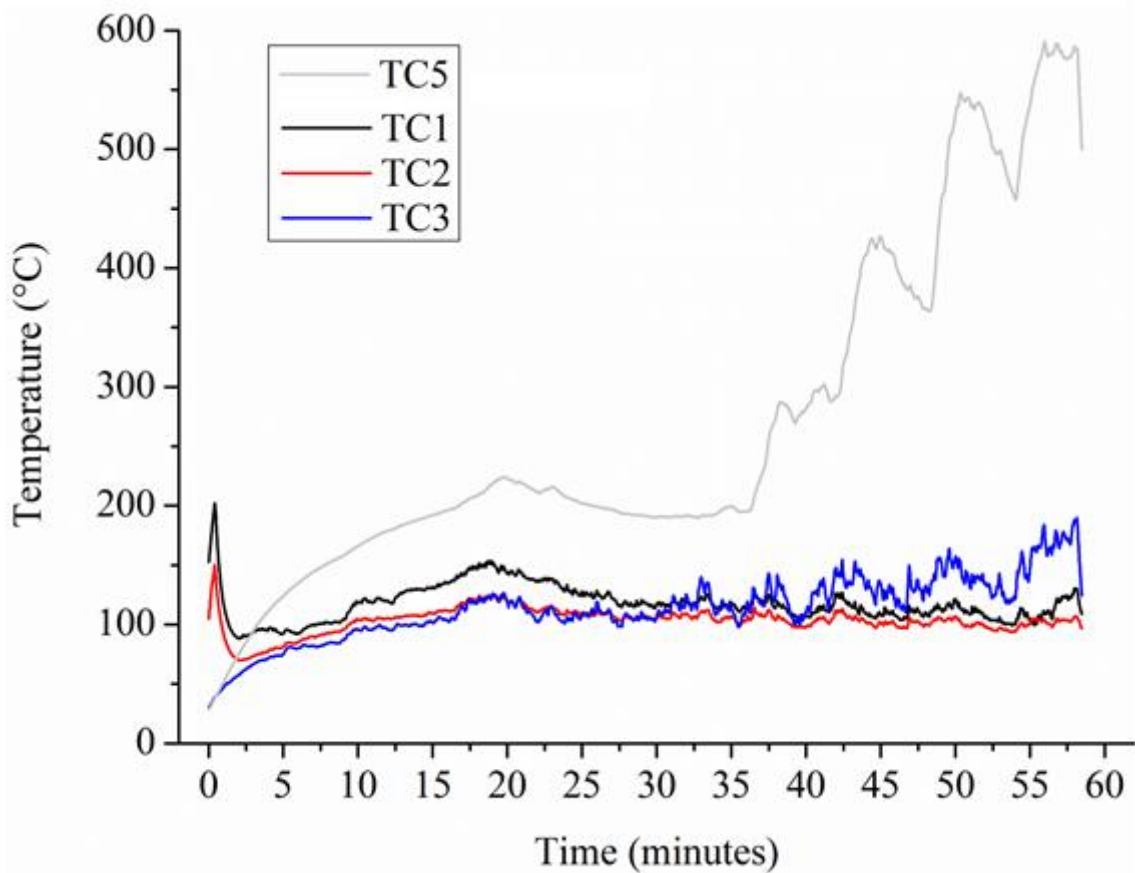
Figure 4.14 – Internal burner system temperature with increasing flow rates of air

Case B: Propane flow rate 3.9 (LPM), Air mover closed

The flow rate of propane was increased to 3.9 LPM. The initial value for λ was 0.25 and the air to fuel ratio was 3.9. The flame was long, unstable and a flickering orange until the value for λ was increased to 0.37 after 18 minutes (1080 seconds) the flame became green at the base and the body of the flame constantly switched between blue and orange. At this point there was a decrease in the temperature recorded by thermocouple 5. This was apparently caused because the length of the flame decreased. The long orange flame surrounded the thermocouple when the value for λ was less than 0.37 as the flow rate of air increased the flame reduced in size and the flame was no longer in contact with the high temperature thermocouple (TC5). After 27 minutes (1620 seconds) the flow rate of air into the Coandă was set to 42 LPM and the value for λ increased to 0.43. At this point the flame became a small, stable blue flame this caused an immediate increase in the flame temperature, see Figure 4.15. The temperature in the burner recorded directly after the flame (TC5) continued to increase as the flow rate of air to the Coandă ejector increased. The flame remained blue

and stable until the flow rate of air reached 50 LPM, the maximum flow rate available on the rotameter. The maximum temperature monitored by TC5 was 909°C when the value for λ was 0.51 at 39 minutes (2340 seconds). Once the blue flame had stabilised, when λ was increased to 0.43, as the flow rate of air to the Coandă increased the flame became shorter and the blue tail shortened until the flame became cone shaped.
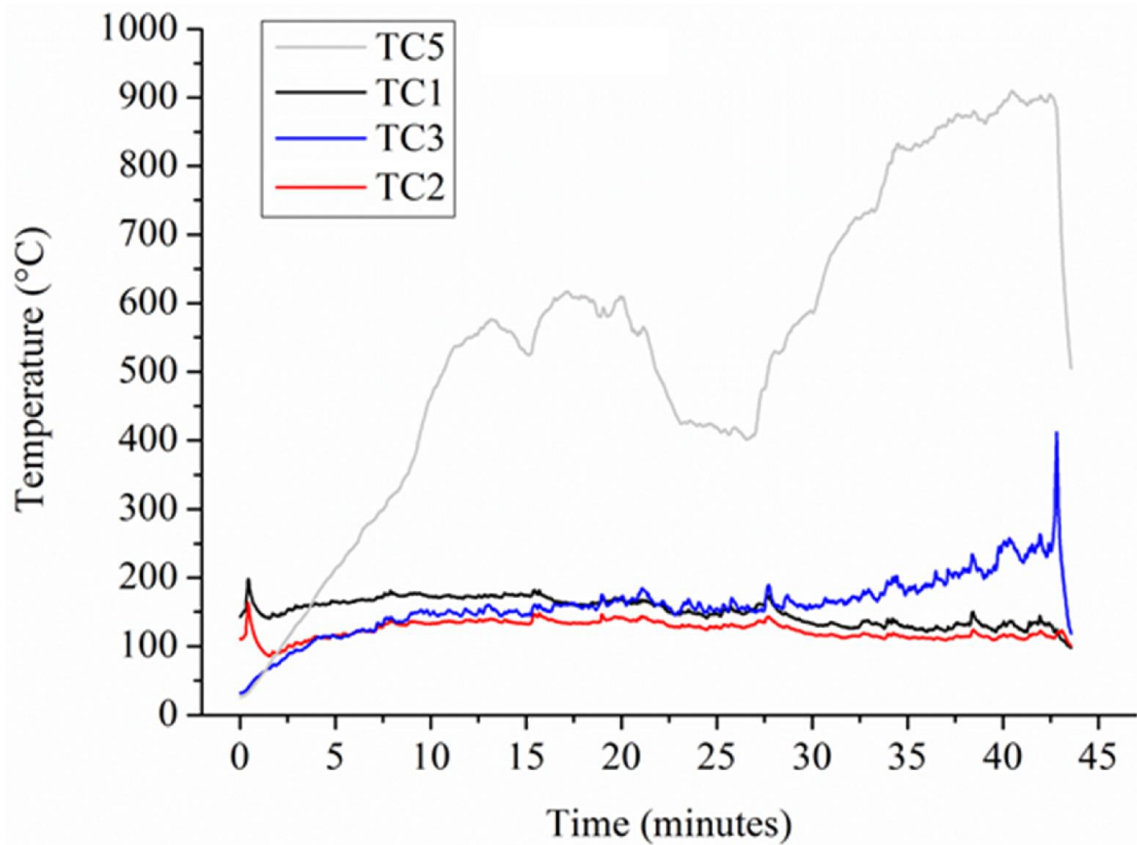
Figure 4.15 – Internal burner temperature with increasing flow rates of air

Figure 4.16 – Flame shape and colour (Left: $\lambda = 0.33$, centre: $\lambda = 0.39$, right: $\lambda = 0.49$)

The temperatures at the front of the burner unit monitored by TC1 and TC2 remained constant throughout the experiment at temperatures between 120°C and 180°C. The temperature at the burner outlet increased for the remainder of the experiment before stabilising after 15 minutes at around 160°C. After 27 minutes, the flame stabilised and became blue in colour, at this

point the temperature at the duct outlet increased steadily and reached a temperature of 260°C.

Case C: Propane flow rate 5.3 (LPM), air mover closed

The flow rate of propane was increased to 5.3 LPM which equates to 0.6 kg/hr. The initial value for λ was 0.31. As with cases A and B the flame was long, unstable and orange in colour. The change in the flame appeared when λ was increased to 0.36. At this point the flame was stable and blue with a green coloured cone at the base. The maximum value of λ was 0.39 because the maximum flow rate of air to the burner was capped by the capacity of rotameter which was 50 LPM (3 m^3/hr).
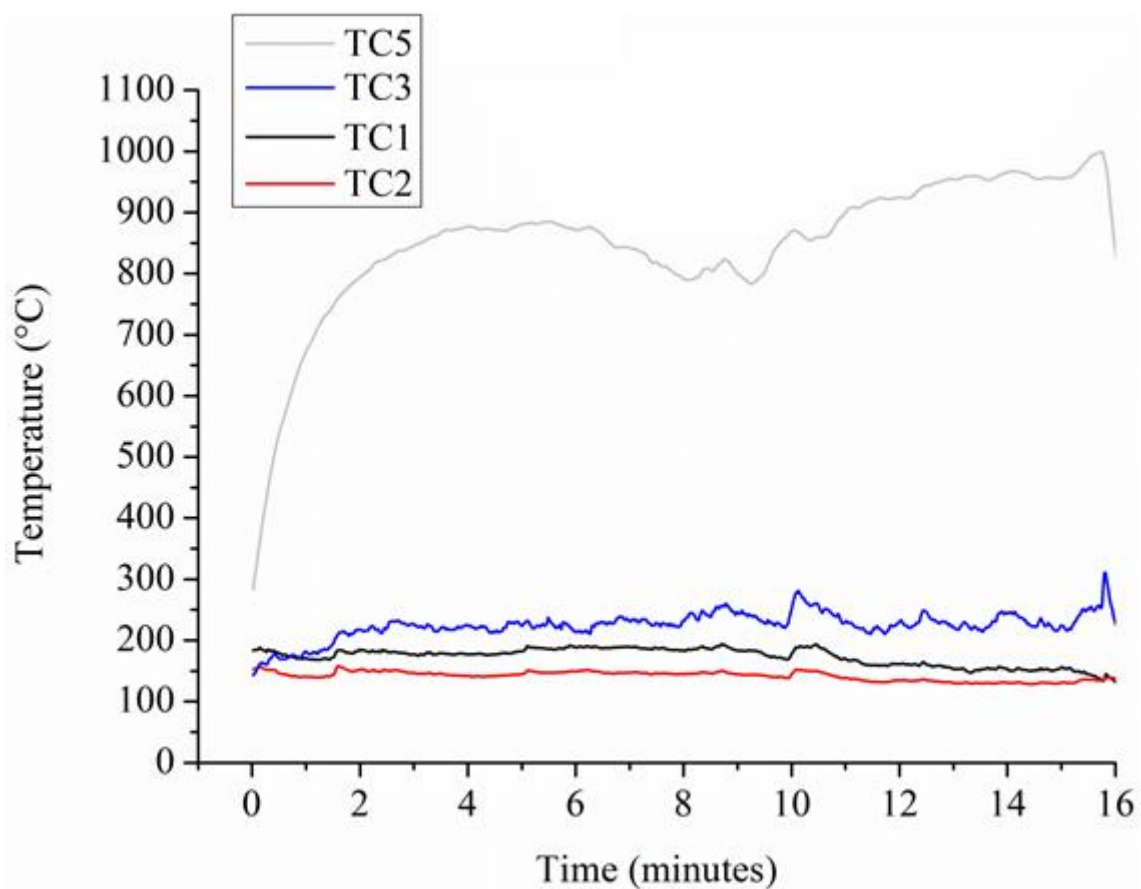
Figure 4.17 – Internal burner temperature with increasing flow rate of air

Figure 4.17 shows a rapid initial increase in the flame temperature. The larger flow rate of propane, compared with cases A and B, meant the flame was longer in length. The high temperature thermocouple was totally engulfed by the large orange flame thus the temperature was greater than in previous cases. The temperature recorded by TC5 dropped slightly after 6 minutes only to increase again at 9 minutes. In a similar fashion to case B this was most likely caused by the flame decreasing in size so that it no longer touched the thermocouple. The

flame temperature increased at 9 minutes when the value for λ was 0.36 which also coincided with the flame changing to a stable blue flame.

The temperature at the front of the burner unit which are monitored by TC1 and TC2 stay relatively constant throughout the experiment. This is similar to the temperature profiles in cases 1 and 2 where the temperature in this area of the burner system remains constant despite the size and structure of the flame.

Case D: Propane flow rate 2.6 (LPM) - Air mover open

The air mover at the front of the burner was then opened. With the air mover open there should be recirculation of combustion gases back through the burner which should increase the temperature at the base of the burner unit.

In case D the flow rate of propane was set at 2.6 LPM. The initial value for λ was set at 0.15. The flow rate of propane was 0.16 m^3/hr and the flow rate of air was 0.6 m^3/hr. The flame at these conditions was long and orange. The flame began to change in colour and reduce in size when the value for λ was increased to 0.25 (9 minutes) at this value the flame was green at the base and the flame was mainly blue with hints of yellow. The flame became a smaller dark blue flame once the value for λ increased to 0.37 (21 minutes), when compared to case A the value at which the flame became stable and totally blue was reduced. In case A the flame stabilised when λ was equal to 0.62, this suggests that a significant volume of air was entrained back through the flame region and back through the burner.

The blue flame started to move away from the plate of the burner when λ increased to 0.46 (30 minutes). The flame extinguished when the value for λ was 0.53.

Figure 4.18 indicates the difference in temperature monitored by TC5 and indicates the difference the mixing vessel makes when it was open and closed. Table 4.6 shows the values for λ in relation to Figure 4.18 as time increased.

Time (minutes)	0	3	6	9	12	15	18	21	24	27	30	33
λ	0.15	0.19	0.22	0.25	0.28	0.26	0.34	0.37	0.40	0.43	0.46	0.49

Table 4.6 – Value for λ and resulting time
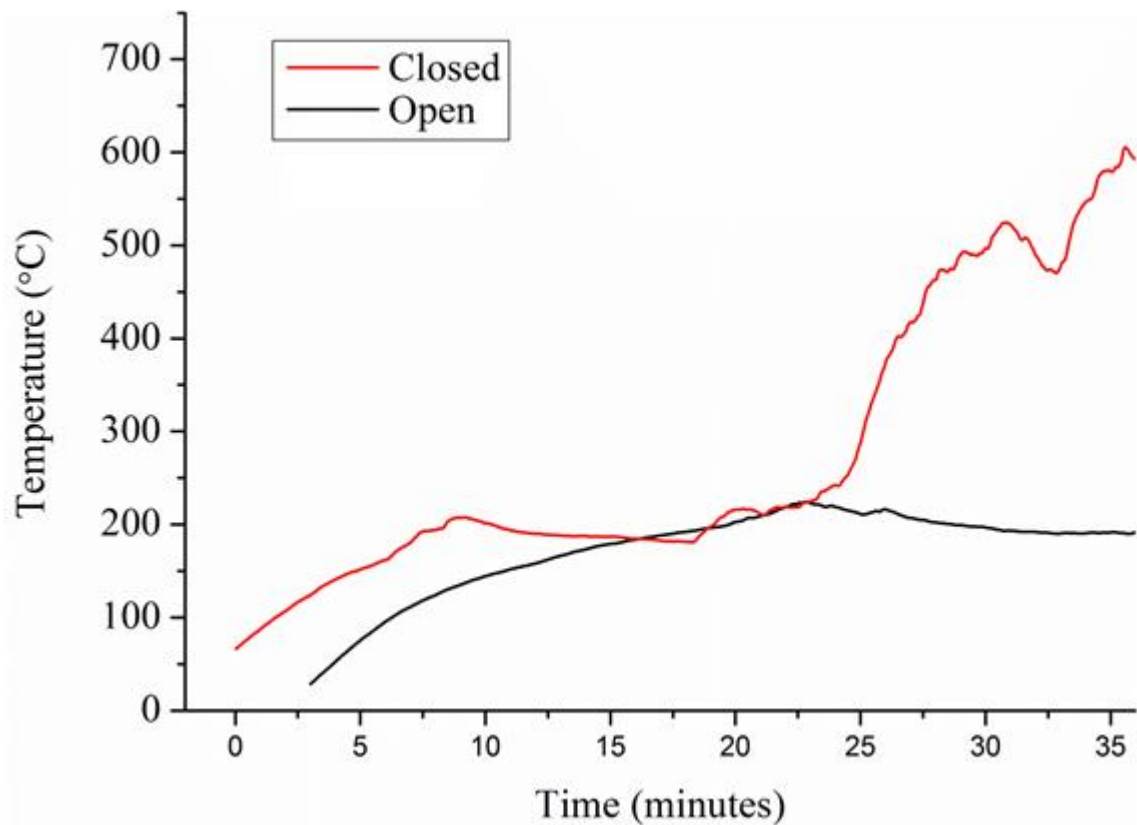
Figure 4.18 – Comparison between temperature recorded by TC5 when the recirculation chamber is open and closed

The key difference between the temperature recorded by TC5 was when the value for λ is 0.40 after 24 minutes at this point the temperate recorded when the recirculation chamber is open the temperature increased rapidly and when the chamber was closed there was a small decrease. The flame at this point, for the open set up, was small, dark blue and stable. The increased temperature could have been caused as the Coandă ejector entrained more gaseous species, including air through the burner unit. As the flow rate of air inserted to the Coandă increased the amount of gas entrained also increases, when the recirculation unit is closed the only gas that can be entrained is the propane as it is inserted into the inlet, but when the unit is open, surrounding gases can be entrained back through burner. It is likely that oxygen contained within air, surrounding the burner system, was entrained thus increasing the air to fuel ratio so that the flame became a stable and blue, despite the value for directly supplied air/fuel ratio being the same.

Case E: Propane flow rate 3.9 (LPM), Air mover open

For case E the flow rate of propane was increased to 3.9 LPM. The flame was long and orange when the value for λ was 0.12, 0.14, 0.16 and 0.19. The flame changed to a mostly blue flame with an orange flame when λ was 0.21 after 12 minutes. The flame became stable and blue when λ was increased to 0.27. The flame remained small and blue until the flow rate

89

of air was increased to 42 LPM (2.4 m³/hr) at this point the flame started to come away from the plate of the burner, the flame extinguished when the air flow rate increased to 42 LPM. The temperature recorded by the thermocouples in the burner can be seen in Figure 4.19.
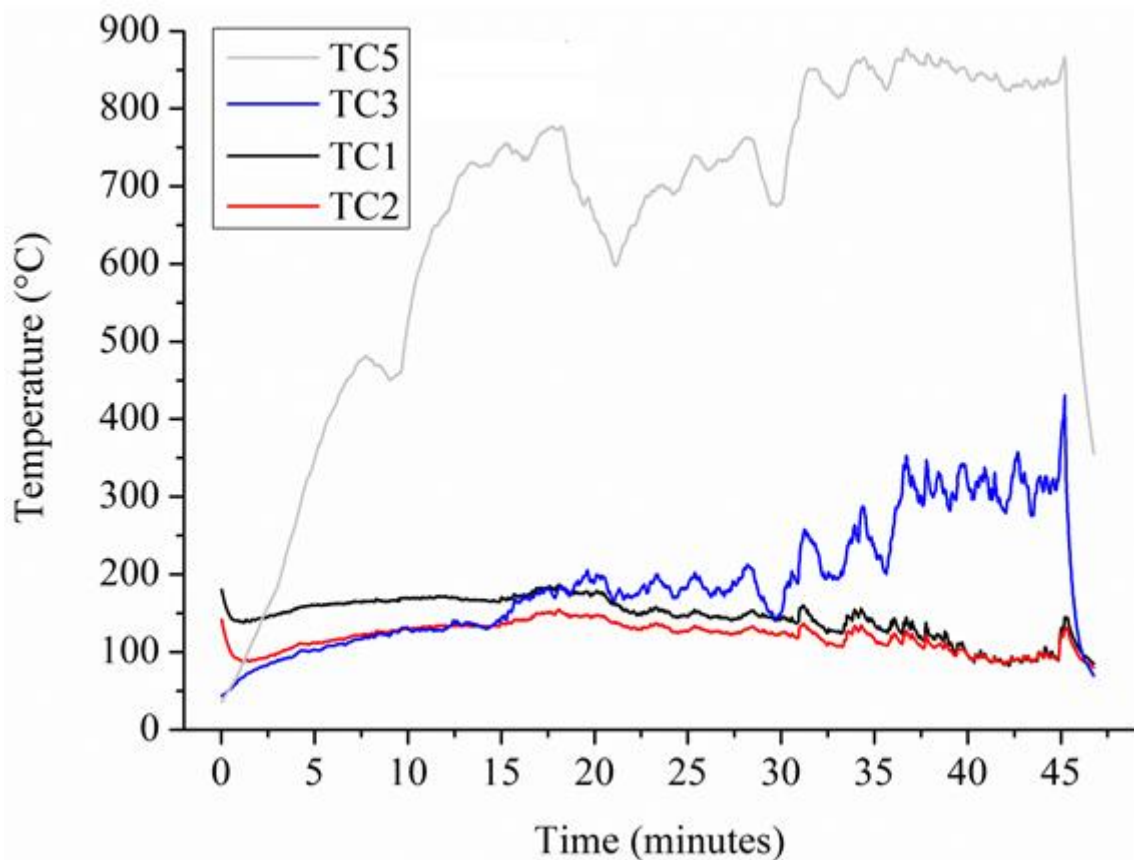
Figure 4.19 – Internal burner temperature as the flow rate of air increased

Case F: Propane flow rate 5.3 (LPM), Air mover open

The final run of the burner system had a propane flow rate of 5.3 LPM (0.32 m³/hr). The flame started off as orange and long as the flame fuel rich. The flame changed colour from orange to blue when λ was increased to 0.22. The flame became a roaring and stable blue flame when λ reached 0.31 after 30 minutes. The flame remained in this state until the flow rate of air was increased to 50 LPM (3 m³/hr) at this point the blue flame began to come away from the plate and eventually went out, whilst the value for λ was 0.37.

4.2.4 Summary of the Burner Results

Six different cases for the burner were analysed. The main focus of the experiment was to determine flame shape and structure at different primary stoichiometric values and to determine the performance in the design of the burner. Soot formation in flames normally results in orange or yellow luminous flame (Gaydon & Wolfhard, 1979). The Coandă burner tested showed that a high temperature blue flame could be produced in primary sub-

stoichiometic conditions. In cases A, B and C when the mixing vessel was closed, only air and propane were supplied into the burner the value for λ at which the flame changed from a flickering orange flame to a smaller blue flame were 0.40, 0.37 and 0.36 respectively.

In cases D, E and F the mixing vessel was open so product gases from the burner could be recirculated back through the burner. In these cases the value for λ at which the flame colour changed were 0.25, 0.21 & 0.22. These calculated values are lower than those compared with the cases set in a closed environment. This suggests that oxygen contained within the surrounding air is entrained back through the burner. When comparing the temperature recorded in cases A and D (Figure 4.18) there is a significant difference once λ reached 0.40 after 24 minutes. In case D the recorded temperature increased substantially and case D remained the same. The design of the outer casing may need to be altered to prevent oxygen in the surrounding environment from entering the burner. The length of the outer casing could be increased or funnelled to prevent oxygen from entering the system.

The design of the burner worked well. There were no problems with igniting the fuel. One area for re-design is to modify the burner/flame stabiliser. This part was designed for propane to have a propane inlet at the front. The inlet was a 10mm hole designed to hold the stainless steel pipe feed in place. This inlet is most likely affecting the flow regime in the burner.

4.3 Pyrolysis of Wood Pellets

4.3.1 Experimental Setup - Pyrolyser

Figure 4.20 shows a schematic diagram of the pyrolyser used for the experimental work and Figure 4.21 shows a photo of unit. The pyrolyser was originally constructed and used in a previous project by Jim Goodfellow. For this project the pyrolyser underwent various modifications so that it was suitable for the experiments. The pyrolyser was primarily designed to produce a tarry gas which was suitable for use in the CTC; hence the design of the pyrolyser was kept simple and easy to operate.
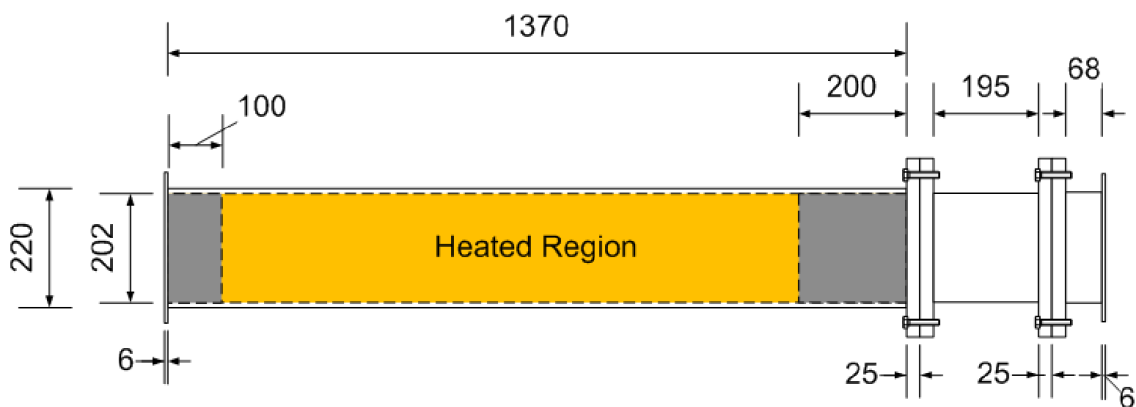
Figure 4.20 – Schematic of the pyrolyser

Figure 4.21 – Front view of the pyrolyser with upper heater raised

Pyrolysis chamber

The pyrolysis chamber has a cylindrical tube placed horizontally and held in position by a supporting frame. The pyrolysis chamber consisted of an 8 inch nominal bore schedule 40 tube. The thickness of the tube walls was 8 mm, the outer diameter was 220 mm and the inner

diameter was 204 mm. The tube was 1370 mm in total length and is made from 316 stainless steel. The pyrolysis chamber has an internal volume of 0.044m^3.

Heating Elements

The pyrolysis chamber was heated by 6 heating elements. The units are helically wound semi-cylindrical ceramic heaters and are rated to temperatures up to 982°C. The heating units were purchased from Omega Ltd, for more information see Omega Engineering Ltd (2012). The heaters were controlled by a central control unit which allowed for the temperature of the heaters to be set to a specific temperature. The 6 heating units surrounded the cylindrical pyrolysis tube and provided external heating. The combined length of the heating system was 1146 mm when the heating units were put together. The heating elements did not surround the whole length of the pyrolysis chamber; at the solid feed end there was a gap of 101 mm and at the gas exhaust end there was a gap of 101 mm. The heating elements used are shown in Figure 4.22 and Table 4.7 indicates the specification of the heaters.
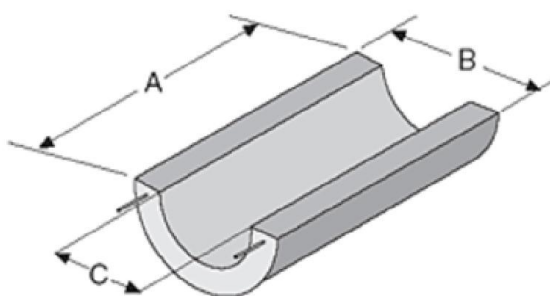
Figure 4.22– Semi-cylindrical heating elements Omega Engineering Ltd (2012)

No of Units	Watts	Volts	Model Number	Dimensions (mm)		
				A	B	C
4	2250	240	CRWS-1210/240-A	300	360	250
2	3400	240	CRWS-1810/240-A	460	360	250

Table 4.7 – Specification of the heaters

Fuel Tray

The pyrolysis unit was designed for batch reactions. A measured sample of wood pellets was placed inside a fuel tray which was then loaded into the pyrolyser. The fuel tray is shown below in Figure 4.23. The tray was 920 mm long, 72 mm wide and 72 mm high.

Figure 4.23 – Fuel tray

Butterfly Valve

At the exhaust end of the pyrolyser there was a butterfly valve situated in a pipe to connect the pyrolyser to the Coandă tar cracker. The butterfly valve was used to gain greater control of gas flow exiting the pyrolyser. When the valve was opened more pyrolysis gas would exit the unit. The outer diameter of the pipe was 127 mm. The length of the pipe was 220 mm and the butterfly valve was situated 125 mm from the flange at the pyrolysis end, see Figure 4.24.
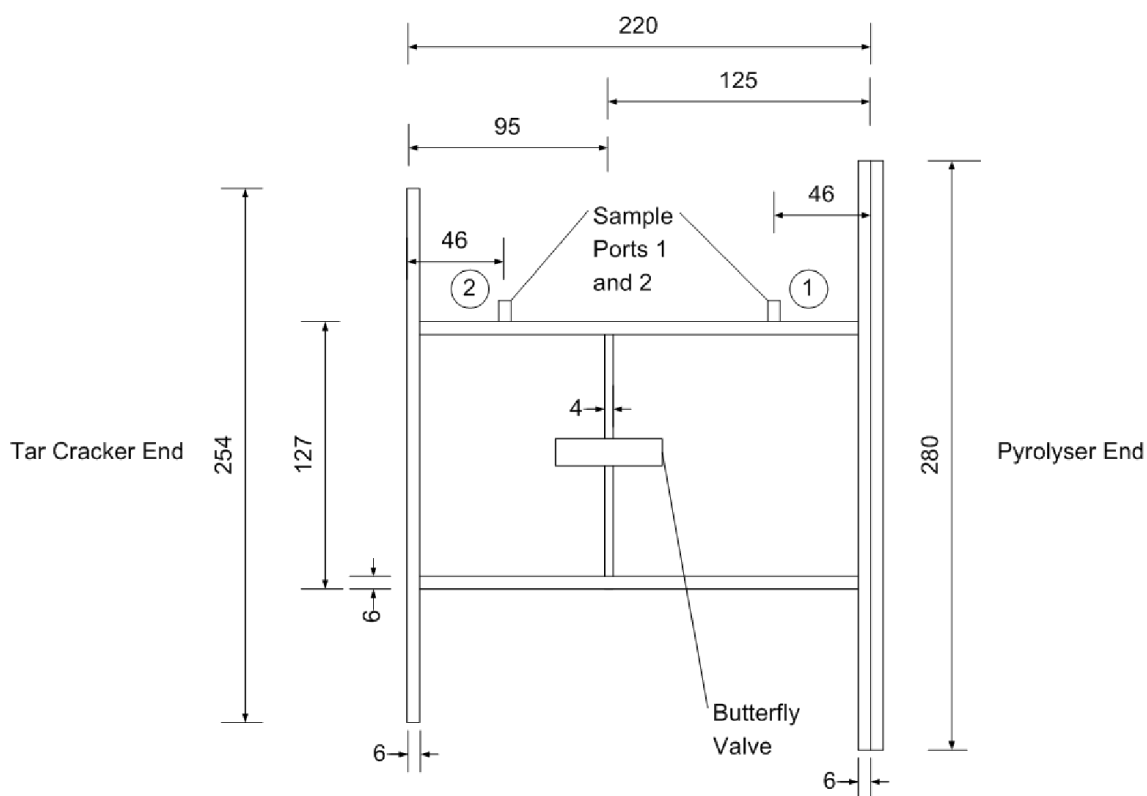
Figure 4.24 – Dimensions of the pipe containing the butterfly valve (All values in mm)

The pipe containing the butterfly valve had flanges on either end allowing for this unit to connect to the pyrolysis chamber and the tar cracking unit. The flange at the pyrolysis end had 6 holes and had a diameter of 280 mm. At the opposing end the flange has 12 holes and had a smaller diameter, 254 mm. The section of pipe that contained the butterfly valve was designed

94

to be as short as possible to reduce the gas residence time from the pyrolyser to the tar cracking system and to prevent tar contained within the gas from cooling and condensing. The pipe has two sampling ports (1 and 2); pyrolysis gas can be taken from these ports and analysed.

Tar Trap

Due to the nature of the operation, the gases produced from the pyrolyser will contain condensable tar. To collect tar for analysis a tar trap was designed. The tar trap was based on recommendations from a technical report by Good et al. (2005) but does not follow the report exactly. A technical drawing for the tar trap is shown in Figure 4.25. The tar trap accommodated six connected impinger bottles which were filled with isopropanol or glass wool to capture condensable material for further analysis and also prevented condensable species from entering the gas chromatograph. Isopropanol (propan-2-ol) was the solvent recommended by Good et al. (2005) as it is less toxic than alternatives such as dichloromethane.
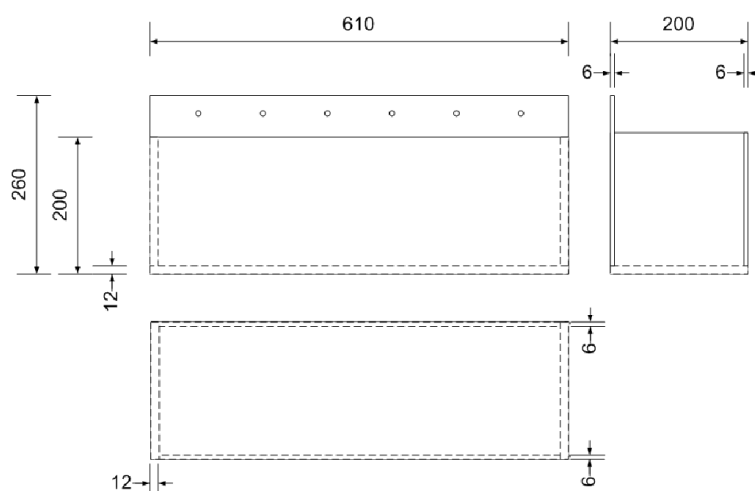
Figure 4.25 – Technical drawing of the impinger tar trap (All values in mm)

Figure 4.26 – Impinger tar trap

Bursting Disc

A bursting disc was installed at the opposite end of the reactor from the tar cracker. The disc was made from graphite and was 4 mm thick. The bursting disc was designed so that it could be quickly attached and removed from the loading end of the pyrolyser. This allowed for quick loading of the fuel tray into the pyrolyser. If the pressure inside the pyrolyser became too high, the bursting disc would burst to direct the contents of the pyrolyser away from the operator.

Purge Gas

Nitrogen gas was purged into the reactor to create an inert, oxygen free atmosphere. The flow rate of nitrogen was controlled by a FL-2014 series acrylic flow-meter purchased from Omega Engineering LTD. The range of the flow meter was 0-10 LPM.

ABB Gas Chromatograph

The gas chromatograph system used to analyse the gases being produced from the pyrolyser was manufactured by ABB, the model number was PGC2000. A thermal conductivity detector (TCD) is used on the column. TCD filaments work on the basis that a heated body loses heat at a certain rate depending on the surrounding gas and its composition. The rate of heat loss is monitored by the filament so that any change results in a proportional change in the bridge output.

Both a reference and measurement filament are used in the TCD. A reference carrier gas flows across both the reference and measurement filaments so that both filaments indicate the same temperature and thus a zero output is shown on the bridge. When the analyser is run the gas sample flows past the measurement filament and, depending on its composition, changes the thermal conductivity and hence the temperature of the filament, which results in a change in the electrical resistance. The bridge monitors and senses the change in current and then either increases or decreases the current flow through the bridge to compensate. The change in current flow to the bridge is proportional to the concentration of the component in the sample.

Three carrier gases were used: nitrogen, hydrogen and helium. The carrier gases purge the columns and sweep the detector in the detector cell as well as flushing the columns. The pressures of the carrier gases were set according to the manual. Nitrogen was set at 49.5 PSIG, helium to 88 PSIG, hydrogen to 57.5 PSIG and the air supply was set at 60 PSIG.

The accuracy of the analyser depends on the accuracy of the calibration gas used to calibrate the unit. In this case the accuracy of the calibration gas is 5%. The GC was calibrated before

each experiment. There are 7 components of interest in the experiment (hydrogen, nitrogen, methane, oxygen, carbon monoxide, propane and carbon dioxide). These components are measured on two method tables that run at the same time on a master and slave loop, Table 4.8 and 4.9 indicate the measured component and the method table it is analysed on.

Method Table 1		
Component	Calibration Gas Concentration (mol.%)	Time of Analysis (seconds)
H_2	30	092
O_2	2	177
N_2	77.4	204
CH_4	8	271
CO	20	303
Method Table 2		
CO_2	20	185
C_3H_8	1	415

Table 4.8 – Measured components and relative calibration gas concentration

Method Table 1		
Valve	Time Valve Opens (seconds)	Time Valve Closes (seconds)
1	5	90
2	35	111
3	390	520
4	35	285
Method Table 2		
5	5	310

Table 4.9 – Gas chromatograph valve opening and closing times

Five internal valves control the injection of the sampled gas into 10 internal columns. On the master loop valve 1 injects five seconds after the analysis is started. This is for the measurement of hydrogen. Valve 1 closes after 90 seconds. Valve 2 and 4 open at 35 seconds, valve 2 closes at 111 seconds and valve 4 at 285 seconds respectively. Valve 3 opens at 390 seconds and closes at 520 seconds. On the slave loop valve 5 injects after 5 seconds and then closes at 310 seconds, carbon dioxide and propane are the two components analysed on this

loop. Valve 2 provides the sample so that oxygen and nitrogen can be analysed and valve 4 allows for the analysis of methane.

4.3.2 Experimental Procedure

Figure 4.27 shows the flow diagram of the pyrolyser. The main issue with the pyrolyser was dealing with the tarry gas that was produced in regard to its collection and preventing tar in the gas from entering the gas chromatograph and interfering and blocking the molecular sieves in the column.
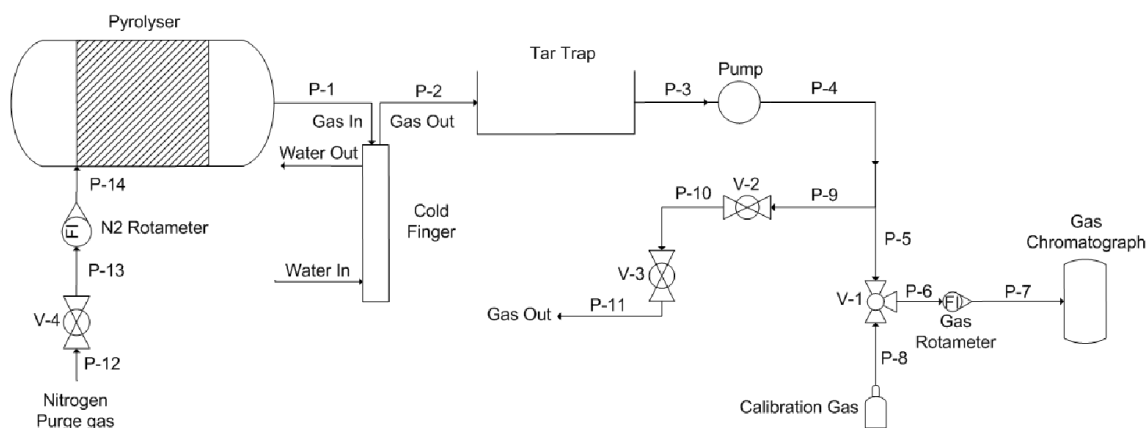
Figure 4.27 – Flow diagram of the pyrolyser

Start-up Procedure

1. The gas chromatograph was switched on, purge gases of helium, nitrogen and hydrogen were turned on at flow rates designated by the ABB gas chromatograph manual. Air was supplied to the gas chromatograph and heated so the internal components were heated to 140°C. The gas chromatograph was left to warm up for a minimum of two hours. The stability of the unit was checked by monitoring the reactor temperature and the detector reading which both have to be stabilised to ensure accuracy.

2. Once the gas chromatograph has reached a stable point a calibration test was ran according to the operator's manual.

3. The pyrolyser is then turned on and the desired temperature set (500, 600, 700 or 800°C) and then left to heat. The temperature of the pyrolyser tube is monitored by a k-type thermocouple which is situated at the base of the unit and in direct contact with the internal chamber.

4. Five of the six impinger bottles were filled with 200 ml of isopropanol and the sixth was packed with glass wool to remove tar from the pyrolysis gas. All the pipes were checked to ensure that they were connected securely.

5. The extraction unit was turned on.

6. Water to the cold finger was turned on.

7. When the pyrolyser had reached the desired temperature nitrogen is purged to the pyrolyser (Opened V-4). The flow rate was set at 8 LPM by a rotameter and the pyrolyser was left to purge for 10 minutes.

8. Wood pellets were then weighed out into the fuel tray. For each experiment 250 grams of the fuel was used as this provided a reasonable amount of tarry pyrolysis gases without overloading and over pressuring the pyrolysis chamber.

9. The fuel tray was loaded into the pyrolyser. The bursting disc was removed to allow for the loading. Once the fuel tray was in the pyrolyser the bursting disc was re-attached.

10. 30 seconds after the wood pellets were loaded the sample pump was tuned on. A gas sample was taken from sample port 2 shown in Figure 4.24.

11. The gas travelled down a stainless steel pipe with an internal diameter of 4mm and external diameter of 6mm (P-1). The gas is then cooled by a flow of running water. Moisture and tar that are contained in the gas drop out and into a collection vessel at the base of the cold finger. The gas is then brought through the impinger bottles in the tar trap where tar was captured by the solvent.

12. Gas that was released at P-11 was monitored by a flame. When the gas flowing out ignited and there was a small steady flame valve 1 was opened to allow the cleaned pyrolysis gas into the gas chromatograph. A steady flame normally took about 2 minutes from when the pump was turned on to appear.

13. A rotameter was used to monitor the flow rate of the sample gas. For accurate results the gas chromatograph requires the flow-rate of the calibration gas to be the same as the measured gas. For all of the experiments in this section the rotameter was set so the flow-rate was 20 cm^3/min (0.0012 m^3/hr). Valves, V-2 and V-3 controlled the flow-rate of pyrolysis gases through the rotameter and into the gas chromatograph for analysis. If both V-2 and V-3 were closed all the pyrolysis gas will flow into the gas chromatograph.

14. The gas chromatograph is then started to analyse the gas sample.

15. After 90 seconds of gas flow into the gas chromatograph the pump was turned off.

16. Once the gas chromatograph has performed the analysis the gas concentrations were recorded.

Shut-Down Procedure

1. The electric heaters were turned off. And the pyrolyser left to cool to ambient.

2. The gas chromatograph was turned off and left to cool. The carrier gases remained on for 30 minutes providing a purge to the internal parts of the gas chromatograph.

3. The water supply to the cold finger was turned off and the collected condensable phase (tar and moisture) collected for further analysis.

4. The purge gas to the pyrolyser was turned off

5. The extraction unit was turned off.

6. Isopropanol and collected tar in the impingers in the tar trap were collected for further analysis.

7. Once the pyrolyser had cooled to ambient the fuel tray was removed and a sample of the wood pellet char collected for further analysis.

4.4 Experimental Issues

4.4.1 Errors with Gas Analysis

From the first run of the pyrolysis experiment a number of errors became apparent. The main issue was the total run time of the procedure which was not long enough to produce a sustained sample of product gas for analysis by the gas chromatograph. This issue with the supply of gas from the pyrolysed wood pellets would also prevent the CTC running smoothly, as the fuel to feed the desired flame would not be available.

The pyrolysis experiments were performed using a batch loading system. Wood pellets were loaded into the pyrolyser and heated in the reactor. Two minutes after the initial loading a dark grey gas became visible; the gas would exit the pyrolyser through the butterfly valve and be vented through the extraction unit. The grey coloured pyrolysis gases would continue to be produced and appear visible for about 6 minutes after the pellets were initially loaded, giving a four minute window for a gas sample to be taken.

The pyrolysis gases appeared darkest and most prominent between three and four minutes from the initial loading point. Therefore there was only a short time space, less than six minutes, to take a sample of the gas from the pyrolyser and have it analysed by the gas chromatograph. This was an issue due to the operation of the gas chromatograph. The equipment is designed to monitor and analyse the gas composition of continuous processes so its accuracy when used to analyse one sample becomes questionable. Due to the 6 minute window for a sample to be taken and the total run time of the gas chromatograph was nine and half minutes only one incomplete sample of gas could be analysed per experiment. Table 4.10 shows the relationship between the key sampling mechanisms into the gas chromatograph and a visible description of the pyrolysis gas produced.

Action	Time (Seconds)
Load wood pellets into pyrolyser	0
Visible pyrolysis gases exiting reactor	120
Turn on pump for sampling	120
Start gas analysis	210
Valves 1 and 5 in the gas chromatograph opens	215
Valves 2 and 4 in the gas chromatograph opens	245
Valve 1 closes	300
Valve 2 closes	321
Visible pyrolysis gases are reduced	360
Valve 4 closes	495
Valve 5 closes	520
Valve 3 opens	600
Valve 3 closes	730
Gas analysis ends	780

Table 4.10 – Key times for pyrolysis gas sampling

Another problem with the pyrolysis being batch and the gas analyser designed for continuous sampling is that it was difficult to select a certain time at which the sample should be taken. The pyrolysis of wood pellets into permanent gases and condensable gaseous species is affected by the heating rate. The higher the temperature of the pyrolyser the faster the heating rate of the wood pellets would be. Therefore when the pellets were loaded into the pyrolyser at 500°C the pyrolysis reaction was slower when compared with 800°C. In each of the experiments the pump was turned on 2 minutes after the pellets were loaded. From when the

pump was turned on it took roughly 90 seconds for the pyrolysis gases to travel from the pyrolyser through the tar traps and into the gas chromatograph.

Using Table 4.10 it can be seen that valves 1 and valves 2 open and close before the gas production from the pyrolysis of wood pellets has stopped. Valve 1 controls the supply of sample gas for the hydrogen concentration to be analysed. Valves 2 and 4 controlled the gas supply for the analysis of oxygen, nitrogen, methane and carbon monoxide. Valve 5 in the gas chromatograph closed 160 seconds after the visible production of pyrolysis gases has significantly reduced this is most likely the reason why the results for propane and carbon dioxide were not accurate.

4.4.2 Effectiveness of the Cold Finger and Tar Trap

After a number of pyrolysis only experiments were performed, the poor effectiveness of the cold finger and the impinger tar trap was observed. There was a large amount of tar accumulation in the pipe containing the butterfly valve and also in the cold finger which was causing the cold finger to become blocked and thus caused problems with the pump and flow of gas to the gas chromatograph. The pipe containing the butterfly valve was modified so that tar that condensed in this region could be removed more easily.

Tar condensed and then blocked in the cold finger which caused issues with respect to the durability and repeatability of the experiments. After each run of the pyrolyser the cold finger would need to be cleaned with isopropanol to remove the built up tar. Therefore a replacement device was designed and installed where the cold finger had been previously. The design of this unit is discussed in section 5.1.3.

4.4.3 Summary of the Pyrolysis Experiments

The running of the pyrolysis experiments led to a number of issues with the design of the system. The key problem was the length short experimental time caused due to the nature of having a single batch load of wood pellets to the pyrolyser. These experimental issues are addressed in chapter 5.

5. Experimental: System Improvements

5.1 Technical Modifications

5.1.1 Feeding System

A continuous batch feeding system was chosen for the redesign of the feeding mechanism. This modification should allow for a more conclusive analysis of the effectiveness of the CTC system. Firstly; the sampling issues for gas analysis would be solved as the total run-time of the pyrolyser would be extended allowing for one or more complete gas sampling procedures. The total cycle time for gas analysis is 570 seconds (9 minutes and 30 seconds). For a realistic analysis of the gas produced, both by the pyrolyser and in the combined experiment, a minimum of three gas compositions results was required. Therefore the feeding system was designed to be able to provide wood pellets and more importantly the resulting tarry pyrolysis gases for a minimum of twenty-eight minutes and thirty seconds.

There were a number of secondary considerations that affected the design of the system. The feeder should be reliable, simple to operate and work with as few moving parts as possible. Reliability is an issue due to the nature of the pyrolysis environment. The produced tarry gas is likely to condense upon and foul any materials that it comes in contact with, causing damage to equipment, therefore the parts of the feeding system should only be in the presence of the tarry gases for as little time as possible.

The temperature at which the pyrolysis is performed affects the rate at which wood pellets are required to be loaded. The higher the temperature the faster the solid wood pellets degrade into gaseous products therefore the loading mechanism should be able to be controlled so that the loading interval can be changed to suit the pyrolysis temperature. The simplest way to do this is to have the loading mechanism controlled by a human. The final design of the feeding mechanism restricted the amount of time the feeding mechanism was in contact with the tarry gases, was simple to operate and allowed for a change in the loading time interval. A technical drawing for the repeatable batch style system is shown in Figure 5.1.
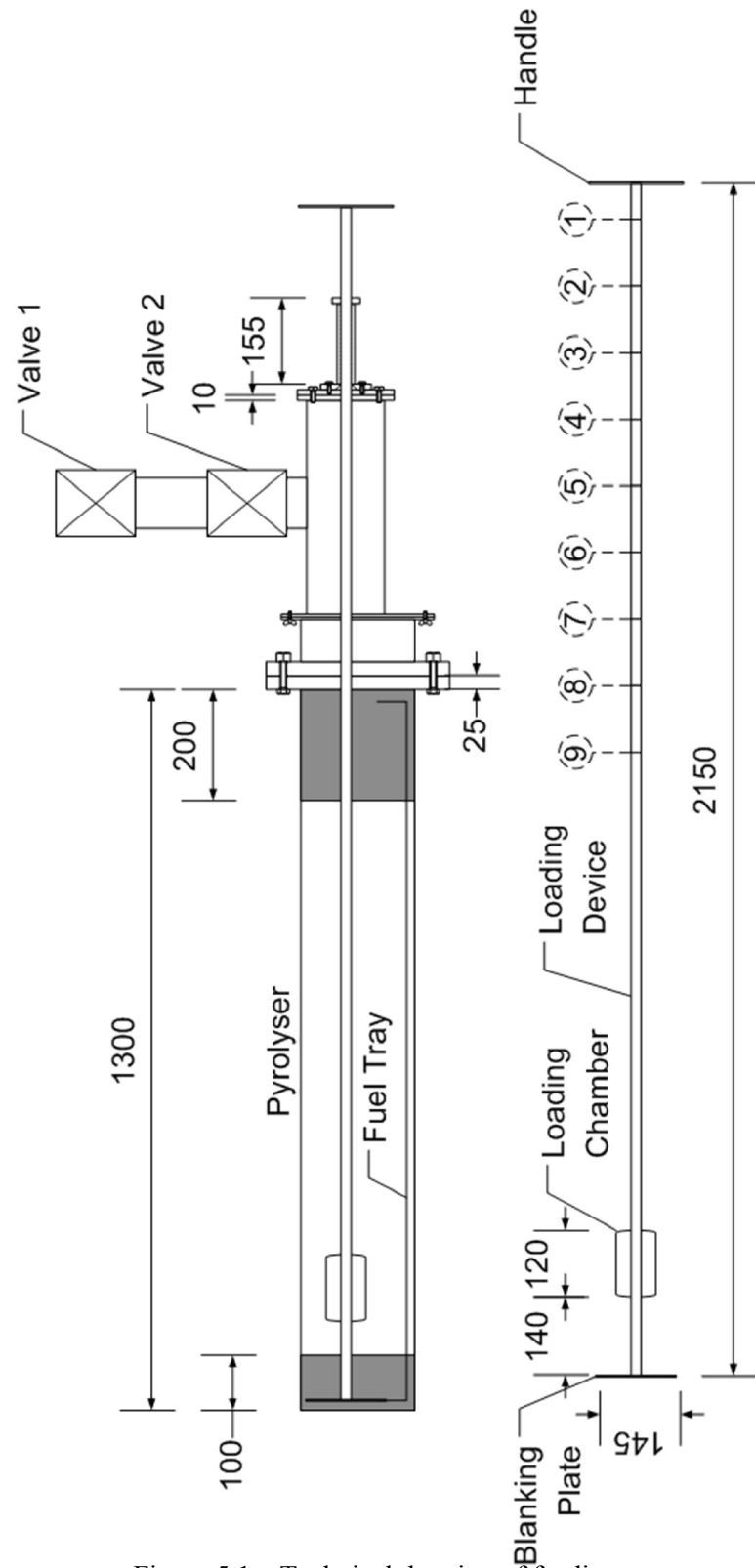
Figure 5.1 – Technical drawing of feeding system

5.1.2 Description of the Feeding System

The feeding system is made up of four key components: loading valves 1 and 2, the loading device, fuel tray and the loading device body.

Loading Device

The loading device is made from a long cylindrical mild steel tube with an outer diameter of 18mm and wall thickness of 2mm. The total length of the unit is 2150mm. At the loading end of the pyrolyser there is a circular blanking plate, made from mild steel which has a diameter of 145mm. The blanking plate was implemented to close off the pyrolysis chamber from the feeding unit. When the loading device is fully withdrawn from the unit the blanking plate becomes flush to the wall where the pyrolyser and feeding system are joined, thus preventing any tarry gases from exiting the pyrolyser, condensing and fouling any equipment. Figure 5.2 shows how the blanking plate works.

Blanking plate – prevents any tarry gases from exiting the pyrolyser and fouling the loading valves.
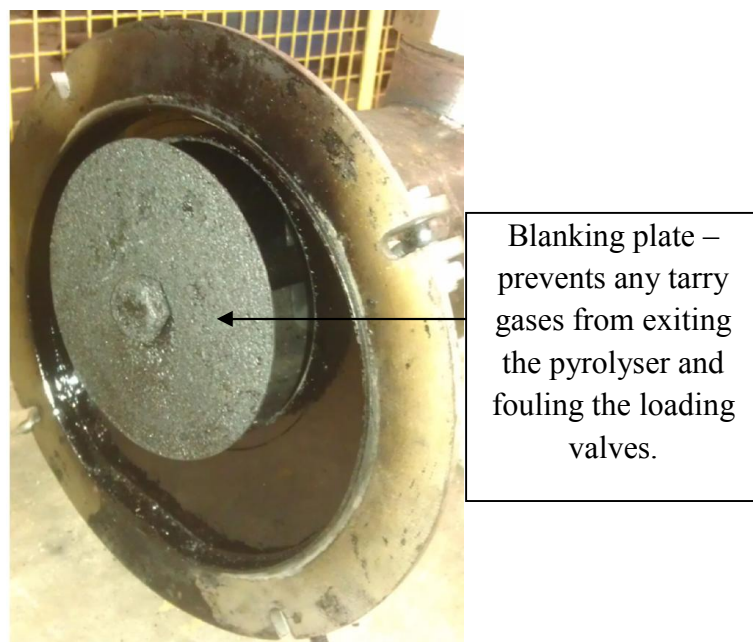
Figure 5.2 – Blanking plate

Figure 5.2 shows how the blanking plate creates an effective seal to prevent tarry gases from leaving the pyrolysis chamber. The photo was taken after less than ten total runs of the pyrolyser. There is a clear build-up of tarry deposits showing the fouling capability of the produced tar.

The blanking plate has a second useful design feature; it prevents the loading device from being pulled out of the pyrolyser and acts as a set point for the loading chamber. When the loading vessel is pulled out of the pyrolyser the blanking plate then shuts against the outer chamber and the loading chamber aligns with valve 1 and 2 allowing for fuel to be dropped into the loading chamber through both valves. This mechanism is shown is in Figure 5.3.
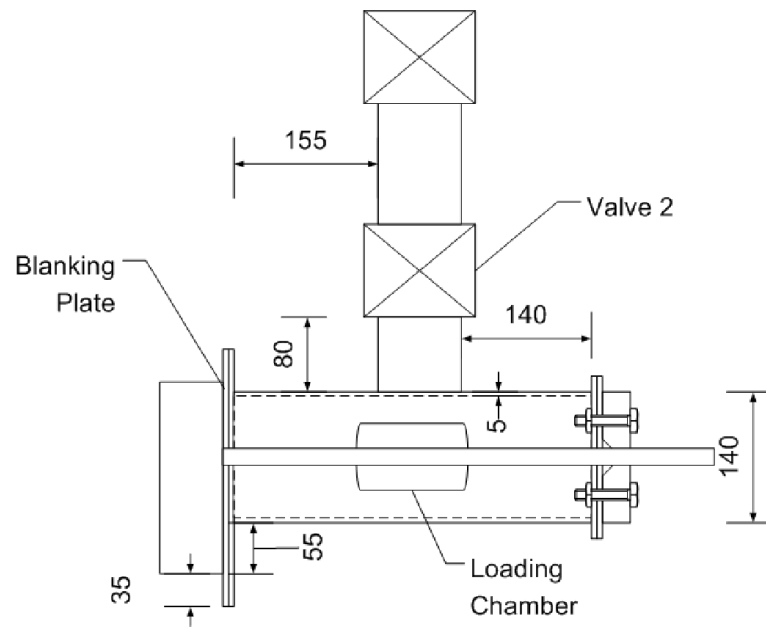
Figure 5.3 – Loading chamber aligned with valves

The loading chamber is made from mild steel. The chamber is 120mm wide with a depth of 105mm. The height of the chamber is 80mm shown in Figure 5.4.
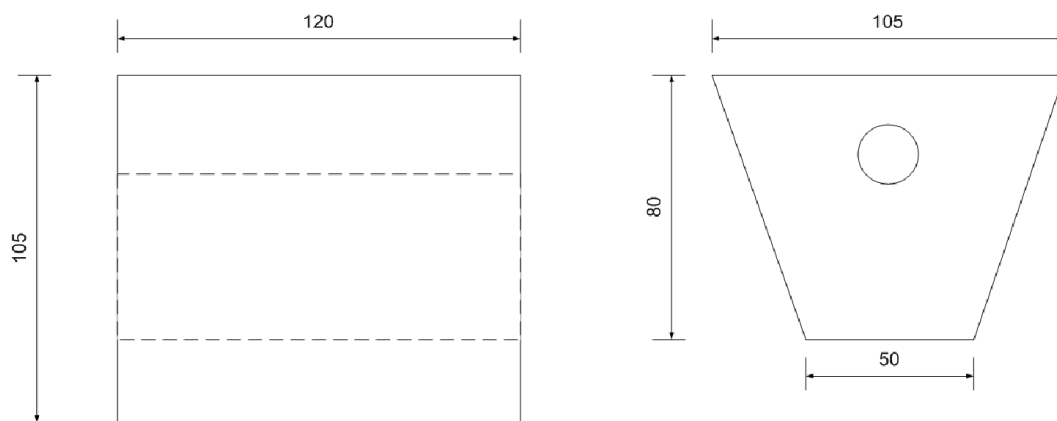
Figure 5.4 – Loading chamber dimensions
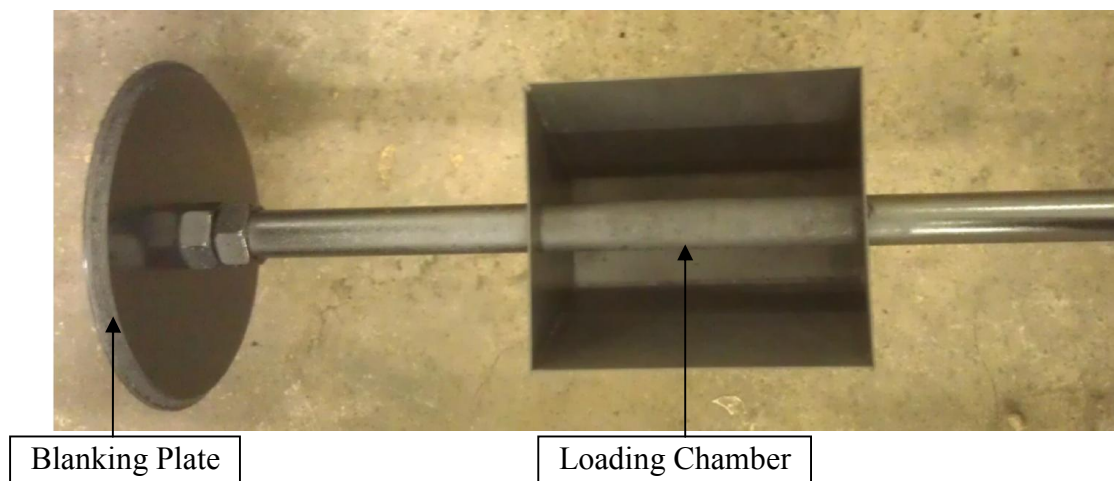
Figure 5.5 – Loading chamber

On the stem of the loading vessel nine set points have been marked. The set points correspond to the position of the loading chamber in the pyrolyser when the wood pellets are loaded into the fuel tray, which is positioned in the pyrolyser. There are 9 loading points in total with a gap of 120mm between each point. Having set points allows for a good spread of wood pellets in the fuel tray and prevents wood pellets building up and spilling over, exiting the fuel tray and touching the hot surface of the inner walls of the pyrolyser. During the operation of the pyrolyser the first batch of wood pellets will be loaded at point 1, the next to point 2 and the process repeated until pellets have been loaded at each of the nine loading points where the process can be repeated. The nine loading points can be seen on the loading device on Figure 5.1.

Fuel Tray

The fuel tray where the wood pellets are loaded is placed inside the pyrolyser before the start of the experiment. The tray can be removed from the loading end of the unit so that char samples can be collected, weighed and analysed. The fuel tray is made from mild steel and is 1420 mm long, 200 mm wide at the top, 116 mm wide at the base and 90 mm high. The wall thickness is 2 mm. The fuel tray is shown in Figure 5.6.
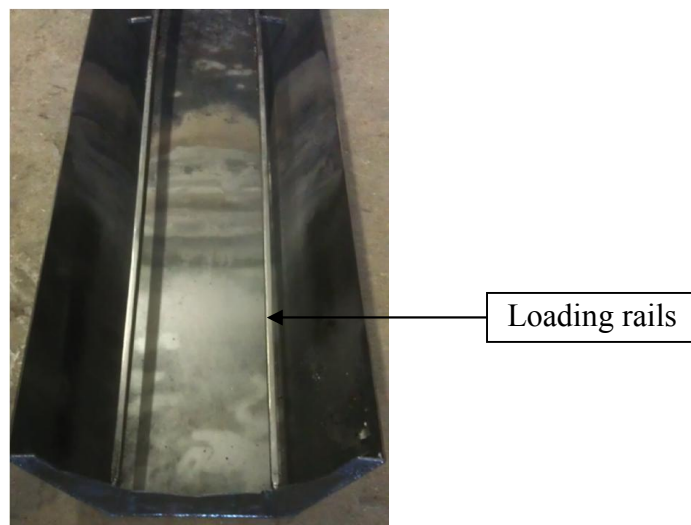
Figure 5.6 – Loading ails on the fuel tray

The fuel tray had two rails placed along the entire length of the unit. The rails were 5 mm wide and 40 mm high. The loading chamber slid along the rails and into the pyrolyser, the central pipe which made up the main body of the loading vessel is above centre on the loading chamber so that when the unit was rotated the chamber rotated without becoming obstructed by the rails thus allowing for wood pellets to be deposited into the fuel tray. Once the chamber was rotated and the pellets were emptied the loading chamber was withdrawn back

to its resting position under the loading valves, with the blanking plate flush and the pyrolysis chamber closed.

Loading Valves 1 and 2

The loading valves prevented any pyrolysis gases from exiting the system and stop air rom leaking into the pyrolyser. Two three inch ball valves were used, the valves are made from brass which has been chrome plated, polytetrafluoroethylene (PTFE) seats were used in the valves, which are pressure rated up to 20 bar. The dual valve system allowed for pellets to be loaded into the system with only a small amount of ambient air entering the system per load. Between valve 1 and 2 was a section of 3" mild steel pipe which was threaded at either end so that the valves were attached to one another. A second section of 3" was welded on to the main body of the feeding system so that valve 2 was connected to the main body of the feeding system.
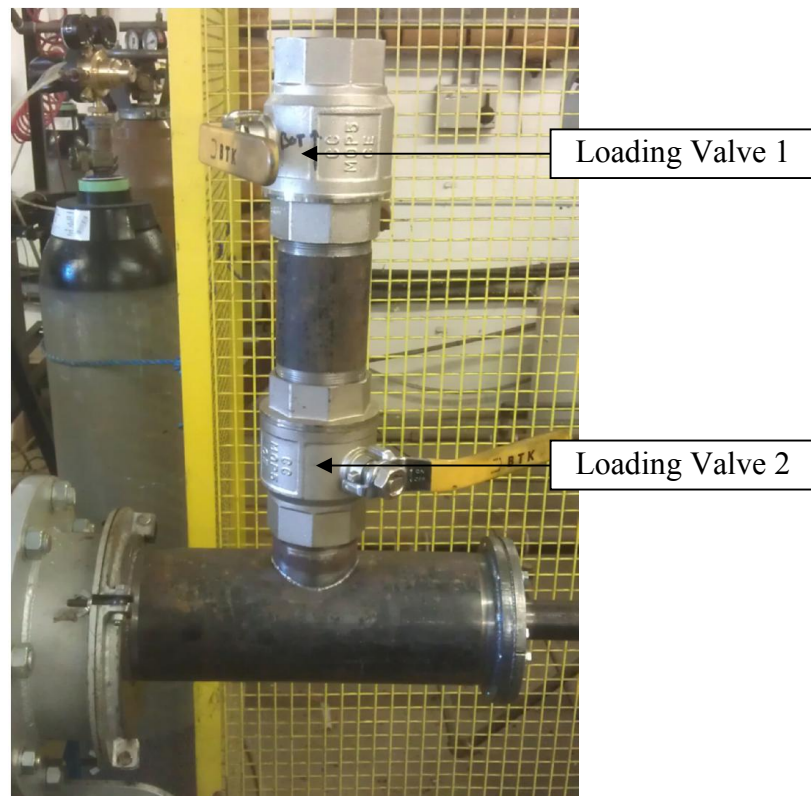
Figure 5.7 – Dual valve feeding system

Stage 1: The designated amount of wood pellets was loaded. Valve 1 was opened and the wood pellets are emptied into the chamber between valves 1 and 2. Valve 1 was then closed. Only a small volume of surrounding air is contained in this region allowing for the minimum amount of interference to the inert pyrolysis environment once the pellets are fully loaded.

Stage 2: Valve 2 was opened and the wood pellets are deposited into the feeding chamber. Valve 2 was then closed.

Stage 3: The wood pellets were now securely in the loading chamber were pushed into the chamber to the desired loading point. The rails on the fuel tray provided support to loading chamber.

Stage 4: Once at the desired loading position the loading chamber was completely rotated. The wood pellets were dropped in to the fuel tray.

Stage 5: The loading chamber was then withdrawn from the pyrolyser and placed in the default position (the blanking plate is flush against the end of pyrolyser and the loading chamber is underneath the loading valves).
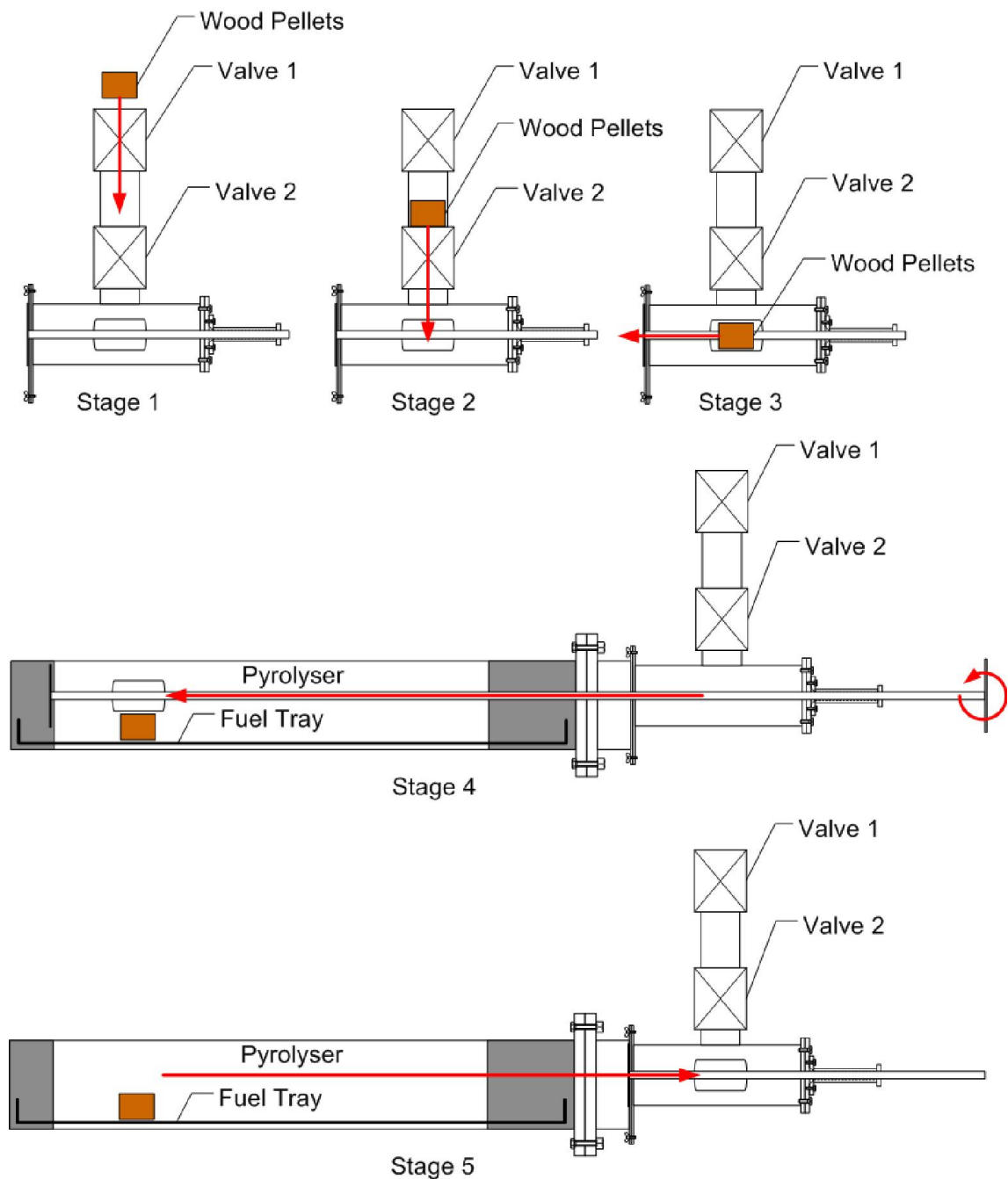
Figure 5.8 – Dual valve feeding method

Feeding Device Body

The main body of the feeding system was made from a 5" mild steel pipe. On the end that connected to the pyrolyser there were four rotating wing nuts. The main body can be easily connected by positioning the two parts together and then tightening the wing nuts. The wing nuts were used to allow for quick access to the pyrolyser to allow for comfortable access to the fuel tray once the experiment had been completed.
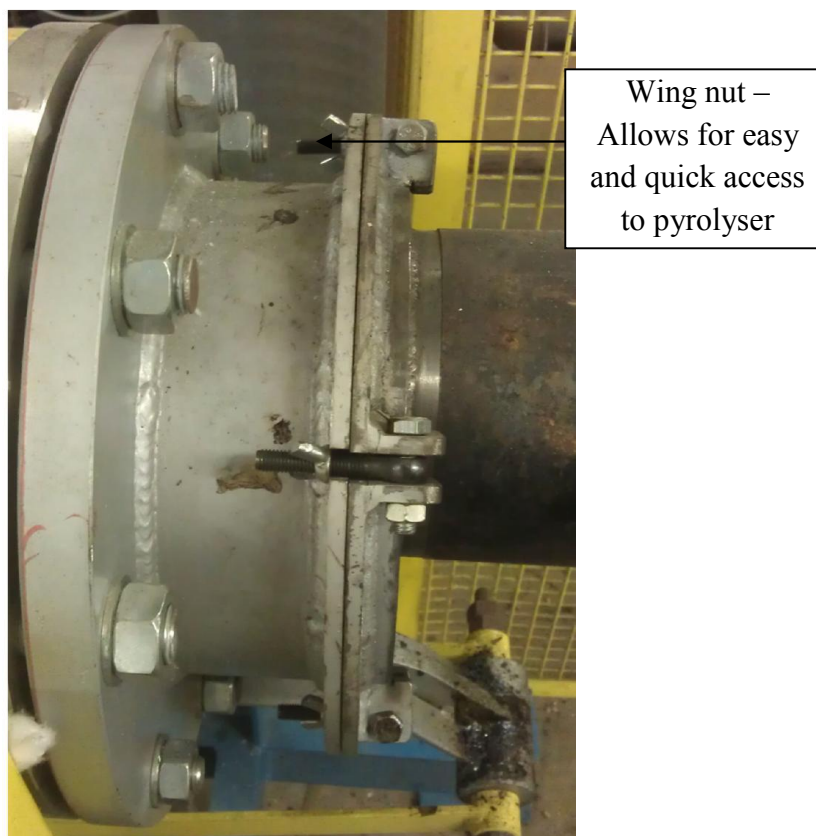
Figure 5.9 – Wing nuts connecting pyrolyser to feeding system

5.1.3 Tar Traps

To improve collection of tars produced, two tar traps were added to the gas and tar sampling lines. Both tar traps were based on the same design. The first of the units contained a water cooled outer jacket to cool the sampled gas. The design of tar trap systems was made so that the gases sampled from the pyrolyser and from after the CTC would have to pass through a larger volume of isopropanol when compared to the original impinger collection system. The water cooled tar trap/cold finger was made up of three pipes of decreasing diameter size, situated within one another. The inner pipe carried the pyrolysis gas to the base of the unit and had an internal diameter of 4mm. The middle pipe contained isopropanol and has an internal diameter of 15.6mm. The outer pipe acted as a water jacket and kept the isopropanol at a reduced temperature suitable for condensing tar vapour found in the gas. At the base of the unit is a ball valve which allowed for the removal of the solvent. A technical drawing of the unit is shown in Figure 5.10. The second tar trap which did not have a water jacket and consisted of the 4mm I.D pipe within the 15.6mm I.D pipe which contained isopropanol.
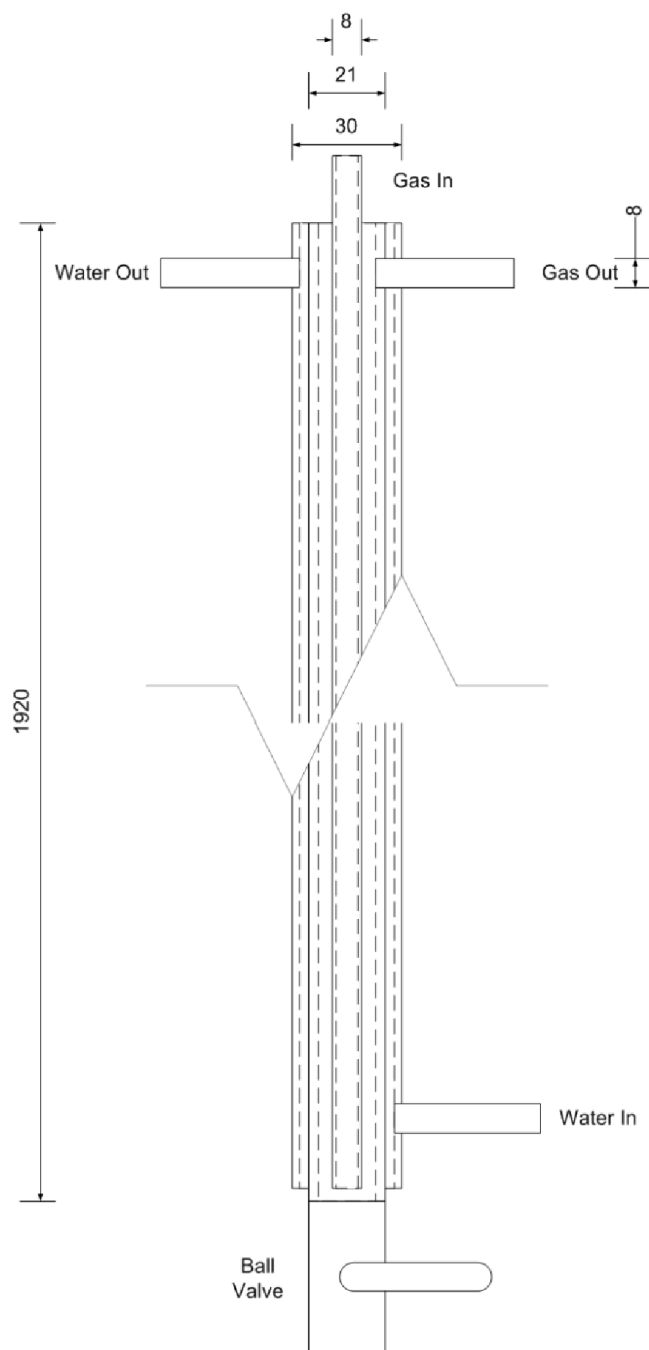
Figure 5.10 – Tar trap/cold finger (All values in mm)

The new tar traps were found to be more effective than the previous method which used a cold finger followed by the impinger tar trap. Further modifications were made to the experimental setup to collect additional data to be used for analysis and comparison. A wet gas meter was installed along the sample line to monitor the amount of gas that was brought through the tar traps. This allowed for calculation into the amount of tar produced per unit of gas and also quantification data for individual tar species. The wet gas meter was positioned after the pump on P18 (see Figure 5.21). The wet gas meter was manufactured by Alexander Wright and measures the amount of gas in cubic feet. The reading for the meter is read and

recorded before and after every run. The accuracy of the wet gas meter is ±0.5% at full scale. The total value of sampled gas was converted into cubic feet to normal meters cubed.

5.2 Combined Experiment

The combined experiment was then commissioned; there were further experimental issues with sampling the treated gas from the end of the burner. The combined experiment was ran with the same burner design setup as describe in section 4.2.1. Gas samples were taken from after the flame in the burner and analysed by the gas chromatograph. The gas results were not as expected with the analyser reading that the sampled gas was found to be air. The sample line was checked for leaks but none were found. The gas chromatograph sampling air was caused by recirculation of air from atmosphere which entered the outer casing. The CTC was redesigned to prevent this from happening. Section 5.2.1 shows the modifications made before the final design was completed.
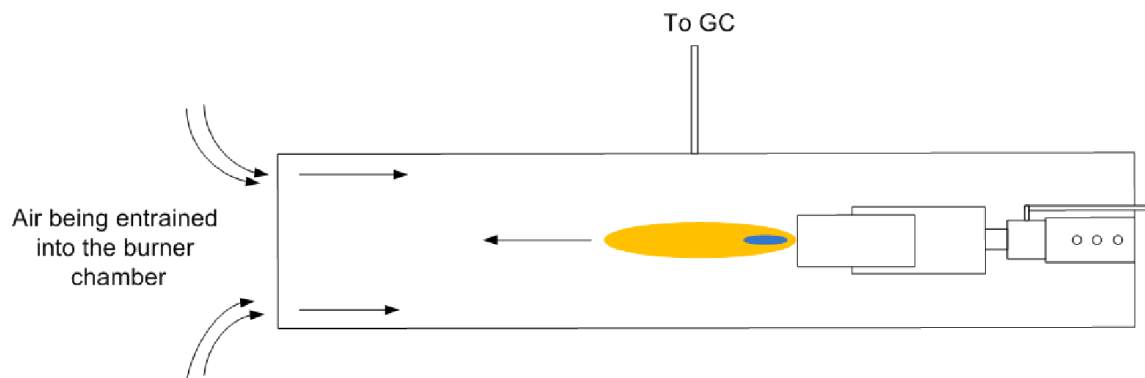
Figure 5.11 – Ambient air entraining into the burner chamber

5.2.1 Modifications to the CTC

Blocking Plate (Version 2)

To prevent the recirculation of air into the burner chamber a blocking plate was made and situated in the outer casing. The plate was made from mild steel and has a thickness of 3mm. The blocking plate fits tightly into the outer casing. The central hole to allow for the exhaust of the gases is 50 mm in diameter. The blocking plate can be seen in Figure 5.13.
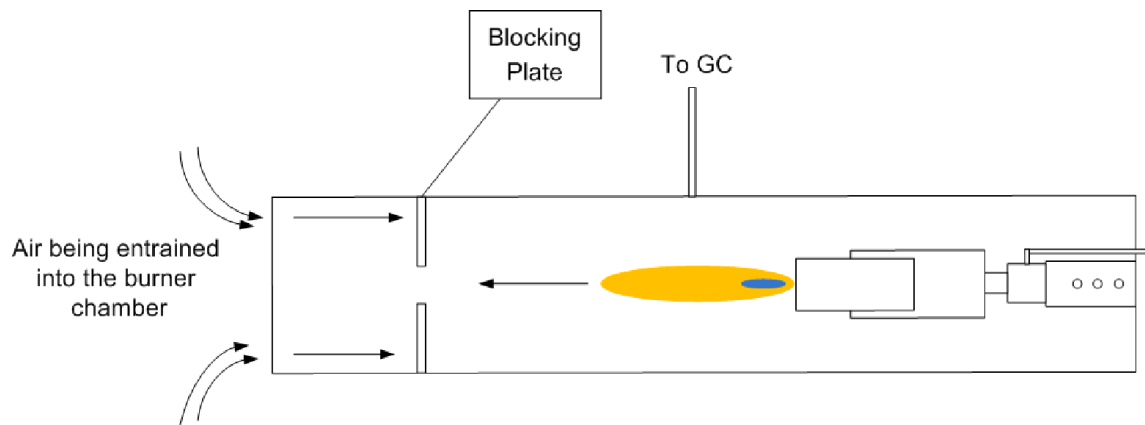
Figure 5.12 – Blocking plate inserted burner outer chamber
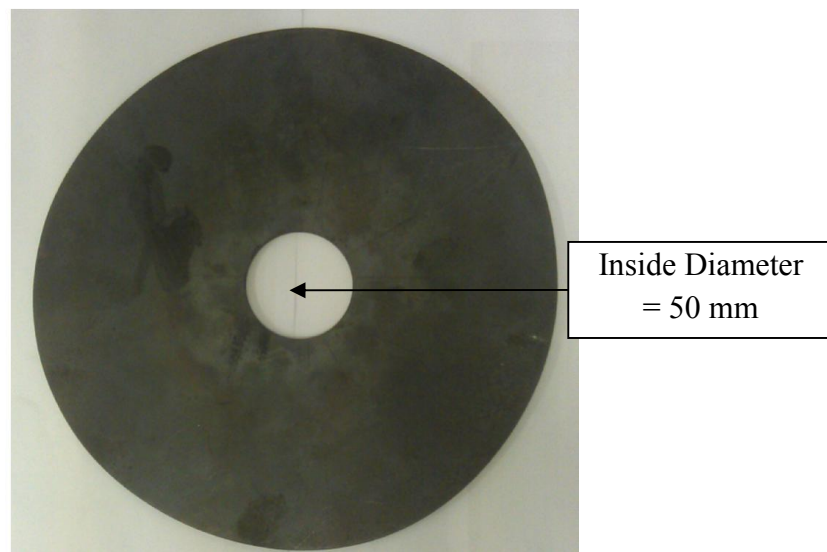
Figure 5.13 – Blocking plate

Despite the changes in the burner design the blocking plate had an adverse effect on the burner. When the burner was ran with propane as the only fuel, the flame would not stay ignited. The burner was using the oxygen from the entrained air to fuel the propane combustion and preventing this oxygen from entering the chamber extinguished the flame. The flame would not stay lit despite increasing the flow of air into the Coandă ejector. It was therefore considered that using a blocking plate to prevent air from entering the burner and being samples was not the way forward and instead a complete re-design of the burner was required.

Tunnel Burner (Version 3)

The burner was redesigned to be a more simple design, similar to the Coandă burners used by Prior, (1977) and O'Nions, (1997). In version 2 of the CTC the Coandă ejector was connected directly to the flame stabiliser by means of a tunnel burner, which was effectively a pipe. The

post Coandă chamber and flame stabiliser were removed. At the end of the burner there was a nozzle to stabilise the flame. A technical drawing of the nozzle is shown in Figure 5.14.
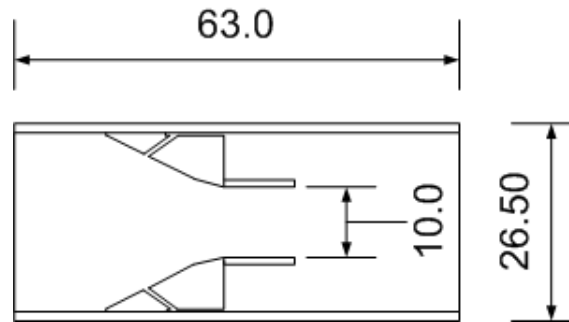
Figure 5.14 – Technical drawing – Nozzle burner version 3

In the centre of the burner there is a 10mm outlet where the main body of the flame forms. The nozzle of the burner has two angled sections to direct the gases through the outlet. There is a small annular gap at the outside of the nozzle where a secondary flame forms. There are four evenly spaced holes which connect the centre of the burner to the annular slit. The width of the gap was 0.2mm. The total length of the nozzle burner is 63mm.

The new burner improved the performance of the system. The burner stayed alight when propane and air were combusted and when the blocking plate was inserted in to the outer chamber. When the nozzle burner was ran with tarry pyrolysis gases there were obvious flaws in the operation of the burner. Due to the small outlet size of the nozzle when the flow rate of air to the Coandă was increased to 50 LPM the Coandă ejector was not operating properly. As the flow-rate of air through the Coandă increased so too does the entrainment and 'suction' of the ejector. The small outlet diameter meant that the burner could not cope with the increased flow throughout thus causing a backup of pressure. When version 2 of the CTC was ran with the pyrolysis gases due to the loss of this suction affect caused by the Coandă jets the pyrolysis gases were not entrained through the burner. This meant that the flame from the burner was unreliable and there were also heavy losses of the pyrolysis gases as the build up of gases increased causing the gases to bypass the burner and exit the combustion system.

Increase Burner Size (Version 4)

To prevent the backing up of pressure an up-scaled version of the nozzle burner was designed. The outlet of the burner was increased from 10mm to 15mm.
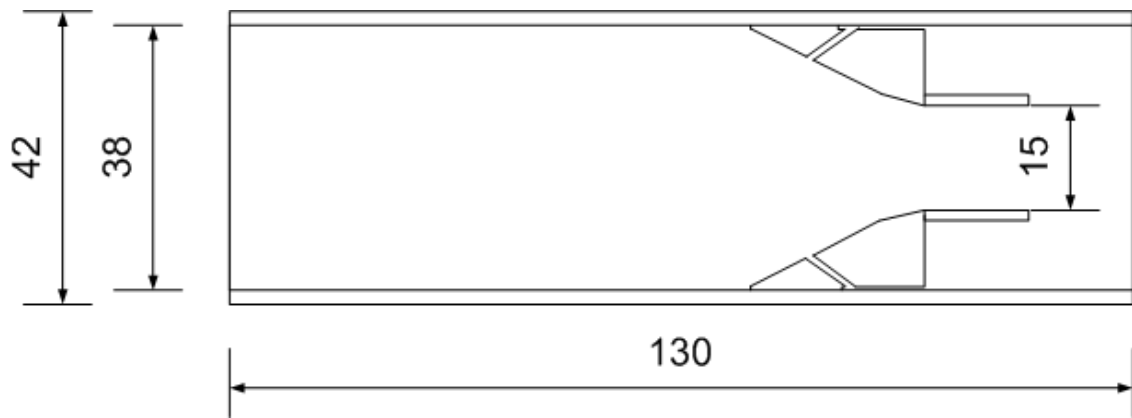
Figure 5.15 – Technical drawing – Nozzle burner version 4

There were still issues with the flame staying lit when the blocking plate was inserted into the outer chamber of the burner although there were certainly improvements, with respect to maintaining the flame stability, when compared with previous versions of the burners.

One of four holes leading to the annular outlet

15mm burner outlet

Annular slit
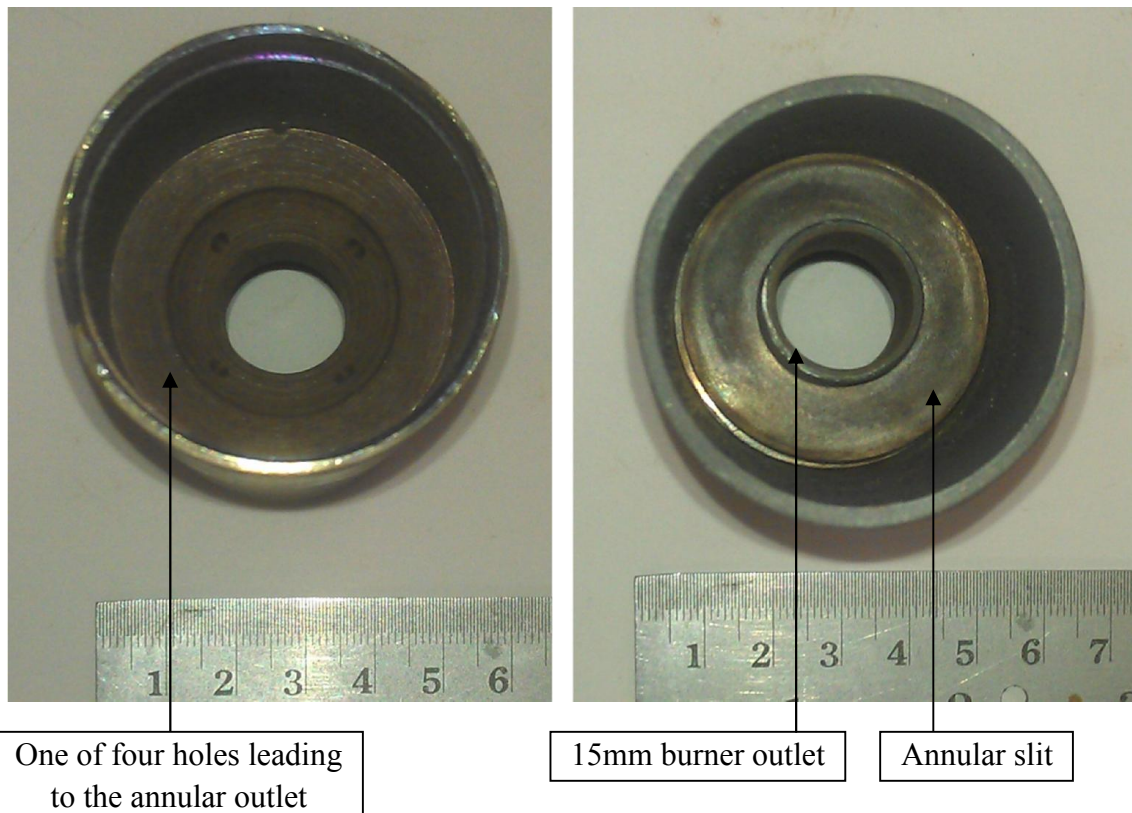
Figure 5.16 – Large nozzle burner

Decrease the diameter of the outer casing (Version 5)

To prevent air from entering the burner from the exhaust of the unit an outer casing to house the burner with a smaller diameter was designed and installed. The current diameter of the outer casing is 252mm. For version 5 of the burner setup the outer casing was designed to have an outer diameter of 76mm which was a considerable reduction. The smaller diameter

would allow the flame to take up the whole area of the outer casing and prevent any recirculation of air around the outer edges of the casing. The diameter of the unit had to be large enough so that recirculation of flame species can occur. The outer casing with the smaller diameter should also have the same sample ports as the previous incarnation so that flame temperatures can be monitored and produced gases can be sampled. Despite these alterations there were still issues with the burner. The final version of the burner design elongated the chamber of the tunnel so that the total length of the burner was increased. This alteration was done to ensure that there is perfect mixing of air and the fuel used (propane or pyrolysis gases). Version 6, the final design of the burner is shown in Figure 5.17.
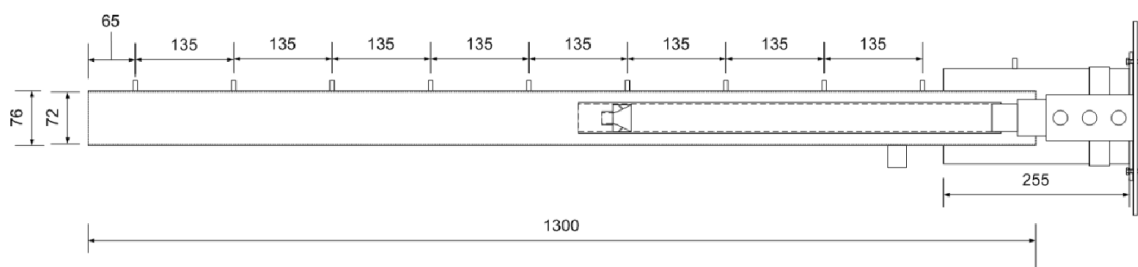
Figure 5.17 – Technical drawing of the final design of the Coandă burner

Figure 5.18 – The Coandă burner

The outer casing is made up of two components parts. The first part was the chamber which connected to the flange of the pyrolyser. This unit was made from mild steel. 6 screws 8mm screws are used to attach the device to the pyrolyser. Like the previous outer casing there is a mechanism built in so that the recirculation holes of the mixing vessel can be opened and closed. A rotating sleeve is used with a connecting bolt which is screwed to the mixing vessel.

The first part of the unit, which connected to the pyrolyser, was 255mm in length with an outer diameter of 130mm. There was a single sample port built into the vessel which can be used to monitor the temperature or be used to take a gas sample.

The second part of the unit was a long cylindrical vessel. The total length was 1295mm, the outer diameter was76mm and the inner diameter was 72mm. The unit was made from mild steel. There were nine 7/8" fittings for sampling. The outer casing was wrapped in k-wool to insulate the combustion chamber. The device slid onto the end of the Coandă ejector and fitted inside the first part of unit described above. There are eight 12mm holes are the end pyrolyser end of the chamber which allowed for recirculation of the hot gases produced from the flame, shown in Figure 5.19.
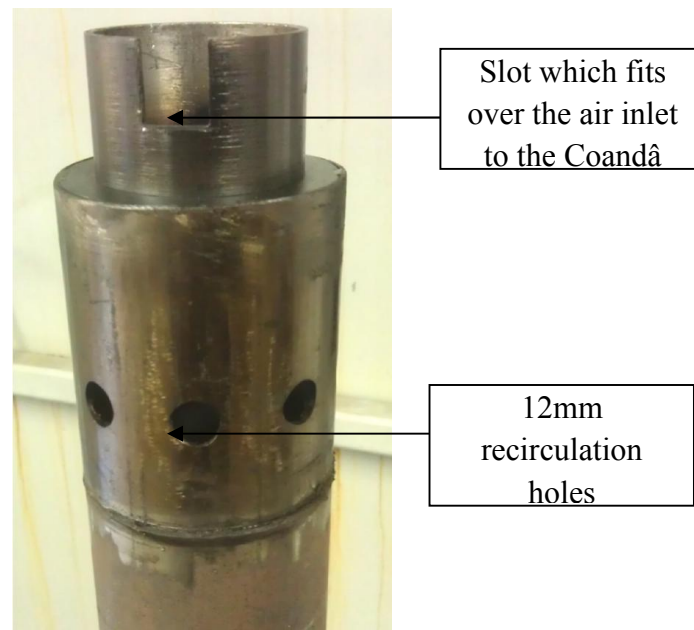
Figure 5.19 – Pyrolyser end of the outer chamber

5.3 Experimental Setup of the Combined System

A schematic diagram and flow diagram for the final design of the combined system is shown in Figure 5.20 and 5.21 respectively. 6 thermocouples were used to monitor temperatures in the CTC. Table 5.1 indicates the position and type of thermocouple using the sample port numbers as shown in Figure 5.20.

The R-type thermocouple which has a higher working temperature range is placed directly in the flame (sample port 9) produced by the CTC, so that the flame temperature can be monitored and recorded. The sampled gas is taken from point sample port 8 which is also in the flame region of the CTC. Six k-type thermocouples are placed in various positions in the CTC. These thermocouples monitor both the flame temperature and also the temperature towards the inlet of the CTC, where hot combustion gases are entrained from the flame region back towards the Coandă inlet.

Sample Port	Description
1	k-type thermocouple
2	-
3	k-type thermocouple
4	-
5	k-type thermocouple
6	-
7	-
8	Gas and tar sample
9	R-type thermocouple
10	k-type thermocouple
11	-
12	k-type thermocouple

Table 5.1 – Positions of thermocouples and gas sampling line

Gas Flow-meters

The flow rate of air to the CTC was measured and controlled by a FL-2017 series acrylic flow-meter purchased from Omega Engineering LTD. The limit of the flow-meter was 10-100 LPM. The accuracy at full scale was ±5%. During the running of the CTC experiments the value from the flow meter was recorded. The flow rate of air was kept constant during the complete run-time of the experiment. This value was used to calculate the air-fuel ratio in the system as described in Section 6.3.
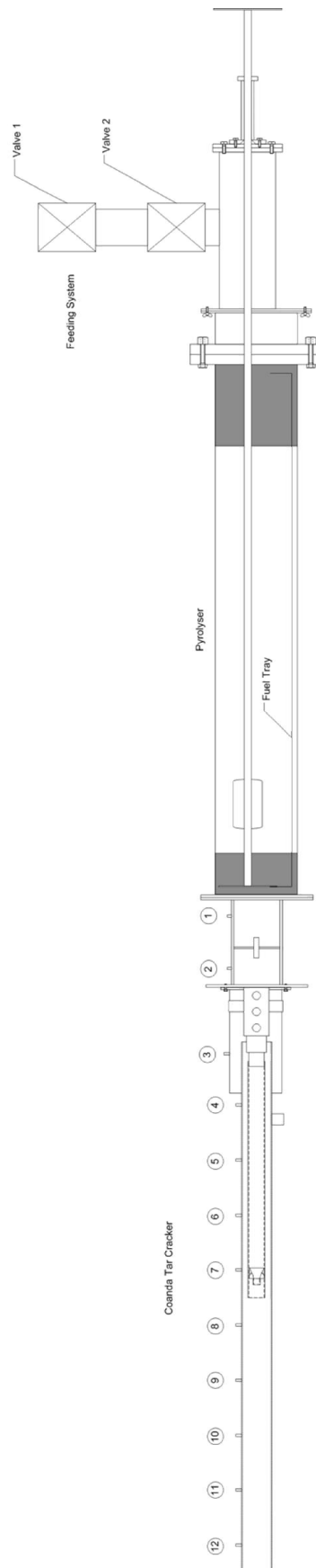
Figure 5.20 – Schematic of the CTC
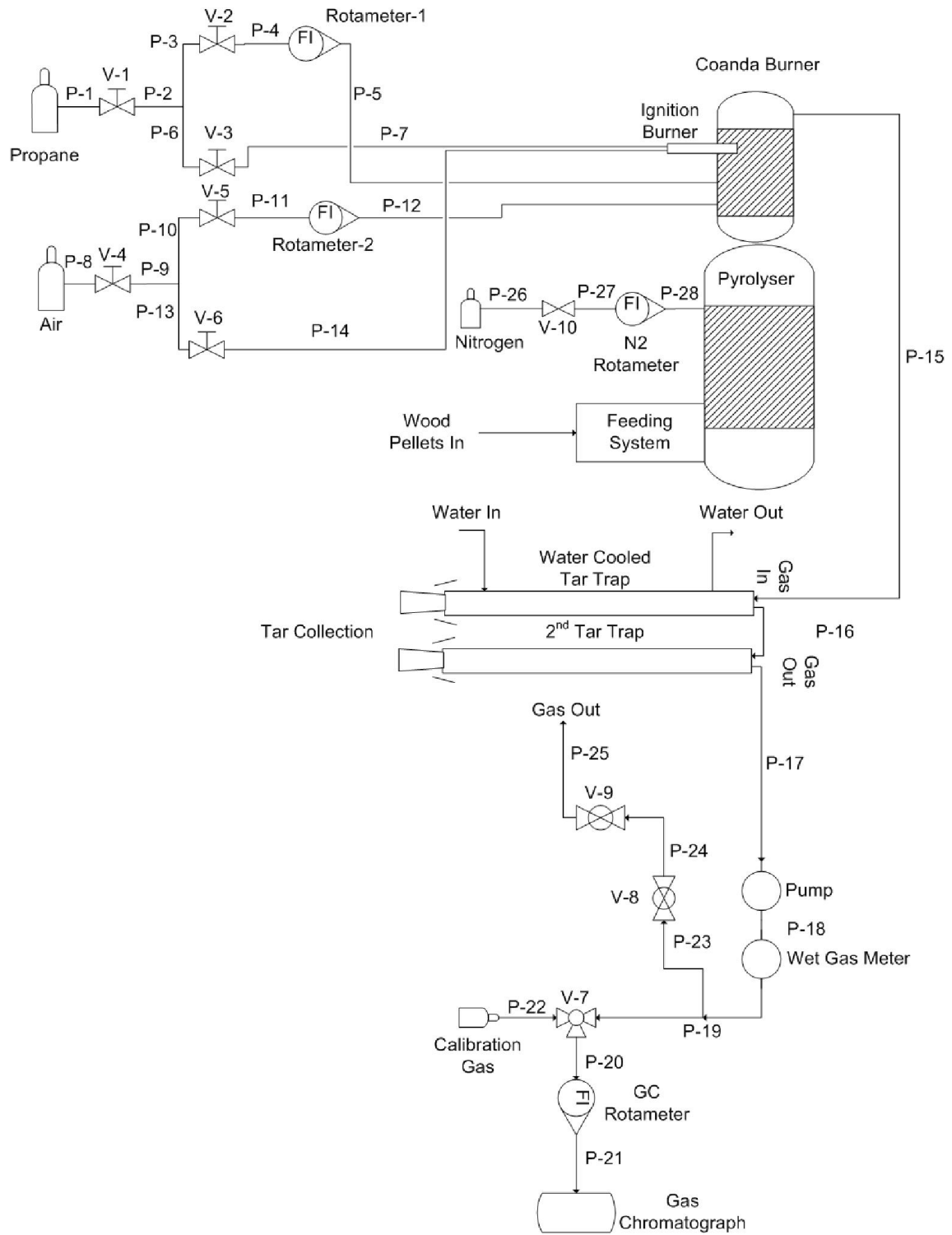
Figure 5.21 – Flow diagram of the combined experiment

5.3.1 Experimental Procedures

Start-Up Procedure

1. The gas chromatograph and the purge gases were turned on and left to stabilise and warm up.

2. The pyrolyser was turned on and the required pyrolysis temperature set (500, 600, 700, 800°C).

3. The water cooled tar trap was filled with 150ml of isopropanol, the 2nd tar trap was also filled with 150ml of isopropanol.

4. The extraction unit was turned on.

5. Water to the water cooled tar trap was turned on.

6. 10 batches of 100 grams each of wood pellets were weighed out and placed in containers.

7. When the pyrolyser has reached the desired temperature nitrogen gas was purged into the pyrolyser (Opened V-10). The nitrogen flow rate was set at 8 LPM and left to purge for 10 minutes.

8. The gas chromatograph was calibrated using the calibration gas.

9. The burner using propane only was turned on and the data logger started so the flame temperature and internal temperature could be recorded and monitored. (See chapter 4.2.2 for the start-up procedure).

10. The first batch of wood pellets was feed into the pyrolyser. Depending on the pyrolysis temperature the resulting feed rate of the pellets was altered, this is shown in Table 5.2.

Pyrolysis Temperature (°C)	Wood Pellet Feed Rate (seconds)
500	120
600	120
700	100
800	80

Table 5.2 – Pyrolysis temperature versus wood pellet feed time

11. The flame was monitored visually. The flame would change colour, structure and shape once the pyrolysis gas were being entrained through the Coandă burner. Once

the flow of pyrolysis gas was constant and substantial enough to maintain combustion in the flame the flow of propane into the burner was shut off (Closed V-2). This normally took around 60 seconds from when the wood pellets were loaded.

12. Once the flame was stable the pump was turned on and the gas sampled and analysed by the gas chromatograph. The reading on the wet gas meter was recorded.

13. The flame was monitored throughout the experiment. If the flame went out the ignition burner would be turned back on to re-ignite the flame from the Coandă burner.

14. The experiment was run until the final of the ten batches of wood pellets had been pyrolysed.

15. Readings from the GC were recorded. Three complete readings were taken from each experiment.

Shut-Down Procedure

1. The CTC was shut down and flow rates of propane and air turned off.

2. The electric heaters were switched off and the pyrolyser cooled to ambient.

3. The gas chromatograph was turned off at the mains, the carrier gases remained on for 30 minutes to purge the internal columns.

4. The water supply tar traps was turned off and the isopropanol and collected tar were removed for analysis. Solvent samples from the tar traps were collected and stored.

5. The tar trap pipe in the interconnecting pipe was checked for tar build-up.

6. The extraction unit was turned off.

7. The purge gas to the pyrolyser was turned off.

8. Once the pyrolyser has cooled to ambient the wood pellet char was removed and collected.

5.4 Tar Analysis

The collected tar samples were analysed by Nicholls Colton Ltd. Two types of analysis were used. The first method was for semi-volatile organic compounds (SVOC). For this a portion of the solvent sample was taken and then spiked with internal standards analysed using a Shimadzu GC-MS - QP2010 Plus in full scan mode. The second method of analysis was for volatile organic compounds (VOC) in which samples were diluted and made up to 10ml using

de-ionised water and then analysed using a Shimadzu GC-MS - QP2010 Plus in scam/sim mode. Due to financial constraints the tar samples could only be analysed once.

5.5 Overview of Experiments

This section presents an overview of the experiments to be completed in the final experimental phase. The experiments were performed to analyse the effectiveness of the CTC for tar destruction. For this analysis a comparison is made from tar yields from the pyrolysis only experiments and the tar yields when the CTC was used to treat the pyrolysis gas. Four pyrolysis temperatures were tested (500, 600, 700, 800°C) to enable a comparison into the affect of the temperature on the products from each experiment and to also allow for analysis into the effectiveness of the CTC over a wide range of pyrolytic conditions, with respect to the gas and tar composition and volume of the pyrolysis gas that entered the CTC. The analysis looks at the gravimetric yield as well as some key individual tar species (benzene, naphthalene and toluene). By looking at and understanding the composition and concentration of certain tar species it is possible to determine how the pyrolysis temperature affects the formation and destruction of tar species in the pyrolysis stage as well as what effect the high temperature and oxidation regime in the CTC has.

Secondly; in each of the experiments there are two additional products that are analysed; char and the product gas. Char from each experiment was analysed to determine what affect the pyrolysis temperature has on their chemical properties (ultimate and proximate analysis) and the calorific value. Finally the gas from each experiment was analysed to quantify the permanent gas species produced from the pyrolysis only experiments and the combined experiment. Table 5.3 shows the names and gives the details of the experimental programme.

Name	Pyrolysis Temperature (°C)	Description	Products and Analysis	
Pyro500	500	Pyrolysis Only	**Tar**	Composition Gravimetric analysis
Pyro600	600			
Pyro700	700		**Gas**	Composition
			Char	Proximate analysis (TGA) Ultimate analysis Calorific value
Pyro800	800			
CTC500	500	Pyrolysis and CTC	**Tar**	Composition Gravimetric analysis
CTC600	600			
CTC700	700		**Gas**	Composition
			Char	Proximate analysis (TGA) Ultimate analysis Calorific value
CTC800	800			

Table 5.3 – Overview of planned experiments

5.6 Summary

Chapter 5 details the improvements that were made to the experimental rig to improve the performance of the system. Three major alterations were made. Firstly, the wood pellet feeding system was improved to allow for longer operational time. The feeding system was changed from a batch to a repeating continuous system. Secondly, the CTC was modified to improve the stability of the flame and to prevent any surrounding air from entraining into the burner and lastly the tar/gas sampling line was enhanced so that higher volumes of tar can be captured.

6. Experimental: Results and Discussion

6.1 Introduction

This chapter presents the results and discussion from the experimental study and details the key findings of the research study. The performance of the CTC is evaluated by comparing the composition and quantity of sampled and collected 'tar' when wood pellets are pyrolysed and when the pyrolysis gas is treated in the CTC. Additionally the gas composition from both sets of experiments is evaluated as well as a discussion of the effect of temperature on the produced char.

6.2 Pyrolysis - Tar Analysis

6.2.1 Pyrolysis Only – Gravimetric Tar

Table 6.1 and Figure 6.1 highlights the gravimetric tar yields obtained from the pyrolysis only experiments. Not all of the produced gas and vapourised tar were processed in the sampling lines, thus the gravimetric tar yield was calculated using the total amount of tar collected in the tar traps in relation to the volume of gas sampled in each individual experiment.

Experiment Name	Pyrolysis Temperature (°C)	Gravimetric Tar Yield (g/Nm^3)
Pyro500	500	78.59 ±5.78
Pyro600	600	31.41 ±2.24
Pyro700	700	18.03 ±0.48
Pyro800	800	16.55 ±0.46

Table 6.1 – Quantity of individual tar species per unit of sampled gas

There is a clear reduction in the tar yield as the pyrolysis temperature increased from 500 to 800°C. At 500°C, the yield was 78.59 g/Nm^3; there was a steady decrease as the pyrolysis temperature increased to 600°C. The results for the gravimetric tar yields at 700 and 800°C are similar, 18.03 and 16.55 g/Nm^3.

The reduction in gravimetric yield was expected and fits in with previous research into the pyrolysis of biomass by Boroson et al., (1989) & Morf et al., (2002). The liquid or 'tar' phase of the products from biomass pyrolysis starts to reduce at temperatures between 450 – 550°C (Neves et al., 2011), this is caused because the increase in temperature causes secondary conversion of the initial volatiles species, thus causing an increase in the gas yield and a reduction in the liquid yield.
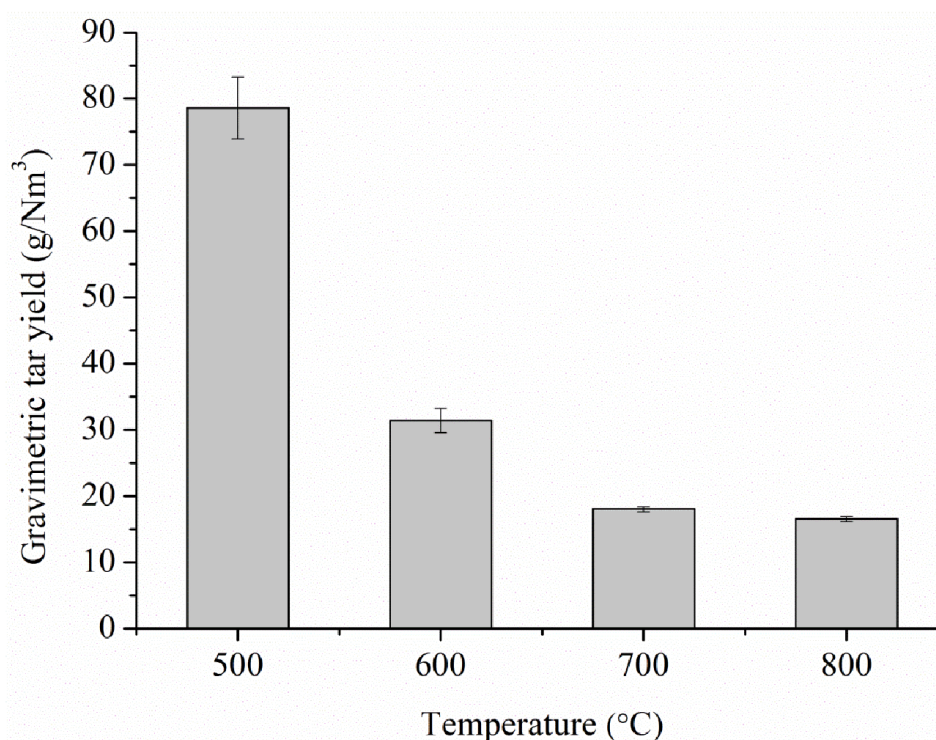
Figure 6.1 – Gravimetric tar yield

6.2.2 Tar Composition

Table 6.2 indicates the yields of the key tar species per litre of sampled gas. The table highlights the tar species that were found in the highest concentrations. The complete tar analysis determined the yields of over a hundred tar species. The complete list can be found in Appendix II. Low yields of larger PAH species such as chrysene (C18H12), pyrene ($C_{16}H_{10}$), phenanthrene ($C_{14}H_{10}$) and fluorene ($C_{13}H_{10}$) were found. The low yields of larger PAH species could be caused by the sampling method used to collect tars contained in the gas. A pump was used to drive the sampled gas through the tar traps causing a reduction in the residence times of the tars and gas, thus minimising potential secondary reactions in which larger PAH can be formed. These larger tar compounds are found in a number of studies which evaluated the tar composition when biomass fuels were pyrolysed in similar temperature ranges and conditions (Brage et al., 1996 & Zhang et al., 2010).

The analysed tar species are mainly aromatic. The yield of benzene in g/Nm3 of sampled gas increases steadily with pyrolysis temperature. At 500°C the yield of benzene is 1843, this increases to 5495 as the pyrolysis temperature increased 600°C. The highest yield of benzene (10718 g/Nm^3) was found at 700°C before it decreased at 800°C to 7385 g/Nm^3. Toluene followed a similar trend; the yield increased as the pyrolysis temperature increased from 500 to 700°C before reducing at 800°C, the highest pyrolysis temperature.

Other species that are found in notable values are mostly aromatic compounds (xylene isomers, styrene, propylbenzene isomers and trimethylbenzene isomers) and are classified as secondary tars according to Milne et al.,(1998). Xylene reaches its highest yield at a pyrolysis temperature of 600°C, before gradually reducing as the pyrolysis temperature increased. Ethylbenzene follows a similar pattern, reaching a maximum concentration at 700°C before it decreased. Ethylbenzene is reduced more readily at higher temperatures through methyl abstraction producing toluene and methane (Bruinsma & Moulijn, 1988).

			Pyro500	Pyro600	Pyro700	Pyro800
			Pyrolysis Temperature (°C)			
			500	600	700	800
Determinant	Formula	M_w	g/Nm^3 of gas sampled			
Benzene	C_6H_6	78	1843	5495	10718	7385
Dichloromethane	CH_2Cl_2	85	67	75	106	36
Toluene	C_7H_8	92	2301	3815	4016	3364
Phenol	C_6H_6O	94	2	4	3	3
Styrene	$C_6H_5CH=CH_2$	104	280	818	1016	936
Ethylbenzene	$C_6H_5CH_2CH_3$	106	293	314	107	107
Xylene isomers	$C_6H_4-CH_3, CH_3$	106	959	1002	681	627
Propylbenzene isomers	C_9H_{12}	120	56	34	-	-
Trimethylbenzene isomers	C_9H_{12}	120	128	98	36	48
Naphthalene	$C_{10}H_8$	128	191	1401	2772	2521

Table 6.2 – Quantity of individual tar species per unit of sampled gas

There are a number of reactions that biomass tars can undergo at increased temperature. There are four key reactions that can take place. Reactions 1 and 2 are tar polymerisation reactions whereas reactions 3 and 4 are tar cracking reactions. Polymerisation reactions are not as important as tar cracking because tar destruction is the main focus of this study. The four reactions are detailed below:

1. Reactions between gaseous/liquid tar species and ash/char

2. Reactions between tars in the liquid phase

3. Decomposition reactions in the gas phase under inert conditions

4. Reactions between gaseous tar species and permanent gas species which causes tars to decompose.

(Vreugdenhil & Zwart, 2009)

The key reactions for the pyrolysis only experiments are 3 and 4, decomposition and heterogenous reaction. The reactivity of the tar in these reactions can be affected by two sets of parameters. The first set of parameters are standard conditions which affect the chemical reaction rates. The second set relates to the types of biomass tars formed:

1st set - standard

- Reaction temperature

- Residence times at the reaction temperature

- Partial pressure of the gaseous tars and permanent gaseous species

2nd set – tar type

- The concentration of primary, secondary and tertiary tars

- The chemical composition (carbon, hydrogen, oxygen) of the tars

- The concentration of key tar species such as naphthalene, pyrene, benzene and phenol

(Vreugdenhil & Zwart, 2009)

Benzene, toluene and naphthalene are the tar species that appear in the highest concentrations. These compounds are aromatic and the most difficult of the produced tar species to destroy (Fassinou et al., 2009). The increase in pyrolysis temperature causes the destruction of unstable tar species and supports the formation of the stable aromatic species discussed above.

Phenol is found in small concentrations when compared to the major aromatic compounds reported, other primary tars were completely absent from the analysis. Phenol was found in much larger quantities in a pyrolysis study by Brage et al., (1996) and Fassinou et al., (2009). Phenol is the only primary tar found in a high concentration, which is surprising as primary tar species are normally the dominant tar class at pyrolysis temperatures between 500 and 700°C (Milne et al., 1998). The absence of primary tars must be put down to experimental error when the tars were analysed.

6.2.3 Analysis of Benzene

Figure 6.2 indicates the relative concentration of benzene contained within the collected and analysed tar. The relative concentration of benzene increases from just below 30 to 55% as

the pyrolysis temperature increased from 500 to 700°C. The mass.% of benzene then reduced to 49% of the total amount of tar as the temperature increased to 800°C

	Pyro500	Pyro600	Pyro700	Pyro800
	Pyrolysis Temperature (°C)			
	500	600	700	800
Determinant	(mass/total mass)%			
Benzene	29.9	41.9	55.1	49.1
Toluene	37.4	29.1	20.6	22.4
Ethylbenzene	4.8	2.4	0.6	0.7
Xylene isomers	15.6	7.7	3.5	4.2
Dichloromethane	1.1	0.6	0.5	0.2
Styrene	4.6	6.2	5.2	6.2
Propylbenzene isomers	0.9	0.2	*	*
Trimethylbenzene isomers	2.1	0.7	0.2	0.3
Naphthalene	3.1	10.7	14.2	16.8
Phenol	*	*	*	*

Table 6.3 – Relative concentrations of key tar species against pyrolysis temperature

*   *indicates reading is below detection limit*
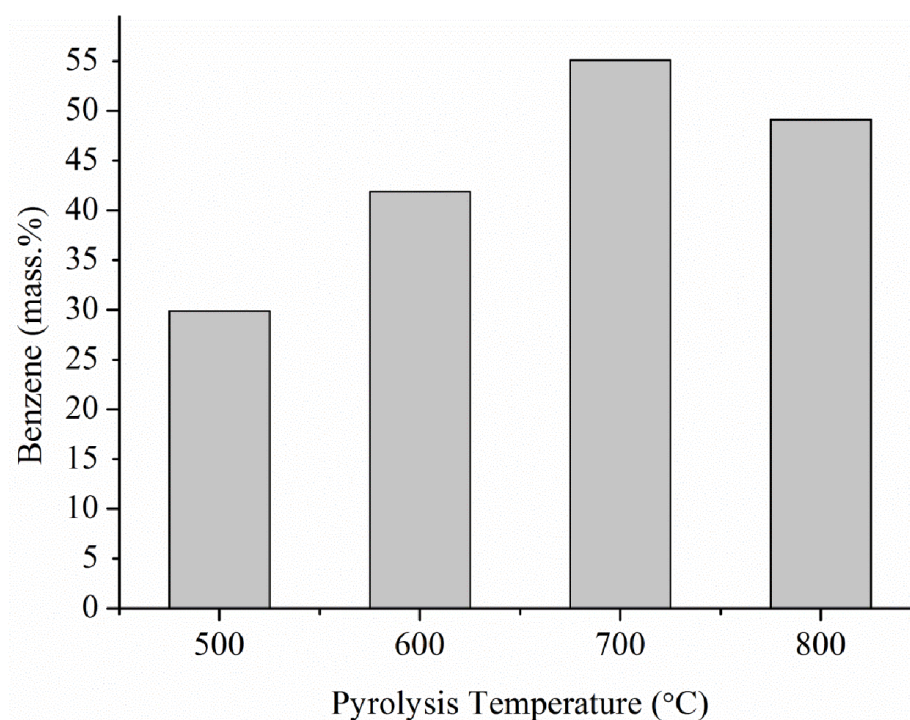
Figure 6.2 – Relative concentration of benzene contained in tar against pyrolysis temperature

Benzene is a very stable compounds and is difficult to destroy, even at high temperatures (Zhang et al., 2010; Jess, 1996; Bruinsma & Moulijn, 1988). The chemical stability of benzene is shown in Figure 6.2 where benzene alone amounts for over 40% by mass at pyrolysis temperatures above 600°C. However, the yield of benzene was reduced when the pyrolysis temperature is increased to 800°C thus showing that thermal destruction of benzene is possible when the pyrolysis temperature is high enough.

The thermal destruction of benzene is caused by hydration, the addition of water, or one of its elements. The benzene ring is broken and hydrogen is added to the reaction thus causing the production of permanent gas species which are smaller hydrocarbons such as methane, ethane and ethylene, as shown in Figure 6.3.
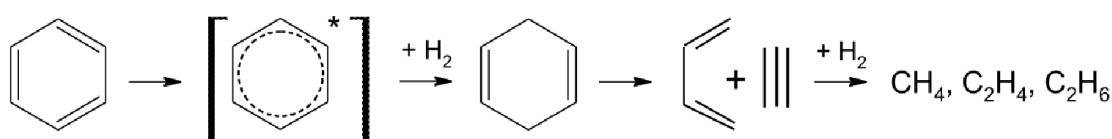
Figure 6.3 – Hydration of benzene into permanent gas species (van der Hoeven, 2007)

There is gradual increase in methane produced as the pyrolysis temperature increased (see Table 6.12). Benzene begins to thermally destruct at temperatures between 700 and 800°C, which resulted in a significant reduction in benzene and an increase in the yield of methane.

According to Vreugdenhil & Zwart (2009) radical reactions play the biggest role in thermal tar cracking. There are five key reaction steps:

1. Radical forming reactions caused by the breaking of bonds

2. Propagation reactions causing the creation of new chemical bonds

3. Hydrogen transfer

4. Isomerisation reactions

5. Termination reactions where two radicals react with each other

Benzene can be affected by the first reaction step which forms two free radicals which react further to create other products. Figure 6.4 (a) indicates how two radicals are formed when benzene is broken down thermally. A benzene radical and hydrogen radical are formed. It is expected that increasing the temperature of pyrolysis promotes this reaction as the bond dissociation energy has to be overcome so that the reaction can take place. Both produced radicals can react further with other species or with other radicals to form new permanent species or additional radicals. The breaking of the covalent bonds to form two radical species is called homoylsis. Figure 6.4 (b) shows how toluene can break down to form radicals.
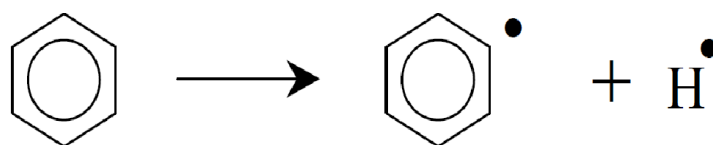
Figure 6.4 (a) – Benzene radical forming reaction (Vreugdenhil & Zwart, 2009)
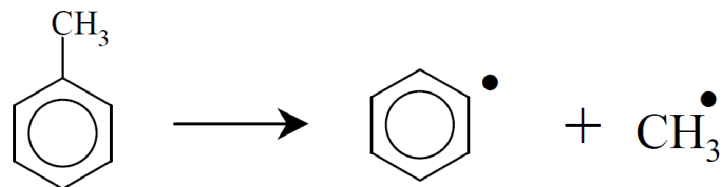
Figure 6.4 (b) – Toluene conversion to radicals

The radicals generated through the radical forming reactions, as shown through the breakdown of benzene and toluene in Figures 6.4 (a) and (b), can react again with other species to form other tar species and additional radicals (Vreugdenhil & Zwart, 2009). These reactions are key in the production of naphthalene and other larger PAH species as well as the production of permanent gas species and in particular hydrogen. The yield of hydrogen greatly increases as the pyrolysis temperature increased. The propagation reactions of benzene and toluene are detailed below. As shown in Figure 6.5 toluene reacts with a hydrogen radical to form benzene in permanent form and a methyl radical. This reaction can explain why the increase in pyrolysis temperature from 500 to 700°C resulted in a decrease in the relative concentration in toluene but an increase in benzene, see Table 6.3. When the pyrolysis temperature reaches 800°C reaction shown in Figure 6.5 is no longer the key reaction as the temperature and conditions are high enough to cause the decomposition of benzene causing an increase in the yield of permanent gas species as already discussed.
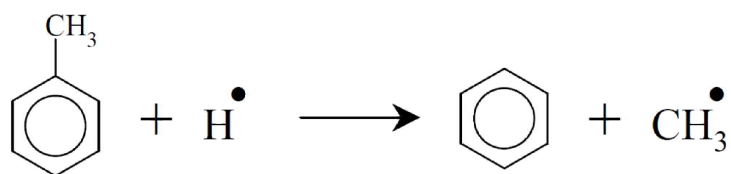
Figure 6.5 – Propagation of toluene and a hydrogen radical
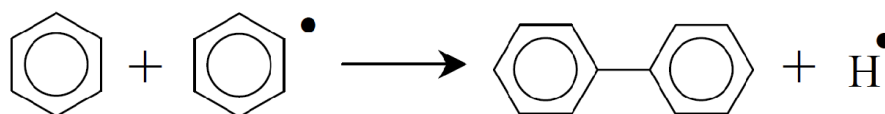
Figure 6.6 – Propagation of benzene and benzene radical

Hydrogen transfer reactions continue the production of radicals as a hydrogen atom is transferred from one molecule to another with a radical being released. This is shown in

Figure 6.7; a large PAH species reacts with a benzene ring, the hydrogen atom is transferred causing the production of a benzene radical.
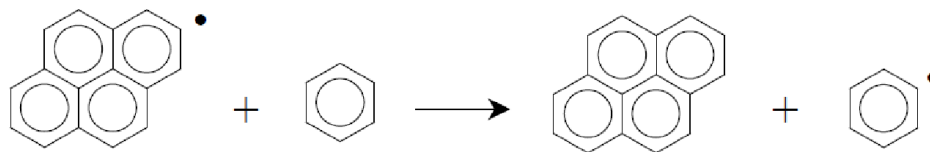
Figure 6.7 – Hydrogen transfer

Termination reactions (5) allow for the production of permanent species as two radicals combine to produce a stable electron pair. One of the key reactions present is the combination of a hydrogen radical and a methyl radical to form methane as shown in Figure 6.8.

$$CH_3^{\bullet} + H^{\bullet} \longrightarrow CH_4$$
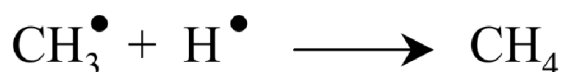
Figure 6.8 – Radical termination reaction

6.2.4 Toluene

Figure 6.9 shows the relative concentration of toluene with increasing pyrolysis temperature. Toluene is another of the most prevalent species formed during biomass pyrolysis. The mass.% of toluene decreased as the pyrolysis temperature increased from 500 to 700°C, at this point, however, the mass.% of toluene increased from 20.6 to 22.3%. Toluene contains a methyl group which detaches from the benzene group to form benzene as shown in Figure 6.10. The increased pyrolysis temperature promotes this reaction. Thus as the temperature increases the total mass of toluene is shown to decrease.

Figure 6.10 shows the cracking scheme for toluene as shown by van der Hoeven et al., (2006). Toluene is broken down into a number of products (benzene, methane, and hydrogen) through the addition and subtraction of hydrogen radicals. Benzene is produced through the addition of a hydrogen radical which caused the methyl group to break away from the structure. The reduction of toluene to methane and hydrogen can be shown when looking at the gas compositions in Table 6.11. There is a large increase in the concentration of hydrogen as well as an increase of methane. The reduction of toluene may have caused the increase in the yields of these permanent gases.
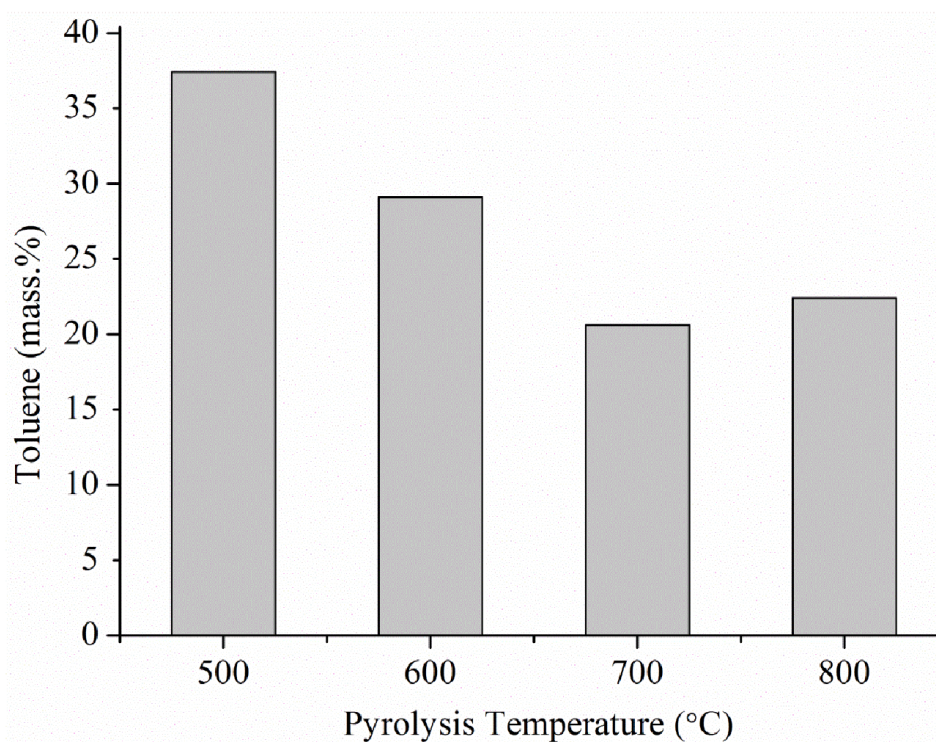
Figure 6.9 – Relative concentration of toluene contained in tar against pyrolysis temperature
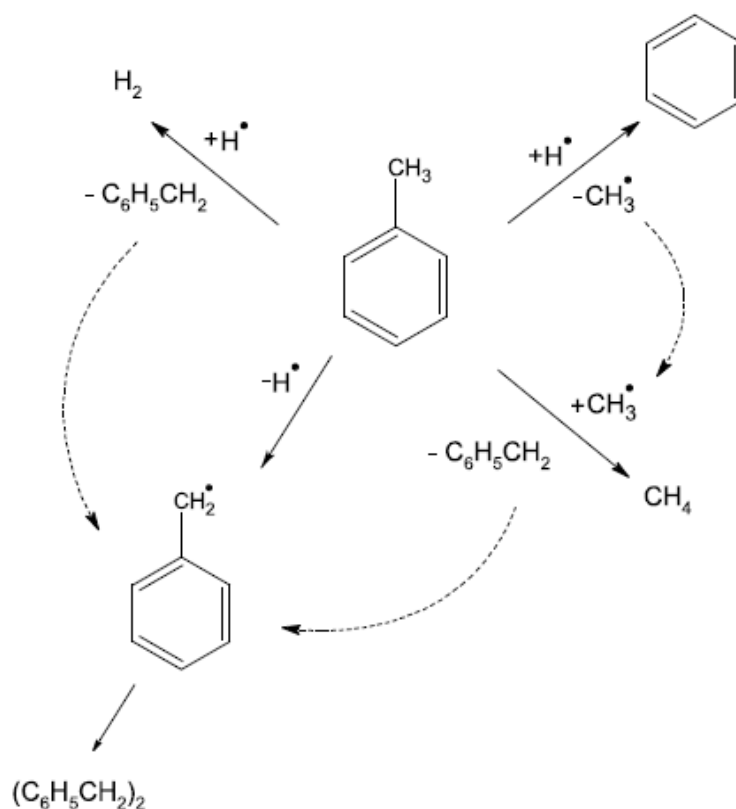
Figure 6.10 – Thermal tar cracking scheme for toluene (van der Hoeven, 2007)

The relative concentration of toluene increases from 20.6 to 22.3% as the pyrolysis temperature increased which was not expected. Toluene is a more reactive tar species when compared with benzene. According to (Jess, 1996) toluene is more reactive than both

naphthalene and benzene in pyrolytic conditions. Jess (1996) concluded that the order of reactivity of these three tar species is: toluene >> naphthalene >> benzene. When looking at the results there was a decrease in the yield of benzene as the pyrolysis temperature increased from 700 to 800°C. Toluene and naphthalene are more reactive so it would be assumed that these two tar species would thermally destruct more readily than benzene, however this was proven not to be the case.

Toluene can also react through a homolysis reaction. In this reaction a methyl radical and benzene radical are formed. The rate of this reaction is linked to the temperature. Therefore as the pyrolysis temperature is increased there should be a breakdown of toluene to form these two types of radicals. The reaction scheme is shown in Figure 6.4 (b).

From the results the relative concentration of toluene decreases steadily as the pyrolysis temperature increases before increasing as the temperature reaches its maximum of 800°C. Toluene is the most reactive and requires the lowest temperatures to decompose. Although Jess suggests that the temperature required for full conversion is over 1000°C these temperatures were not present in the pyrolyser. The reduction of toluene at temperatures lower than those recorded by (Jess, 1996) can be attributed to the different gas compositions and the presence of non-carbon atoms (N and O) which decompose at lower temperature when compared with sole PAH compounds. In the results presented here toluene is decomposed at lower tempertures. Gas species are produced through primary and secondary pyrolysis reactions. The presence of these gases, especially hydrogen promotes the production of hydrogen radicals which causes a propagation reaction leading to the destruction of toluene.

6.2.5 Analysis of Naphthalene

Naphthalene is another key tar species that plays an important role in the formation and destruction of tar species produced through pyrolysis. Figure 6.6 shows how naphthalene can be formed through the reaction of a benzene ring and a benzene radical. In this reaction naphthalene and a hydrogen radical are formed. The relative concentration of naphthalene increases gradually as the temperature of pyrolysis increases as shown in Figure 6.11. At 500°C the relative concentration of naphthalene is below 4%. However this relative concentration reaches a maximum of 16.7% which is almost equal to the relative concentration of toluene. It is thought that propagation reactions that cause smaller tar species to polymerise into larger ones play a key role in the production of naphthalene and other PAH as well as hydrogen which can be seen due to the increase in the yield of hydrogen as the pyrolysis temperature increases.
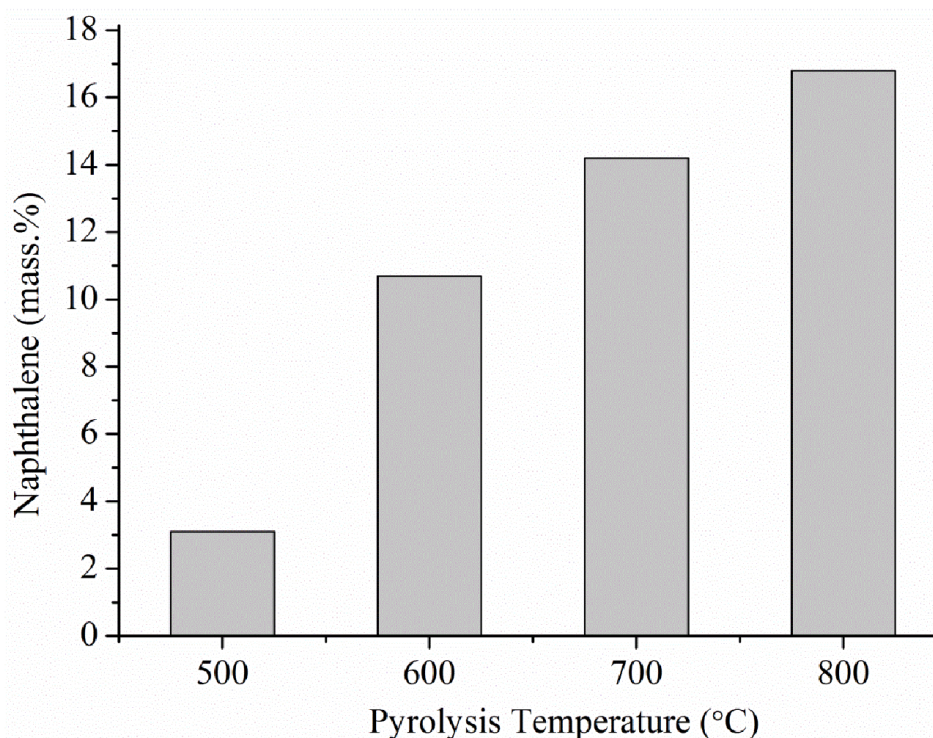
Figure 6.11 – Relative concentration of naphthalene contained in tar against pyrolysis temperature

6.3 Tar Composition after CTC Treatment of Pyrolysis Gases

By comparing the results from the tar analysis it is possible to assess the effectiveness of the Coandă burner as a means of destroying tar. There are a number of previous studies that have used two stage systems to test for tar destruction (Ahrenfeldt et al., 2013a; Su et al., 2011; Wu et al., 2011; Chen et al., 2009; Fassinou et al., 2009). In most of these cases the second stage applied high temperatures and/or the addition of oxygen, to treat a tarry pyrolysis gas produced in the first stage.

The majority of these studies did not utilise a partial combustion system with a controlled burner, as is the case in this work. Instead oxygen and or air are supplied into a high temperature second stage unit and then react with the fresh pyrolysis vapours. Not having a burner which requires a stable flame makes for easier control of the equivalence ratio. In these experiments the stability and the control of the flame were important factors. By using a burner, heat can be produced from combusting a small portion of the permanent gases produced from pyrolysis to produce heat, this heat can then be used to thermally destroy tar species. Using a burner also promotes the production of radicals which contribute to tar destruction. The problem with using a combustion device rather than purely mixing oxygen with the pyrolysis gases is that of keeping a stable and lit flame, which becomes very difficult

especially when operating at reduced equivalence ratios used by other authors. In previous studies it has been shown that it is important to use excess air ratios below 0.7. Having such a low amount of air entering the combustion system inevitably created problems with keeping the flame ignited.

In Wu et al., (2011) gases produced from the slow pyrolysis of rice straw pellets at 500°C were partially oxidised at equivalence ratios (ER) from 0.0 to 0.4 and at reactor temperatures between 700 to 1100°C. Results from this study showed that increasing the ER led to an increase in tar destruction and an increase in the conversion of primary tars to permanent gaseous products, namely carbon monoxide, methane and hydrogen.

The work performed by Houben, (2004) is the most similar to the work presented in this paper. In this work a micro-swirl burner is used to partially oxidise with naphthalene, used as a model tar component, in an artificial producer gas. The excess air ratio, λ, was varied from 0.19 to 0.75. It was shown that when not counting benzene as a tar component, the naphthalene in the artificial gas could be reduced by as much as 95% either through polymerisation or cracking. Naphthalene was cracked when λ was less than 0.4 and the fuel hydrogen concentration was greater or equal to 20% by volume. When conditions were not within this limit naphthalene was primarily converted into other species by polymerisation.

In theory, using a Coandă burner should allow for combustion at equivalence ratios that are close to 1, which was the case in previous studies by Prior, (1977) and O'Nions, (1997). As a reference, the lowest air to fuel ratio, before the burner became unstable, achieved by O'Nions was 1.03. However in those studies more traditional fuels were used, namely propane and oil and the fuel supply was constant, which was not the case with the gas from the pyrolyser, which fluctuated due to the feeding method. It was found that the flame of the burner would not ignite or quickly extinguish when the ER was reduced to the stoichiometric levels used by other researchers. The only way to keep the flame lit was to operate the CTC at above stoichiometric values. Ultimately this would lead to the complete combustion of the pyrolysis gases rather than partial oxidation. This, however, should ensure that produced tars are destroyed in the flame but will almost certainly mean that the produced gas will have a low energy content, as the active ingredients, namely CO and H_2, are combusted and removed from the gas.

The value for λ was calculated by first working out the mass of air required to completely combust the wood pellets added to the pyrolyser. It was calculated that to combust 1 kg of wood pellets 5.52 kg of air was required. From the pyrolysis only experiments the yield of char was known (see Section 6.5), the remaining mass which would enter the Coandă burner

was used for the basis of the calculations. From this it is possible to calculate the air required to fully combust the volatile portion of the wood pellets; the permanent gases and tars in vapour form. The flow rate of air entering the burner was recorded throughout the experiment and by knowing the pressure at which air is fed into the Coandă burner it is possible to calculate the mass flow of air in kilograms, which can then be divided by the stoichiometric value to work out the excess air ratio. The value for λ was calculated using Equation 6.1. This is the same technique used by Ahrenfeldt et al. (2013a) to calculate the excess air ratio used in his work.

$$\lambda = \frac{\dot{m}_{air,supplied}}{\dot{m}_{air,stoich}}$$

(Eqn. 6.1)

6.3.1 Experimental Description

The primary issue was the stability of the flame in the burner and also ensuring that the flame remains ignited throughout the entirety of the experiments. At 500, 600 and 700°C there were numerous issues with these two problems. The flame was extremely sensitive especially when wood pellets were being loaded into the pyrolyser. When the pellets were loaded into the pyrolysis chamber and the blanking plate which separates the feeding and pyrolysis systems opened, the flame would often extinguish.

There were also issues with controlling the flow of air into the Coandă burner, it was difficult to maintain the stability and consistency of the flame. If the flow rate of air was too low or too high the flame would struggle and would go out. The most successful experiment was when the pyrolyser was run at 800°C. During this experiment the flame remained stable despite loading issues.

The issue with flame stability creates problems along the sampling line. Firstly the tars collected in the tar traps will not be purely from the combusted gases and instead will be contaminated by the tars contained within the gases that were not treated by the Coandă burner. This contamination also caused issues with the gas samples. It is expected that the composition of the gases post burner will be different from the pure pyrolysis products. It should be noted that during the 700°C experiment there were short periods of time when the Coandă burner was not in operation and untreated pyrolysis gases and vapours will have been collected along the sampling line and caused contamination to the tar analysis and the gaseous results.

6.3.2 Temperature and Conditions in the CTC

This section highlights the temperature in the CTC as recorded by the thermocouples in the unit. As previously discussed high temperatures play an important in role in destroying tar, as the high temperature causes bonds to rupture and promotes the formation of permanent species.

Figure 6.12 indicates the temperature in the CTC when the pyrolysis temperature was 800°C. Port 9 indicates the flame temperature which reaches temperatures above 1200°C and reaches a maximum temperature of 1325°C. Figure 6.12 indicates the fluctuations in the flame caused when wood pellets were loaded into the pyrolyser. For the displayed results wood pellets were loaded every 80 seconds (1 minute and 20 seconds). The downward deviations in the flame temperature are observed when the wood pellets are loaded. The flame from the CTC was re-ignited as soon as possible by using the ignition burner. The k-type thermocouples situated after the flame (ports 10 and 12) indicate the drop in temperature caused by the flame going out. Once the flame from the CTC is re-ignited the temperature 'recovers' instantly.

The temperatures at ports 3 and 5 are low when compared with the flame temperatures. This could be an indication that the hot combustion gases are not re-circulating to the secondary inlet of the Coandă inlet because the gaseous entrainment is satisfied by pyrolysis gases.
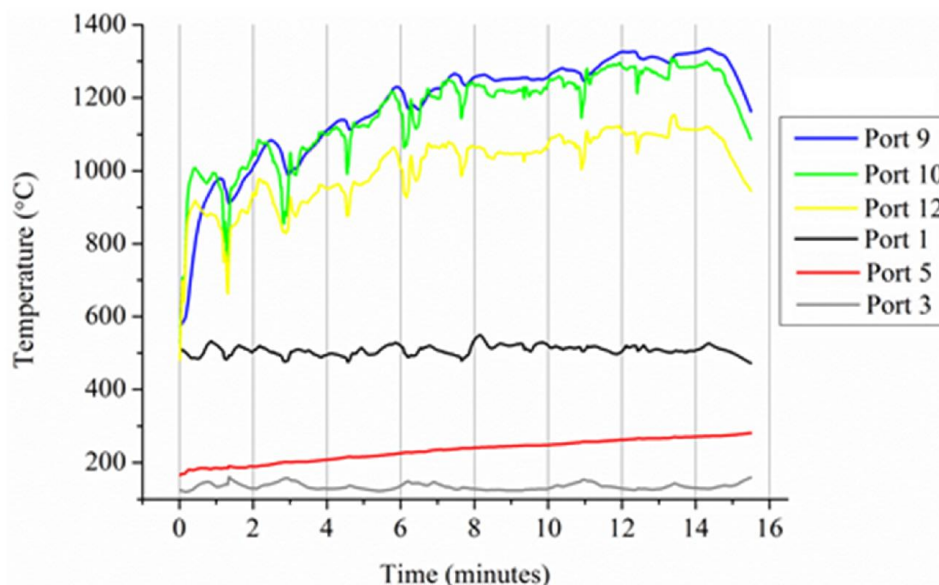
Figure 6.12 – Temperature in the CTC for the 800°C pyrolysis case

Figure 6.13 shows the comparison of the flame temperature in the four experiments. The flame temperature in the CTC800 experiment is consistently higher than the other three cases. The flame temperature in the CTC700 maintains a temperature consistently above 900°C once issues with the flame stability were resolved. In the CTC700 case there was a significant drop

in the temperature between 6 and 8 minutes caused by the flame extinguishing and resulting issues with re-igniting the flame.

Each of the four cases indicates similar trends; at the beginning of each experiment there is an initial increase in the flame temperature. Each case also indicates deviations caused by the instability of the flame. Reductions in flame temperature coincide with the loading of the wood pellets to the pyrolyser. The average temperature of the CTC500 and CTC600 cases is similar with only a couple of degrees difference, although the maximum temperature observed in the CTC700 case (915°C) is higher. The average and maximum flame temperature are shown in Table 6.4. In the CTC700 case the average temperature was determined to be 857°C.
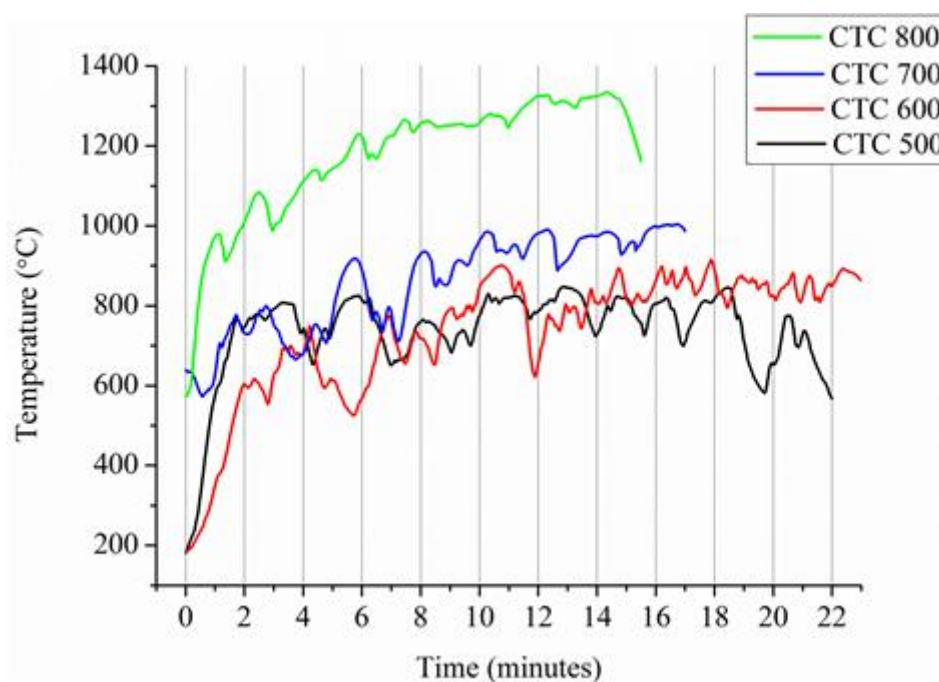
Figure 6.13 – Comparison of flame temperatures

6.3.3 Tar Results – Pyrolyser and CTC

Table 6.10 shows the results for some of the key tar components collected in the tar traps after the pyrolysis gases have gone through the Coandă burner. The average and highest recorded temperature of the burner was recorded from an R-type thermocouple positioned after the main body of the flame, port 9, as discussed previously. These values give an indication of the overall temperature in the combustion environment. Table 6.4 shows how again the stable aromatic tar species are most abundant, benzene and toluene are the most common tar species.

	CTC500	CTC600	CTC700	CTC800
	Pyrolysis Temperature (°C)			
	500	600	700	800
Average Temperature of CTC (°C)	735	737	857	1178
Maximum Temperature in CTC (°C)	847	915	1004	1335
Value for λ	1.5	1.8	1.8	1.7
Determinant	mg/Nm^3 of gas sampled			
Benzene	385	327	763	350
Toluene	223	129	241	132
Ethylbenzene	19	7	8	5
Xylene isomers	60	26	41	28
Dichloromethane	30	29	61	94
Styrene	56	26	60	36
Naphthalene	253	121	276	*
Phenol	0.2	0.2	0.1	*

Table 6.4 – Yield of key tars

*   indicates reading is below detection limit*

When comparing the tar concentration it is obvious to see that there is an impressive reduction in the amount of tars produced per unit of gas. The highest reduction occurs when the pyrolyser was run at 800°C, comparing the results from Pyro800 and CTC800. Benzene is reduced from 7385 to 350 mg/Nm^3 of sampled gas, toluene is reduced from 3364 to 132 mg $/Nm^3$ of gas, a reduction of 94%; naphthalene is completely destroyed. The high rate of tar reduction in the key tar components can be seen in Figure 6.14 which compares results from both sets of experiments.

The experiment performed at 800°C is the most successful in terms of tar destruction which can be put down due to the high temperature in the burner environment. The maximum temperature of 1335°C was recorded which is high enough to thermally crack tar. Wu et al., (2011) performed experiments into both inert and partial oxidation treatment of tar compounds. Under the inert conditions, it was found that increasing the temperature led to a positive relationship to tar cracking, the high temperature is one of the key reasons for the increase in tar conversion.
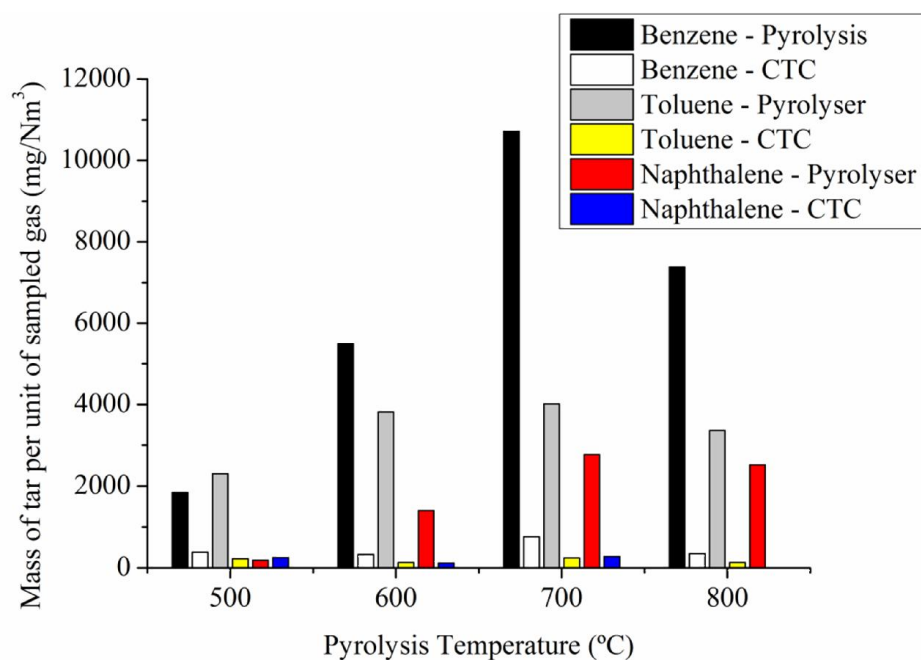
Figure 6.14 – Comparison of key tar components from pyrolysis only and Coandă burner experiments

Due to the nature of this system it is not possible to quantify and deduce the total amount of tar and gas produced when the dual system is used, which was possible in the pyrolysis only tests as a mass balance around the system could be performed. However when looking at the relative concentrations of individual tar species found in the product gas it is possible to draw a number of conclusions into the how tar species are affected by the addition of oxygen and increased temperature in the CTC. Table 6.5 shows the relative concentrations of key tar species found after the tarry gases produced in the pyrolyser had been treated in the CTC.

	CTC500	CTC600	CTC700	CTC800
	Pyrolysis Temperature (°C)			
	500	600	700	800
Determinant	(mass/total mass)%			
Benzene	37.2	48.8	52.6	54.1
Toluene	21.5	19.2	16.6	20.5
Ethylbenzene	1.8	1.1	0.5	0.8
Xylene isomers	5.9	3.9	2.8	4.3
Styrene	5.5	3.9	4.1	5.5
Naphthalene	24.5	18.0	19.0	-

Table 6.5 – Relative concentration of tar species

*   indicates reading is below detection limit

Benzene, toluene and naphthalene are again the most prominent species found in the combined experiment. As previously discussed benzene and toluene are stable tar compounds that are difficult to destruct even in high temperature and radical producing regimes that are apparent in the flame of the CTC.

6.3.4 Gravimetric Tar Analysis

Table 6.6 shows the gravimetric tar yields from the pyrolysis gases treated by the CTC. The results for each case show that there is a dramatic reduction in the overall yields when the gases are treated. In each case the level of tar is reported to be less than 3 (g/Nm^3). The *conversion %* in Table 6.6 relates to the total % of tar that is converted when the results from the pyrolysis only and CTC experiments are compared. The highest conversion rate is at a pyrolysis temperature of 500°C; this rate of conversion applies to the high gravimetric yields found in the pyrolysis only experiments. The lowest gravimetric tar yield was found when the pyrolysis temperature was 800°C.

Experiment Name	Pyrolysis Temperature (°C)	λ	Gravimetric Tar Yield (g/Nm³)	Conversion %
CTC500	500	1.5	2.49 ±0.08	96.8
CTC600	600	1.8	2.46 ±0.04	92.2
CTC700	700	1.8	2.97 ±0.04	83.5
CTC800	800	1.7	1.98 ±0.06	88

Table 6.6 – Gravimetric tar yield after CTC treatment
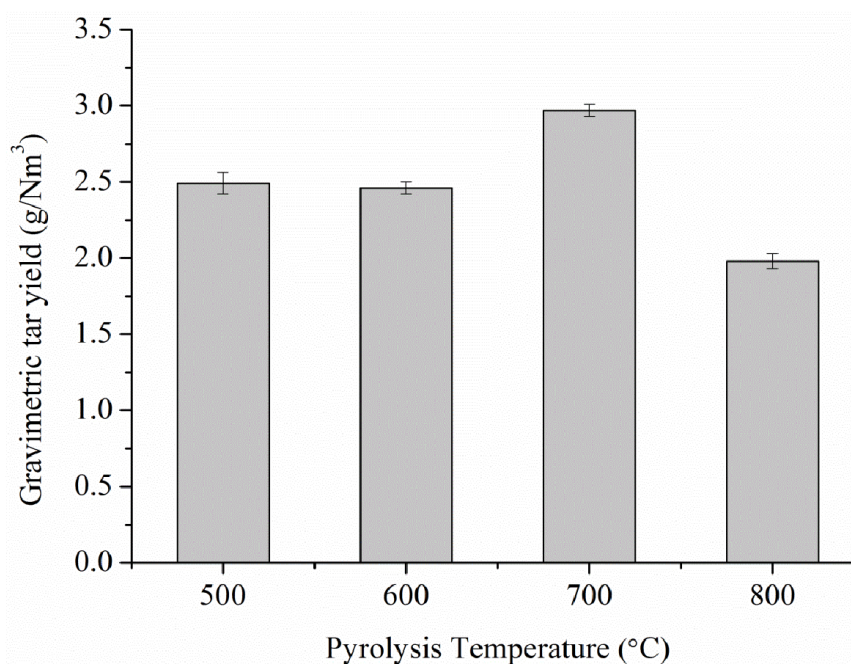
Figure 6.15 – Gravimetric tar yield after CTC treatment

143

6.3.5 Analysis of Benzene

Benzene makes up 54% of the total amount of tar when the experiment was run at a pyrolysis temperature of 800°C (see Figure 6.16). The reduction in tar is due to a number of factors and not just the presence of oxygen. As the burner is run at greater than stoichiometric conditions in all four cases oxygen cannot come into direct contact with all of the tar vapours contained in the treated pyrolysis gas. Thus further presence of oxygen must promote certain reactions, which in turn leads to the destruction of tar species. Furthermore the increase in temperature in the flame will aid the tar cracking process. As Jess (1996) has shown; toluene, benzene and naphthalene can all decompose when the temperature is high enough. The flame temperatures used are high enough to cause decomposition through thermal cracking. As well as the increased temperature caused by combustion in the flame it is expected that intermediate gas products produced when permanent gas species are combusted are required for effective tar cracking (van der Hoeven, 2007).
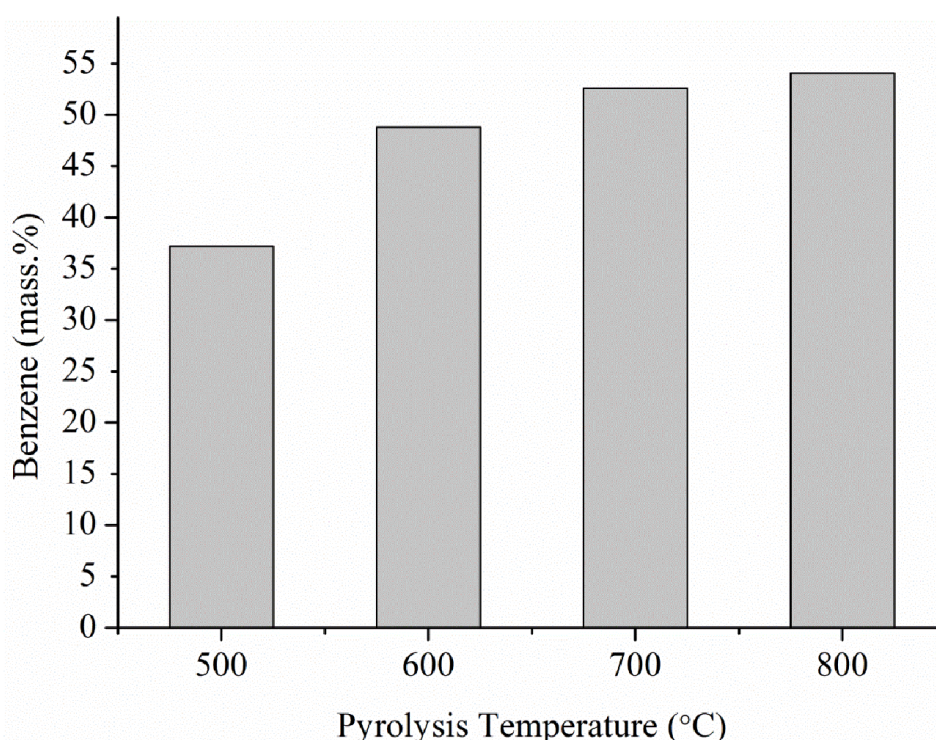
Figure 6.16 – Mass.% of benzene contained in tar after partial oxidation treatment

Due to the equivalence ratio being higher than stoichiometric, analysis into the combustion of tar species is required. Venkat et al., (1982) and Brezinsky, (1986) performed extensive studies on the high temperature oxidation of aromatic hydrocarbons in a turbulent flow reactor. The mechanism for benzene oxidation was sequenced into a series of events. Firstly benzene and phenyl (C_6H_5) are converted to oxygenated C_6 species. This is then broken down into a C_5 species; this is followed by the appearance of C_4 species through the oxidative

process which rapidly produces many C_2 species. Carbon monoxide forms early and the carbon dioxide forms after the carbon monoxide concentration reaches high levels (Venkat et al., 1982). The complete destruction pathways of benzene with a radical pool of H, OH, O and HO_2, radicals which would be present in the flame, is reported in(Brezinsky (1986).
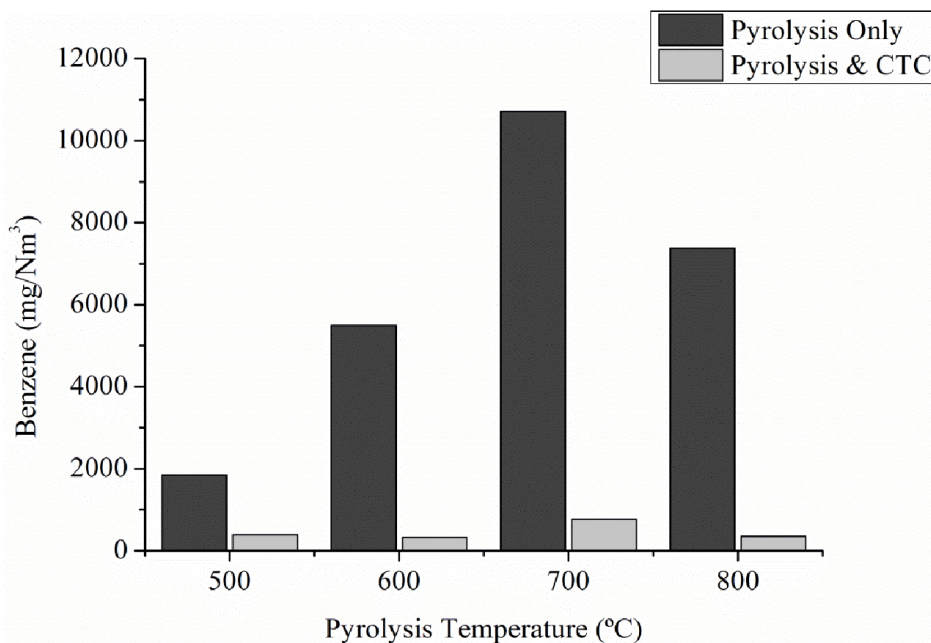
Figure 6.17 – Benzene comparison

Figure 6.17 shows a comparison between the benzene yield from the pyrolysis only and the CTC. There is a very clear reduction in the benzene yield when the CTC was used.

6.3.6 Naphthalene Analysis

Perhaps more interesting is that the relative concentration of naphthalene is not measurable when the CTC was run in conjunction with the pyrolyser at 800°C. In effect the naphthalene is efficiently destroyed. The destruction of naphthalene can be attributed to the hydrogen present in the pyrolysis gas that is partially combusted in the Coandă burner. Houben (2004) performed experiments using naphthalene as a model tar gas which was partially combusted in a burner along with a substituted pyrolysis gas. In one experiment performed by Houben (2004) the inlet composition of the combusted gas was altered to determine the effect of hydrogen on the destruction of naphthalene The results show that increasing the molar composition of hydrogen in the fuel gas resulted in a considerable decrease in the final tar concentration. The yield of hydrogen from the pyrolysis stage is at its highest at 800°C. In the results presented by Houben increasing the hydrogen composition in the fuel gas led to a decrease in tar species with a high number of rings. When the molar composition of hydrogen was set at above 25% (molar percent) the resulting tar was mainly benzene and one-ringed species, which includes toluene and xylene. Naphthalene is broken down into benzene and

145

other one ringed species such as toluene due to the increased concentration of hydrogen in the pyrolysis gas.
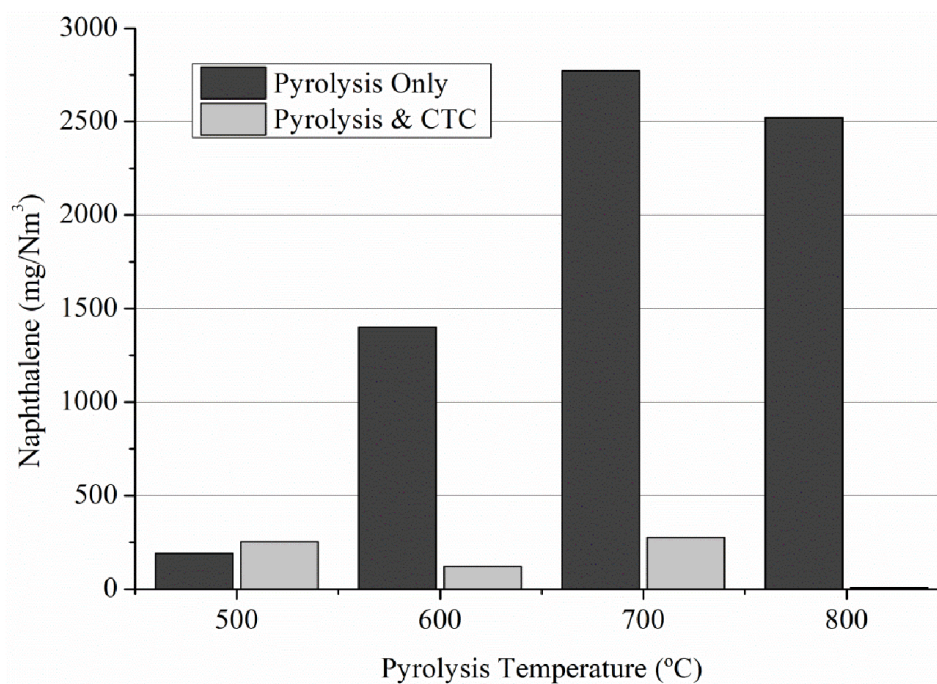
Figure 6.18 – Naphthalene comparison

Ringed structures such as those found in the three tar species considered are affected by reactions with O, HO_2 and O_2. A potential pathway for high temperature reduction was put forward by van der Hoeven, (2007). The ringed structure, in this example benzene, is converted to a phenoxy type radical through either exothermic metathesis reactions with molecular oxygen or through O addition. If the temperature is high enough, which is likely in the flame the phenoxy type radical will decompose and release carbon monoxide. If there is then enough oxygen present further radicals can be formed which can then break down.
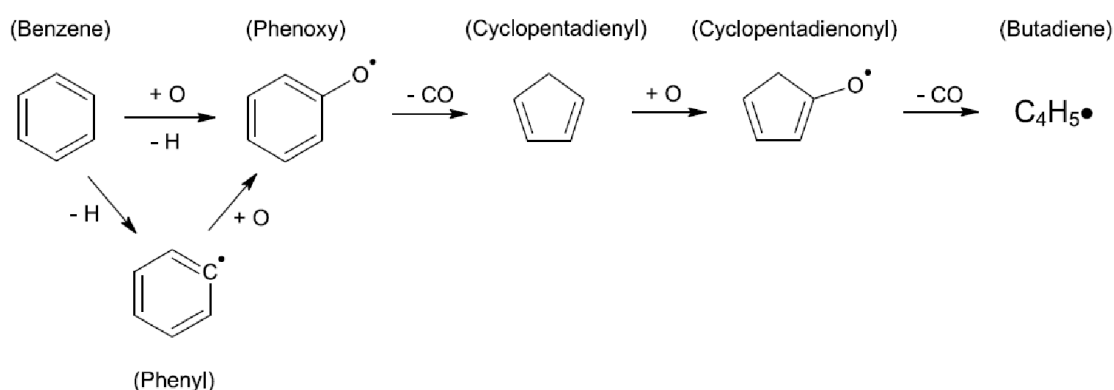
Figure 6.19 – General pathway for ring consumption in high temperature range (van der Hoeven, 2007)

The presence of oxygen in the flame accelerates the chain initiating hydrocarbon decomposition path resulting in faster H-atom abstraction. The presence of oxygen results in the availability of reactive O based radicals. Species that are alkylated are first converted to non-alkylated species such as benzene. In Table 6.5 the reduction in the relative tar concentration of toluene is in tandem with an increase to the relative concentration of benzene apart from when the pyrolysis temperature is 800°C where the relative concentration of toluene increased.

6.4 Gas Analysis

6.4.1 Gas from Pyrolysis

The molar fractions were converted into volume fractions assuming standard temperature and pressure (the compression factor, Z, was assumed to be equal to 1). The results from these gases were taken directly from the readings from the gas chromatograph.

Gas Composition (vol.% dry basis)	GC Cycle		
	1	2	3
Hydrogen	*0**	5.0	5.5
Oxygen	0.2	0.1	1.9
Nitrogen	84.7	47.9	54.6
Methane	1.0	7.6	5.8
Carbon Monoxide	6.5	22.5	16.7
Carbon Dioxide	1.3	*0**	14.3
Total	93.8	83.1	98.7

Table 6.7 – Pyrolysis gas results – 500°C – Pyro500

trace – reported as less than 0.05 vol.% & 0* - suspected error in analysis

Gas Composition (vol.% dry basis)	GC Cycle		
	1	2	3
Hydrogen	0.2	9.7	14.7
Oxygen	0.1	*trace*	*trace*
Nitrogen	63.7	33.8	22.9
Methane	4.3	10	10.8
Carbon Monoxide	17.8	30.3	25.7
Carbon Dioxide	1.4	*0**	*0**
Total	87.4	83.8	74.1

Table 6.8 – Pyrolysis gas results – 600°C – Pyro600

Gas Composition (vol.% dry basis)	GC Cycle		
	1	2	3
Hydrogen	*0**	14.8	16.6
Oxygen	5.7	*trace*	*trace*
Nitrogen	67.7	22.1	26.6
Methane	2.9	12.9	11.8
Carbon Monoxide	10.9	33.6	28.2
Carbon Dioxide	*0**	*0**	*0**
Total	87.2	83.4	83.2

Table 6.9 – Pyrolysis gas results – 700°C – Pyro700

Gas Composition (vol.% dry basis)	GC Cycle		
	1	2	3
Hydrogen	18.8	14.4	15.1
Oxygen	9.8	*trace*	*trace*
Nitrogen	61.5	22.2	26.3
Methane	3.8	12.4	11.4
Carbon Monoxide	12.5	32.5	28.6
Carbon Dioxide	*0**	*0**	*0**
Total	106.3	81.5	81.4

Table 6.10 – Pyrolysis gas results – 800°C – Pyro800

The results show that at each of the four temperatures the first gas result on the initial GC cycle is normally different from the results from the second and third cycle. This is likely to be caused because of contaminants present in the sample line, as indicated by the high concentration of nitrogen. Thus; when the pump was started these contaminated gases entered the GC for analysis, skewing the initial result. At all four pyrolysis temperatures the initial reading has a spike in the volume percent nitrogen. At 500°C the first GC cycle reading for nitrogen was 84.7% before decreasing to 47.9% and then 54.6%. A similar trend is apparent at 600°C where the volume of nitrogen reduces from 63.7% in cycle one, to 33.8% and 22.9% in cycles 2 and 3. This can be attributed to the large volume of nitrogen that was present in the pyrolyser before the pyrolysis reaction started, when wood pellets were loaded into the pyrolyser. The pyrolyser would have been completely purged with nitrogen as this was used to purge the pyrolyser of any oxygen, allowing for the reactions to be pyrolytic rather than combustion reactions.

It is also clear there are still issues when sampling carbon dioxide and propane. Both of these gases are analysed using the second board of the GC. At the experiments at 700 and 800°C no results for carbon dioxide were found to be present in the sampled gas. In the 500 and 600°C experiments CO_2 was found initially, in cycle 1, at low volume concentrations; 1.3% and 1.4% respectively. In the third cycle, at a pyrolysis temperature of 500°C the volume of carbon dioxide was found to be 14.3%. This reading was the singular determination of carbon dioxide in each experiment.

The total volume of permanent gas species was, in most analyses found to be between 10 – 20% less than 100%. In the majority of cases the volume.% is between 80 and 90%. The closest the analysis got to being 100% was in the third cycle of the 500°C experiment, where the total volume % was found to be 98.7%. This was also the only time where a reasonable reading for carbon dioxide was determined; therefore it was assumed that carbon dioxide makes up the majority of the unaccounted permanent gas species. As a result of this the volume of carbon dioxide was determined by difference, as in, the average volume percent of hydrogen, nitrogen, methane and carbon monoxide was deducted from the total (100%). The calculation for carbon dioxide is reflected in Table 6.11.

The GC results for cycle 2 and 3 in all four cases have similar values. For comparison the results from cycle 1 are discarded and the average result from cycle 2 and 3 are taken, this is shown in Table 6.11 and the key gas components (hydrogen, methane and carbon monoxide) are represented graphically in Figure 6.20.

	Pyro500	Pyro600	Pyro700	Pyro800
Gas Composition (vol.% dry basis)	Pyrolysis Temperature (°C)			
	500	600	700	800
Hydrogen	5.2	12.2	15.7	14.7
Oxygen	1.0	*trace*	*trace*	*trace*
Nitrogen	51.3	28.4	24.4	24.3
Methane	6.7	10.4	12.4	11.9
Carbon Monoxide	19.6	28.0	30.9	30.6
Carbon Dioxide	16.2	21.0	16.6	18.5
CO/CO_2 ratio	1.0	1.3	1.9	1.7
H_2/CO_2 ratio	0.3	0.9	0.9	0.8
CH_4/CO_2 ratio	0.4	0.5	0.7	0.6
H_2/CO	0.3	0.4	0.5	0.5
LHV (MJ/Nm^3)	5.2	7.1	9.5	9.2

Table 6.11 – Pyrolysis gas results – Averages

The lower heating value (LHV) of the pyrolysis gas increased as the pyrolysis temperature increased from 500 to 700°C. As the pyrolysis temperature increased 700 to 800°C, the LHV slightly reduced to 9.2 (MJ/Nm^3). Fagbemi et al., (2001) states that the LHV of the pyrolysis gas begins to stabilise at temperatures above 700°C which fits with the results reported in this study. The LHV is lower than the results presented by Fagbemi et al., (2001) and Encinar et al., (2000) who reported LHV's of gases to be slightly higher, in the case of Encinar et al., (2000) the LHV of the gas produced from the pyrolysis of cynara cardunculus is typically (2-3 MJ/Nm^3) higher than the results presented here. This can be attributed to the different biomass fuel and design of the equipment used in the process. The slight decrease in the LHV of the pyrolysis gas as the pyrolysis temperature increased from 700 to 800°C is caused because of the slight decreases in the volumetric yield of hydrogen, carbon monoxide methane.
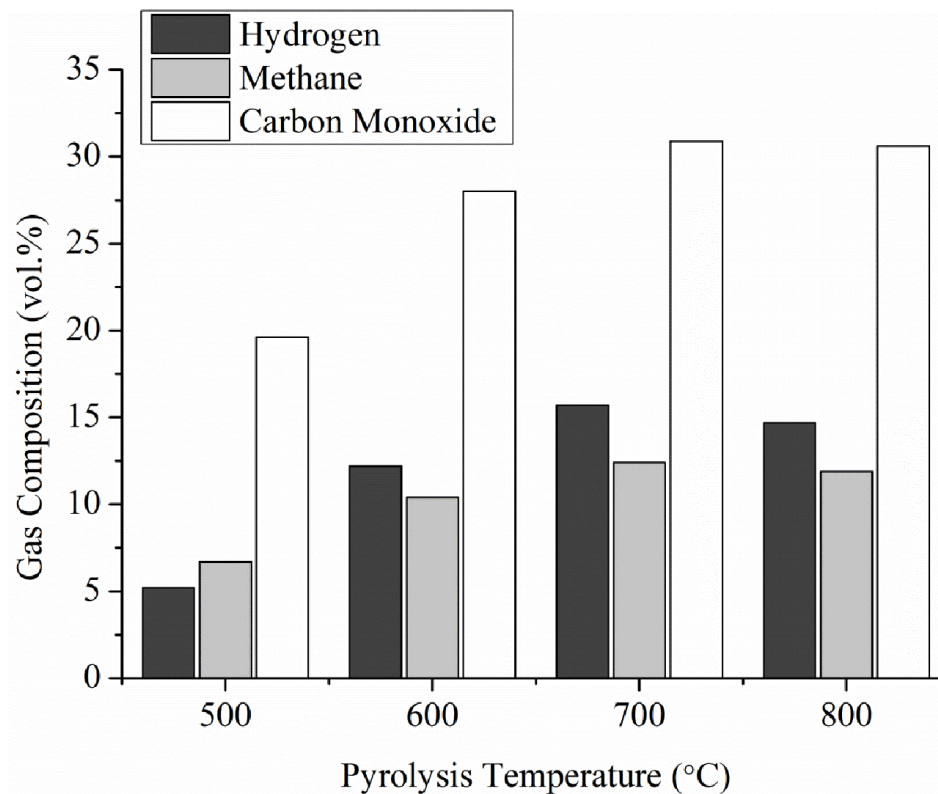
Figure 6.20 – Gas composition vs pyrolysis temperature

The total volume of each individual species could be calculated using data from other sources. This was done by using results from a study by Fagbemi, Khezami, & Capart, (2001). In this study the total amount of gas was recorded per kg of biomass at various pyrolysis temperatures. Wood was one of the biomasses analysed (see Figure 6.21), the results using this fuel were taken accordingly. Figure 6.21 used to calculate the total volume of gas produced, see Table 6.12.
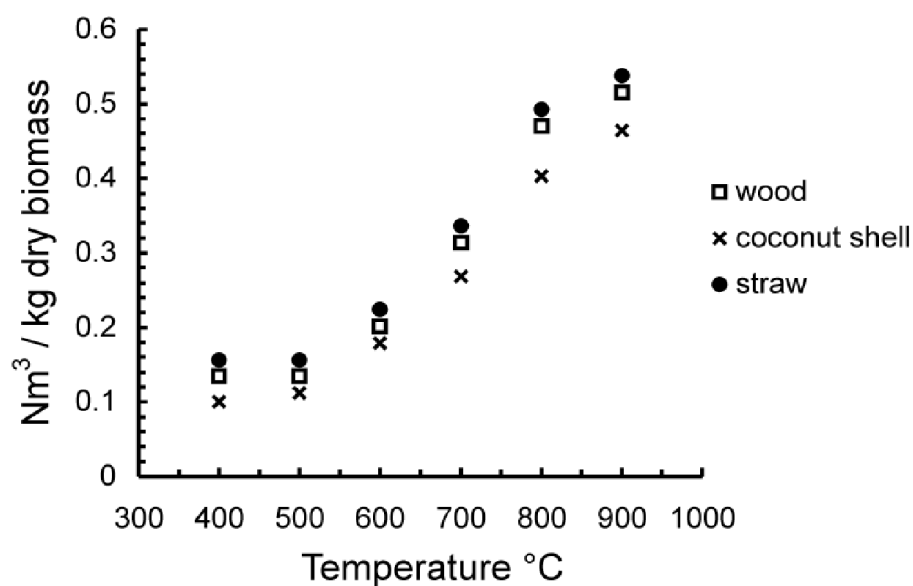
Figure 6.21 – Gas production as a function of temperature (Fagbemi et al., 2001)

Experiment Name	Pyrolysis Temperature (°C)	Gas production per unit of wood pellet (Nm³/kg)	Total gas production (Nm³)
Pyro500	500	0.14	0.14
Pyro600	600	0.2	0.2
Pyro700	700	0.32	0.32
Pyro800	800	0.48	0.48

Table 6.12 – Total gas production (Adapted from Fagbemi et al., 2001)

The volume fractions were multiplied by the value for the total gas production at each of the of four pyrolysis temperatures. Once these values were found the mass of the four analysed gas species was determined using the densities of the individual gases. Adding each of the values gives results for the total mass of the gas produced. Dividing the mass of each individual gas by the mass of wood pellets (1kg) that entered the pyrolyser allowed for calculation into the mass yield of each component gas. Figures 6.22 and 6.23 show the individual gas yields and total gas yield.

	Pyro500	Pyro600	Pyro700	Pyro800
	Pyrolysis Temperature (°C)			
Gas Yield (kg/kg of fuel) $*10^3$	500	600	700	800
Hydrogen	1.4	3.0	5.0	8.3
Methane	14.0	20.8	39.0	45.0
Carbon Monoxide	71.9	97.7	170.2	242.0
Carbon Dioxide	93.4	115.4	144.2	230.9

Table 6.13 – Permanent gas species yields per kg of fuel$*10^3$

The results shown in Figures 6.22 and 6.23 are in good agreement with the gaseous yield results as found by Neves et al. (2011) who analysed pyrolysis yield data from a wide range of studies. All four analysed gas species (CO, CO_2, H_2 CH_4) increased as the pyrolysis temperature increased.
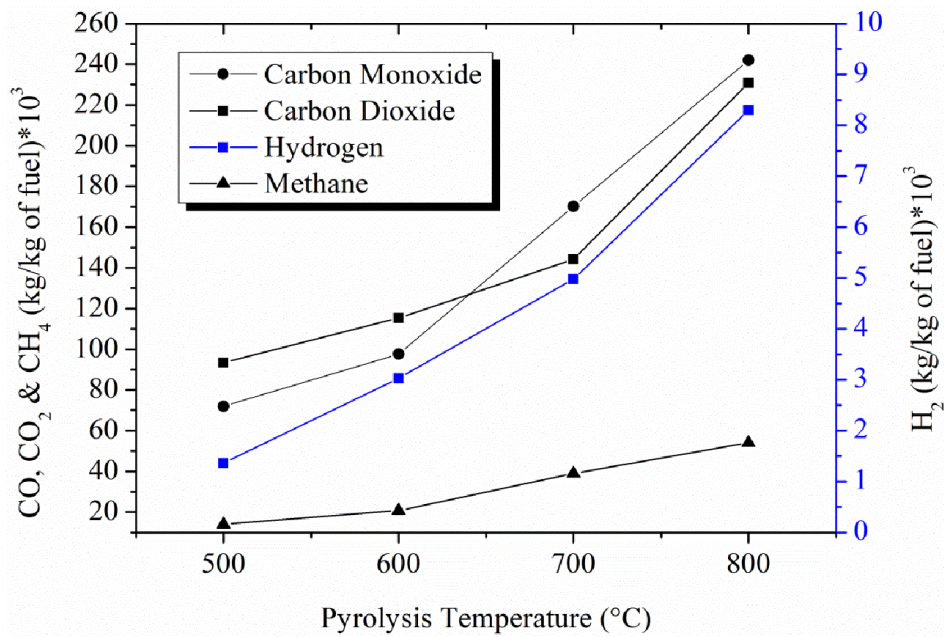
Figure 6.22 – Individual gas yields
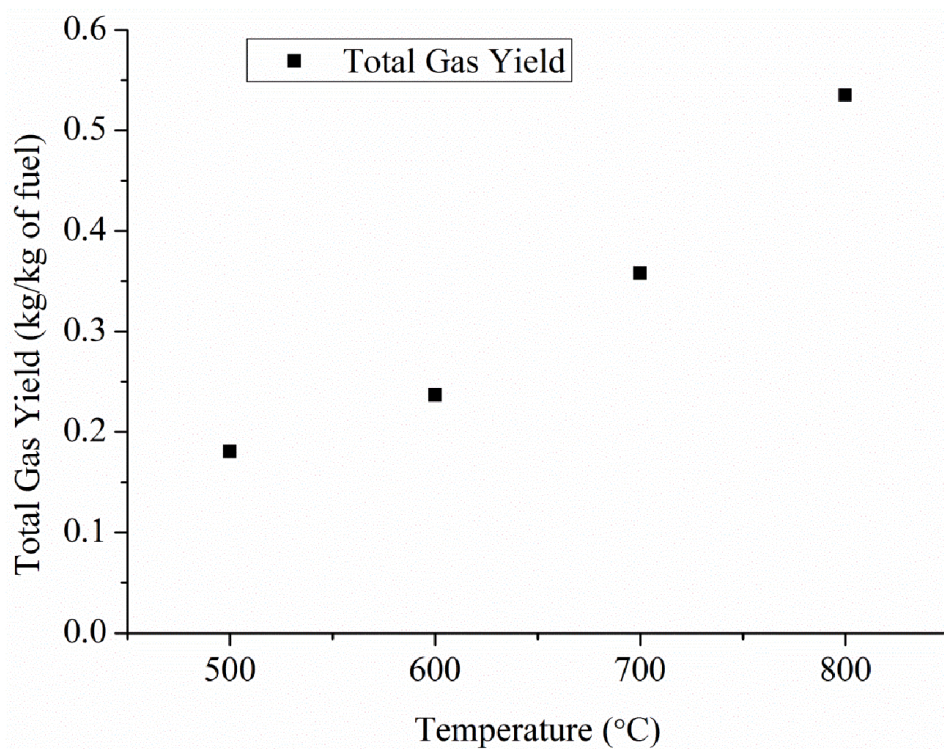
Figure 6.23 – Total gas yield

6.4.2 Hydrogen Analysis

The concentration of hydrogen in the pyrolysis gas increased steadily as the pyrolysis temperature increased from 500 to 700°C before reducing slightly at 800°C. Hydrogen increased from 5.2% at 500°C to 14.7% at 800°C.

The yield of hydrogen increased from just over 0.01 kg/kg of fuel to 0.08 kg/kg of fuel as the temperature increased from 500 to 800°C. There is almost a linear increase in the yield of

hydrogen (kg/kg of fuel) as the pyrolysis temperature increased from 500 to 700°C before increasing more rapidly at between 700 and 800°C. The results presented here compare well with the results from Fassinou et al. (2009). Although the fuel, equipment and residence times were different, the behaviour of the gas yields at increasing temperature is the same. Fassinou et al. (2009) reported an increase in the yield of H_2 from 0.31 ((kg of gas/kg of fuel)*10^3) at 450°C to a yield of 14.07 at 750°C. The yield of hydrogen at 550°C, 1.93 is ((kg of gas/kg of fuel)*10^3) , is comparable at 550°C to results in this study, where the yield was 1.4 at 500°C and 3.0 at 600°C.

Higher yields in hydrogen production are obtained by an increase in pyrolysis temperature. As temperatures increase there is a rise in the number of depolymerisation reactions and cracking reactions, which leads to an increase in hydrogen production.

6.4.3 Methane and Carbon Monoxide Analysis

There is a comparable trend for methane and carbon monoxide, with the composition of both showing a steady increase between 500 to 700°C before reducing slightly at 800°C.

Fagbemi et al. (2001) determined that the concentration of methane reaches a maximum at 750°C which is good agreement with the results presented. The concentration of methane is also within the range found by Fagbemi et al. (2001), who found the concentration to be between 13 and 15% between 700 and 800°C which is slightly above the methane composition in this experiment which was found to be around 12%. Carbon monoxide is formed from decarboxylation as well as depolymerisation reactions, which increase with pyrolysis temperature. Hence the yield of carbon monoxide increases with increasing temperature.

6.4.4 Gas Results – Pyrolyser and CTC

The results for the gas analysis are presented for each of the four pyrolysis temperatures. Due to the stoichiometric ratio required to support the stability of the flame in the CTC there is a heavy reduction in the active gaseous ingredients which are completely combusted. Tables 6.14 to 6.17 indicate the composition of the gas sampled from after the flame in the CTC. In all four cases there is a high volume of nitrogen. This can be explained through the addition of air used in the CTC for combustion. The volume of nitrogen in every GC analysis, apart from the third cycle at 600°C, is above 70% by volume. Nitrogen is non-reactive and dilutes the producer gas.

Due to experimental issues there are thought to be a number of errors with the gas results. The presence of oxygen at high compositions was not expected. Due to the nature of the setup of

the experiment the oxygen introduced to the system through the Coandă burner should be combusted with the pyrolysis gases. There are a number of instances where the oxygen composition is high, this could be due to the flame extinguishing thus there is no combustion reaction, resulting in oxygen being sampled. The composition of nitrogen is increased when compared to the sole pyrolysis experiments. Nitrogen is introduced to the burner through the Coandă so this is to be expected.

Gas Composition (vol.% dry basis)	GC Cycle		
	1	2	3
Hydrogen	*0**	0.3	0.2
Oxygen	24.7	11.8	8.2
Nitrogen	77.4	77.1	78.8
Methane	*0**	0.3	0.2
Carbon Monoxide	0.2	1.7	1.2
Carbon Dioxide	*trace*	11.8	14.1
Propane	*0**	*0**	*0**
Total	102.3	102.5	102.7

Table 6.14 – Combined gas results – 500°C – CTC500

Gas Composition (vol.% dry basis)	GC Cycle		
	1	2	3
Hydrogen	1.9	1.3	4.3
Oxygen	1.3	1.2	5.7
Nitrogen	81.7	75.5	63.6
Methane	*trace*	0.2	4.0
Carbon Monoxide	0.7	2.4	6.2
Carbon Dioxide	*0**	12.1	4.5
Propane	0.4	*trace*	*trace*
Total	86.0	92.7	88.3

Table 6.15 – Combined gas results – 600°C – CTC600

Gas Composition (vol.% dry basis)	GC Cycle		
	1	2	3
Hydrogen	*0**	0.5	3.4
Oxygen	19.4	3.3	17.4
Nitrogen	75.4	76.7	72.0
Methane	*trace*	0	0.8
Carbon Monoxide	0.4	0.6	2.4
Carbon Dioxide	0.61	*0**	4.4
Propane	*trace*	*trace*	*0**
Total	95.8	81.1	100.4

Table 6.16 – Combined gas results – 700°C – CTC700

Gas Composition (vol.% dry basis)	GC Cycle		
	1	2	3
Hydrogen	*0**	3.2	x
Oxygen	15.5	1.2	x
Nitrogen	78	76.8	x
Methane	*0**	*0**	x
Carbon Monoxide	0.3	3.0	x
Carbon Dioxide	0.3	15.5	x
Propane	*trace*	*0**	x
Total	94.1	99.7	x

Table 6.17 – Combined gas results – 800°C – CTC800

6.5 Char Analysis

6.5.1 Char Yield Analysis

Table 6.18 shows a clear indication into how the temperature at which pyrolysis is performed affects the mass of the final product. In each of the four experiments the 1000 grams of wood pellets were loaded into the pyrolyser in 10 sets of 100 gram batches. Table 6.18 shows that as the pyrolysis temperature increases the char yield is reduced. The decrease in the char yield is expected, similar pyrolysis experiments have shown similar results. Fassinou et al., (2009) researched how the temperature, biomass flow rate and residence times influenced the products when pyrolysing pine, the results from this study showed a clear decrease in the

156

yield of char as the temperature of the reactor was increased. This can be explained by the increase in temperature promoting reactions of thermal cracking, depolymerisation and decarboxylation which causes an increase in gas production from the biomass fuel (Fassinou et al., 2009). It is concluded that char production is favoured at lower temperatures whereas high temperatures promote gas formation. The char yield percentages also compare well with the results from Fassinou et al. (2009).

	Pyro500	Pyro600	Pyro700	Pyro800
	Pyrolysis Temperature (°C)			
	500	600	700	800
Char	293.4	227.8	158.9	156.3
Mass loss	706.6	772.2	841.1	843.7
% Mass loss	70.66	77.22	84.11	84.37
% Char Yield	29.34	22.78	15.89	15.63
Calorific Value (MJ/kg)	31.2	28.9	31.1	31.1

Table 6.18 – Char mass loss versus temperature

There is no obvious trend when analysing the calorific value of the chars. It is expected that the calorific value of the char should increase as the temperature at which they were thermally treated increases however this is not the case for these results. The calorific values of the analysed chars are within 10% of each other. The calorific value is closely linked to the amount of fixed carbon contained with the structure of the char. The mass percentage of fixed carbon contained in the char increases as the temperature of the pyrolyser increases (see section 6.3.2), however this does not appear to alter the calorific value in a uniform relationship. This could be that due to all the chars having a high rate of fixed carbon (above 85%) and with the value of fixed carbon being within a small range (between 85.7% and 92.7%) the slight changes in fixed carbon are not enough to result in changes in the calorific value (Encinar et al., 2000).

Ryu et al. (2007) tested batch pyrolysed pinewood at a range of temperatures (300 – 700°C). The results from this study are comparable to results presented here. In experiments performed by Ryu et al. (2007) the mass yield of char dropped steadily as the temperature was increased from 500 to 700°C. At 700°C the char yield in this study is 15.89% which is lower than that found by Ryu et al. (2007) where the char yield was 22%. This difference can be attributed to the fuels used in both experiments being different and also the setup of and

execution of the actual pyrolysis process. Both experiments have similar trends which follow the usual trend as found in other studies on the pyrolysis of biomass; namely (Neves et al., 2011; Demirbas, 2004; Encinar et al., 1996).

6.5.2 Proximate Analysis

The chars were analysed by TGA to determine their inherent properties. Again it is expected that the chars will have similar physical properties to the chars in the pyrolysis only experiment.

	Pyro500	Pyro600	Pyro700	Pyro800
	Pyrolysis Temperature (°C)			
	500	600	700	800
Sample Mass (mg)	13.98	16.16	13.96	12.24
Moisture (%)	1.0	1.2	1.0	0.9
Volatiles (%)	13.9	12.9	6.8	6.4
Fixed Carbon (%)	85.7	85.4	91.3	92.7
Ash (%)	0.0	0.3	0.6	0.0

Table 6.19 – TGA of wood pellet char
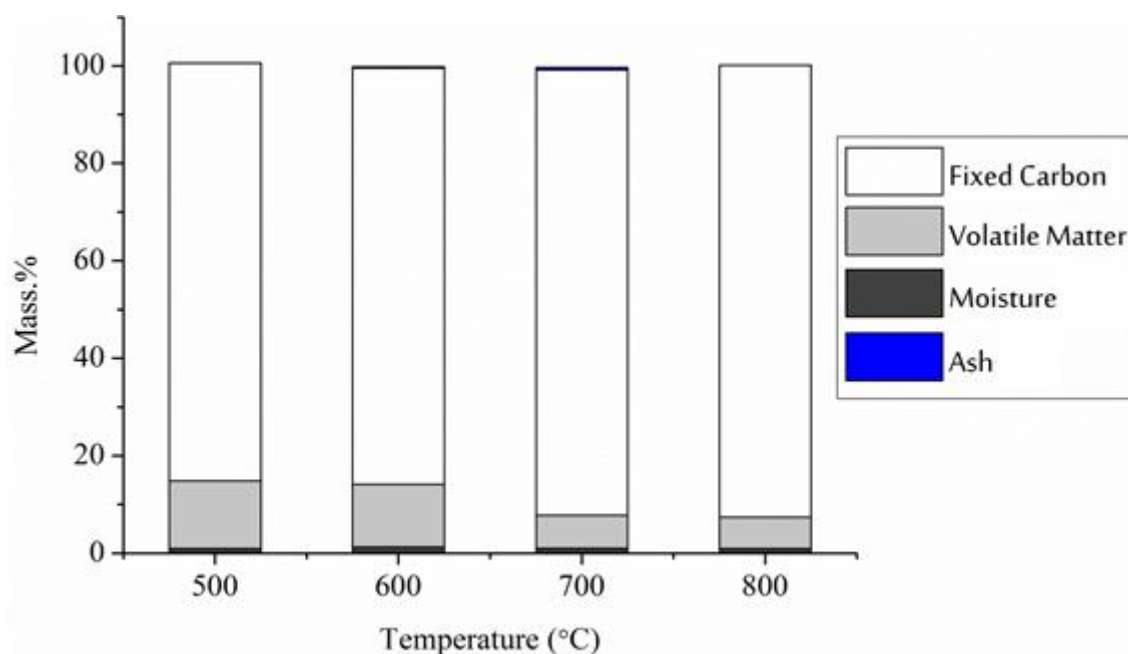
Figure 6.24 – TGA of wood pellet chars

The ash content in the char was below 1% (by mass) of the analysed sampled. There are no obvious trends relating to the amount of remaining ash as the pyrolysis temperature increased. The wood pellets used in the experiments have low ash content so the results are expected.

158

Ryu et al., (2007) performed a proximate analysis on pinewood char samples at a range of different temperatures and found the ash content to be less than 2% in all cases. Fassinou et al. (2009) found that the yield of ash increased gradually from 1 to 1.7% as the temperature increased from 450 to 750°C this trend is not apparent in this study, there is no obvious relationship between temperature and ash content in char.

There is no obvious trend for the moisture content in the chars; the moisture content in each of the four cases was close to 1%. This can be explained due to in each of experiments the pyrolysis temperature is above 100°C meaning that any moisture contained in the wood pellets would have been lost in the pyrolysis process.

The increased pyrolysis temperature led to a decrease in the amount of volatile matter contained within the char sample. The volatile matter content dropped from 13.9% to 6.4% as the temperature was increased from 500 to 800°C. The decrease in volatile matter results in an increase in the fixed carbon content, which is accurate apart from the char pyrolysed at 600°C where the fixed carbon content decreases slightly from 85.7% to 85.4%. This tendency was also found by a number of researchers including (Fassinou et al., 2009; Phan et al., 2008; Ryu et al., 2007; Demirbas, 2004; Fagbemi et al., 2001) when pyrolysing a number of wooden and biomass fuels. The principle behind this is best described by Fassinou et al., (2009) who explains that molecules within biomass crack when they are thermally treated, if the molecules are light than they are more likely to do so. When the temperature at which pyrolysis is performed is increased this phenomenon is intensified therefore the volatile matter content is reduced as the temperature is increased. Demirbas, (2004) determined that increases in temperature reduce the amount of hydrogen and oxygen in the char due to the scission of weaker bonds in the structure of the biochar, thus increasing the temperature increases the percentage of fixed carbon in the char. At 800 and 900°C the mass of fixed carbon is above 90% (91.3% and 92.7% respectively) making the char of a very high quality. Chars of this quality can be used in the metallurgical, chemical, food and pharmaceutical industries (Fassinou et al., 2009).

6.5.3 Thermogravimetric Analysis

Figures 6.25 and 6.26 shows the TG and DTG of the char samples. The shape of the TG and DTG curves for each of the four char is generally very similar. There is a slight decrease in the mass of the sample as the temperature of the analyser is heated from towards 110°C, it is this fraction that equates for the moisture. The curves then stabilise and flat-line until the analyser temperature reaches 350°C. At this point volatiles still contained within the char

structure are released, however as the char sample have already been thermally treated at high temperature the amount of volatiles contained within the sample is low.
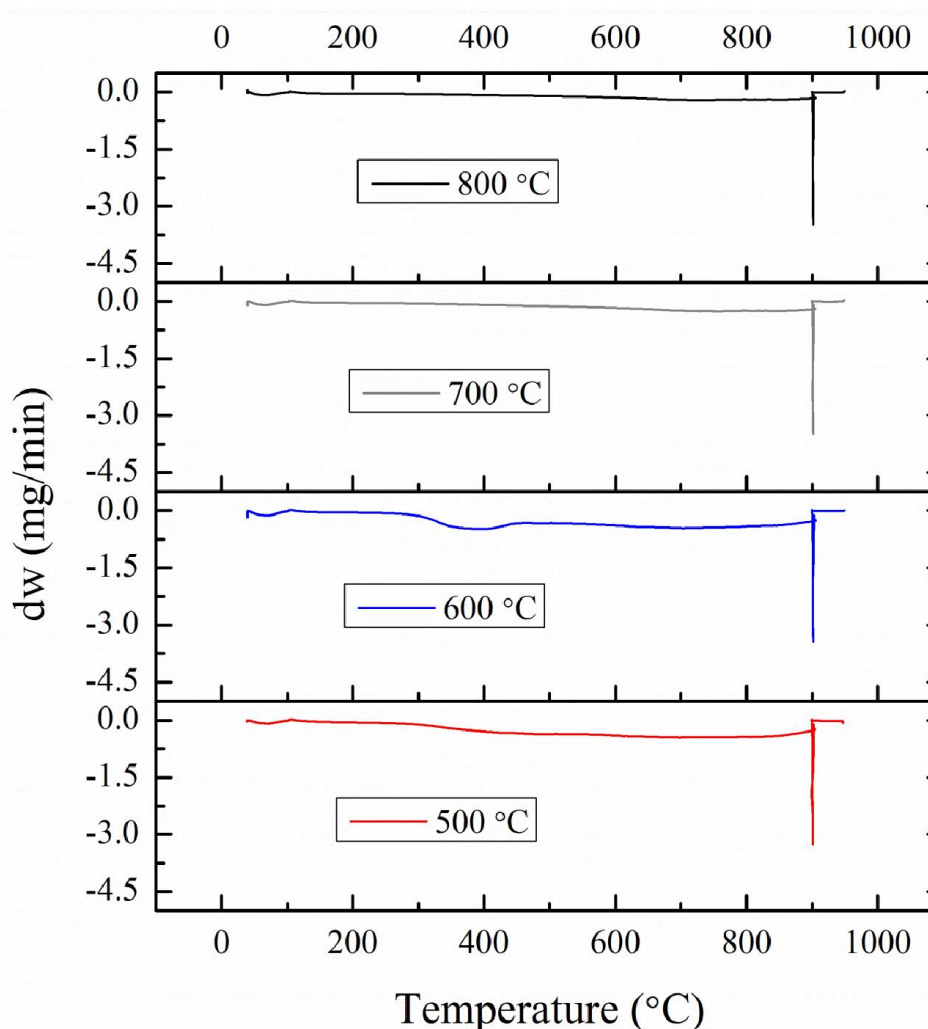
Figure 6.25 – DTG curves of chars

The TG and DTG curves for the chars at 500 and 600°C are similar. Both curves show deviations as the temperature approached 400°C, again this relates to the volatile matter content which was still present in the char samples. The 700 and 800°C also have similar TG and DTG curves due to the low amount of volatiles present. Each of the DTG curves indicates an initial increase in the rate mass loss as the samples were heated from 40 to 110°C; this change in mass is accounted for by moisture leaving the sample.
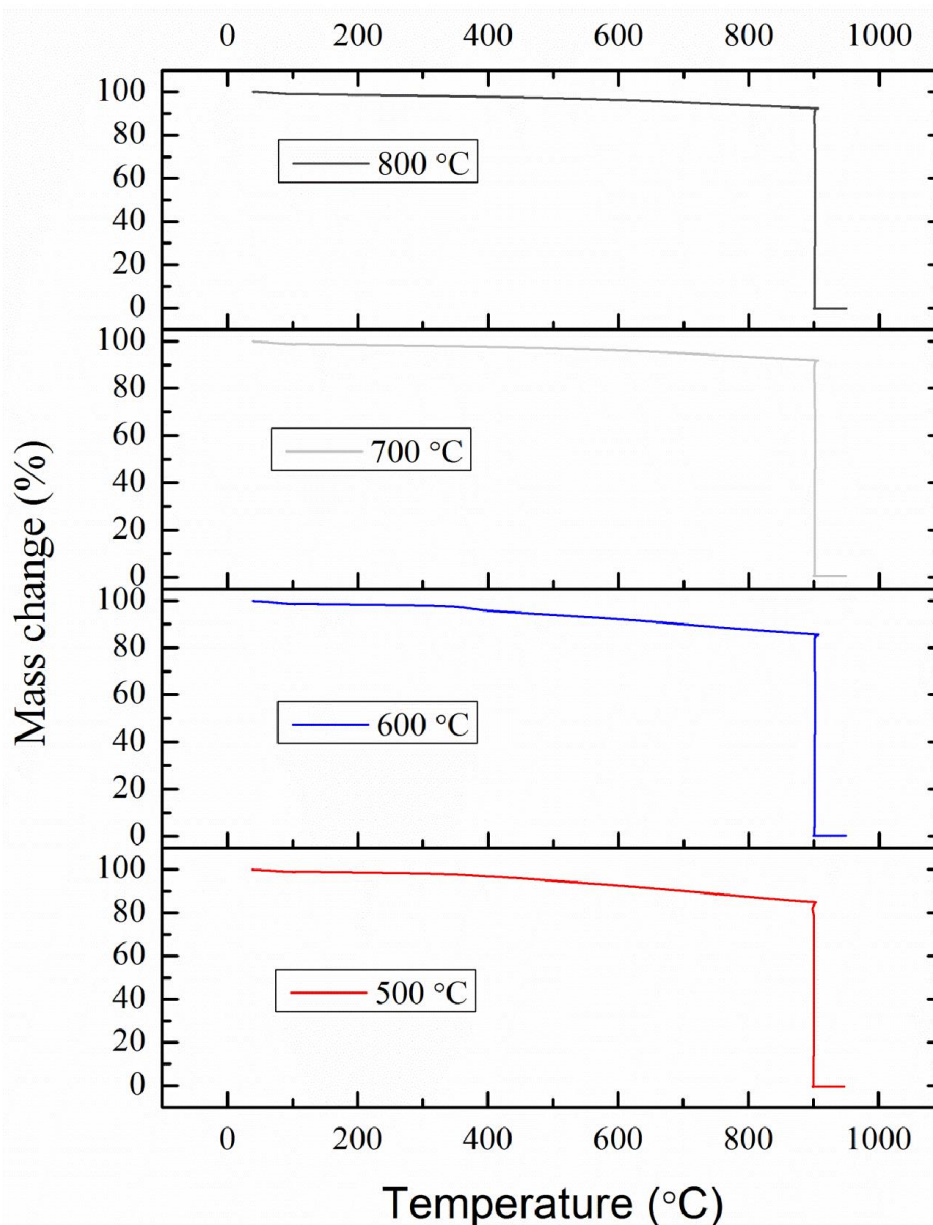
Figure 6.26 – TG curves of wood pellets chars

The most obvious change in the mass of the char happens at 900°C when oxygen is added to the analyser and the char is combusted. In all four cases there is a significant drop in mass when the chars are treated in this environment so that it can be concluded that the majority of the char sample is fixed carbon. In all four samples when oxygen is added (Step 6) to analyse the fixed carbon content the highest rate of change in the mass of the chars is found. In step 7, when the sample is heated from 900 to 950°C, the DTG curve stays constant in all four char samples, this shows that all of the fixed carbon contained within the samples has been removed.

Figure 6.26 shows the rate of change in mass of the sample against time. All four char samples have similar curves. Each curve shows a small rate of change between the second and fourth minute which can be credited to moisture loss. In all four cases the rate of change in

mass goes back to, or very close to zero at minute five. There is a discrepancy in the shape of the curves which show the change in mass as volatile species are removed from the samples. The chars treated at higher temperatures, 700 and 800°C, have reduced deviations due to these chars containing less volatile matter. The curves for all four samples have the biggest rate of change of mass at the same point, when oxygen is added to analyser and the char is combusted. The shape of the curves is very similar which is attributed to the high levels (above 85%) of fixed carbon in the char samples.

6.5.4 Ultimate Analysis

	Pyrolysis Temperature (°C)			
	500	600	700	800
Carbon (mass.%)	80.53 ±0.95	86.98 ±2.78	89.19 ±2.4	94.16 ±1.66
Hydrogen (mass.%)	2.45 ±0.14	1.70 ±0.22	0.91 ±0.11	0.66 ±0.21
Nitrogen (mass.%)	0.32 ±0.04	0.57 ±0.56	0.5 ±0.49	1.01 ±0.92
Oxygen* (mass.%)	16.7	10.75	9.4	4.17

Table 6.20 – CHN analysis of wood pellet chars

* by difference

The carbon content increased with increasing pyrolysis temperature. At 500°C the carbon constituted 80.53 mass.% of the char, this value increased steadily as the pyrolysis temperature increased, and reached a maximum at 800°C (94.16%). This increase was also found by Liu et al., (2010). The hydrogen content decreases with temperature, reducing from 2.45% to 0.66% as the pyrolysis temperature increased.

6.5.5 Char Results - Pyrolyser and Coandă Tar Cracker

It is expected that the char results from the combined experiment will be very similar to the results from the singular pyrolysis experiments. The temperature for pyrolysis is the same; the only difference in these experiments is that the produced gases and tar vapours are sucked through a Coandă burner. The wood pellets are treated under the same thermal conditions therefore the results for the chars should be similar.

	CTC500	CTC600	CTC700	CTC800
	Pyrolysis Temperature (°C)			
	500	**600**	**700**	**800**
Char	203.8	185.4	165.2	154.3
Mass loss	796.2	814.6	834.8	845.7
% Mass loss	79.6	81.5	83.5	84.6
% Char Yield	20.4	18.5	16.5	15.4
Calorific Value (MJ/kg)	33.0	32.5	33.0	32.2

Table 6.21 – Char yield from combined experiment

As expected the char yields show similar trends to those found in the pyrolysis only experiments. As the temperature of pyrolysis increases from 500 to 800°C the yield of char decreases caused by the increase in volatile matter leaving the structure as weaker bonds are readily broken by increases in temperature. Again there is no obvious pattern when examining the calorific value of the produced char.

6.6 Summary

This chapter explores the performance of the CTC and evaluates the system's effectiveness for destroying tar produced from biomass pyrolysis. In the first set of experiments wood pellets were pyrolysed at a series of temperatures (500, 600, 700 and 800°C) the products from the pyrolysis reaction were analysed. The composition of the gas and tar products were analysed evaluated, the char product was tested to analyse its chemical characteristics. In the second set of experiments the pyrolysis gas was treated in the CTC. The effect of the CTC on the gravimetric tar yield and on key tar species (benzene, toluene and naphthalene) was evaluated by comparing the yields and relative concentration of these species before and after treatment with the CTC. The CTC caused a severe reduction in the yields of both the gravimetric tar and the key tar species. The destruction is caused by the addition of oxygen. This increases the temperature through combustion promoting thermal tar destruction and also increases the radical pool, which are key in initiating tar destruction reactions.

7. CFD Modelling

7.1 Introduction

Modelling of the Coandă ejector, which is the key component of the CTC, was performed to determine how certain attributes of the ejector affect its performance. It is considered that understanding what these affects are and knowing what changes could be made could allow for further understanding, development and improvement of the CTC. CFD allows for swift analysis that avoids the requirement for costly experimental equipment and time consuming experimental techniques.

This chapter is divided into 3 main sections. The first section examines some relevant literature on researchers who have modelled Coandă based ejectors. The results from the literature review are used as comparison for the present modelling set-up and results. The chapter goes on to discuss the setup of the geometry, mesh and the computations and conditions in ANSYS Fluent, before the results from the simulations are presented and discussed.

7.2 CFD Modelling of Coandă Ejectors - Literature Review

7.2.1 Optimisation Study of a 3D Coandă Ejector (Kim et al, 2006)

Kim et al. (2006) performed work on Coandă ejectors to study the internal flow patterns and the effect of various design parameters have on the mass flow rate of the induced or secondary flow. Kim et al. (2006) used computation fluid dynamics to perform the required numerical analysis on the ejector. The mesh for the simulation was made up from 350,000 cells in the three dimensional domain, as shown in Figure 7.1. A CFD code called CFD-FASTRAN was used. CFD-FASTRAN is a "density based finite volume computational fluid dynamics code which solves the three-dimensional compressible Navier-Stokes equations in the desired domain" (Kim et al., 2006).
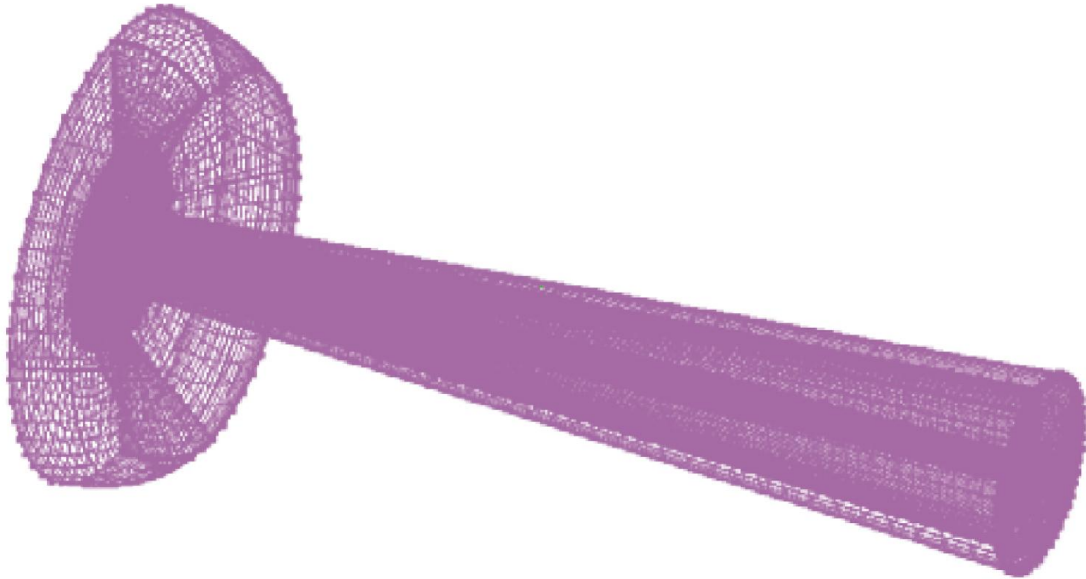
Figure 7.1 – 3D grid system for a Coandă ejector (Kim et al., 2006)

Kim et al. (2006) set up the CFD system so that the reservoir inlet was at a total pressure of 0.6 MPa, the total temperature was set to 300 K. The velocity vectors at the primary flow nozzle exit and the Mach contours at the ejector throat were modelled, see Figures 7.2 and 7.3.
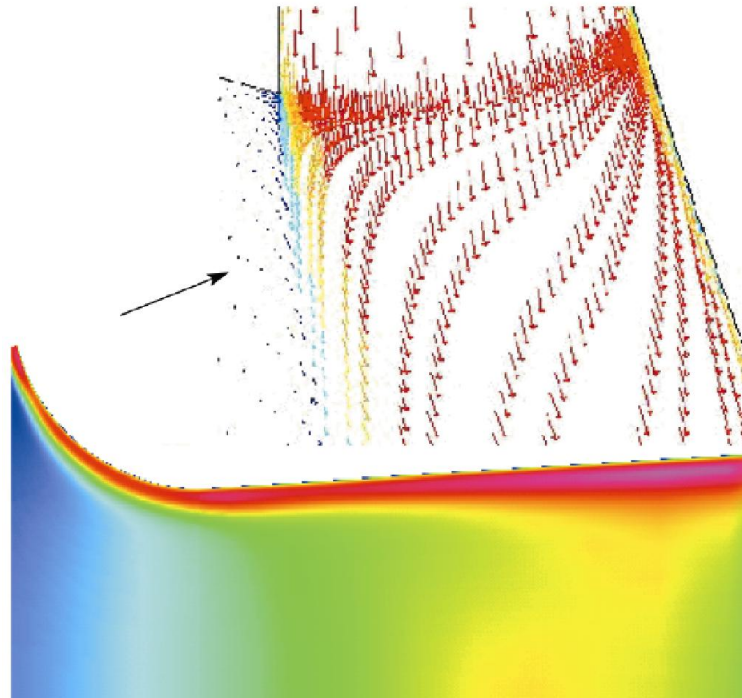
Figure 7.2 – Primary flow nozzle velocity vectors (Kim et al., 2006)
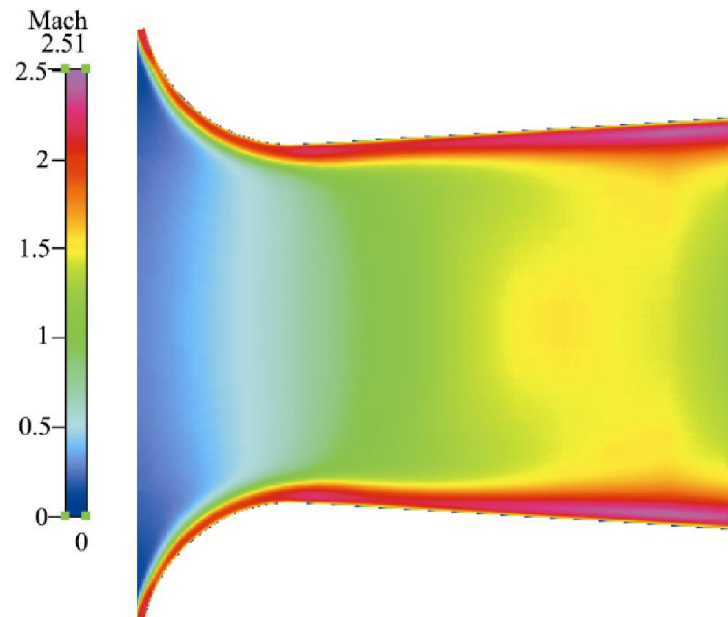
Figure 7.3 – Ejector throat Mach contours (Kim et al., 2006)

Figure 7.2 and 7.3 indicate that the induced or 'secondary' flow does not follow the same path as the primary jet. Kim et al. (2006) also modelled the static pressure at the ejector throat shown in Figure 7.4.
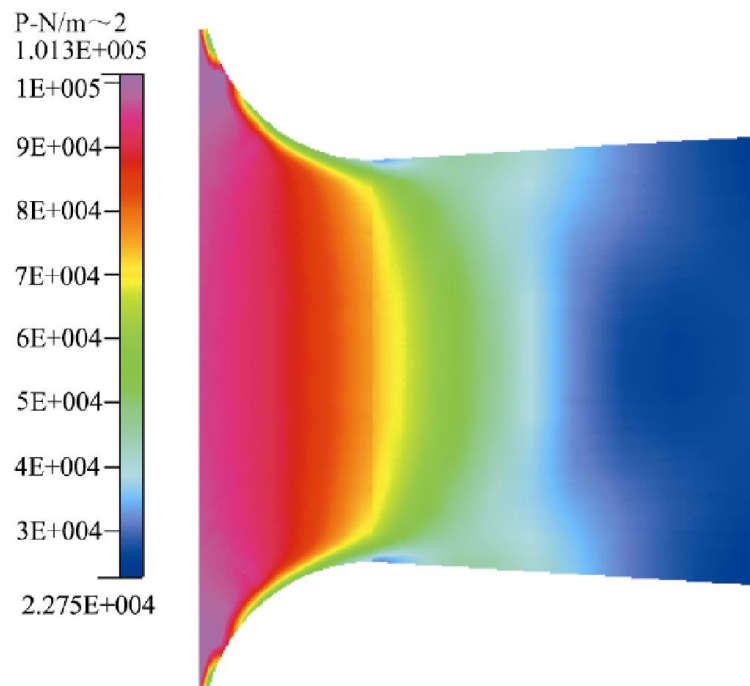
Figure 7.4 – Static pressure at Coandă throat (Kim et al., 2006)

Using Figure 7.4, Kim et al. (2006) concluded that due to good static pressure recovery it can be presumed that the suction on the induced flow is not caused by the primary jets expanding creating a low pressure zone but instead caused by turbulent mixing at the boundary between the two flows generating a dragging effect, which drags the secondary flow along the ejector.

166

Kim et al. (2006) then plotted velocity vectors against a dimensionless number to represent the diameter of the Coandă ejector. From this plot it was concluded that there are two parts; a region of large velocity gradient from the primary flow and a region where the velocity gradient is smaller which is from the induced flow.

Kim et al. (2006) went on to investigate how changing certain geometrical parameters alters the performance of the ejector. The throat gap, *e*, has a large effect on the ratio of mass flow rates. The smaller the throat gap the more enhanced turbulent mixing is at the throat of the ejector therefore causing an increase in the mass flow rate of induced air. Decreasing the throat gap also has crucial impact in the mixing length for the two flows in the ejector. Having a smaller throat gap decreases the mixing length which could indicate a rapid mixing layer growth in the ejector.

7.2.2 Coandă Ejectors for Pneumatic Solid Transfer (Guerriero, 2008)

Guerriero (2008) performed work on modelling Coandă ejectors using FLUENT. In this study a two dimensional model was analysed and the results were compared with experimental measurements gathered from pitot tube and particle image velocimetry (PIV) tests. The model used for the CFD simulations replicated the experimental geometry, as shown in Figure 7.5. The total length of the ejector is 400mm and velocities are measured across the length of the ejector at 0, 50, 100, 200, 300 and 400 mm, see Figure 7.5.
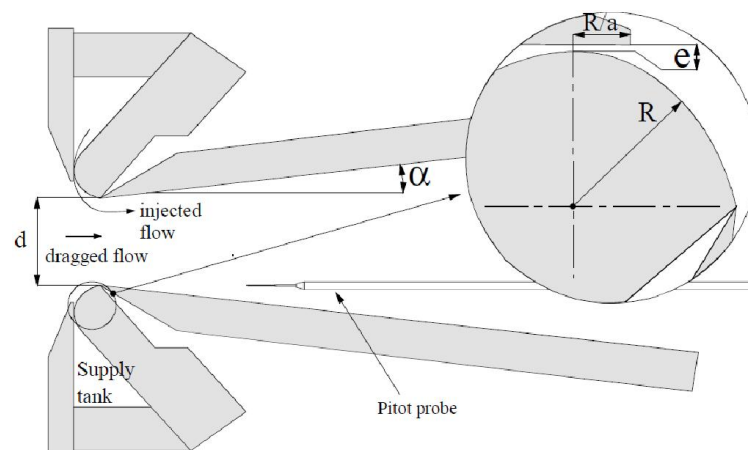
Figure 7.5 – Two dimensional plane of the test rig (Guerriero, 2008)

Where; R is the radius of the curved surface from where primary flow enters

      a is the length of the divergent nozzle after the throat

      e is the width of the primary flow inlet

      α is the angle of the ejector walls

d is the width of the throat of the ejector where flow is induced
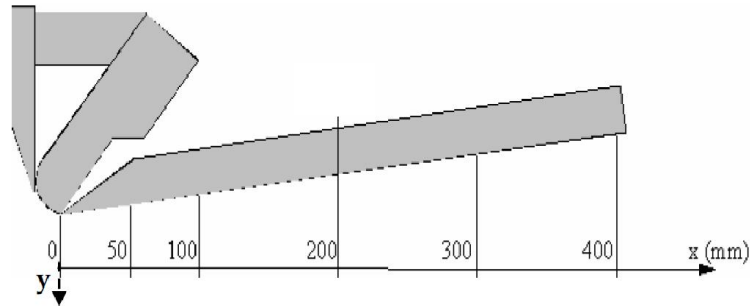
Figure 7.6 – Sections at which the velocity was measured (Guerriero, 2008)

Guerriero (2008) performed analysis using Fluent by comparing different turbulent models that can be selected on Fluent and compared the results from results obtained from PIV tests. It was determined that the model that matched most closely to the experimental data was the RNG model, see Figure 7.7. The re-normalisation group (RNG) method is a turbulence model derived from instantaneous Navier-Stokes equations using a mathematical procedure called re-normalisation group. There are two key differences between the measured and modelled velocities. Firstly at the zone close to the wall there is a large difference which is explained as an experimental problem, because the pitot tube affects the fluid flow in this region, and results in inaccurate measurements. Secondly there are discrepancies for the mixing layer.
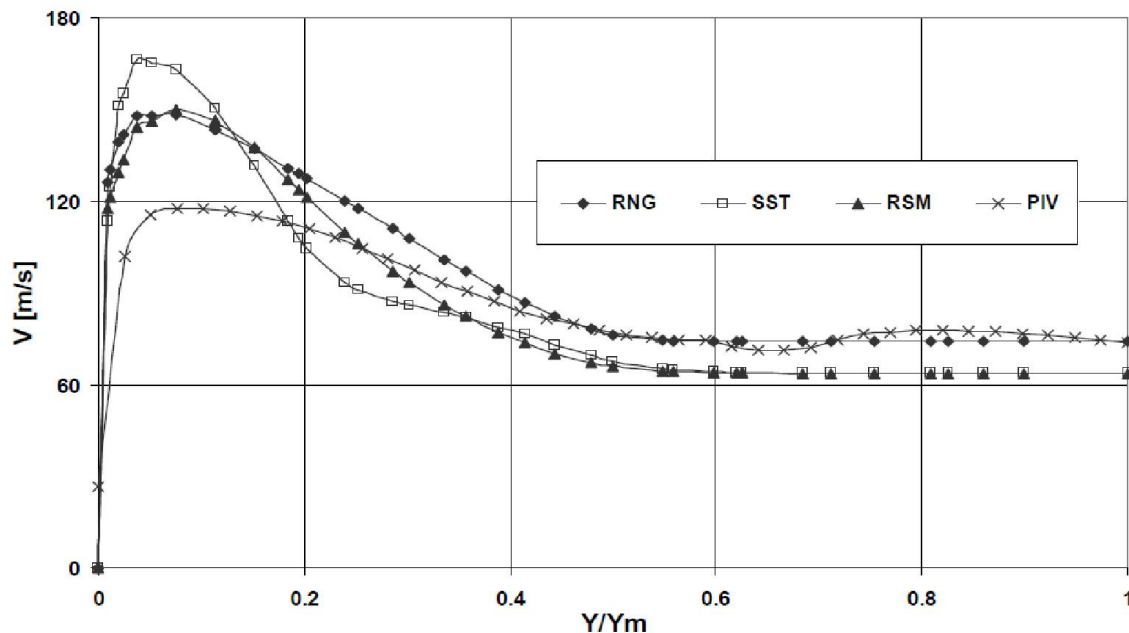
Figure 7.7 – Differences between velocity profiles for a range of turbulent models calculated by Fluent and PIV measurements where x= 100 (Guerriero, 2008)

The CFD simulations performed by Guerriero (2008) proceeded with an analysis on how varying certain geometries in the Coandă affect the performance. It was found that increasing

the value of *e* – the width of the primary flow inlet – increases the injected flow rate causing an increase in the induced flow. This is caused by more momentum being transferred from the primary flow onto the induced secondary flow. This gives a good indication of how the level of induced flow is influenced by the size of the primary flow air inlet, but as Guerriero (2008) notes the performance of an ejector can also be critiqued in terms of the mixing length or the ratio between induced mass flow rate and injected flow. Guerriero (2008) concluded that decreasing the length of *e* decreases the mixing length. This is explained when looking at the velocity profiles in Figure 7.8, there is a flat velocity profile when *e* = 0.05 which indicates that mixing of the two flows is complete. The author explains that this is caused by *"pressure in the primary flow at the nozzle exit is lower and the compression through shock waves is imposed by the external pressure level has to be stronger, which implies a lower primary flow velocity in section 0"*. The lower the Mach number of the primary flow the faster expansion of the mixing layer.
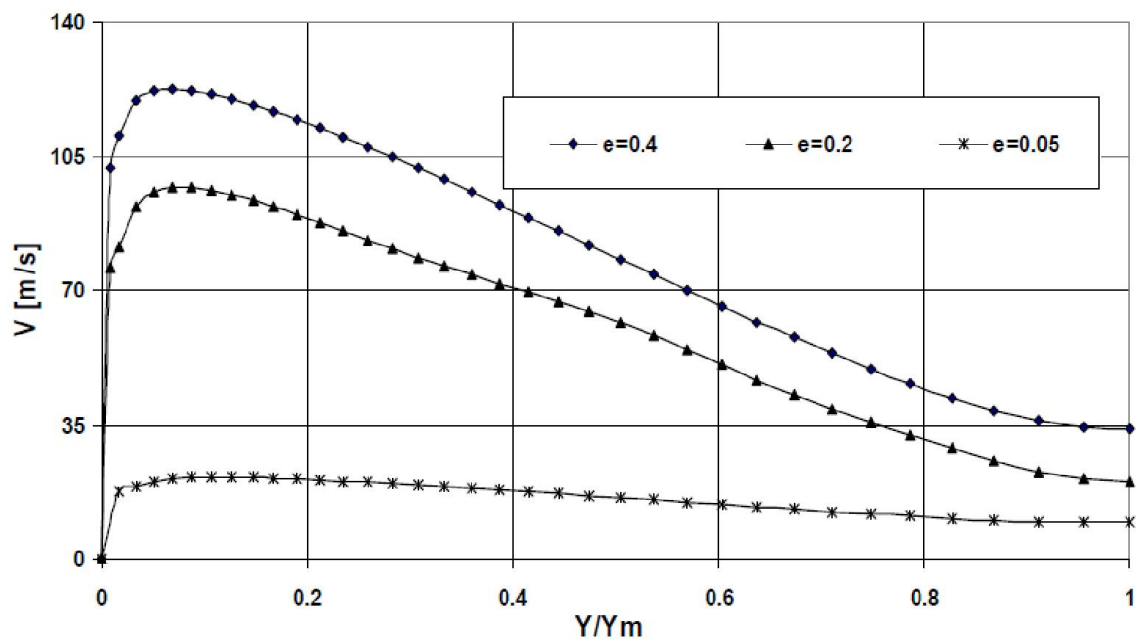
Figure 7.8 – Velocity profiles at x = 400 with varied lengths of *e* (mm) (Guerriero, 2008)

The throat diameter, *d*, was then examined by comparing different lengths. It was found that the induced mass flow rate increases slightly when the diameter was increased because suction of the secondary flow is caused by turbulent effects creating momentum transfer Guerriero (2008). The radius of the curve at the Coandă inlet had little affect on the analysis.

7.2.3 Analysis of Turbulent Flow (Alexandru et al., 2011)

Further work was carried out by Alexandru et al. (2011) on Coandă ejectors to determine and investigate how ejector performance is affected by altering various geometric parameters. Alexandru et al. (2011) used Fluent in conjunction with Gambit to generate and analyse the models. The three dimensional geometry used is shown in Figure 7.9 and the primary flow inlet is shown in Figure 7.10. The results obtained by the authors were set when the pressure at the primary flow inlet was set at 5 bar and when e = 0.25mm, R_1 = 7.5mm for the first case and where e = 0.4mm and R_2 = 37.5mm.
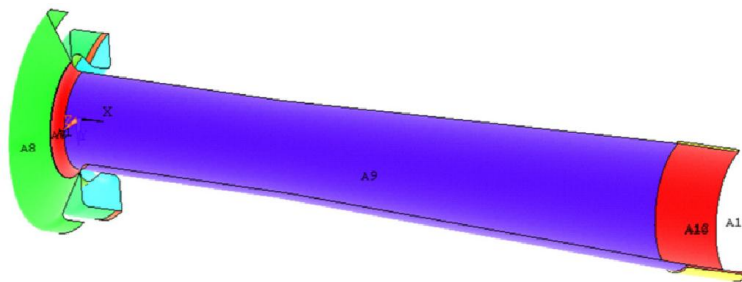
Figure 7.9 – Three dimensional geometry of Coandă ejector (Alexandru et al., 2011)
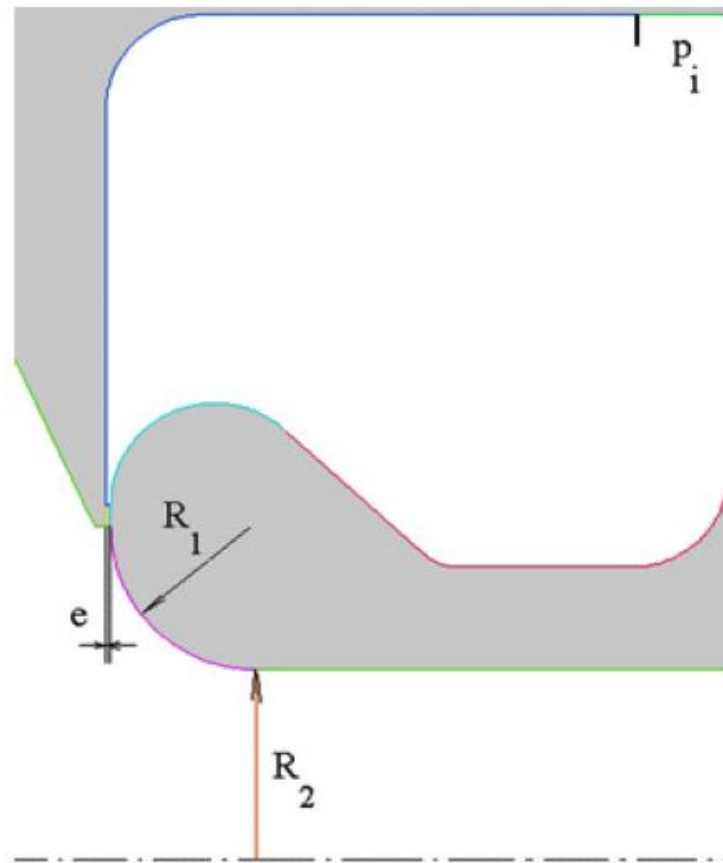
Figure 7.10 – Primary flow inlet (Alexandru et al., 2011)

Alexandru et al. (2011) results are similar to that of Kim et al. (2006). Mach number contours were modelled (see Figure 7.11) and it was determined that the induced flow does not follow the same pattern as that of the primary flow and the mixing of the two flows occurs in the divergent part of the ejector.
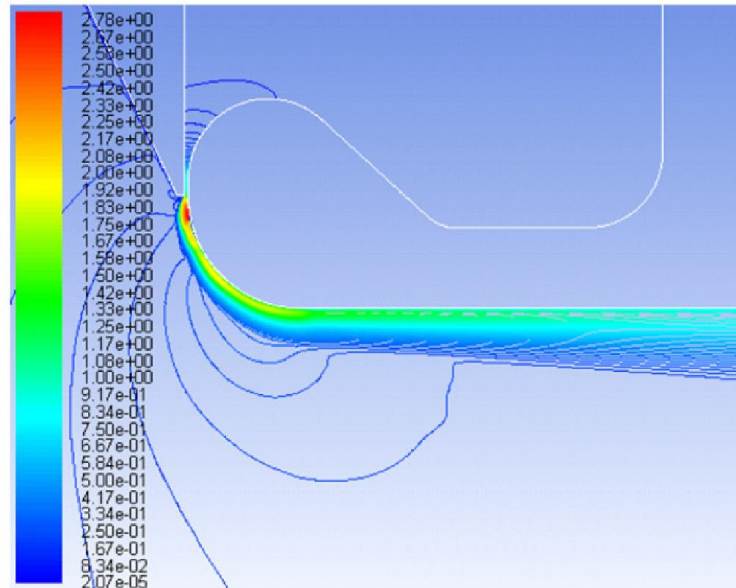
Figure 7.11 – Mach contours (Alexandru et al., 2011)

The authors then plotted the flow velocity at x = 0 and x = 550 for different Coandă diameters and Coandă gap widths. Again, in results similar to that of Kim et al. (2006) the plots can be split into two parts; large velocity gradients from the primary flow and small gradients for induced flow. When comparing the mass flow rate for different Coandă diameters, Alexandru et al. (2011) notes that larger the diameter, and thus larger cross section, only has an incremental increase to the overall mass flow rate.

7.2.4 Summary of Literature

It is concluded by the authors that from the computational results the Coandă gap, *e*, has a significant impact on the ratio of mass flow between primary and induced air as well as having a strong control on the mixing length. Decreasing the value of, *e*, leads to shorter mixing lengths which could indicate rapid mixing and later growth.

7.3 Introduction to Modelling

A two dimensional axisymmetric model was used for the CFD simulations. The geometry of the actual ejector used in the CTC was replicated as accurately as possible. The model was devised to be set up in two dimensions for a number of reasons. The primary reason was that a three dimensional model would require a large number of elements which would increase

the time required to run the simulations. ANSYS workbench version 14.5 was used for each part of the modelling system.

7.4 Geometry and Mesh Setup

As discussed the 2D model used to represent the CTC was drawn to be as geometrically close to the Coandă ejector used in the experimental system. A number of key parameters affect the overall performance of the ejector, these include; the Coandă gap width, the length of the divergent nozzle and the radius of the curve (Guerriero, 2008).

The success of the model depends on accuracy of the air injection through the Coandă gap. Primary air is required to adhere to the curved surface, and pass momentum onto secondary flow which is present at the inlet of the ejector. The key parameter in the Coandă ejector is the Coandă gap width, *e*. The value for *e* used in the experimental setup was measured to be 0.08mm. The geometry used for the Coandă ejector is shown in Figure 7.12.

Air enters the system through the air inlet at a determined pressure, in the experimental programme the air pressure was 5.2 barg. Air is ejected towards the Coandă curve by the divergent nozzle. The divergent nozzle was positioned 2 mm from the centre of the radius of the Coandă surface; this was done to ensure that the injected air is affected by the Coandă affect. The Coandă curve has a radius of 5mm. The Coandă ejector inlet where the secondary flow is entrained is 25 mm, this means that the total diameter of the inlet is 50 mm which is the same as the ejector used in the experiment, see Figure 7.12.
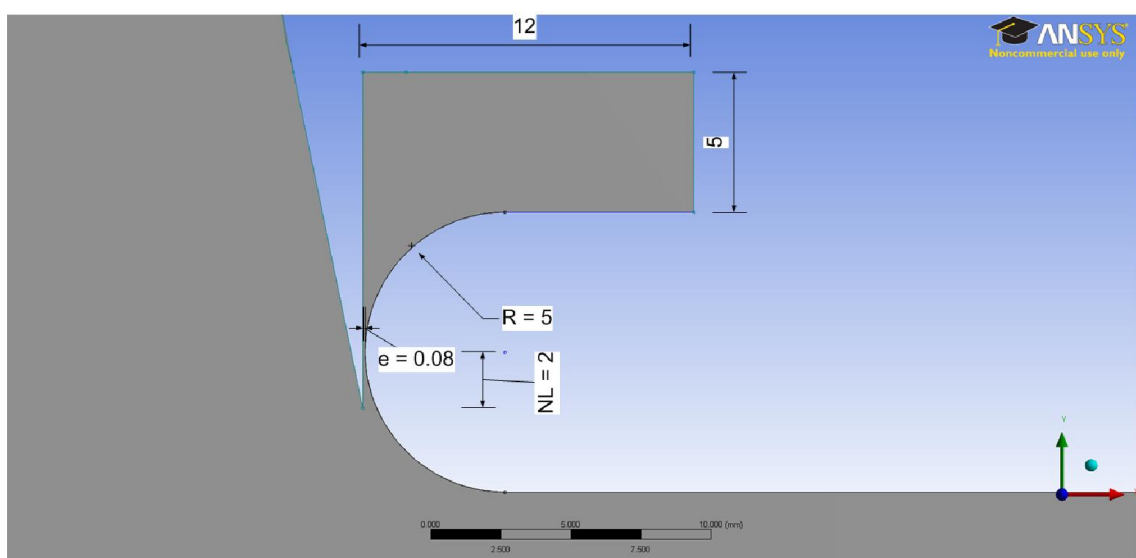
Figure 7.12 – Coandă Inlet

Additional key features for the model relate to the inlets of secondary flow into the computation domain, the positioning of the inlets was performed to replicate the position of

ambient air around the inlet of the ejector. Although this setup is different from the experimental rig where only the ejector inlet is enclosed by an outer casing, this was done to keep the model simple. Figure 7.14 indicates the position of the three secondary air inlets. *Ejector inlet 1* is positioned to the left of the Coandă ejector and is 60 mm in length, *Ejector inlet 2* is positioned adjacent to Ejector inlet 1 and is 70 mm in length, and the third inlet creates a complete boundary around the Coandă ejector and is 15 mm in length (see Figure 7.13). The three inlets allow for creation of a reservoir of secondary flow.
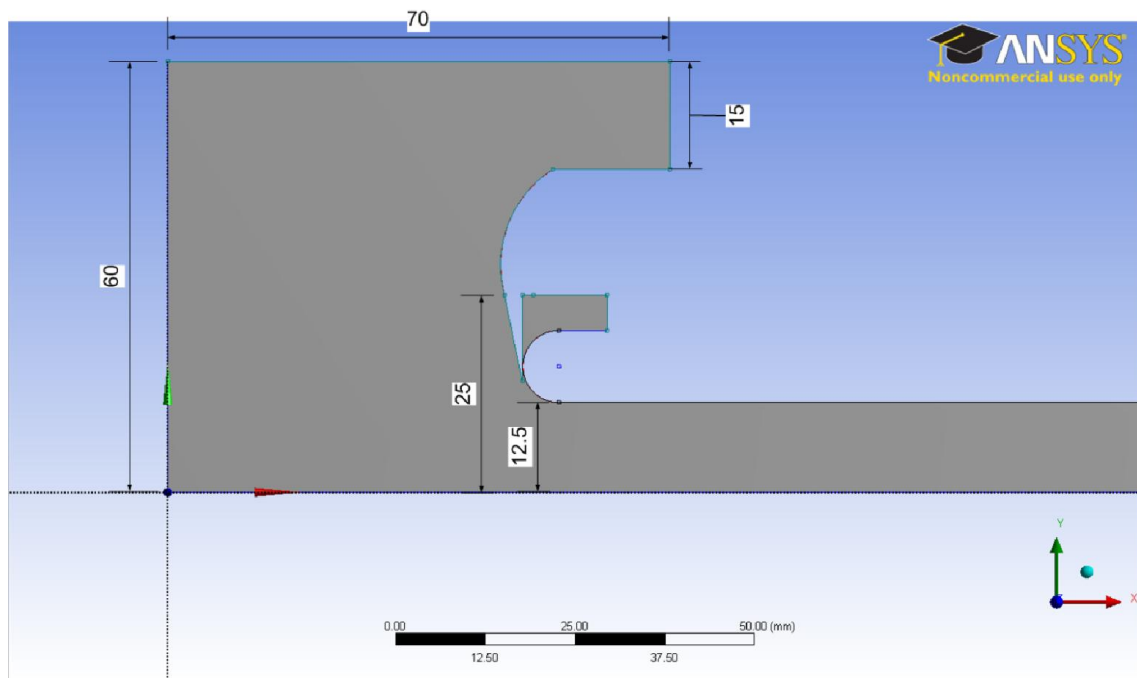
Figure 7.13 – Ejector inlets
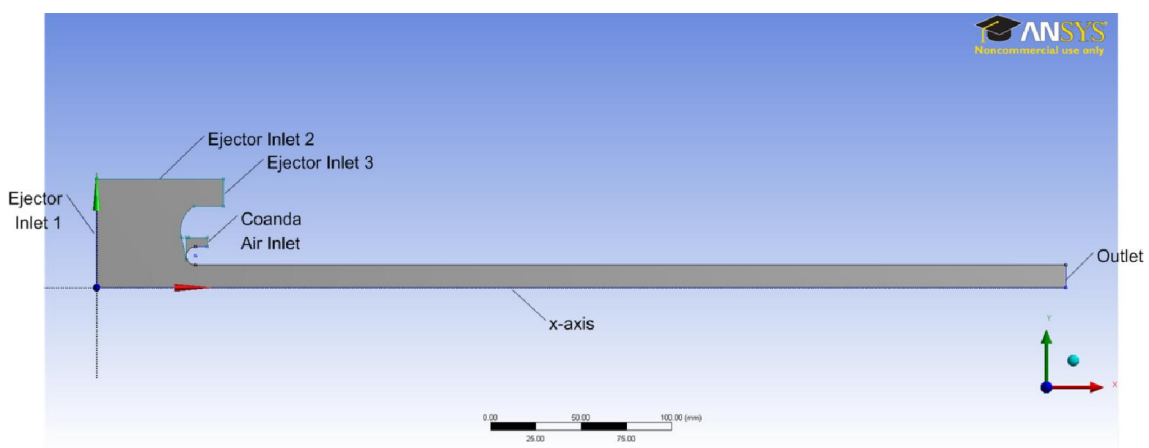
Figure 7.14 – Complete geometry

The x-axis runs along the length of the ejector, the Coandă ejector is axisymmetric so only half of the geometry is required to be modelled, reducing the time required to compute the model. The outlet of the ejector is positioned to the right of the ejector. The diameter of the ejector was kept constant from the Coandă inlet to the outlet.

The mesh was setup using the in-built meshing software in ANSYS workbench. The number of elements and nodes was kept below 40000 to reduce computational time. For all cases the advanced size function was set to *Proximity and Curvature*. The proximity setting ensures that all small 'gaps', such as the one for the Coandă gap are meshed more finely to provide a more accurate solution in these regions.

The quality of the mesh was reviewed by checking the skewness and orthogonal quality. The skewness is seen as one of the primary measures for evaluating the mesh quality (ANSYS, 2012), and determines how close a face or cell is to ideal, see Figure 7.15. The value of the skewness for a cell is ranked from 0 to 1. With 0 being ideal and 1 being degenerate. The average skewness of the mesh was determined to be 0.01, which is rated as an 'excellent' quality according to ANSYS, (2012).
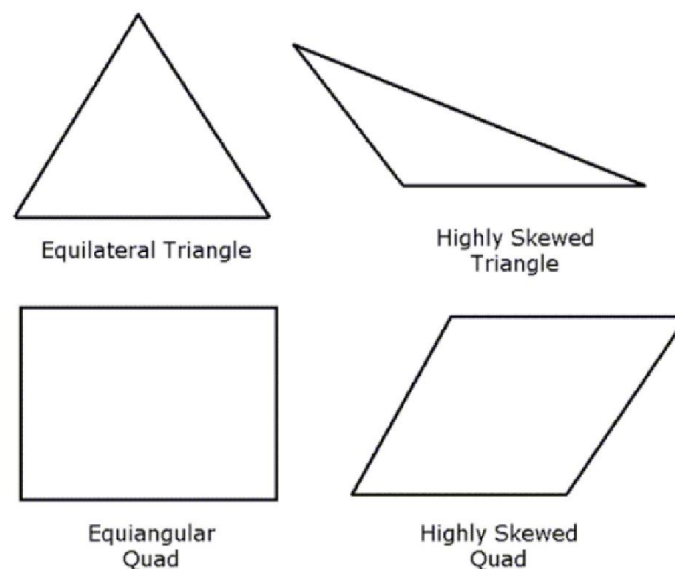
Figure 7.15 – Skewed and ideal equilateral and triangles (ANSYS, 2012)

The orthogonal quality was the second parameter used to determine the mesh quality. The range is between 0 and 1, with 1 being the best. The average orthogonal quality was determined to be 0.99. The mesh was considered to be valid for analysis because of the values for the average skewness and orthogonal quality. The final mesh is shown in Figure 7.16.
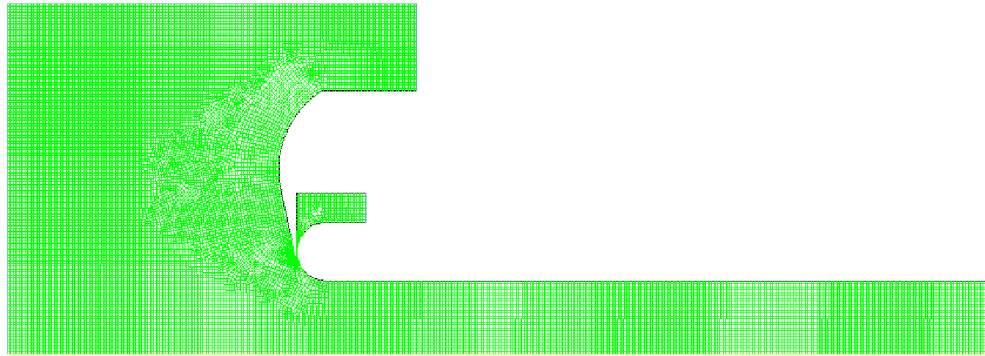
Figure 7.16 – Final mesh

7.5 FLUENT Setup

FLUENT has, over the past twenty years, become the leading software for CFD analysis and is well respected in industry and academia. FLUENT software allows for fast alterations of certain conditions in the computational model and this allows for quick and accurate comparison of numerous conditions. The ability to change such parameters allows for comparison and analysis of a number of cases and provides an insight into how such changes affect the flow field within the ejector.

7.5.1 FLUENT Theory – Governing Equations

This section describes briefly the fundamentals of the governing equations used for the CFD analysis. The governing equations are for all CFD problems are based on:

- Mass conservation

- Newton's second law (F = ma)

- Energy conservation

(Guerriero, 2008)

Some of the key aspects of the three governing equations are explored below, further details can be found in all CFD manuals and books;

Mass conservation equation

$$\frac{\partial p}{\partial t} + \nabla \cdot (\rho \vec{v}) = S_m$$

<div align="right">Eqn 7.1</div>

S_m acts as a source and is the mass added to the continuous phase from the dispersed second phase or from other sources defined by the user (ANSYS, 2010a). For two dimensional axisymmetric geometries, such as the one used in this simulation, the mass conservation equation can be given as:

$$\frac{\partial \rho}{\partial t} + \frac{\partial}{\partial x}(\rho v_x) + \frac{\partial}{\partial r}(\rho v_r) + \frac{\rho v_r}{r} = S_m$$

<div align="right">Eqn 7.2</div>

Where x is the axial coordinate, u_x is the axial velocity; r is the radial coordinate and u_r, the radial velocity.

Momentum conservation equation

Conservation of momentum in an non-accelerating reference can be described as:

$$\frac{\partial}{\partial t}(\rho \vec{v}) + \nabla . (\rho \vec{v} \vec{v}) = -\nabla \rho + \nabla . (\bar{\bar{\tau}}) + \rho \vec{g} + \vec{F}$$

<div align="right">Eqn 7.3</div>

Where p is the static pressure, $\bar{\bar{\tau}}$ is the stress tensor and $\rho \vec{g}$ and $\vec{F}$ are the gravitational body force and external body forces.

The Energy Conservation Equation

The energy equation is defined in Fluent as:

$$\frac{\partial}{\partial t}(\rho E) + \nabla . (\underset{v}{\rightarrow} (\rho E + \rho)) = -\nabla . (\sum_j h_j J_j + S_h$$

<div align="right">Eqn 7.4</div>

Where:

k_{eff}	-	the effective conductivity
J_j	-	the diffusion flux of species j
S_h	-	the heat of the chemical reaction

7.5.2 FLUENT Theory - Viscous Models

There are a number of different models that can be used for modelling turbulence in ANSYS FLUENT. The available k-ε models include; standard, RNG, and realizable. As well as these, there are k-φ models such as the standard and SST (Shear Stress Transport). Although each model has basic similarities, there are some differences such as the method used to calculate the turbulent viscosity and the terms used to describe the generation and destruction in the ε equation (ANSYS, 2010a).

In previous studies where Coandă ejectors were modelled two models have been principally used. Firstly, the standard k-ε model with non-equilibium wall functions and secondly the k-φ with SST (shear stress transport). These two models are considered in this work. More information on these models is available in the FLUENT theory guide (ANSYS, 2010a).

7.5.3 Set-up of FLUENT Calculation

This section discusses the setup and the boundary conditions for the calculations. The mesh was imported to FLUENT and the calculation defined. The parameters for the solution method are shown below.

Solver

- Type – Density-Based
- Velocity Formulation – Absolute
- Time – Steady
- 2D Space – Axisymmetric

Notes on the solver options – the density based model is recommended because 'air' is set as an ideal gas. The density based solver was used by other researchers including Alexandru et al. (2011); Guerriero (2008); Kim et al. (2006).

Models

- Energy
    - On
- Viscous
    - Model - k-omega
    - k-omega Model – SST
    - k-omega Option – Compressibility Effects

Materials

- Fluid

    o Air

    o Density – Ideal Gas

Boundary Conditions

- Coandă Inlet – Pressure Inlet

- Momentum

    o Reference Frame - Absolute

    o Gauge Total Pressure (Pascal) - 520000

    o Supersonic/Initial Gauge Pressure (Pascal) – 520000

    o Direction Specification Method – Normal to Boundary

- Turbulence

    o Specification Method – Intensity and Hydraulic Diameter

    o Turbulence Intensity (%) – 40

    o Hydraulic Diameter (mm) – 5

The turbulence intensity is defined as the ratio of the root-mean-square of the velocity fluctuations to the mean flow velocity (ANSYS, 2010b). A turbulence of 1% is considered to be low and values greater than 10% are thought to be high. The turbulent intensity used in the model was the same as used by O'Nions (1997) although it is higher than the turbulence intensity used by (Guerriero, 2008) at the primary or Coandă inlet who used a turbulent intensity of 1%. The hydraulic diameter for the outlet was calculated assuming that there was fully developed flow, therefore $L=D_H$ (ANSYS, 2010b). It should be noted that (Guerriero, 2008) performed a comparison into how the turbulent intensity at the Coandă inlet affects the numerical analysis. It was determined that changing the turbulent intensity from 1% to 10% had no impact on results.

The boundary conditions for the *Ejector Inlet 1*, *2* and *3* are shown in Table 7.1. Each of the ejector inlets was configured as a pressure inlet.

Boundary Condition	Ejector Inlet 1	Ejector Inlet 2	Ejector Inlet 3
Momentum			
Reference Frame	Absolute	Absolute	Absolute
Gauge Total Pressure (Pascal)	0	0	0
Initial Gauge Pressure (Pascal)	0	0	0
Turbulence			
Specification Method	Intensity and Hydraulic Diameter	Intensity and Hydraulic Diameter	Intensity and Hydraulic Diameter
Turbulent Intensity (%)	1	1	1
Hydraulic Diameter (mm)	70	60	15

Table 7.1 – Boundary conditions for the ejector inlets

The boundary conditions for the outlet are shown below, it is assumed that the flow in the body of the ejector is full-formed so the hydraulic diameter is the same as the width as the outlet.

- Outlet – Pressure Outlet
- Momentum
    - Backflow Direction Specification Method – Normal to Boundary
    - Gauge Pressure (Pascal) – 0 - constant
- Turbulence
    - Specification Method – Intensity and Hydraulic Diameter
    - Turbulence Intensity (%) – 1
    - Hydraulic Diameter (mm) – 12.5

Once the boundary conditions were set the solution was initialized using the hybrid method. The solution method is described below:

- Solution Methods
    - Formulation – Implicit
    - Flux Type – Roe-FDS
    - Gradient – Least Squares Cell Based

o Flow – Second Order Upwind

o Turbulent Kinetic Energy – Second Order Upwind

o Specific Dissipation Rate – Second Order Upwind

Finally the axis was defined as an axis and the remaining parts were set as walls. The first simulation was then run until the solution convergence was achieved this normally occurred at around 2100 iterations.

7.6 Modelling Results

7.6.1 Analysis of Case A

Case A acts as the baseline case, from which other simulations, where certain parameters are changed, can be compared. The boundary conditions and geometrical parameters are the same as discussed sections 7.2 and 7.33. The key features for the model are presented in Table 7.2.

Dimension	Unit	Case A
Coandă gap, e	mm	0.08
Nozzle length, NL	mm	2
Radius, R	mm	5
Nozzle Ratio, R/NL	-	2.5
Diameter, D	mm	25
Pressure of air at inlet	Pascal	520000

Table 7.2 – Case A: Key parameters

Velocity vector analysis

A way to analyse the fluid velocity in the Coandă ejector is to look at velocity vectors. Figure 7.17 indicates the velocity vectors at the inlet of the Coandă ejector.
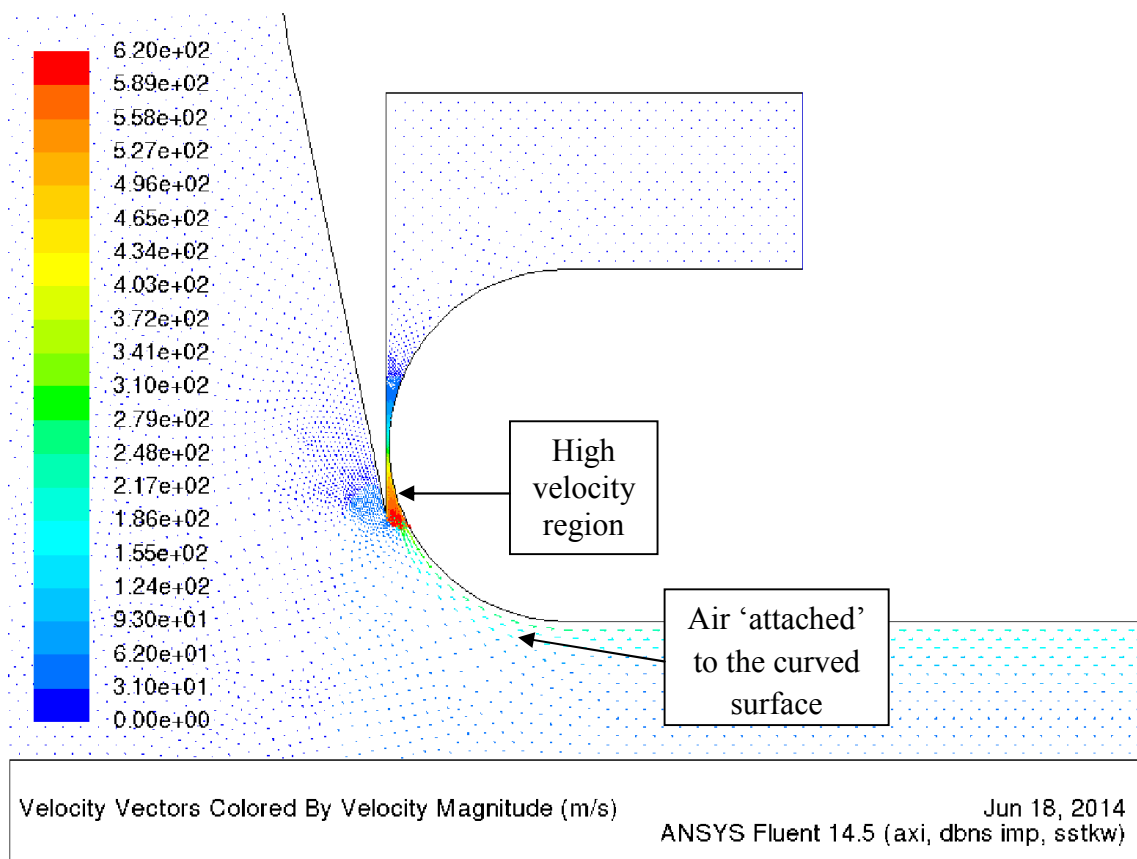
Figure 7.17 – Velocity vectors at the Coandă inlet

Figure 7.17 shows how the Coandă gap creates an area of high velocity. Air enters from the Coandă inlet at a gauge pressure of 5.2 bar, the velocity of the fluid in this region is comparatively slow, as shown by the dark blue coloured vectors. After entering into the system primary air was injected through the Coandă gap. At this point because of the small size of the gap there was a dramatic increase in the velocity of the primary flow. Fluid velocity increases to a peak velocity of 617 m/s, shown by the red coloured vectors in the high velocity region. The high velocity fluid attaches to the curved Coandă surface and the flow is directed to along the body of the ejector. The light blue arrows show where the air 'attaches' to the Coandă surface and continues along the length of the ejector.

The secondary flow enters into the computational system through one of three pressure inlets. The inlets are at atmospheric conditions. In the region before the Coandă ejector throat the fluid is at reduced velocities. This region acts as a reservoir for the secondary flow.

Figure 7.18 indicates how the high velocity primary air entrains the secondary fluid by dragging to the outlet of the ejector. Figure 7.18 shows how underneath the Coandă gap there is an increase in the fluid velocity as momentum from the injected flow is passed to the surrounding secondary fluid. After this initial increase there is a reduction in the velocity of

the secondary fluid, signified by the dark blue section of reduced velocity (0-30 m/s) fluid between the two regions of higher velocity.

The injected primary air and entrained secondary air mix along the length of the ejector and momentum is passed from the higher velocity primary air to the secondary flow. The mixing between the two flows is discussed later in this chapter.
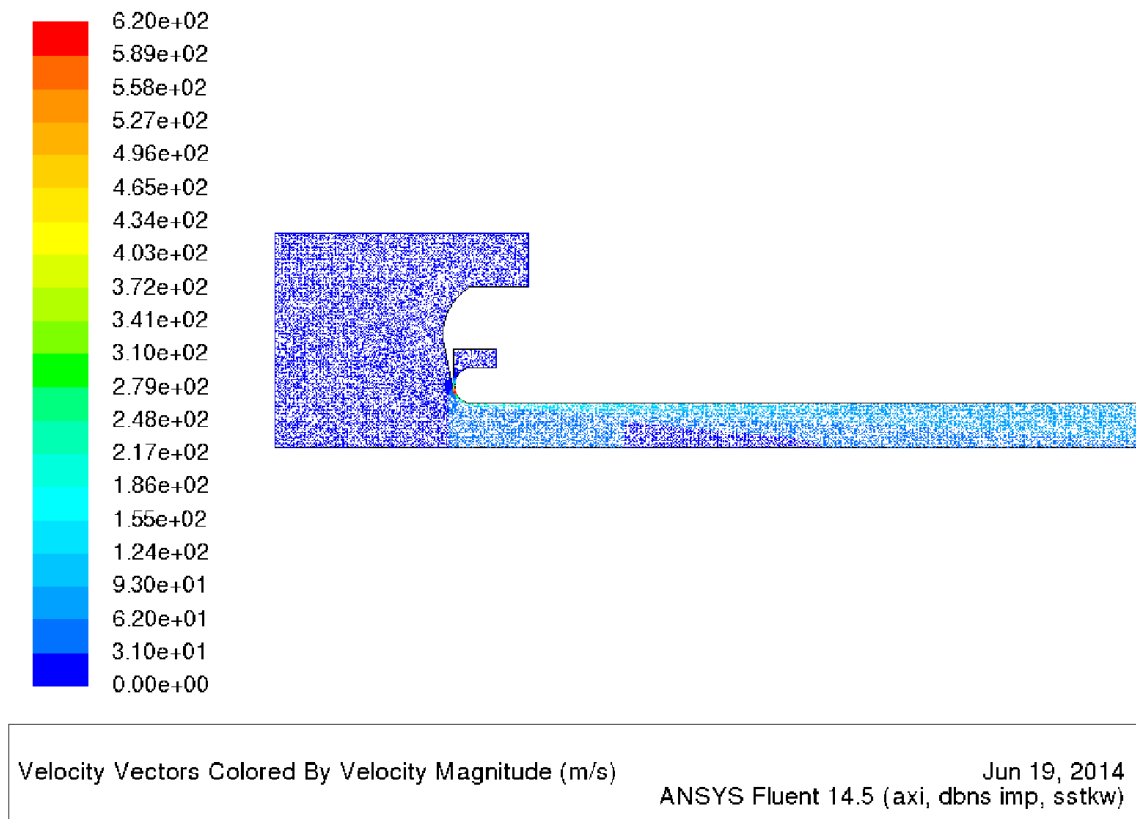
Figure 7.18 – Velocity vectors in the Coandă ejector

Particle track analysis

The particle track analysis gives a good indication of the pathways of the primary flow and the secondary flow. These two streams do not follow the same path. The pathlines entering the computational domain from *Ejector Inlet 1*, see Figure 7.19, shows how the secondary fluid is dragged along the length of the ejector. Figure 7.21 shows the pathlines from the Coandă inlet. The adhesion to the curved surface is obvious. Once the fluid enters through the Coandă gap and adheres to the Coandă surface there is little deviation as the fluid travels along the body of the ejector. Each of the pathlines are shown to follow a similar path to each other. The primary fluid only interacts with the secondary fluid in a small region at the top of the ejector.
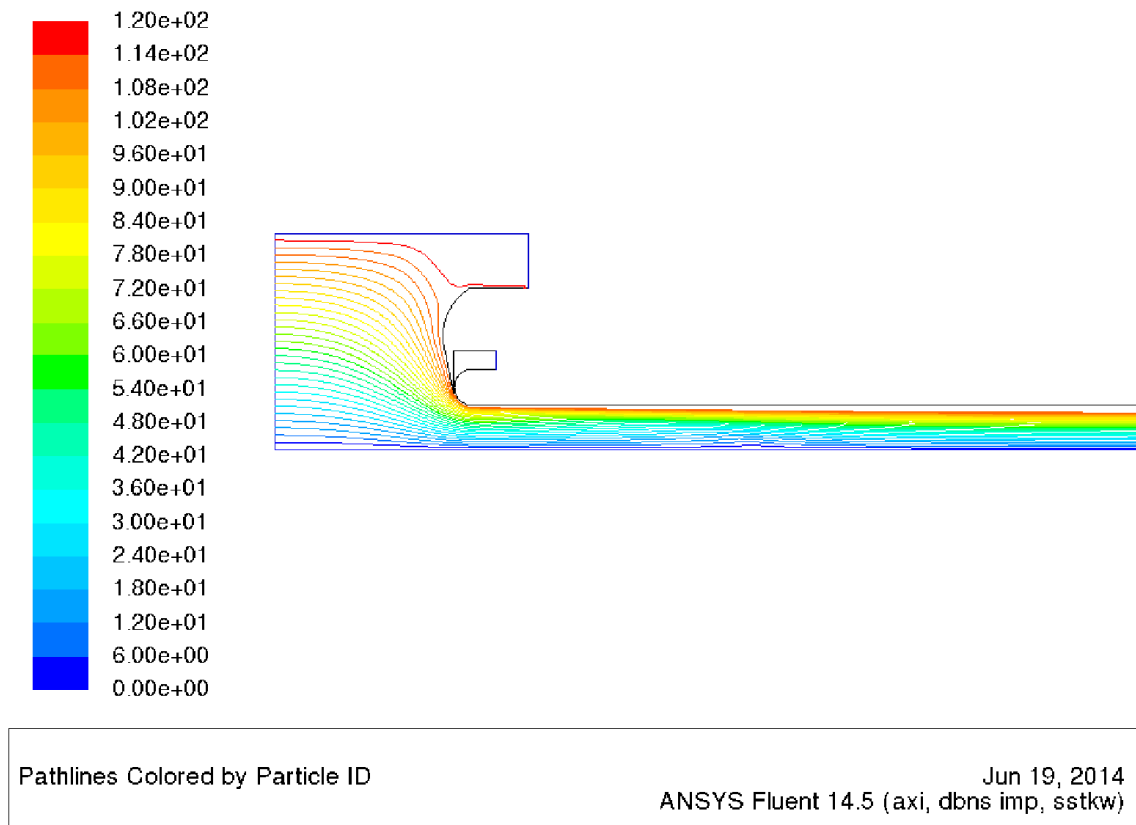
Figure 7.19 – Particle tracks from Ejector Inlet 1

Figure 7.20 shows how secondary flow entering from ejector inlet 1 interacts with the Coandă ejector. Figure 7.20 indicates the velocity of the pathlines along the length of the ejector. As the secondary fluid enters the ejector it is at low velocities between 1 and 10 m/s. The secondary fluid moves steadily towards the Coandă throat, as the fluid becomes closer to the throat there is an increase in velocity, signified by a lighter blue coloured velocity vectors. Fluid that is closer to the Coandă gap is dragged along the ejector at higher velocities. In the throat region, beneath the Coandă gap there is an initial increase in the velocity of the secondary fluid, caused by the high velocity primary fluid, entering the ejector body through the Coandă gap, passing momentum to the secondary fluid. This dragging force is caused by the turbulent shear stress as well as viscous effects Kim et al., (2006).

As the secondary fluid flows along the body of the ejector there is an equalisation between the induced flow along the diameter of the ejector. The difference in velocity between the induced flow that was closer in proximity to the Coandă gap at the throat of the ejector and the induced flow that entered the ejector in the middle of the ejector (x=axis) reduces along the length of the ejector.

2.00e+02
1.90e+02
1.80e+02
1.70e+02
1.60e+02
1.50e+02
1.40e+02
1.30e+02
1.20e+02
1.10e+02
1.00e+02
9.00e+01
8.00e+01
7.00e+01
6.00e+01
5.00e+01
4.00e+01
3.00e+01
2.00e+01
1.00e+01
0.00e+00
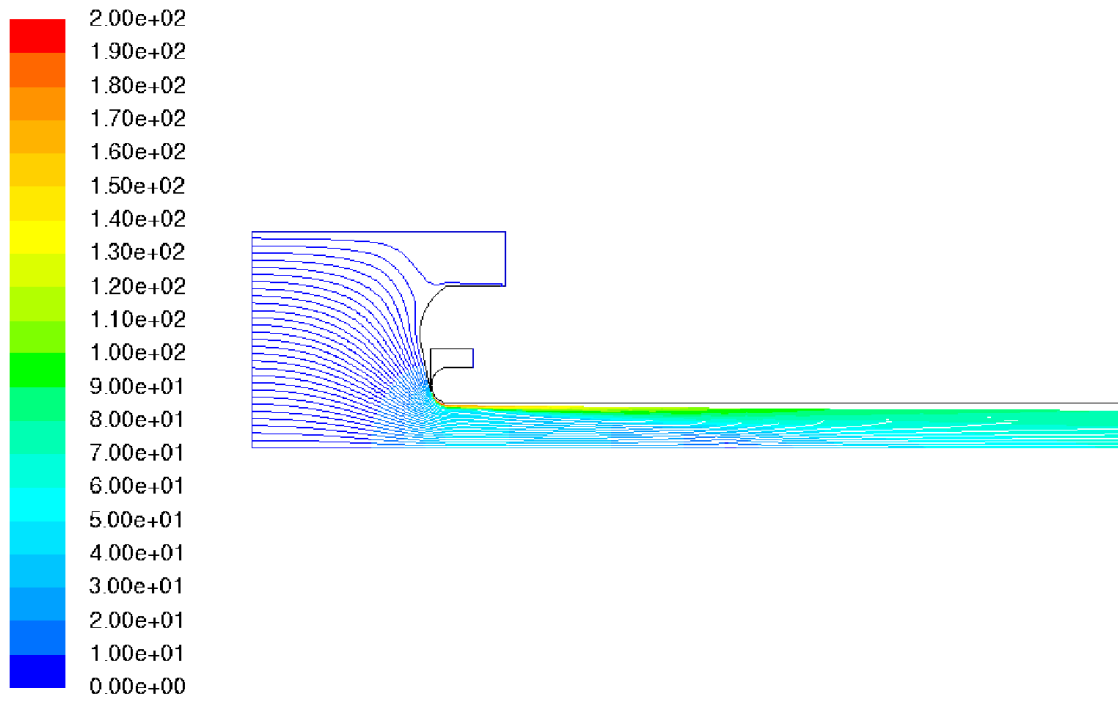
Pathlines Colored by Velocity Magnitude (m/s)   Jun 19, 2014
                                          ANSYS Fluent 14.5 (axi, dbns imp, sstkw)

Figure 7.20 – Particle tracks by velocity magnitude from Ejector inlet 1

9.00e+00
8.55e+00
8.10e+00
7.65e+00
7.20e+00
6.75e+00
6.30e+00
5.85e+00
5.40e+00
4.95e+00
4.50e+00
4.05e+00
3.60e+00
3.15e+00
2.70e+00
2.25e+00
1.80e+00
1.35e+00
9.00e-01
4.50e-01
0.00e+00
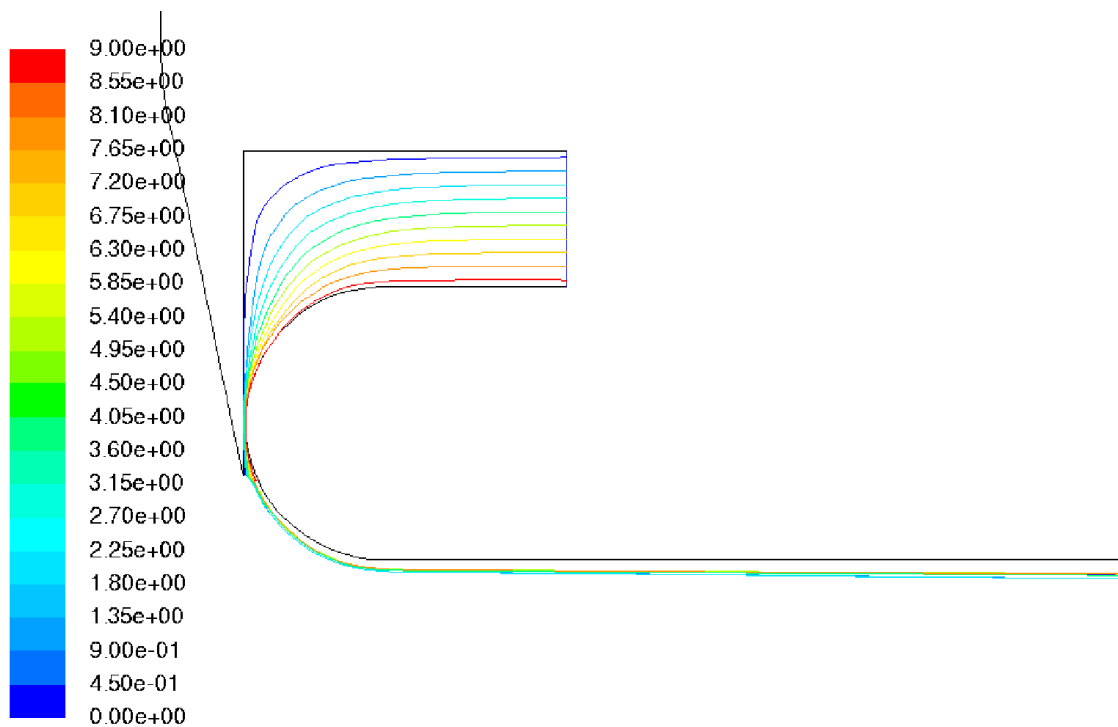
Pathlines Colored by Particle ID   Jun 19, 2014
                                          ANSYS Fluent 14.5 (axi, dbns imp, sstkw)

Figure 7.21 – Particle tracks from Coandă Inlet

Velocity Profiles along the ejector

To analyse the ejector eight points along the length of the ejector are used to analyse the velocity along the length of the ejector. At these intervals the velocity profile across the y axis was analysed. The intervals were set at various values of x along the x-axis shown in Figure 7.22. The values for y were non-dimensionalised by dividing the y co-ordinate from where the velocity value as taken with the diameter of ejector, 12.5 mm. The 8 points were chosen to determine how the velocity profile changes from the initial injection into the ejector body to the end of the burner body where the burner tip is located.
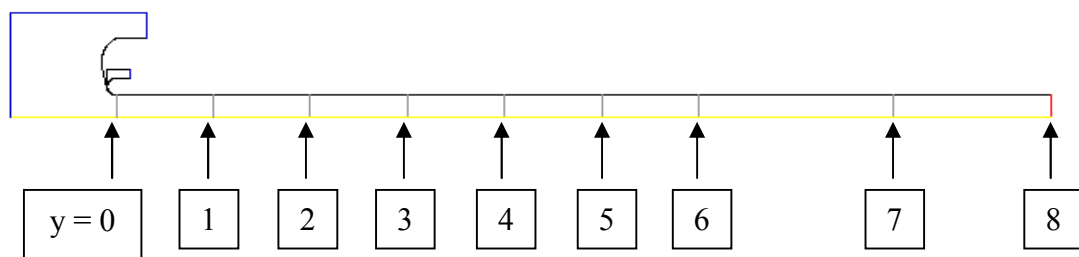
Figure 7.22 – Analysed points along the length of the CTC

Point	1	2	3	4	5	6	7	8
x	0	50	100	150	200	250	300	400

Table 7.3 – Surface along ejector body in relation in inlet
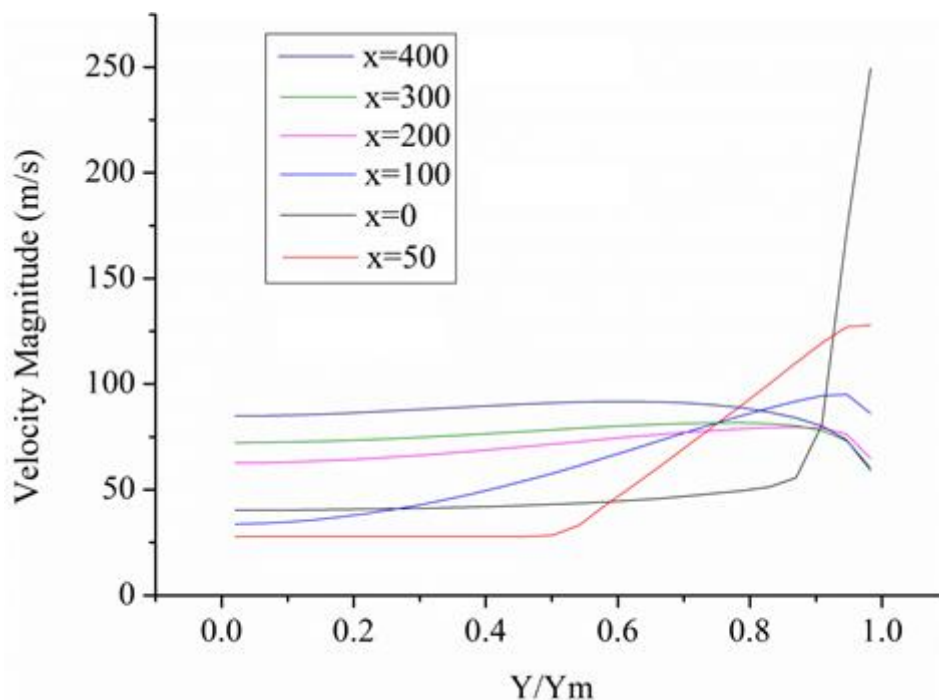
Figure 7.23 – Velocity profiles at various points along the ejector

Figure 7.23 shows the velocity profiles at six points along the length of the Coandă ejector. At x=0 the changes in velocity across the diameter of the ejector is apparent. When y/ym is close to 1, close to the top of the Coandă ejector, the velocity is at its highest point, the velocity at this point is around 240 m/s.

The high velocity can be attributed to the injected air that passes through the Coandă gap. The air attaches to the curve of the Coandă and, although, reducing from the velocity from when air initially exits the Coandă gap, the velocity is still high close to the wall when compared with velocities along the axis. The velocities reduce as the examined position moves away from the surface of the wall and closer to the axis of the ejector.

The determined velocity profiles are similar to those found by Guerriero (2008) who performed numerous CFD simulations on a Coandă ejector. In this study various geometrical parameters where altered to determine how these factors affect the flow velocity and relationship between the injected primary flow and induced secondary flow. Despite this, Guerriero (2008), who used different geometrical set-up and boundary conditions found similarities between the velocity profiles. In the majority of the cases interpreted by this author the highest velocities were found at positions closest to the walls of the ejector where air had been injected.

Guerriero (2008) considered that if the velocity profile at any point along the axis is flat then complete mixing has been achieved, because the velocities for primary and secondary flow are equal. A flat velocity profile across the width of the ejector was also considered to indicate well mixed flow by Alexandru et al. (2011). The flat profile refers to a small change in the velocity magnitude across the diameter of the ejector.

Figure 7.23 shows the velocity profile at a position 50 mm (x = 50) from the inlet. When comparing the velocity profile at the inlet (Figure 7.23) it can be seen that the overall velocity at the region close to the wall has reduced from close to 250 m/s to around 130 m/s. Interestingly, the velocity magnitude is lower at positions close to the centre of the ejector, at x = 50. This can be explained by the high initial velocity creating an initial influx of momentum for secondary fluid in the stagnant region. After this initial change in velocity there is a small region where the velocity reduces in a position after the Coandă throat.

Of the evaluated points along the x-axis the first to have a flat profile is at x=200 (see Figure 7.23. Therefore at this point it can be assumed that mixing between primary and secondary flow has been completed which has implications on the design of the burner. A Coandă type burner was used as a tar cracker of its ability to operate at less than stoichiometric levels and yet still maintain a high temperature, blue-flame, which is required for thermal tar cracking. In

the experimental programme discussed in previous chapters the key issue was its ability to maintain a stable flame in the burner when propane fuel was used. It was determined that this issue was caused because the fuel and oxidant were not fully mixed along the length of the ejector, hence at the exit of the burner, where a tip was inserted to provide flame stability a stable flame could not be maintained. By extending the length of the Coandă burner it was possible to improve the mixing between the fuel and oxidant and create a stable flame. In the experimental programme the length of the burner extension was done on a trial and error basis. A first a long chamber was used, which solved the issue and it was not investigated further; however based on the results from this simulation it may be possible to shorten the length of the burner to make the process more streamlined. If the combustion products are fully mixed at x=200 then it should be possible to shorten the burner so that the tip is placed at this point.

7.6.2 Comparison of Viscous Models

As discussed in the introduction two models were considered to simulate the turbulence in the Coandă ejector. The k-φ model with SST is preferred by Alexandru et al. (2011) and Dumas et al. (2014) whereas the k-ε is recommended by Guerriero (2008) and Kim et al. (2006). This section compares the difference in the results when both models were used. Other parameters for the geometry and boundary conditions were kept the same, see Table 7.2.

Figures 7.24, 7.25 and 7.26 indicate how the two turbulence models yield similar results. In Figure 7.24 there is a slight discrepancy when Y/Ym is 0.95, but the velocity profiles and magnitudes are very similar close to the wall and in the main body of the ejector. In Figure 7.25, the velocity profiles at x = 50, there is a slight difference in the velocity magnitude at positions where Y/Ym are between 0 and 0.5. Figure 7.26 shows the profiles at x = 400 which is close to the outlet of the ejector again there is little difference between the results.

Although the difference between the turbulent models is slight the k-φ model with SST was chosen to be used for the remaining simulations.
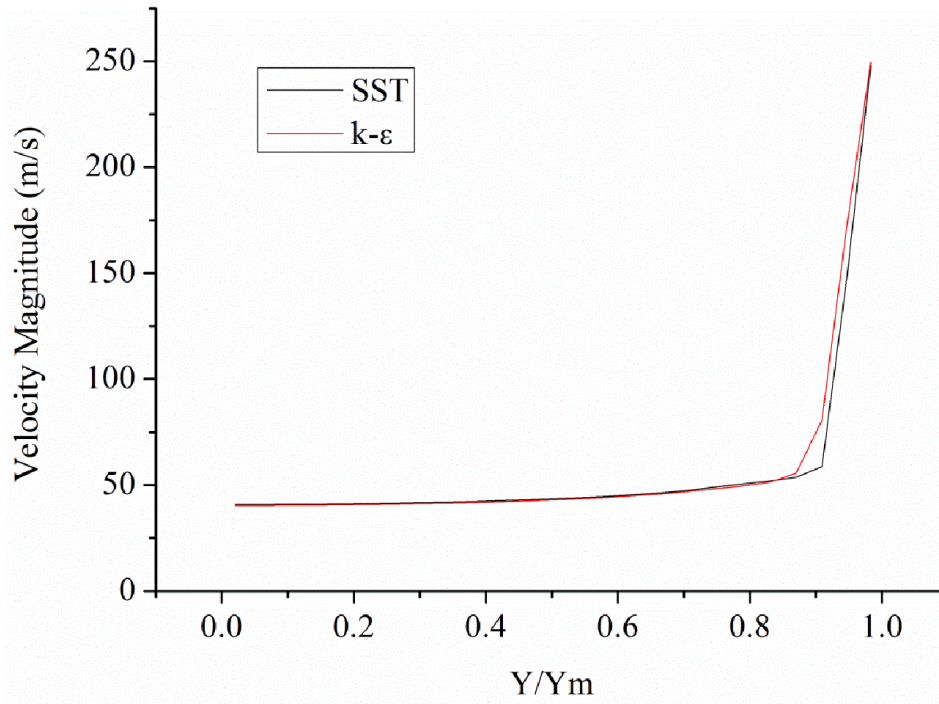
Figure 7.24 – Comparison of viscous models - Velocity profiles at x=0
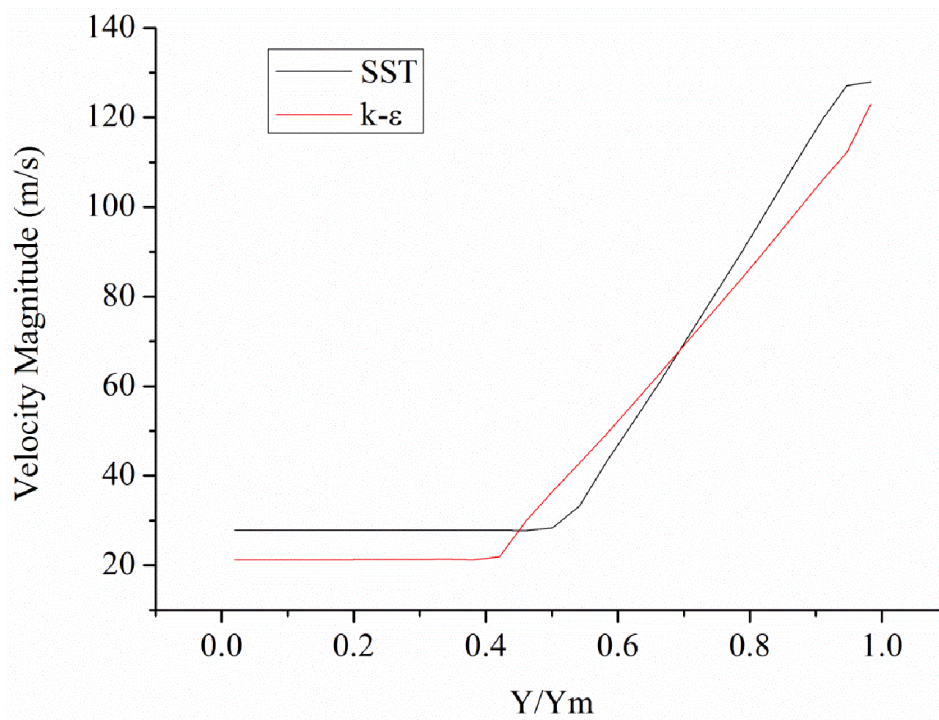
Figure 7.25 – Comparison of viscous models - Velocity profiles at x=50
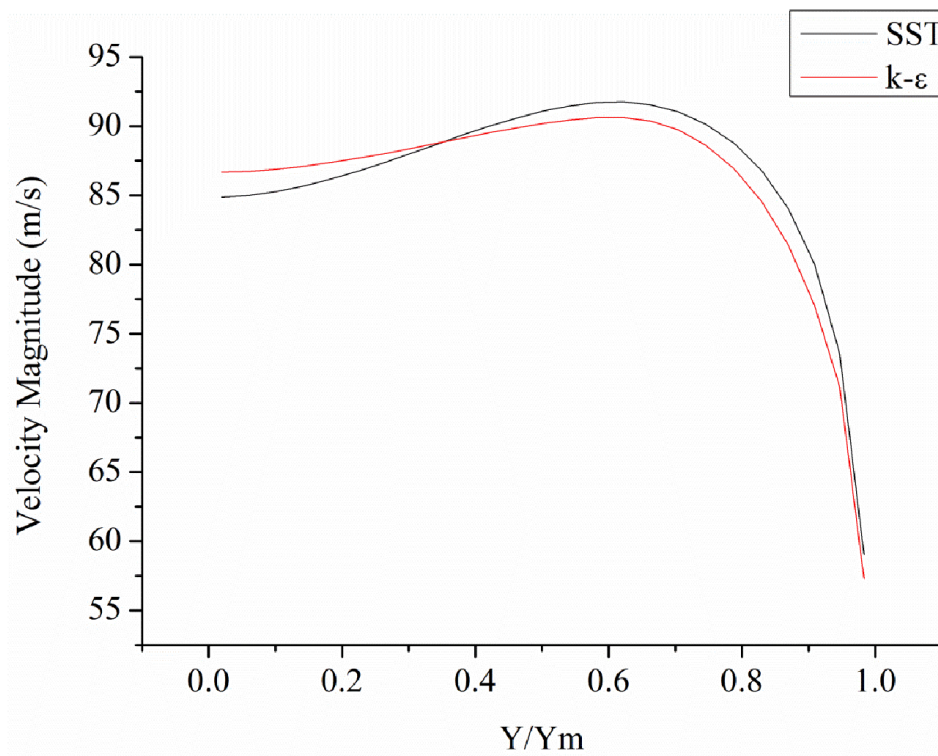
Figure 7.26 – Comparison of viscous models - Velocity profiles at x=400

7.6.3 Comparison of Inlet Pressure Case A vs D vs E vs G

One of the key parameters that can be changed is the pressure at the Coandă inlet. In this section the effect of the inlet pressure on the performance of the ejector is analysed. Table 7.4 shows the four inlet pressures used for the analysis. The lowest inlet pressure is 420,000 and the highest is 720,000 Pascals.

Dimension	Unit	Case A	Case D	Case E	Case G
Coandă gap, e	mm	0.08	0.08	0.08	0.08
Nozzle length, NL	mm	2	2	2	2
Radius, R	mm	5	5	5	5
Nozzle Ratio, R/NL	-	2.5	2.5	2.5	2.5
Diameter, D	mm	25	25	25	25
Pressure of air at inlet	Pascal	520000	620000	420000	720000

Table 7.4 – Analysis of pressure at Outlet
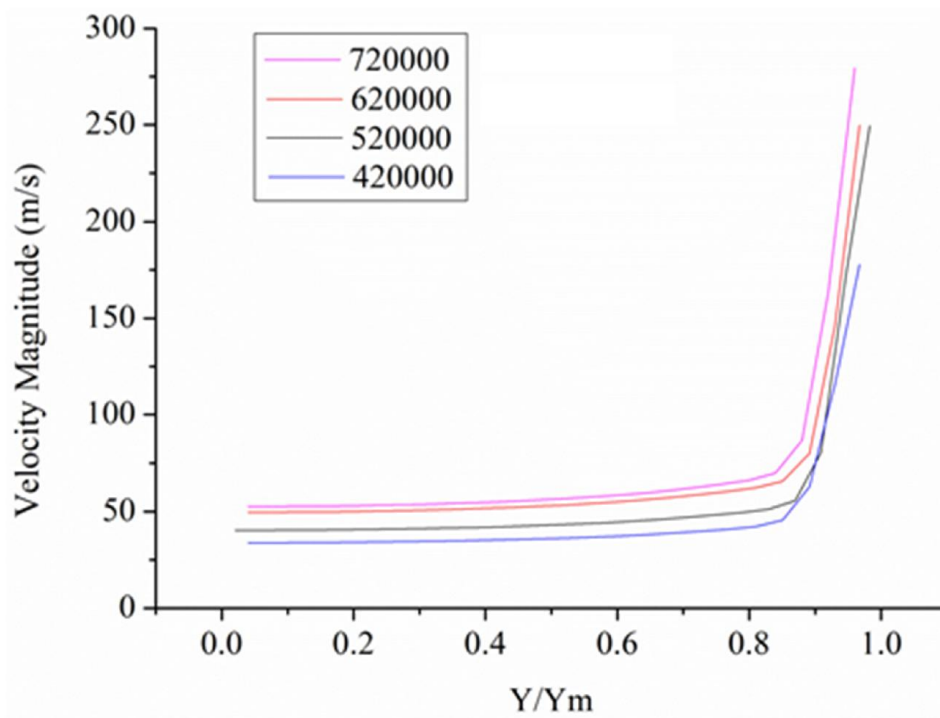
Figure 7.27 – Comparison of inlet pressure – Velocity profiles at x = 0

Figure 7.27 shows how increasing the Coandă inlet pressure results in an increase in the velocity at the Coandă throat inlet. In Case G, where the pressure is highest, the velocity along the length of the ejector is greater than in the other cases. There is a considerable difference between the velocity at regions close to the Coandă gap. At the lowest pressure the velocity is around 175 m/s, at the highest inlet pressure the velocity is around 280 m/s.
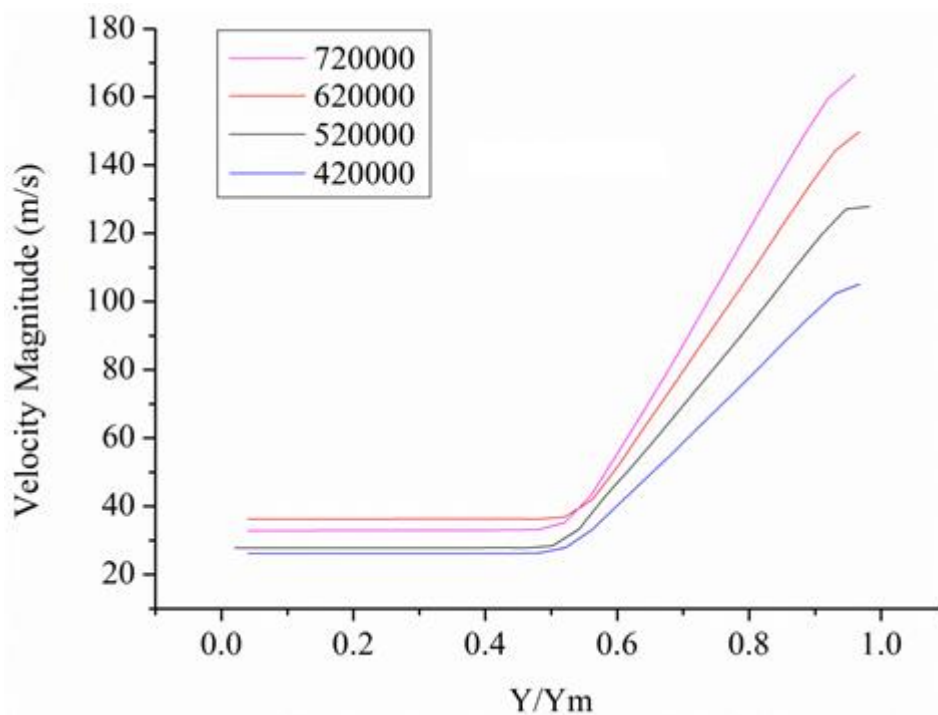
Figure 7.28 – Comparison of inlet pressure – Velocity profiles at x = 50
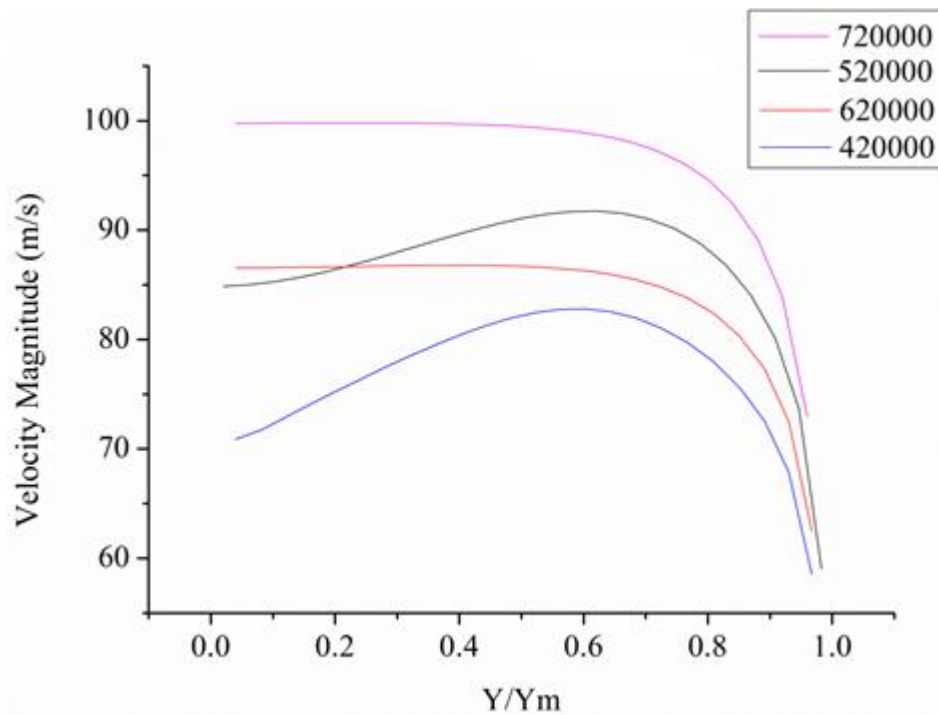
Figure 7.29 – Comparison of inlet pressure – Velocity profiles at x = 400

7.6.4 Comparison of the Coandă gap width

There are a number of parameters which can be altered to analyse the performance of the ejector. The principal parameters that can be changed are the Coandă gap width, the length of the nozzle in relation to the radius of the curved surface and the radius of the Coandă curve. The radius of the Coandă curve has little effect on the performance of the ejector (Guerriero, 2008; Kim et al., 2006). This section examines the effect of the Coandă gap width.

Table 7.5 shows the key parameters of Case A and C. For case C all the key parameters are kept the same apart from the Coandă gap width that is increased from 0.08 to 0.2 mm.

Dimension	Unit	Case A	Case C
Coandă gap, e	mm	0.08	0.2
Nozzle length, NL	mm	2	2
Radius, R	mm	5	5
Nozzle Ratio, R/NL	-	2.5	2.5
Diameter, D	mm	25	25
Pressure of air at inlet	Pascal	520000	520000

Table 7.5 – Key parameters – Comparison of Coandă gap width

Figures 7.30, 7.31 and 7.32 show the velocity profile across the ejector at x = 0, x = 50 and x = 400 respectively. At the inlet of the ejector when the Coandă gap was 0.2 mm the velocity is

higher across the width of the ejector. At positions close to the wall, where Y/Ym is 1 the velocity for Case C is around 375 m/s which is considerably larger than the velocity in Case A. Similar results were found by (Guerriero, 2008; Kim et al., 2006).

Increasing the Coandă gap increases the flow rate of injected primary air, this causes an increase in the secondary flow rate as there is a higher rate of momentum that is passed between the flow (Guerriero, 2008). The velocity at x = 50 and x = 400 (Figures 7.31 and 7.32) is higher for Case C across the length of the ejector, resulting in a higher flow rate.

Decreasing the Coandă gap width also reduces the mixing length. Figure 7.32 shows that the velocity profile for Case A (*e* = 0.08) is slightly 'flatter' than that of Case C. The flatter profile indicates that there is increased mixing between the two flows.
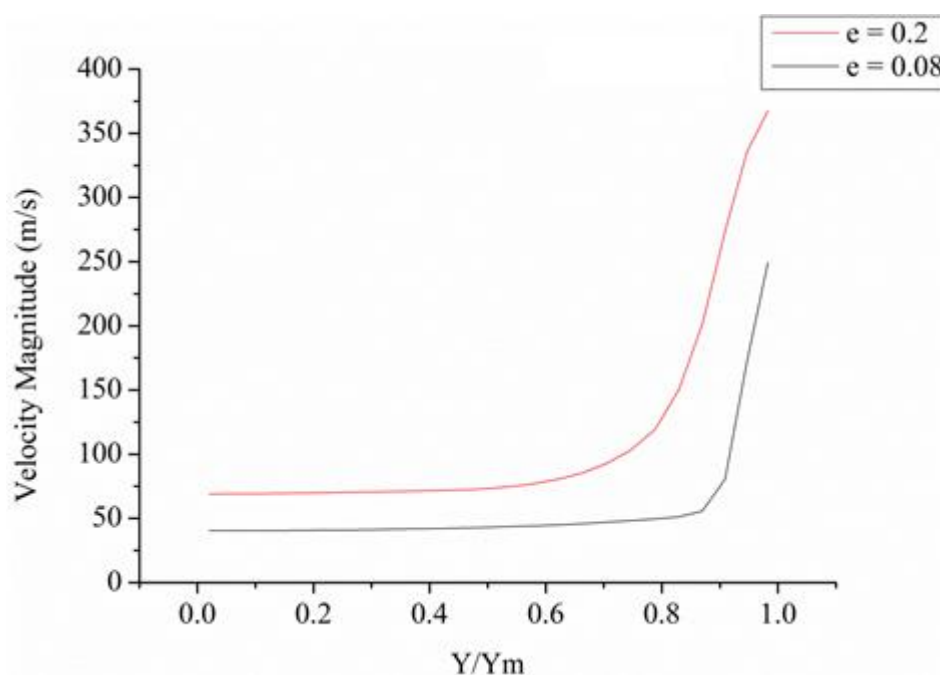
Figure 7.30 – Comparison of Coandă gap width – Velocity profiles at x = 0
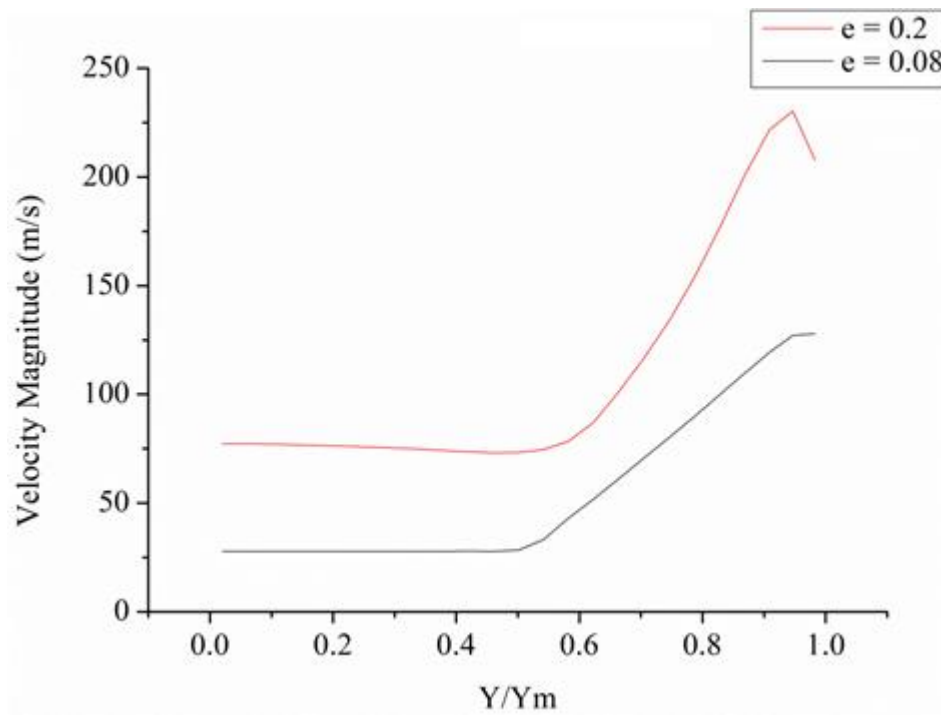
Figure 7.31 – Comparison of Coandă gap width – Velocity profiles at x = 50
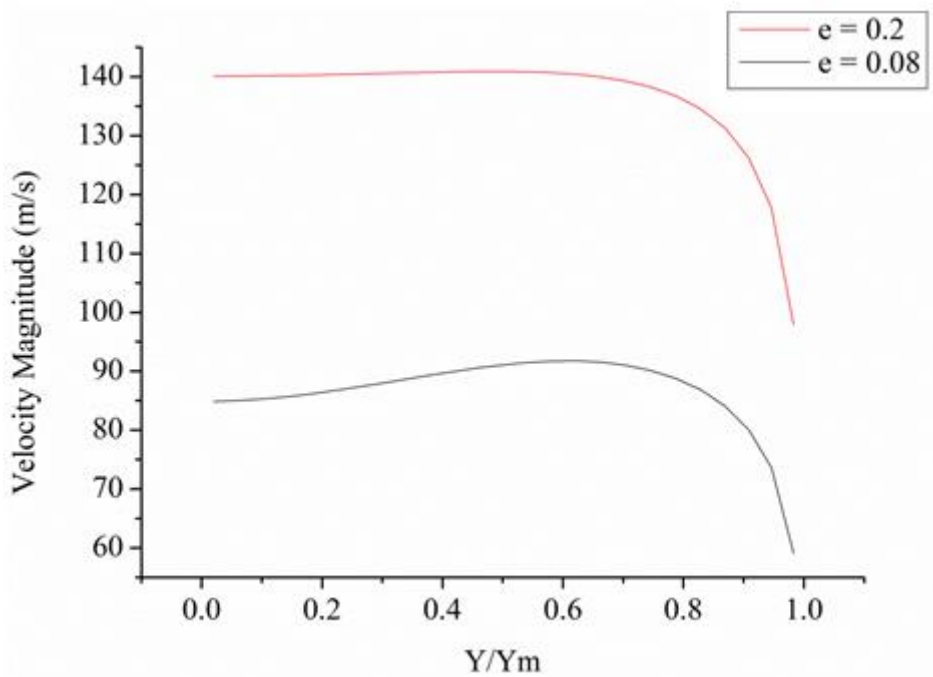
Figure 7.32 – Comparison of Coandă gap width – Velocity profiles at x = 400

7.7 Summary

This chapter has analysed how changing certain key parameters in a Coandă ejector effects the performance of the unit. A base case (Case A) which used similar geometries and input parameters as the device used in the experimental programme was modelled and then compared against additional cases. The key parameters that were examined were the comparing the viscous models used in the simulation, the inlet pressure at the Coandă inlet and the length of the Coandă gap. To analyse the performance of the ejector, velocity at set points along the length of the ejector were analysed. When the velocity profile was 'flat' it determined that mixing between primary and secondary flow was complete.

The viscous models analysed were the k-φ model with SST and the k-ε model. There was very little difference when comparing the velocity profile x = 0, 50 and 400. Increasing the inlet pressure in the primary air reservoir increased the velocity magnitude (m/s) close to the walls of ejector in the Coandă throat (x = 0). Increasing the pressure at the inlet increased the velocity along the width of ejector at x = 400.

8. *Applications and Developments*

This chapter looks at ways in which the design of the system can be developed and optimised as well as looking at potential industrial applications. Firstly discussion into how the existing system can be optimised to operate more efficiently is explored. Next two potential industrial developments are explored. The first considers adapting the current design of the CTC to produce biochar by recycling the heat from the combusted volatiles to power the pyrolysis reaction. Secondly, the CTC is expanded into a three-stage gasifier to produce a tar-free, low calorific value gas. Finally two potential commercial systems are analysed.

8.1 *Optimisation of the Existing System*

The existing dual pyrolysis and tar cracking system requires further development so that it can be operated efficiently. There are a number of design features of the existing unit that require improvement; preliminary the feeding mechanism, removal of produced char, and the CTC design can all be modified to improve the overall quality of the system. There are a number of factors to consider when describing and evaluating potential alterations. The dual system should be able to run for long periods without the need for maintenance or the need for a person to control the system, the entirety of the system operation should be automated.

8.1.2 *The Feeding Mechanism*

The existing design provides raw fuel in batch feeding method, which is controlled manually. The batch style feeding system created a number of issues and problems with the control of the system and maintaining the flow of the gas that is supplied to the tar cracking stage. As previously discussed, in the experimental section, the batch supply method caused fluctuations in the volume of gas which entered the CTC, thus resulted in issues with flame stability, as the fluctuations changed the required fuel to air ratio which kept the flame within stability limits. To resolve this issue a continuous feeding system would be required for the first, pyrolysis stage. Screw feeding systems are commonly used in pyrolysis reactors and offer the most viable solution.

Installing a screw feeding system has the added benefit of removing the requirement of a person to manually push the raw biomass into the pyrolyser. The screw feeding system also allows for further control of the residence time of the biomass particles in the pyrolyser, allowing for further control of the system. This would allow for more flexibility and control into the desired pyrolysis products. The rate at which the screw feeder rotates has a direct effect on the residence time of the biomass particles in the high temperature pyrolysis environment.

A screw-feeding system would be unproblematic to retrofit into the existing horizontal set-up of the pyrolyser. Figure 8.1 indicates a method into how a simple screw feeding system could be implemented into the chamber.
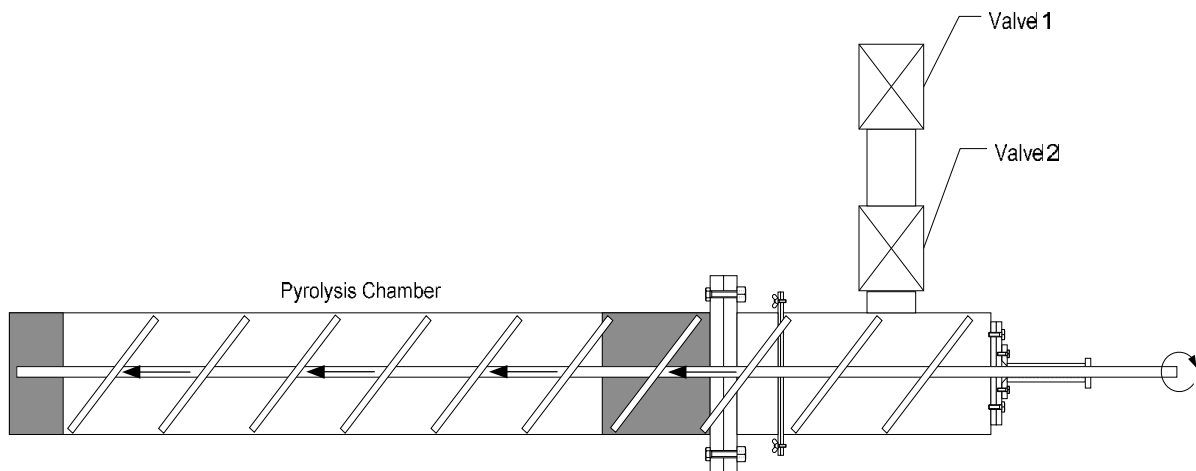
Figure 8.1 – Screw feeding system

The screw feeding system would augment the existing dual-lock hopper system that is present in the batch feeding system. The dual-lock hopper system prevents the leakage of gases in and out of the pyrolyser thus preventing oxygen from entering the chamber and pyrolysis gases from exiting. A small electric motor would be required to drive the screw feeding system forward, it is expected that the motor would have to operate at a low rate of revolutions. The forward and constant motion of the rotation of the screw ensures that the supply of raw biomass is maintained throughout the operation.

In order to allow for continuous operation further enhancements are required. At present a known amount of wood pellets are fed through the dual-valve system manually. By installing a hopper (see Figure 8.2) and using automated valves that open at set time intervals would alleviate the need for the manual input. In the current system wood pellets are collected in a fuel tray placed inside the pyrolyser, this creates issues as the produced char needs to be removed from the system once the raw biomass has been converted to char. By installing a char collection unit at the end of the pyrolysis chamber (see Figure 8.3) so that produced char can drop down once it has passed through would allow for uninterrupted operation.
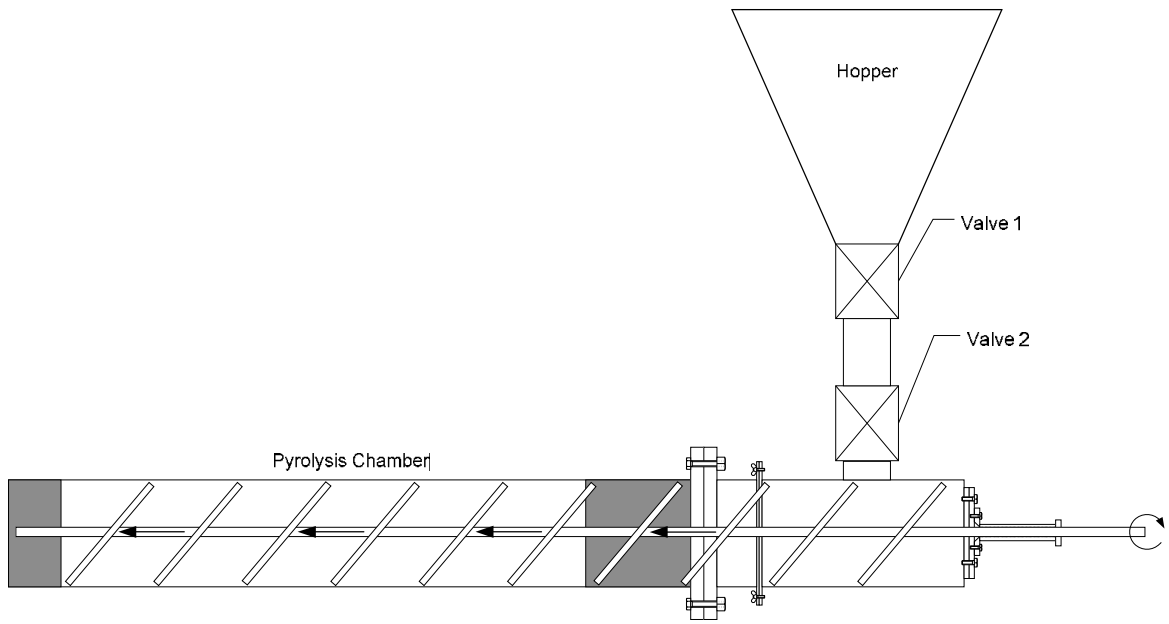
Figure 8.2 – Screw feeding system with hopper
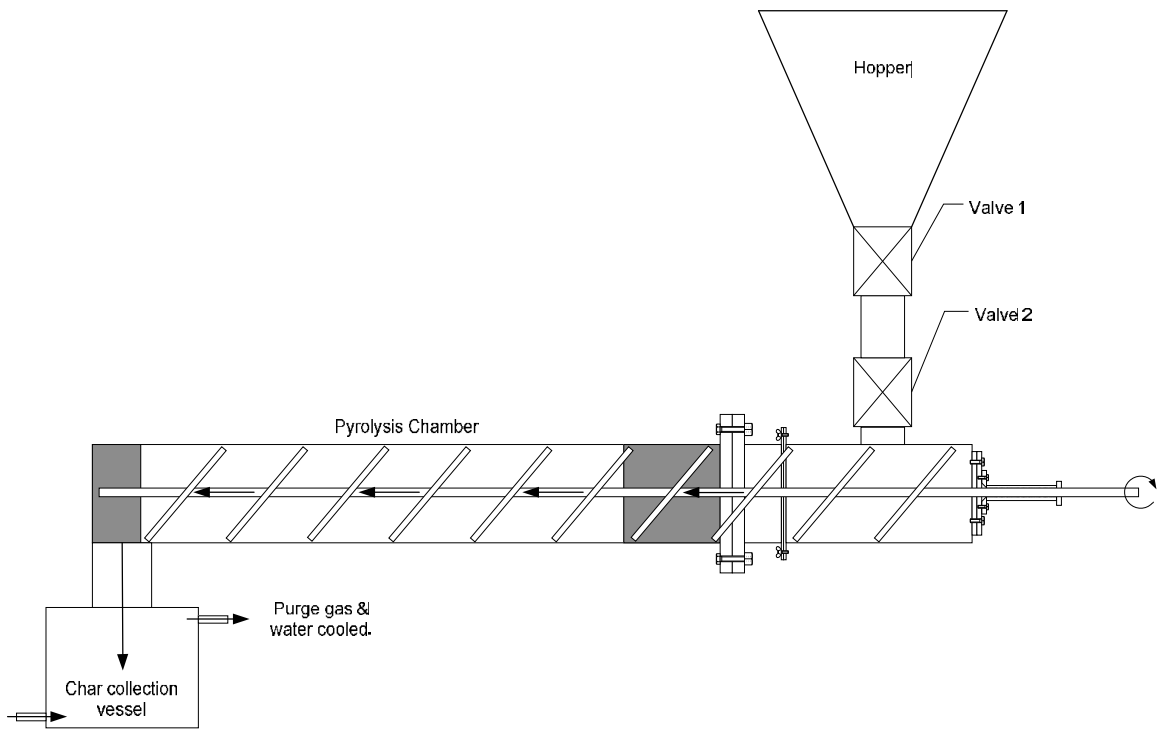
Figure 8.3 – Char removal system

8.1.3 Re-design of the CTC
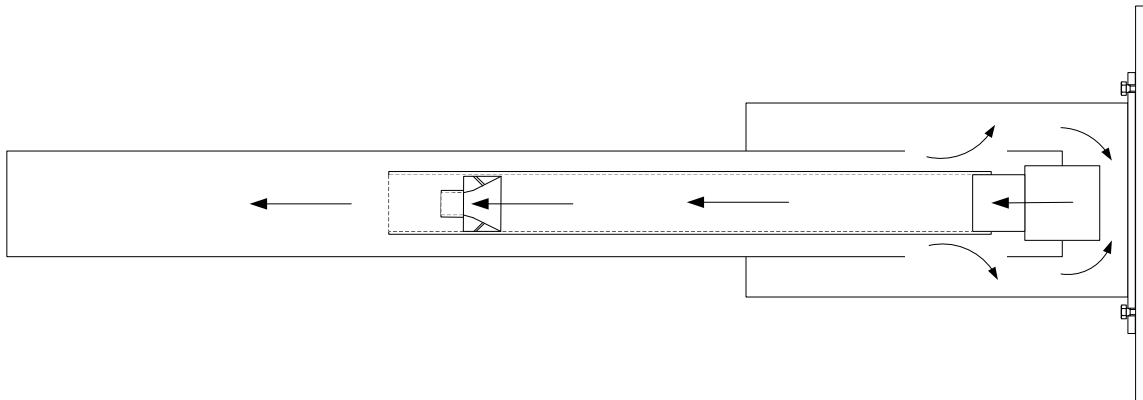
Figure 8.4 – Proposed re-design of the CTC

The design of the CTC can be improved to ensure that the system is more effective at cracking tar vapours. In the current design a mixing vessel/pre-Coandă chamber is situated before the Coandă ejector system. The mixing vessel provides a space where hot recycled gases and fresh pyrolysis gases can be pre-mixed before entering the ejector and then the tunnel burner. The mixing vessel is a key component as it allows for the whole CTC system to be attached to the pyrolyser. In the proposed system, shown in Figure 8.4, the mixing vessel is removed; instead the Coandă ejector is positioned so that there is a complete annular gap before the inlet to the ejector which will ensure that there is improved mixing between the recycled gases from the flame and the fresh gases produced in the pyrolysis stage.

A further design development is to decrease the length of the tunnel burner. The results from the flow field analysis using CFD proved that there is complete mixing between the injected air flow and secondary air flow at a much shorter length than the existing tunnel burner. Once the gases are completely mixed the gases should be combusted, reducing the overall length allows for a more compact unit.

There is also further scope to re-design the burner tip to enable increased flame stability. The current design is effective when there is a constant supply of gas but it could be possible to increase flame stability by adjusting and improving the burner tip design. This would be done by testing a number of individual designs and determining their effectiveness.

8.1.4 Feed Material

Wood pellets were used for the experimental tests, for a number of reasons that have been previously highlighted; they are easy to handle, are reliable and uncomplicated to source. Wood pellets were suitable for the project but other biomass fuels could also be used. Due to

the chemical make-up of solid biomass material there are certain trends that are apparent when biomasses are pyrolysed. The key tendencies for the products with increasing pyrolysis temperature from 400 – 1000°C are; gas yield increases and char yield decreases (Neves et al., 2011). The tar yield reaches as maximum at around 500°C before decreasing as the temperature increases. The common traits of biomass should allow for the existing system to operate with a number of biomass materials including; straw and wood chips; however due the different shapes modifications to the feeding system may be required. A second option would be to optimise the design of the system so that liquid biomass materials could be processed. Sewage sludge could potentially be used in the system. Sewage sludge pyrolysis was reviewed by Fytili and Zabaniotou, (2008), although tests would be required to determine whether the overall system could manage the higher moisture content of the fuel as the increased volume of water vapour produced in the pyrolysis stage could have a negative effect on flame stability.

8.2 Modifications for Char Generation

This section looks at modifications that could be made to the existing system so that the process is developed to create biochar from raw biomass. Although the initial aim of the project was to develop a system to create a producer gas for electricity generation, there are characteristics of the existing design which, with some modifications, could potentially allow for a biochar generation system to be developed. In this chapter two existing commercialised char generation technologies (PYREG and Pacific Pyrolysis) are reviewed. Next, modifications to the existing system are proposed. Finally, a brief exploration into the potential applications for the produced biochar is discussed.

As discussed in the experimental section operating the CTC at the reduced stoichiometric conditions required for partial oxidation of tar vapours caused reliability issues with respect to flame stability. It is anticipated that operating the burner at an ER of 1 or greater than 1 would result in a stabilised and constant flame. However, doing this would lead to complete combustion of the pyrolysis gases and the produced gas would not contain any of the useful gases such as hydrogen, carbon monoxide and methane as these would be fully combusted. The tar components in the gas would also be destroyed. As shown from the experimental section the temperature of the flame and resulting gas produced is high enough for thermal tar destruction; for each of the 4 cases the flame temperature was greater than 800°C. This high temperature gas could be used to provide the heat for the pyrolysis stage thus creating a cyclic process where the pyrolysis of the raw biomass is powered by the heat generated from the combustion of the pyrolysis gases in the CTC. Currently electric heaters are used to provide

the required heat for the pyrolysis reaction. The proposed system is similar to the commercial PYREG reactor which produces a biochar using the heat from the combusted pyrolysis gases and recycling this to drive the pyrolysis reaction of the raw biomass. The design features of the PYREG reactor are discussed in Section 8.2.1.

8.2.1 The PYREG Reactor

The PYREG reactor is a commercial unit, a diagram of the system is shown in Figure 8.5 and the system numbered system components is shown in Figure 8.6.
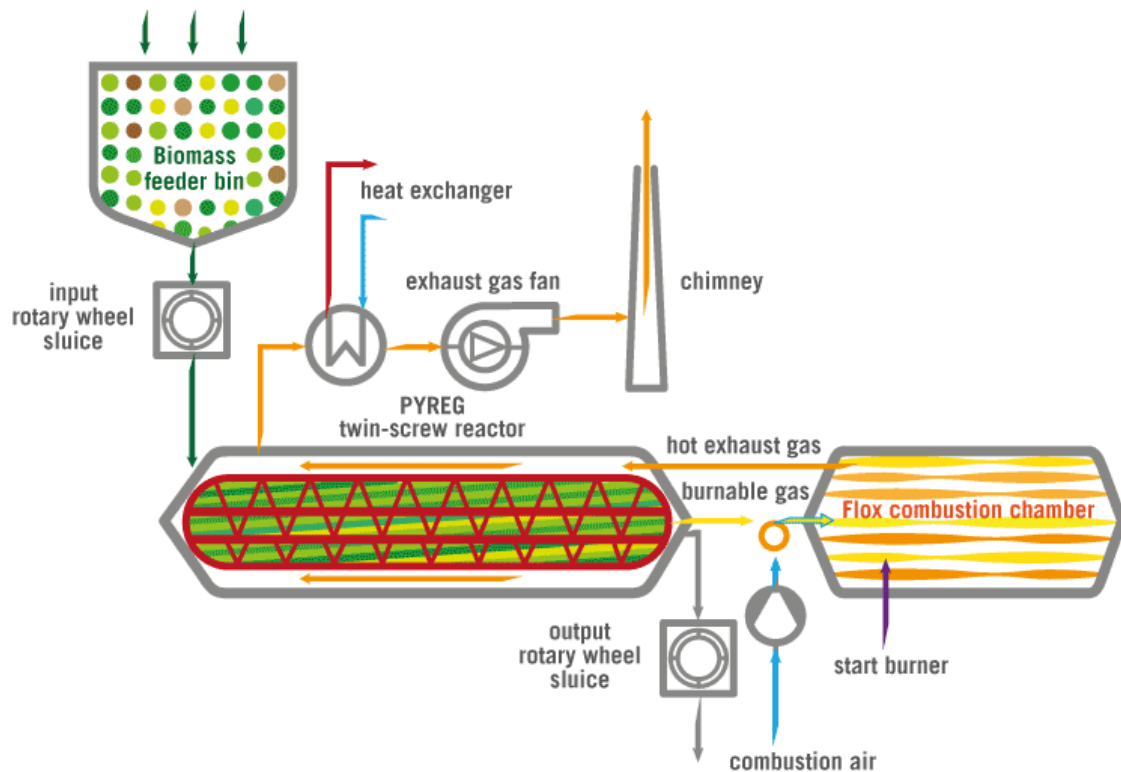
Figure 8.5 – Diagram of the PYREG system (PYREG, 2011)
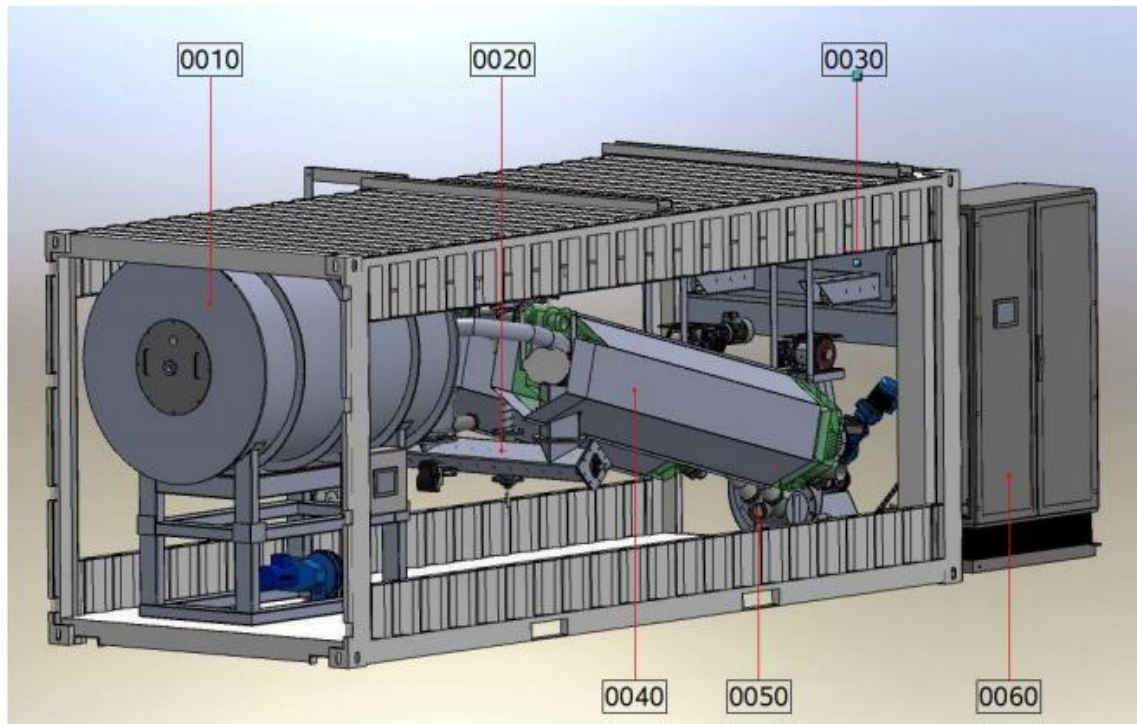
Figure 8.6 – System components (PYREG, 2011)

1. Combustion chamber

2. Biochar discharge conveyor

3. Feeding system

4. Reactor

5. Exhaust system with option for heat recovery

6. Control cabinet

Figure 8.5 shows an overall flow diagram for the PYREG system. Biomass is stored in a bin/hopper and fed to the PYREG reactor by a motor driven rotary valve, the total volume of the feed hopper is $2.2m^3$. The design of the rotary valve prevents air from entering the system. The PYREG reactor uses a twin screw system. The screws are interlocked and helical in shape as a result the biomass fuel cannot become 'trapped' against the hot walls and the biomass is constantly moved around in the system allowing for uniform heat distribution and continuous transport of fuel along the length of the reactor. A central column which contains the twin screw mechanism is surrounded by an outer chamber. As discussed, the heat required for pyrolysis is achieved by recuperating the heat from the exhaust gas created from the combustion of the pyrolysis gas in the FLOX combustion chamber (see Figure 8.5). The upper temperature limit in the PYREG reactor is 800ºC.

The FLOX combustion chamber combusts the pyrolysis gas at temperatures up to 1250 C. The flow rate of air to the chamber is regulated by an adjustable air fan. The combustion air can also be pre heated by using any excess heat that is not used in the PYREG twin-screw reactor. A start-up time of 45 minutes is needed before the PYREG can be operated using the heat of the combustion gases produced when the burnable pyrolysis gas is burned. In the start-up procedure natural gas is supplied to the start burner to produce the required heat for pyrolysis. Once the temperature is high enough for pyrolysis the supply of natural gas can be removed and the entire process becomes self-perpetuating.

The produced biochar exits the PYREG reactor through a rotary valve, it is then transported using a screw conveyor into the settling bin where the biochar can be utilised or prepared for another process. The PYREG is kept at a negative pressure by using induced draft fans this is done to prevent the escape of flammable gases from the system.

The PYREG has been operated using a number of different biomass fuels, including miscanthus, willow, coffee pulp, horse manure, poultry litter and sewage sludge. The minimum general requirements for the material properties are that the calorific value should be greater than 10 MJ/kg and the moisture content should be less than 50%.

8.2.2 The PACIFIC Pyrolysis Reactor

A second company which provides a commercial biochar production system is Pacific Pyrolysis. Figure 8.7 gives a description of the process. The simplified diagram indicates how the process works. Wet biomass is fed into the rotary dryer. The dry biomass is then fed into a pyrolysis kiln where there are two products; biochar and 'syngas', a portion of the syngas is fed back in the rotary dryer to drive the drying of the wet biomass. The produced gas is then sent to a gas clean-up system before being combusted in an engine where electricity is generated. Char produced in the pyrolysis kiln in then treated further in a char conditioner before a final biochar product is produced.

Similarly to the PYREG system a wide range of feedstocks have been demonstrated, these include;

- Wood waste

- Paper sludge

- Animal manure

- Crop residues

- Industrial organic waste
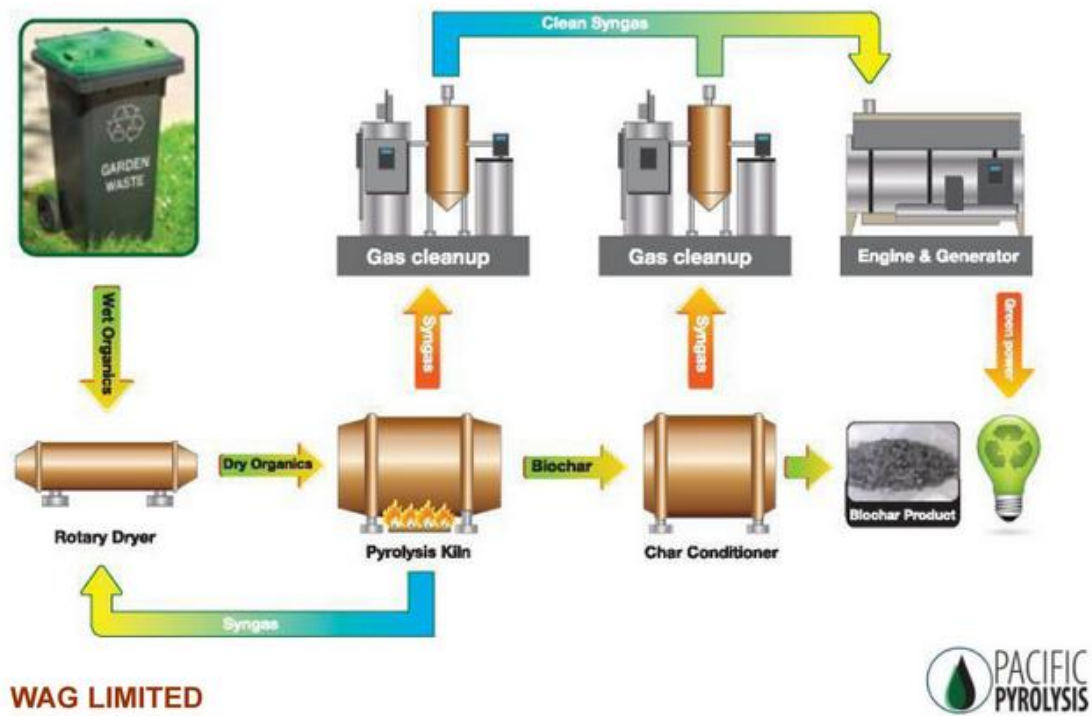
Figure 8.7 – Flow diagram of the Pacific pyrolysis system

Figure 8.8 shows the design for a commercial plant which is capable of processing 4 tonnes of raw biomass per hour.
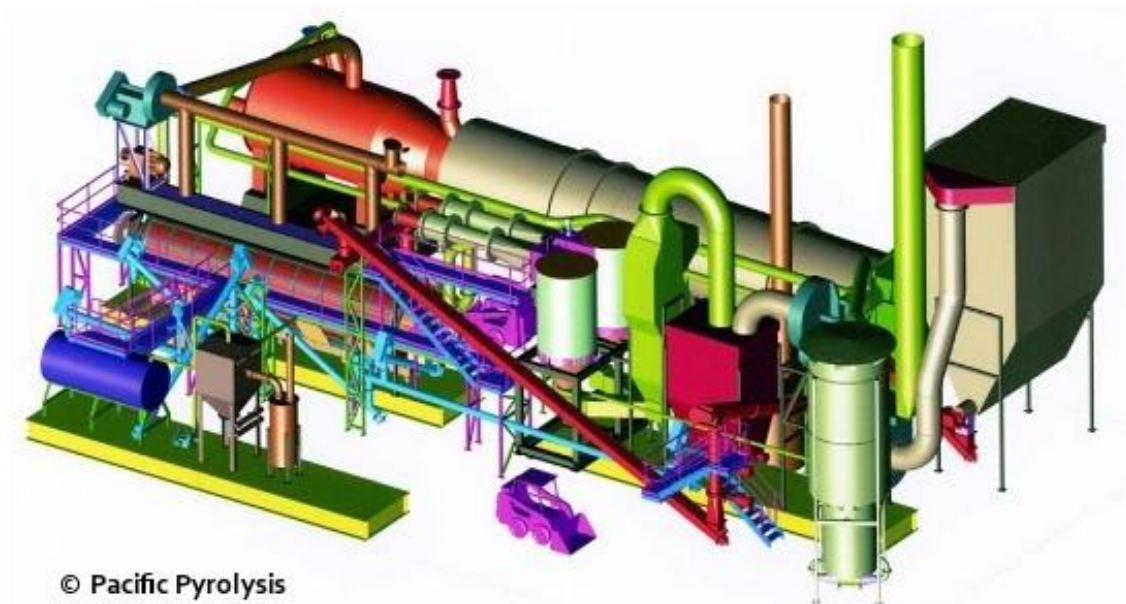
Figure 8.8 – Commercial 4 tonnes per hour pyrolysis plant

8.2.3 Technology Comparison

Table 8.1 gives a comparison of some of the key features of the two plants, the PYREG reactor and the PyroChar 4000 by Pacific Pyrolysis, that have been described previously in section 8.2.1 and 8.2.2.

		PYREG 500	PyroChar 4000
Feed rates	kg/hour	40 – 180	166
	Tonnes/day	1 – 4.3	4
	Tonnes/year	365 – 1500	1460
Feed materials	Lopping residues Mischantus, willow Coffee pulp and grounds Horse manure Poultry litter Sewage sludge Paper fibre		Wood waste Bagasse Paper sludge Animal manure Crop residues Municipal green waste Crop residues
Fuel Requirement	Moisture Content	< 50%	< 70%
	Calorific Value	> 10 Mj/kg	n/a
	Particle Size	< 30 mm	< 40 mm

Table 8.1 – Comparison of commercial biochar technologies

Table 8.1 indicates the similarities between some of the key features of the two technologies. The feed-rates for both facilities are similar when looking at the yearly feed rates. There is likely to be some discrepancies in the values depending on the biomass fuel used, and the values also assume constant operation for a year. A complete year of continuous operation is unlikely due to technical issues that require shut-downs to solve and fix any technical problems.

Both technologies can operate using a large proportion of available biomass material; ranging from solid wood to various sludges. However both have limitations regarding the fuel quality required. The maximum moisture content for the PYREG 500 is 50%, the PyroChar 4000 has a slightly higher threshold with the facility being able to process fuels containing up to 70% moisture. The lower value fuel moisture limit could create difficulties for the PYREG 500 when ran with liquid based fuels such as sewage and other sludges which have a high moisture content thus the fuel may require drying before they are processed. The PyroChar 4000 has a dryer which pre-treats any wet biomass alleviating this concern.

The required particle size is also relatively small for both systems. The PYREG 500 can operate with fuels that are less than 30 mm, slightly less than the PyroChar which can function with particle sizes less than 40 mm. Size reduction pre-treatments for some larger woody biomass materials may be required to reduce the particle size to the working limits, such processes will add to the overall operational cost.

8.2.4 Proposed Modifications

The existing dual-system could be retrofitted and used for char generation similar to how the PYREG is operated. The produced pyrolysis gas in the first stage would be fully combusted by the CTC, thus higher flow rates of air would be required to the CTC. The hot combustion gas would then be recycled to provide the heat required to drive the pyrolysis reaction. Additional design features, some of which that have already been previously discussed, would also be required for the system. Figure 8.9 shows a potential design of a char generation system which incorporates the discussed design features.
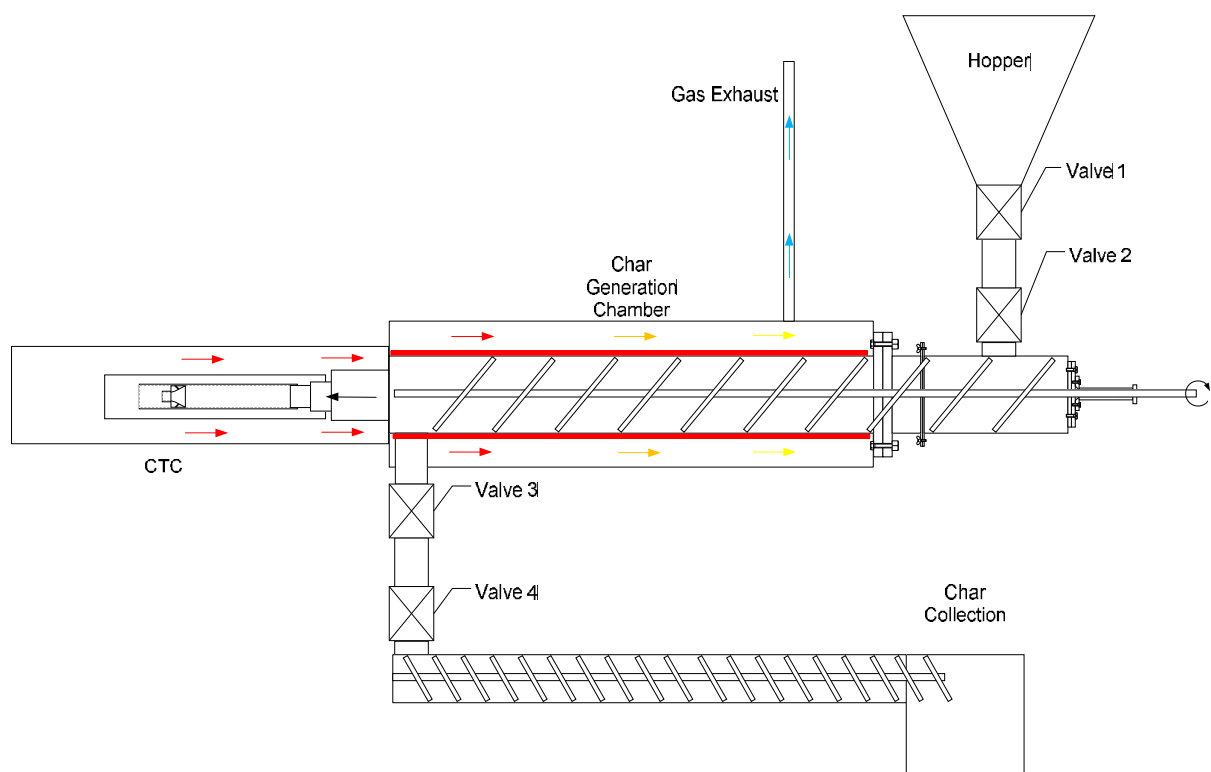
Figure 8.9 – Potential design for char generation

In the proposed char generation system biomass would enter the system through the hopper. Valve's 1 and 2 would act as a double lock hopper. The opening and closing of the valves would be automated. The design of the valves would depend on the biomass fuel used and the rotational speed at which the screw feeder which transports the biomass through the char generation chamber is rotating at. The screw feeder transports the biomass along the length of

the vessel; to create a uniform heat distribution a screw feeding system which prevents the biomass from becoming trapped against the hot walls of the chamber may be required. The PYREG system uses a twin screw feeder which could potentially be used in this system. Alternatively the design of the screw would complement the chosen biomass material.

The CTC would operate solely as a burner and the gases would be completely combusted. To begin the process a start-up gas would be required to be combusted in the CTC; propane is the most likely option as this was used in the previous experimental tests. Once the gas temperature had reached high enough levels to pyrolyse the biomass in the char generation chamber (see Figure 8.9) the supply of gas to the burner could be removed. The high temperature gas is recycled to provide heat to the char generation chamber. This is shown in Figure 8.9 by the coloured arrows; there is heat transfer from the outer chamber containing the high temperature combustion product gases through the walls of the char generation chamber. The design of the unit would have to be considered so that the transport of heat is efficient. The walls of the inner chamber should be as thin as possible. The gas is then sent to exhaust. A unit for heat transfer between the air used for combustion in the burner would be used so that the combustion air entered the burner at above ambient levels, in turn, creating an improved combustion environment.

The char produced in the char generation chamber would exit through valves 3 and 4 using a dual lock hopper system similar to the feeding system. These valves would also be automated. A second screw feeding system would then transport the char to a collection vessel; it is likely that this screw feeder would be water cooled to reduce the temperature of the produced char.

8.2.5 Biochar Applications

The char generated by the pyrolysis stage could be used for carbon sequestration in soil. Putting biochar into soil has two potential positive effects. Firstly for establishing a 'long-term sink for atmospheric carbon dioxide in terrestrial eco-system' (Laird et al., 2009). This alone has the potential to reduce greenhouse gas emissions by creating a permanent store for carbon dioxide in soil. The second positive outcome is that the presence of biochar in soil could potentially bring benefits to soil fertility and, thus, increase crop yields.

An extensive review on biochar application to soils was performed by Verheijen et al (2010) this report described the effect of biochar on soil with respect to its inherent properties as well as discussing some of the wider implications such as the overall impact on atmospheric emissions. The key findings from the study were presented. Positives include; a general increase in plant production when biochar is present, an increase in earthworm abundance and

a liming effect to the soil. There were also a number of negatives such as; soil loss through erosion, risk of soil contamination and soil compaction. There are also still a large number of unknowns which need to be researched some of which are caused by the lack of long-term studies in this area.

Jeffery et al (2011) looked solely at the crop productivity, which is perhaps the most attractive benefit of biochar in soil, by using meta-analysis. The aim of the study was to determine whether there is a link between the presence of biochar in soil and crop productivity. The results from this review of other studies showed a small, but significant, overall increase, with a grand mean increase of 10%. In the analysed studies the impact on crop productivity ranged quite dramatically, from -28% to 39%. The positive effects of biochar were predominantly found in soils which were either neutral or acidic or when the soils had a coarse or medium texture. The authors suggest that the crop yield increase can be attributed to biochar creating a liming effect and improving the water holding capacity of the treated biochar treated soil. However it should be noted that only short term studies, which are limited between one and two years, were available for analysis and some of these studies were missing key information regarding the type of soil and important data sets. But overall the effect of biochar is concluded to be positive for crop production.

8.3 Three-Stage Gasification System

A second potential development is to add a third stage to the existing system. The three stage system would use the pyrolysis stage and the Coandă tar cracking stage that are present in the existing system but with an added third stage which acts as a char gasification stage. The present horizontal setup will most likely have to be changed so that the three stage system is a vertical design. Figure 8.10 and 8.11 shows a potential downdraft and updraft setups that could be used for the system.

Biomass is fed into system, most likely via the means of a screw feeder so that the feed rate is constant throughout the operation. The biomass would be fed into the first stage where a traditional pyrolysis reaction would take place. The products from this would be a tarry gas and a char. The tarry gas, entrained by the injection of air through the annular slit of the CTC, is then treated in this region, at substiochiometric conditions producing a high temperature blue flame. This process results in the removal of tar from the gas.

The second product, char, produced in the pyrolysis stage is dropped into the bottom of the unit by using a rotating gird. The speed at which char drops down would be controlled. It is thought that the char dropping through the ejector would not have an adverse effect on the

operation of the CTC, although experimental tests would be required. The design of the system could be such that residual heat from the partial combustion of the pyrolysis gas can be used to drive the pyrolysis of fresh biomass as it enters the pyrolysis chamber. The char drops down onto a fixed bed. The char is gasified with air, oxygen or steam to form permanent gas species. Air and oxygen would promote the formation of carbon monoxide but if steam was used hydrogen formation would be more prominent. The setup of the three stage gasifier could either be updraft or downdraft, as indicated in Figures 8.10 and 8.11. It is likely down draft would be preferred as passing the gas through the char bed can have further advantages with respect to removing tar from the producer gas. A second rotating ash grid is used so that ash is removed from the fixed char bed.

The char that is passed through the cracking stage is charged to a fixed bed. The char undergoes reactions depending on the gasifying agent selected. This agent will have an effect on what the potential applications the producer gas could be used for. Using air has the advantage that the partial combustion generates a heat supply for the gasification reactions and the char and tar content is moderate (Wang et al., 2008) however using air as the agent has a detrimental effect on the heat value of the gas, resulting in the LHV of the gas to be less than 6 MJ/Nm^3. The presence of nitrogen in air also results in a large volume of nitrogen being present in the final gas product. Using steam results in a producer gas with a higher heating value, nominally between 10 and 15 MJ/Nm^3, the gas is also hydrogen rich, which makes it preferential for certain applications such as the Fischer-Tropsch synthesis. Using steam as the agent can increase the amount of tar in the producer and an external heat source is required for gasification.
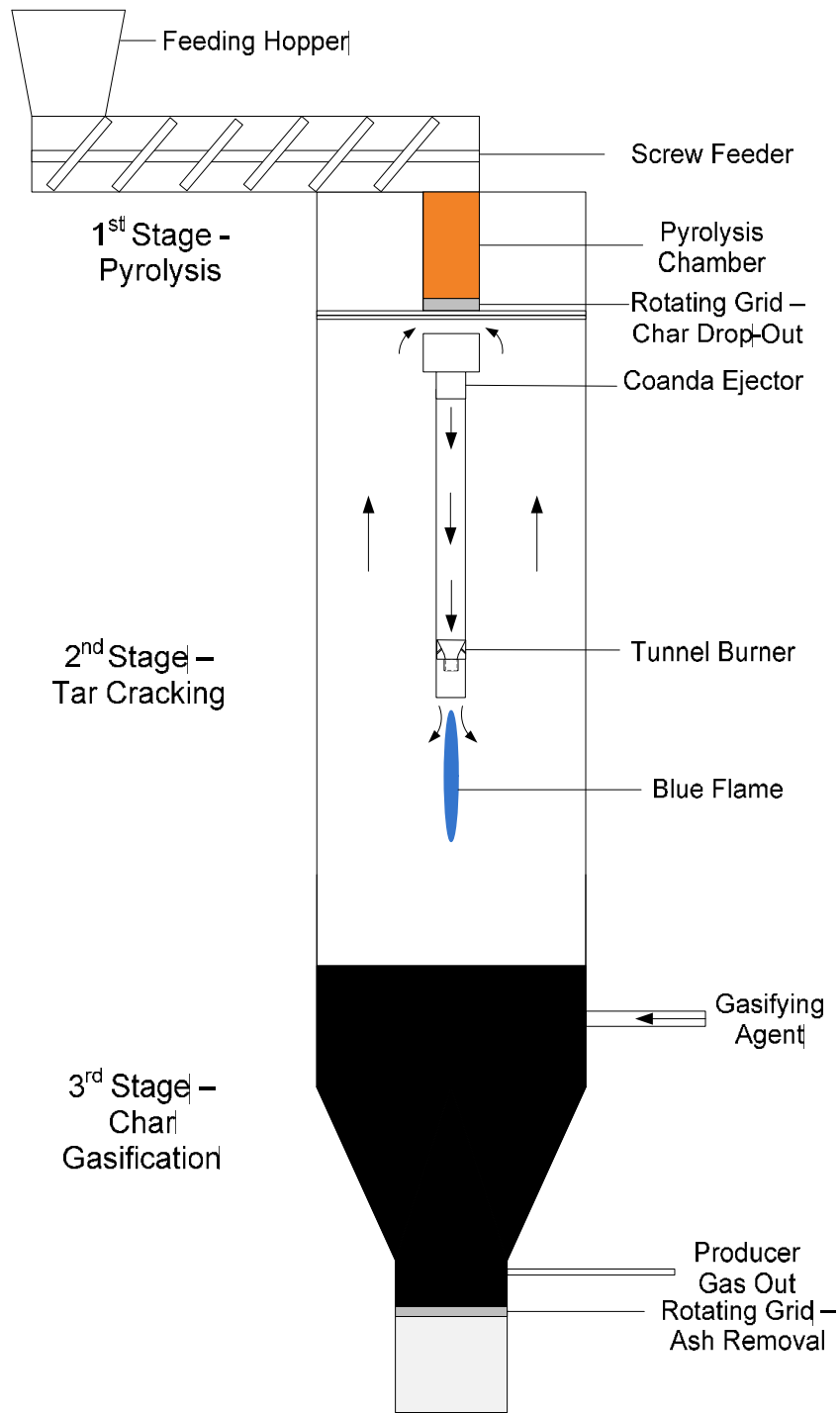
Figure 8.10 – Downdraft-three stage CTC gasifier
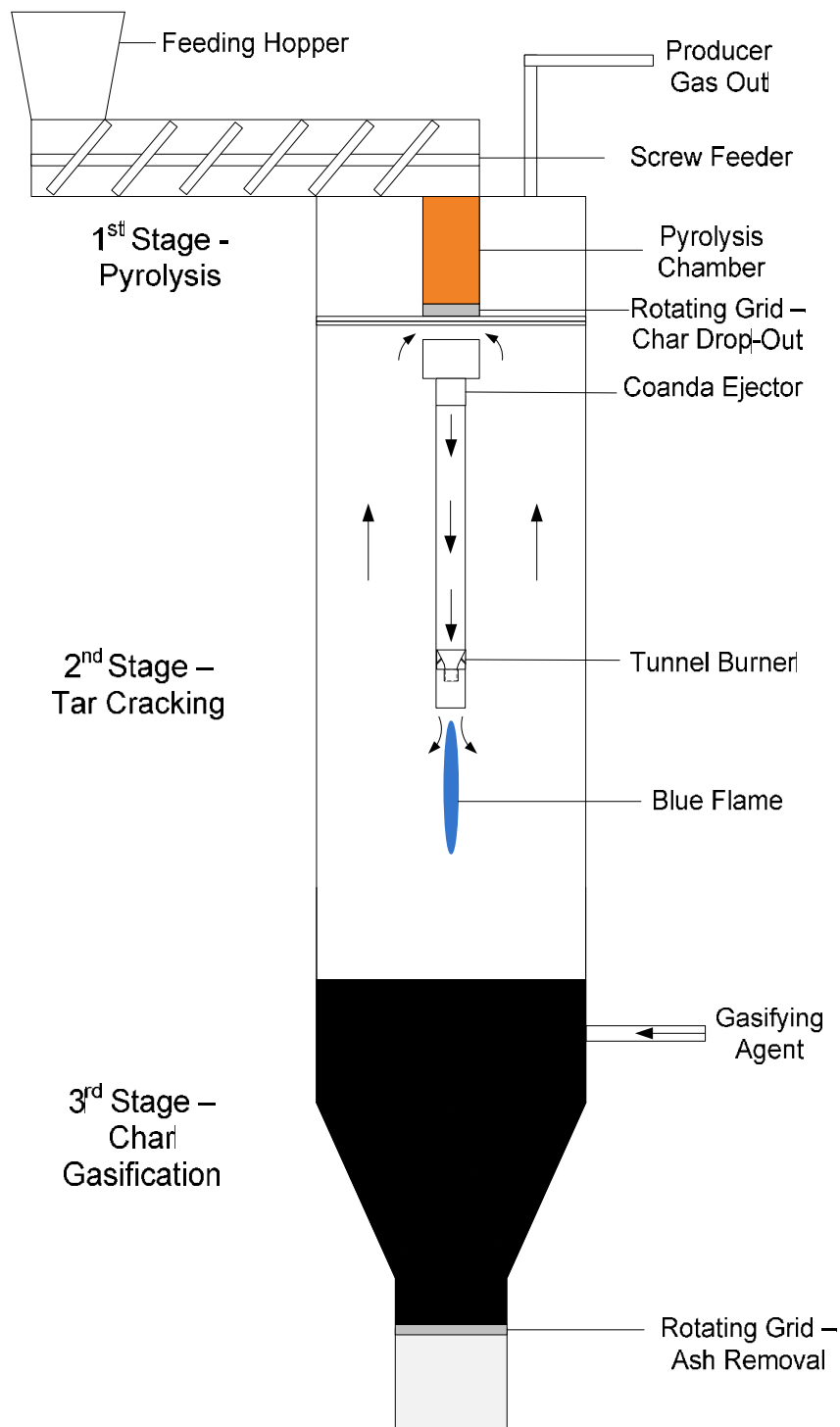
Figure 8.11 – Updraft three-stage CTC gasifier

8.3.1 Applications of the Three Stage System

The produced low calorific value gas from the three stage system could be used in a variety of applications. There are a number of factors which affect the type of end use for the produced gas. The gas quality can be separated into three key factors; the calorific value, the composition and the tar content. Results showed that gas composition from the dual system contained only a small volume of hydrogen and carbon monoxide which are the active

ingredients, using a three stage system should increase the yields of these useful gases. There were also a large volume of gases such as nitrogen and carbon dioxide which are not useful for end-use applications, which again, is likely to be an issue for the proposed three staged system. The addition of nitrogen as a purge gas in the pyrolysis stage and the addition of nitrogen in the air used for combustion in the CTC means that there is a large, unavoidable, volume of nitrogen in the product gas. A high volume of nitrogen can cause further issues if the gas is combusted; it is likely that NOx will become a potential emissions issue. The tar yield is effectively reduced by the CTC but the yield is still too high to be used in high end applications such as for Fischer-Tropsch. Therefore the most likely end uses of the produced gas will be for power generation.

Depending on the gasifying agent used the heating value of the gas produced in the three stage system is likely to be high enough to be utilized in a gas turbine or engine for energy production. The most likely scenario for the three stage system is to be used for power generation in small scale systems. Having an in-built tar cracking system, the CTC, should reduce the requirement for expensive gas treatment facilities such as using catalysts or gas scrubbers. The economics of small scale systems is such that operation rates should be as low as possible so that the overall cost for electricity is reduced. It is likely that the proposed system could be used for rural electrification in developing countries. Producer gas can be used directly combusted to generate steam for power using a steam turbine, the efficiency of the process is, however, limited to the limit of the steam turbine (Wang et al., 2008). If the producer gas is of high enough quality with respect to tar content and calorific value the gas can be fed into gas turbines or gas engines directly. When used in these situations the gas is first cooled to increase the energy density (Wang et al., 2008).

A local biomass energy source would be found and the used to power the process. Due to the size of the process a gas engine would be used rather than a turbine because they are cheaper.

In order to be used for power generation in a gas turbine the producer gas must meet a number of requirements. The gas must contain low levels of solids and liquids (tars) but levels of chlorine and sulfur can be tolerated by the turbine (Bridgwater, 1995). Table 8.2 highlights the fuel specifications required.

Parameter	Value
Minimum LHV (MJ/m^3)	4 – 6
Minimum hydrogen content (vol. %)	10 – 20
Minimum delivery temperature (^{o}C)	450 – 600
Tars at delivery temperature	All in vapour form
NH$_3$	No limit
HCl (ppm)	<0.5
S	<1
Maximum particulates (ppm)	-
Particle size (μm) > 20	<0.1
10 - 20	<1
4 – 10	< 10

Table 8.2 – Producer gas specifications for use in gas turbines (Adapted from Bridgwater, 1995)

For gas engines the tolerance impurities in the producer gas is higher than that of gas turbine engines. Table 8.3 shows a comparison between gas turbines and engines.

		IC engine	Gas turbine
Particles	mg/Nm^3	<50	<30
Particle size	μm	<10	<5
Tar	mg/Nm^3	<100	-
Alkali metals	mg/Nm^3	-	0.24

Table 8.3 – Comparison between gas specifications between internal combustion engines and gas turbines (Hasler & Nussbaumer, 1999)

Producer gas can be used in spark ignition engines. A typical diagram of a spark engine is show in Figure 8.12. The producer gas is sent through a gas clean-up system which consists of a centrifugal dust collector and a filter before passing through a cooling system. A carburettor, which mixes the producer gas and air, is then used before the combustion mixture is passed into the spark ignition engine. Suction from the engine draws the producer gas and air into through the gas clean-up system. For maximum combustion power the mixture between producer gas and air should be slightly lean when compared to the stoichiometric value (Reed & Das, 1988).
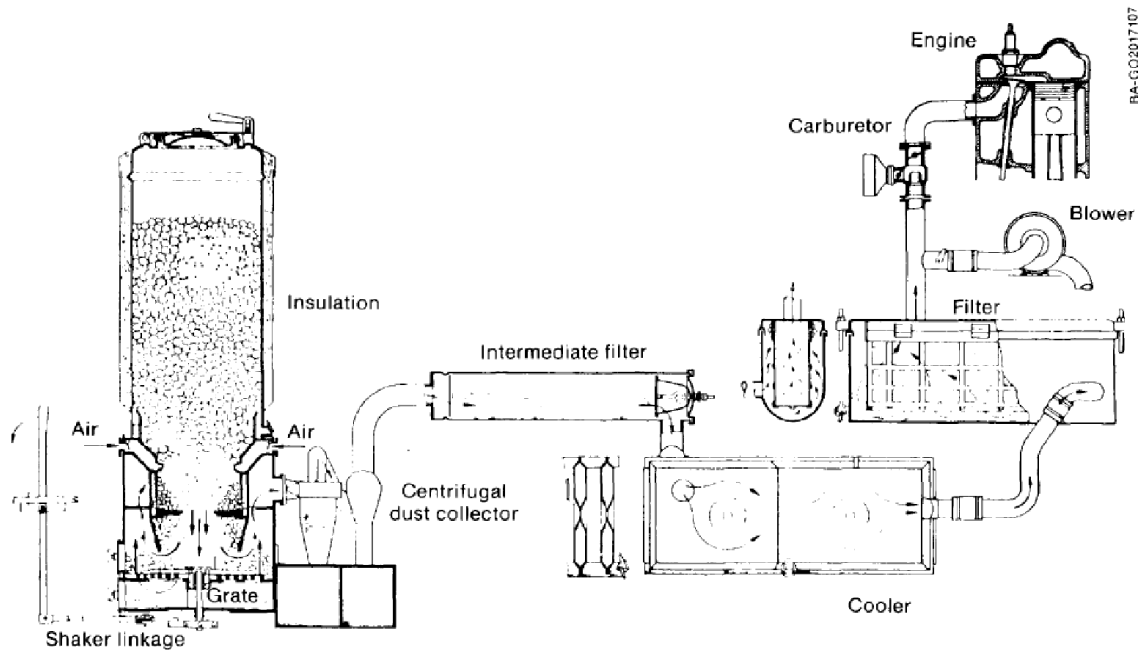
Figure 8.12 – Typical set up of a spark-ignition engine (Reed & Das, 1988)

Diesel engines can also be operated on producer gas in an "aspirated" mode. Air and producer gas is, firstly, mixed and a small quantity of diesel fuel is introduced continuously to ensure that there is ignition in the gas mixture. The injection of diesel needs to be timed so that the engine operation runs smoothly. Table 8.4 shows some of the key advantages and disadvantages to some of the potential energy conversion applications.

Energy Conversion Device	Net electrical efficiency of gasification plant	Advantages	Disadvantages
Steam turbine	10-20%	• Turbine components are adapted from combustion products • High availability due to long maintenance intervals • High specific work (kJ/kg yielded for working fluid)	• Expensive • At small sizes electrical efficiency is low • Partial load decreases efficiency significantly • Large plant size due to size of condenser and boiler
Gas turbine	15-25%	• Good electrical efficiency even at small sizes • Compact • High availability due to long maintenance intervals • Good for CHP due to high exhaust	• Turbine components are exposed to combustion products • Partial load decreases efficiency significantly • Moderately expensive

		temperatures	
Externally fired gas engine	10-20%	• Turbine components are adapted from combustion products • Acceptable electrical efficiency even at small sizes • High availability due to long maintenance intervals • Good for CHP due to high exhaust temperatures	• Expensive • Heat exchanger is exposed to high temperatures • Partial load decreases efficiency
Gas engine	13-28%	• Good electrical efficiency even at small sizes • Inexpensive • Durable and reliable • Partial load effects efficiency only marginally	• Short and expensive maintenance intervals • Engine components are exposed to high temperature combustion products

Table 8.4 – Advantages and disadvantages of energy conversion systems for biomass producer gas

CHP Small-Scale Gasification Systems

Current state of the art gasification systems offer cogeneration of both heat and electricity and are seen as the most efficient way of using biomass resources (Ahrenfeldt et al., 2013b). Using a combined heat and power (CHP) system for small scale systems (less than 10MW) offers, attractive and potential lucrative alternative to biomass combustion, such small-scale systems could provide a biomass to power efficiency of 35-40%, which compares favourably to conventional technologies (Ahrenfeldt et al., 2013b).

The *"Viking"* gasifier is a two-stage process that is characterised by having separated pyrolysis and gasification stages with a high temperature tar cracking zone (Henriksen et al., 2003). Wood chips are used for the fuel in the system. A process flow-sheet for the plant is shown in Figure 8.13. The original demonstration facility had a nominal thermal input of 70kW but the unit was successfully scaled up to a 20kWe (electrical) facility, with plans afoot to build a 500kWe plant. Data from the 70kW demonstration facility is presented in Table 8.5.

	Unit	Value
Thermal input	kW	70
Feedstock	-	Wood chips
Electric Output	kW	17.5
Thermal Output	kW	39
Overall electric efficiency	%	25

Table 8.5 – Key data from the demonstration facility (Ahrenfeldt et al., 2013b)

Figure 8.13 – Process flow sheet of the Viking gasifier

The current design of the CTC could be adopted to provide both electrical and thermal power in a similar method to the "Viking" gasifier shown in the Figure 8.13. The design of the gasification unit could be the same as the system shown in Figure 8.10 or the system could be re-designed to create a clearer separation between the pyrolysis and gasification stages, as shown in the "Viking" gasifier.

The first stage would be a pyrolysis system using a screw feeder which feeds both char and tarry gases to the second gasification stage. The CTC unit would be fitted between the described systems to crack tar, thus reducing the overall tar content in the producer gas. A down-draft gasifier would also be used to further reduce the tar content in the producer gas.

Using the produced high temperature gas for district heating is a logical solution for creating a more efficient and viable process. When using an engine for electricity generation the producer gas is normally required to be cooled, using this heat for district heating rather than it going to waste makes the process more efficient. Figure 8.13 shows that heat from gaseous exhaust of the engine is supplied back to the pyrolyser to power the reaction, which again increases the overall efficiency of the system, as heat is recycled for useful means. Figure 8.14 shows a simple diagram of how the CTC could be installed into a three-stage system which could be used for CHP.
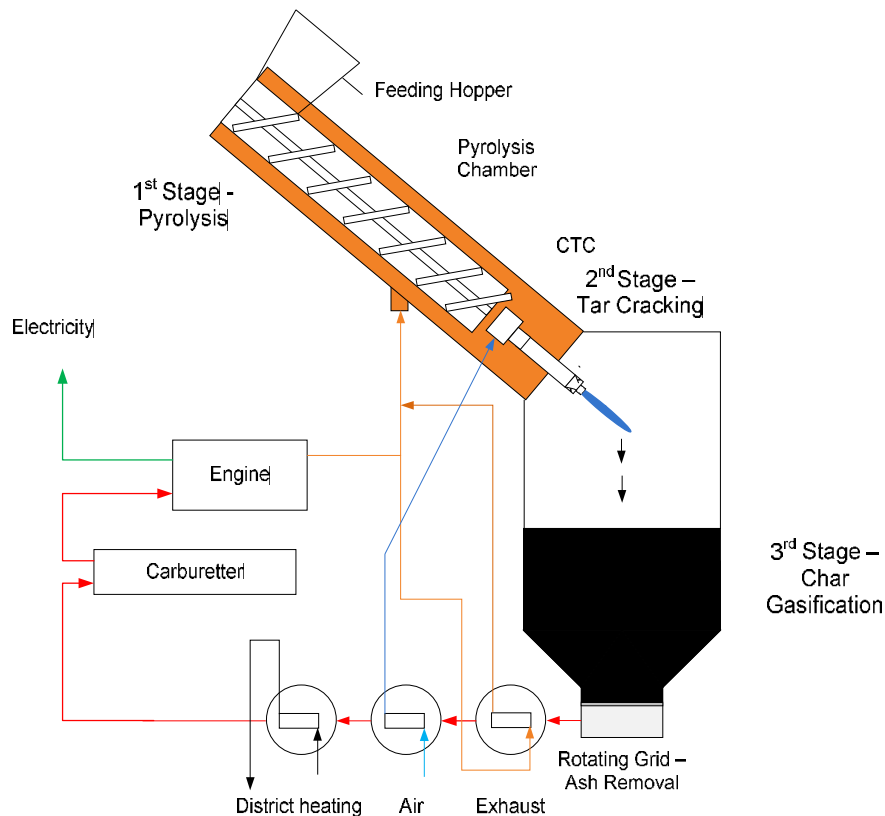
Figure 8.14 – Schematic of a potential three-stage CTC gasifier with CHP

Figure 8.14 shows how a potential three-stage tar cracking gasifier could be used for a CHP system using both an engine for electricity generation and thermal energy in a district heating system. In the first stage the biomass fuel is pyrolysed, some of the heat for pyrolysis could be provided from exhaust from the engine, which is transferred to the pyrolysis chamber in two ways. In the first the exhaust is transferred directly to the chamber, in the second the exhaust gas is passed through a heat exchanger situated at the product gas exit at the bottom of the gasifier. Heat from hot product gas is passed to the exhaust gas which is then supplied to the pyrolysis chamber.

In the second heat exchanger air used for partial oxidation in the Coandă ejector is pre-heated by, again, using the heat of the product gas. In the third heat exchanger heat from the product gas is transferred to a district heating system. The product gas is then mixed with air in a carburettor before being combusted in an engine to generate electricity.

8.4 Analysis of Proposed Systems

There is considerable scope for how the existing dual pyrolysis and CTC system could be developed to be commercialised and used in industry. This section discussed two of the likely potential applications for the system.

The first discussed system was to modify the existing design to convert the operation for biochar generation. There are number of issues with the stability of the flame when the produced gas is partially combusted in the CTC. For partial combustion low stoichiometric rates of air required to destroy tar but, at the same time, keep the energy content of the gas high enough. This low stoichiometric level of oxygen supplied has caused issues. By increasing the supply of oxygen so that the CTC operates above an ER of 1 should ensure that the stability of the flame. The hot combustion gases produced would then be recycled to drive the pyrolysis of the biomass to the char. The proposed system is a continuous process with biochar being the only product. Further modification to the existing design would be required. A continuous screw feeder would be installed to supply fresh biomass to the pyrolysis chamber and also to remove the produced biochar.

The resulting biochar has a number of uses. Biochar has been used in soil to improve quality, resulting in improved crop yields, although further research is required to determine the long-term advantages and disadvantages of using biochar in soil. Using biochar in this way also means that carbon is sequestrated for long time periods. Currently PYREG technology is the market leader in producing biochar. Further experimental activities would be required to determine the most efficient design of the unit as well as to determine the most effective way to operate the burner so that it is appropriate for the proposed system. Investigations into different biomass feed stocks would be required. In particular; animal wastes, sewage sludge and other waste materials from industry which could potentially be treated by the system forming a useful product.

The design development of the three stage system is also discussed. The proposed system has many benefits when compared to other systems. Using the CTC to remove tar from the gas reduces the requirement and need for expensive gas cleanup equipment which is normally needed in small-scale gasification units. The CTC removes the tar species produced when

biomass is pyrolysed resulting in a low yield of tar in the final producer gas. There is also no cost to replace catalysts or dispose of any effluents produced when tars are removed by scrubbers. The additional third stage where char produced from the pyrolysis stage is gasified should also result in an overall increase in the heating value of the gas. The produced gas is likely to be used in an engine or turbine downstream of the process for power production.

A second option for the three-stage system is for it to be modified to be used for a CHP system, where the heat from the producer gas is processed in heat exchangers for numerous useful methods. Hot gases can be used to drive the pyrolysis reaction, combustion air for the Coandă can be pre-heated and heat can be transferred to a district heating scheme. It is this modern, state of the art setup that is likely to be most commonly used in biomass gasification system. The CTC has an advantage over other existing systems because of its inherent ability to destroy problematic tar species in the second stage.

8.5 Commercialisation Scenarios

The previous chapter discussed and evaluated some of the potential industrial applications the CTC could be developed into. This section looks at requirements, both technical and practical, as well as looking at costs from existing commercial systems to offer a basic insight into what the costs for building and operating the systems would be.

Firstly, adapting the CTC for char generation is pursued and compares the proposed device with the PYREG 500 and the PyroChar 4000. Secondly costs from a small-scale (200 kWe) gasifier operating with two different energy conversion systems is evaluated to offer a comparative example for the proposed three-stage gasifier. This section is devised to give an insight into the future of the technology and not a complete techno economic assessment. As such an evaluation of the costs of similar industrial systems is performed to offer an indication into the costs for building and operation. The two proposed systems are in their infancy, and although could offer solutions to energy problems and fit into emerging biomass markets the devices have yet to be proven on an experimental scale, as such a complete techno-economic assessment is not warranted. However the evaluation of existing devices should provide a basic judgement into what the costs of the system might be. For a complete techno-economic evaluation numerous parameters would be required to be known. The fuel used in the operation would have a key impact on the overall cost. The location of the system is also important and whether there was a local biomass source available would also affect the associated costs.

8.5.1 Char generation system

For industrialisation the size of the component parts of the system would need to be increased. The system can be divided into three sections: feeding, pyrolysis and gas combustion. The PYREG500 can process between 40 and 180 kilograms of biomass per hour; the PyroChar operates at the upper part of this range at 166 kg/hour. The modified experimental system should be able to process a similar amount of biomass; for this section a biomass feed-rate of 160 kilograms per hour will be used for the basis of the calculations. There are also further considerations that need to be dealt with when appraising the system for up-scaling. Additional requirements such as storage, automation and controls are required to allow the system to operate in industry, but again are beyond the scope of this section.

There are a number of issues that would have to be addressed regarding the design of a large scale reactor of this kind. The primary concern is the operation of the Coandă burner and whether the system could run with a higher gaseous throughput reliably. The increase in gas production from the greater flow-rate of biomass being processed in the pyrolysis zone could create problems with the Coandă burner and experiments would be required to determine if the system could handle the throughput. Alternatively a re-design of the system could be required to ease the operation.

The current size of the Coandă ejector used in the experimental setup has a throat diameter of 25mm. Larger throat ejectors are available from the BeckAir Ltd the company from where the ejector was purchase from. The different sizes can be seen in Table 8.6.

Part Number	Throat Diameter mm	Air consumed SLPM	Outlet Airflow SLPM	Consumed: Outflow	Diameter mm	Length mm	Material
BRJ25S/S	25	397	5500	1:13.9	50	85	Stainless Steel (304)
BRJ40S/S	40	510	10600	1:20	63	95	Stainless Steel (304)
BRJ50S/S	50	962	17000	1:17.7	90	135	Stainless Steel (304)
BRJ75S/S	75	1416	33333	1:23.5	132	165	Stainless Steel (304)

Table 8.6 – Available Coandă ejectors (Adapted from Beckair, 2013)

Table 8.6 shows the different ejector sizes that are available from Beck-Air. The largest throat diameter available is 75mm which is three times the current size of ejector used in the CTC at present. Increasing the size of the unit also has an effect on the ratio or air consumed by the ejector through the annular slit and the total amount of air that is entrained through the body of the ejector. Increasing the throat diameter from 25mm to 75mm increases the ratio of consumed to outflow air from 1:13.9 to 1:23.5, further experiments would be required to determine what the maximum size of the ejector could be effectively utilised. Alternatively a series of smaller Coandă burners could be set-up to process and then recycle gases to and from a larger pyrolysis chamber.

The temperature at which pyrolysis is performed also has a key effect on the yield and the quality of the char. The design of the system should enable for control of the pyrolysis temperature, this will most likely be done by adding cold air to the hot combustion gases for cooling purposes before the gases are recycled to the outer chamber of the pyrolysis zone. Table 8.7 indicates how the pyrolysis temperature affects the conversion of biomass to char using the desired feed-rate of wood pellets to the system.

		Pyrolysis Temperature (ºC)			
		500	600	700	800
Pellet Throughput	kg/hr	160	160	160	160
	kg/day	3840	3840	3840	3840
	kg/year	1,401,600	1,401,600	1,401,600	1,401,600
	tonnes/year	1402	1402	1402	1402
Char Conversion	%	20.3	18.5	16.5	15.4
Char Output	kg/hr	32	30	26	25
	kg/day	780	710	634	591
	kg/year	284,525	259,296	231,264	215,846
	tonnes/year	284.5	259.3	231.3	215.8

Table 8.7 – Effect of temperature on char yield

8.5.2 Potential costs for char generation

As discussed this section highlights some potential options for the CTC to become a commercial or industrial device. This section looks at some of the costs that would be associated with building, commissioning and running a potential char generation system. The

method that has been chosen for the costing is to compare the system with an existing commercial unit. Economic information regarding the PYREG500 is shown in Table 8.8.

Associated Cost	Cost (£)	
Investments	Reactor	249000
	Storage and Feeding	48140
Operating and Maintenance		12450
Wood Pellets Cost (per annum)		145457
Total		455047

Table 8.8 – Estimated costs for a PYREG500 (Gustafsson, 2013)

Table 8.8 gives a brief indication into some of the potential costs for the building of a PYREG500 unit. The proposed char generation system is likely to incur similar costs but that is beyond the scope of this section. Wood pellets were chosen for the fuel for the calculation; although because wood pellets are a high grade biomass fuel it is unlikely that they would be used in such a system. The cost of wood pellets was calculated by multiplying the cost per tonne of wood pellets (£104/tonne) from Sikkema et al., (2011) by the total feed rate required per year.

8.6 Potential costs for the three-stage gasifier

For commercialisation of the three stage gasifier the process will be kept to the small scale to fill a void in the market. In most probability the gas produced from the gasifier will be converted into power via an internal combustion engine, as this is currently the most common technique for energy conversion (Bocci et al., 2014) or using an externally fired gas turbine.

In a study by Arena et al., (2010) a comparison between using a gas engine and an externally fired gas turbine using the producer gas from a fluidised bed gasifier with a plant capacity of 200 kWe was performed. The results from this study are shown in Table 8.9.

	Externally-fired gas turbine	Gas engine
Total energy conversion efficiency, %	27.1	23.0
Waste export, kg/kg fuel	Gas: 6.64 Liquid: 0.11 Solid: 0	Gas: 32.25 Liquid: 0 Solid: 0.01
Exhaust gas temperature (°C)	145	313
Total plant costs, £/kWe	5000	6300
Operating costs, (£/year)/kWe	780	570
Internal rate of return (IRR), %	13.2	13.0

Table 8.9 – Cost comparison from two biomass gasification to energy conversions systems with reference to a nominal plant capacity of 200 kWe

8.7 Summary

This chapter explored how the CTC could be developed to improve the efficiency and operation of the system, as well as potential commercial applications. The key development for the CTC is the feeding system. Adding a screw-feeding system would provide a continuous supply of fuel to the pyrolyser which would alleviate some of the operational issues previously discussed. Additionally adding a fuel hopper, to maintain a fuel supply, above the dual valve system would allow for longer operational times.

In the second part of the chapter potential applications for the CTC were discussed and analysed. For the first application, the CTC was modified to produce a continuous supply of biochar. In this proposal hot exhaust gases are recycled to provide heat to drive the pyrolysis reaction and convert raw biomass fuel into biochar. The second application discussed was to add a third stage to the system. In this stage char, formed during pyrolysis stage, is gasified forming permanent gas species. Combusting the produced gas in an engine for electricity generation is the desired application.

To determine the effectiveness of both of the discussed methods; mass and energy balances of the complete systems would be required. These balances would include any pre or post processing equipment which may be required. The results would give an indication into the overall energy requirements as well as giving further information regarding the commercial viability and the environmental impact of the technologies.

9. Conclusions, Future Work and Recommendations

The main objective of this research was to develop a Coandă tar cracker to destroy 'tar' produced when biomass is pyrolysed. The CTC utilises a modified Coandă ejector to partially combust 'tarry' pyrolysis gases at sub-stoichiometric air/fuel ratios. Wood pellets were used as the biomass fuel. A two-stage system consisting of a pyrolyser and the aforementioned CTC system was designed and operated. The experimental program consisted of three phases. In the first stage the fuel properties of the wood pellets were analysed and the dual system was tested, first, with propane and then with gases produced from pyrolysis in a single batch mode operation. From this experience the experimental rig was modified to extend the run-time and improve the overall performance of the CTC. In the second stage tar, char and gas products from each experiment were collected and analysed to determine the effectiveness of the CTC for tar destruction. In this section the key conclusions from each chapter of the thesis are presented and highlighted. Secondly future work is proposed, to suggest potential research avenues that are required to be explored to enhance understanding and knowledge of the CTC and related areas of research.

9.1 Conclusions

Literature Review

- The presence of tar in producer gas is a key problem in the success of biomass gasification systems and particularly in small-scale plants where expensive clean-up equipment (scrubbing devices such as OLGA and catalysts) are neither suitable nor cost effective.

- The applications for producer gas from biomass gasification systems are strictly governed by the quantity of tar (mg/Nm^3) contained within the gas. Currently the end-use for producer gas in small-scale biomass gasification systems is likely to be for power generation in a modified internal combustion engine, due primarily to the higher tar tolerance of such systems. The required low limits of tar concentration for 'high end' applications such as gas turbines and fuel cells cannot be met by existing technologies.

- Partial oxidation of biomass gasification producer gas has the potential to destroy tar components within the gas by converting them to permanent gaseous species; however there is a trade-off between tar destruction and the energy content of the gas which is decreased due to the combustion of calorific gaseous components.

- Coandă burners have been proven to produce a high temperature blue flame at sub-stoichiometric air/fuel ratios with both propane and methane. This ability ensures that Coandă burners have the potential to be used for tar destruction using partial oxidation.

Experimental Phase 1

- Wood pellets were used for the experimental tests because of their wide availability and their robustness which makes them easy to handle. The wood pellets were analysed using various techniques. The calorific value of the pellets was 18.0 (kJ/kg); from the proximate analysis using TGA the moisture content was found to be 8 mass.%, the volatile matter content 74 mass.%, fixed carbon 17 mass.% and ash >1 mass.%. The carbon content was 45.6 mass.%, the hydrogen content 6.0 mass.% and nitrogen 0.2 mass.%.

- A Coandă burner fuelled with propane was shown to produce a blue flame at values for λ between 0.35 and 0.40 when the pre-Coandă mixing vessel was closed to prevent re-circulation of any gases. When the mixing vessel was opened the values for λ to produce a blue flame decreased as oxygen from the surrounding air was entrained by the burner and combusted. This prompted a re-design of the combustion system to decrease the diameter of the outer casing to prevent re-circulation of air from the surroundings; meaning that only air that was entered to the Coandă ejector was combusted.

- An initial version of the dual pyrolysis and CTC was designed; constructed and tested a number of operational issues arose. Firstly the single batch feeding system limited the operational time, therefore, there was only a small window for the treated gas to be analysed using the gas chromatograph which affected the accuracy of the gas analysis. The feeding method also affected the production of tarry pyrolysis gas resulting in issues with the functionality of the CTC, which requires a constant supply of gas. These two issues governed that a continuous method for feeding wood pellets to the pyrolyser was required.

Experimental Phase 2

- Tests showed that increasing the pyrolysis temperature from 500 to 700ºC caused an increase in the production of hydrogen, methane and carbon dioxide. As the temperature of the pyrolyser increased to 800ºC, there was a decrease in the yield of gravimetric tar from 78.59 to 16.53 g/Nm³. This reduction can be attributed to higher

pyrolysis temperature causing an increase in thermal cracking and depolymerisation reactions, which in turn promotes production of permanent gas species such as hydrogen, methane and carbon monoxide.

- The use of CTC was proven to be effective at tar destruction. A significant reduction in tar species concentration was observed when processing the gas through the combined CTC combined system. When comparing the Pyro800 and CTC800 cases; the benzene, toluene and naphthalene concentration in the production was reduced by more than 90%.

- The fixed carbon content in the char increased from 85.7% to 92.7% as the temperature increased. The biochar produced from the system has a high calorific value (>28 MJ/kg) and can be used as a valuable fuel in existing heat and power generation.

CFD Modelling

- CFD analysis of the CTC was performed using ANSYS Fluent. A number of cases were tested to determine the effect of some key parameters on the mixing performance of the ejector.

- Two viscous models were analysed; the k-φ model with SST and the k-ε. There was little difference between the two models when analysing the velocity vectors at a number of points along the length of the ejector.

- Increasing the pressure of the reservoir at the Coandă inlet caused an increase in the velocity magnitude at all points analysed in the ejector.

Development and Applications

- Key modifications for the existing system were proposed. The key improvement required is to improve the feeding system so that biomass is continuously fed in to the pyrolysis zone using a screw feeder.

- A three stage gasifier which incorporates the CTC was proposed. In the first stage the biomass fuel is pyrolysed, in the second stage the produced 'tarry' gas is treated using the CTC; in the final – third – stage char produced from the pyrolysis reaction in the first stage is gasified in a fixed bed.

- A potential system for producing biochar was proposed. In this system the CTC acts as a burner and fully combusts the pyrolysis gases. The produced hot combustion gases are then recycled to provide heat for the pyrolysis of biomass.

General

- Utilising biomass for energy production has the potential to play a vital role in solving a number of global energy and environmental issues. Tar formation in biomass gasification is known as the '*Achilles Heel*' and is the fundamental issue preventing the development of such systems. This thesis explores the development of a novel technology, the CTC, to partially oxidise and destroy tars produced when biomass is thermally treated. The CTC was shown to have a positive impact, and reduces the quantity of key tar species in the produced gas. Although further work is required it is thought that treating gases using a CTC-like device would have a positive impact on the future of biomass gasification systems.

- Although not in the initial scope of the research, the production and application of biochar, which is a bi-product in the current setup of the CTC, became more prevalent. Biochar can be used for both carbon sequestration and soil remediation and its application could have positive implications for storing carbon and improving crop yields.

9.2 Future Work

CTC and Three-Stage Gasifier

- Further study into whether the Coandă tar cracker is suitable for tar destruction is required. A three-stage system should be built which is based upon the designs discussed in chapter 8. There are concerns regarding the flame velocity and whether this will be suitable for use in a fixed bed design; experimental tests will be required on the proposed system.

- A pyrolyser fed by a continuous screw feeding system should be designed and constructed. This rig will allow for more accurate testing of future tar cracking devices as it will provide a continuous and calculable amount of gaseous products dependent on the pyrolysis temperature and feed-rate. This will allow for further in-depth investigations as the supply of a real pyrolysis gas is easily accessed.

- Experiments into using pure oxygen, rather than air, as the oxidising agent that is supplied to the Coandă should be explored. This change will dramatically reduce the quantity of nitrogen and other inert gases in the reaction.

- The set-up of the three-stage gasifier should also be looked into, the positioning of the CTC could be vital to the overall operation of the unit. Further investigation into determining if the heat released in the partial oxidation reaction could be used to power the char gasification should be investigated.

- The tar yield of the producer gas is unlikely to reach low enough yields to be used in advance end-use applications so further investigation into using modified internal combustion engines powered by producer gas should be investigated. The design of the three stage system should concentrate on solely producing a gas for this application.

- Further investigation into the tar cracking mechanism is required. The affect and pathways for partial oxidation should be investigated. This could be potentially performed by taking each of the key tar species individually and analysing the products under a series of unique thermal and oxidative conditions. This should be performed on key tar species (benzene, toluene, phenol and naphthalene). From this experimental data a reaction model for each species could be determined.

Char Generation

- A thorough study of the advantages and disadvantages of biochar should also be looked into. This may involve long term (3+ years) projects with other departments within the University such as the Animal and Plant Sciences department. The wider implications of using biochar as an additive to soil need be explored. These studies will determine if the addition of biochar does improve soil quality and crop growth over a sustained period.

- If biochar is determined to be a useful and sustainable product then the char generation system proposed should be built. There are a number of issues that are required to be solved. Firstly; how to control the recycling of the hot combustion gases; how to accurately control and change the pyrolysis temperature; the effect of the feed rate on the process; the most suitable design and fabrication of the feeding/pyrolysis chamber for efficient heat transfer; whether the Coandă based burner used to combust the tarry gases could be up-scaled to handle a larger feed-rate; if the system could be used to process waste biomass materials to create a useful material and finally if the hot

combustion gases could be used in a further process downstream of the system. Considering and solving all of these features would make for an interesting PhD study.

Additional Remarks

- The mechanism for pyrolysis using microwave pyrolysis needs to be further explored. It is suggested that it is the reactions with, and in the char layer, as species are released from the biomass particle, which causes the production of long chain tar molecules in traditional biomass pyrolysis. Microwave pyrolysis heats biomass internally rather than externally. The author suggests that the tar yield will be reduced because the released species will not undergo as many polymerisation reactions when passed, instead, through cold raw biomass. Proving this theory and understanding the mechanisms could potentially be an important discovery for converting raw biomass into useful and usable materials.

References

Ahrenfeldt, J., Egsgaard, H., Stelte, W., Thomsen, T. & Henriksen, U. B. (2013a). The Influence of Partial Oxidation Mechanisms on Tar Destruction in TwoStage Biomass Gasification. *Fuel*, 112, 662–680.

Ahrenfeldt, J., Thomsen, T. P., Henriksen, U. & Clausen, L. R. (2013b). Biomass Gasification Cogeneration – A Review of State of the Art Technology and near Future Perspectives. *Applied Thermal Engineering*, 50(2), 1407–1417.

Alexandru, D., Florin, F., Horia, D. & Octavian, P. (2011). Numerical Analyis of Turbulent Flow in a CoandăEjector. *PAMM (Proceedings in Applied Mathematics and Mechanics)*, 11(1), 647–648.

Anis, S. & Zainal, Z. A. (2011). Tar Reduction in Biomass Producer Gas via Mechanical, Catalytic and Thermal Methods: A Review. *Renewable and Sustainable Energy Reviews*, 15(5), 2355–2377.

ANSYS. (2010a). *ANSYS FLUENT Theory Guide: Release 13*. Canonsburg, PA: ANSYS, INC.

ANSYS. (2010b). *ANSYS FLUENT User's Guide Release 13*. Canonsburg, PA: ANSYS, INC.

ANSYS. (2012). *ANSYS Meshing User's Guide: Release 14.5*. Canonsburg, PA. ANSYS, INC.

Arena, U., Di Gregorio, F. & Santonastasi, M. (2010). A Techno-Economic Comparison between Two Design Configurations for a Small Scale, Biomass-to-Energy Gasification Based System. *Chemical Engineering Journal*, 162(2), 580–590.

Babu, B. V. (2008). Biomass Pyrolysis : A State-of- the-Art Review. *Biofuels, Bioproducts and Biorefining*, 2, 393–414.

Baker, E. G., Brown, M. D., Elliott, D. C. & Mudge, L. K. (1988). Characterization and Treatment of Tars from Biomass Gasifiers, in: *AIChe 1988 Summer National Meeting*. Denver, Colorada.

Balat, M., Balat, M., Kırtay, E. & Balat, H. (2009). Main Routes for the Thermo-Conversion of Biomass into Fuels and Chemicals. Part 2: Gasification Systems. *Energy Conversion and Management*, 50(12), 3158–3168.

Beckair. (2013). Ringjet Air Amplifiers Datasheet. , 1. Retrieved December 12, 2013, from http://www.beck-air.com/Portals/0/docs/Ringjet Air Amplifiers.pdf

Bergman, P. C. A., Paasen, S. V. B. Van & Boerrigter, H. (2002). The Novel " OLGA " Technology for Complete Tar Removal from Biomass Producer Gas. *Pyrolysis and Gasification of Biomass and Waste, Expert Meeting*, (October).

Bilbao, R., Millera, A. & Arauzo, J. (1989). Thermal Decompostion of Lignocellulosic Materials: Influence of the Chemical Composition. *Thermochimica Acta*, 143, 149–159.

Bocci, E., Sisinni, M., Moneti, M., Vecchione, L., Di Carlo, A. & Villarini, M. (2014). State of Art of Small Scale Biomass Gasification Power Systems: A Review of the Different Typologies. *Energy Procedia*, 45, 247–256.

Boroson, M. L., Howard, J. B., Longwell, J. P. & Peters, W. A. (1989). Product Yields and Kinetics from the Vapor Phase Cracking of Wood Pyrolysis Tars. *AIChE Journal*, 35(1), 120–128.

Brage, C., Yu, Q. & Sjöström, K. (1996). Characteristics of Evolution of Tar from Wood Pyrolysis in a Fixed-Bed Reactor. *Fuel*, 75(2), 213–219.

Breault, R. W. (2010). Gasification Processes Old and New: A Basic Review of the Major Technologies. *Energies*, 3(2), 216–240.

Brezinsky, K. (1986). The High-Temperature Oxidation of Aromatic Hydrocarbons. *Progress in Energy and Combustion Science*, 12(1), 1–24.

Bridgwater, A. V. (1995). The Technical and Economic Feasibility of Biomass Gasification for Power Generation. *Fuel*, 74(5), 631–653.

Bridgwater, A. V. (2004). Biomass Fast Pyrolysis. *Thermal Science*, 8(2), 21–49.

Bridgwater, A. V., Meier, D. & Radlein, D. (1999). An Overview of Fast Pyrolysis of Biomass. *Organic Geochemistry*, 30(12), 1479–1493.

Bruinsma, O. S. L. & Moulijn, J. A. (1988). The Pyrolytic Formation of Polycyclic Aromatic Hydrocarbons from Benzene, Toluene, Ethylbenze,e, Styrene, Phenylacetylene and N-Decane in Relation to Fossil Fuels Utilization. *Fuel Processing Technology*, 18(3), 213–236.

Caputo, A. C., Palumbo, M., Pelagagge, P. M. & Scacchia, F. (2005). Economics of Biomass Energy Utilization in Combustion and Gasification Plants: Effects of Logistic Variables. *Biomass and Bioenergy*, 28(1), 35–51.

Chen, G., Andries, J., Luo, Z. & Spliethoff, H. (2003). Biomass Pyrolysis/gasification for Product Gas Production: The Overall Investigation of Parametric Effects. *Energy Conversion and Management*, 44(11), 1875–1884.

Chen, Y., Luo, Y., Wu, W. & Su, Y. (2009). Experimental Investigation on Tar Formation and Destruction in a Lab-Scale Two-Stage Reactor. *Energy & Fuels*, 23(9), 4659–4667.

Cheng, J. (2010). *Biomass to Renewable Energy Processes.* Boca Raton, Fla. : CRC, c2010.

Circiu, I. & Dinea, S. (2010). Review of Applications on Coandă Effect. History, Theories, New Trends. *Review of the Air Force Academy, The Scientific Informative Review: Henri Coandă 100: Celebrating 100 years from the first jet flight*, 2(17), 14–20.

CPL Distribution LTD. (2014). ENPlus Quality Standards. Retrieved May 1, 2014, from http://www.woodpellets2u.co.uk/enplus-quality-standards

DECC. (2009). *The UK Renewable Energy Strategy* (Climate, Ed.). Department of Energy and Climate Change.

DECC. (2011). *The Carbon Plan: Delivering Our Low Carbon Future*. Department of Energy and Climate Change, London.

DECC. (2012). *UK Bioenergy Strategy*. Department of Energy and Climate Change, London.

Demirbas, A. (2004). Effects of Temperature and Particle Size on Bio-Char Yield from Pyrolysis of Agricultural Residues. *Journal of Analytical and Applied Pyrolysis*, 72(2), 243–248.

Devi, L., Ptasinski, K. J. & Janssen, F. J. J. G. (2003). A Review of the Primary Measures for Tar Elimination in Biomass Gasification Processes. *Biomass and Bioenergy*, 24, 125–140.

Dufour, A., Girods, P., Masson, E., Rogaume, Y. & Zoulalian, A. (2009). Synthesis Gas Production by Biomass Pyrolysis: Effect of Reactor Temperature on Product Distribution. *International Journal of Hydrogen Energy*, 34(4), 1726–1734.

Dumas, A., Subhash, M., Trancossi, M. & Marques, J. P. (2014). The Influence of Surface Temperature on Coandă Effect. *Energy Procedia*, 45, 626–634.

Elliott, D., C. (1988). *Pyrolysis Oils from Biomass* (E. J. Soltes and T. A. Milne, Eds.). Washington, DC: American Chemical Society.

Encinar, J., González, J. & González, J. (2000). Fixed-Bed Pyrolysis of Cynara Cardunculus L. Product Yields and Compositions. *Fuel Processing Technology*, 68(3), 209–222.

Encinar, J. M., Beltrán, F. J., Bernalte, A., Ramiro, A. & González, J. F. (1996). Pyrolysis of Two Agricultural Residues: Olive and Grape Bagasse. Influence of Particle Size and Temperature. *Biomass and Bioenergy*, 11(5), 397–409.

Erlich, C. & Fransson, T. H. (2011). Downdraft Gasification of Pellets Made of Wood, Palm-Oil Residues Respective Bagasse: Experimental Study. *Applied Energy*, 88(3), 899–908.

Erlich, C., Bjornbom, E., Bolado, D., Giner, M. & Fransson, T. (2006). Pyrolysis and Gasification of Pellets from Sugar Cane Bagasse and Wood. *Fuel*, 85(10-11), 1535–1540.

European Committee for Standardisation. (2009). EN 14918:2009 Solid Biofuels - Determination of Calorific Value.

Evans, R. J. & Milne, T. A. (1987). Molecular Characterization of the Pyrolysis of Biomass. 1. Fundamentals. *Energy & Fuels*, 1(2), 123–137.

Fagbemi, L., Khezami, L. & Capart, R. (2001). Pyrolysis Products from Different Biomasses: Application to the Thermal Cracking of Tar. *Applied Energy*, 69, 293–306.

Fassinou, W. F., Van de Steene, L., Toure, S., Volle, G. & Girard, P. (2009). Pyrolysis of Pinus Pinaster in a Two-Stage Gasifier: Influence of Processing Parameters and Thermal Cracking of Tar. *Fuel Processing Technology*, 90(1), 75–90.

Fytili, D. & Zabaniotou, A. (2008). Utilization of Sewage Sludge in EU Application of Old and New methods—A Review. *Renewable and Sustainable Energy Reviews*, 12(1), 116–140.

Gaydon, A. & Wolfhard, H. (1979). *Flames: Their Structure, Radiation and Temperature*. Chapmand and Hall.

Good, J., Ventress, L., Knoef, H., Zielke, U., Hansen, P. L., Wild, P. De, et al. (2005). Sampling and Analysis of Tar and Particles in Biomass Producer Gases - Technical Report. , 1–44.

Gregory-Smith, D. G. & Gilchrist, A. R. (1987). The Compressible Coandă Wall Jet—an Experimental Study of Jet Structure and Breakaway. *International Journal of Heat and Fluid Flow*, 8(2), 156–164.

Guerriero, V. (2008). *Experimental and Numerical Study of Coandă Ejectors and Pneumatic Solid Transport*. PhD Thesis, University of Toulouse, France.

Gustafsson, M. (2013). *Pyrolysis for Heat Production: Biochar - the Primary Byproduct*. Master's Thesis. The University of Gavle.

Han, J. & Kim, H. (2008). The Reduction and Control Technology of Tar during Biomass Gasification/pyrolysis: An Overview. *Renewable and Sustainable Energy Reviews*, 12(2), 397–416.

Hasler, P. & Nussbaumer, T. (1999). Gas Cleaning for IC Engine Applications from Fixed Bed Biomass Gasification. *Biomass and Bioenergy*, 16(6), 385–395.

Heikkinen, J. M., Hordijk, J. C., Jong, W. De & Spliethoff, H. (2004). Thermogravimetry as a Tool to Classify Waste Components to Be Used for Energy Generation. *Journal of Analytical and Applied Pyrolysis*, 71, 883–900.

Henriksen, U. B., Ahrenfeldt, J., Jensen, T. K., Gobel, B., Bentzen, J. D., Hindsqual, C., et al. (2003). The Design, Construction and Operation of a 75kW Two-Stage Gasifier. *ECOS 203*, 8.

Higman, C. & van der Burgt, M. (2008). *Gasification*. 2nd Edition. Gulf Professional Publishing.

Houben, M. P. (2004). *Analysis of Tar Removal in a Partial Oxidation Burner*. PhD Thesis, Eindhoven University of Technology, The Netherlands.

Houben, M. P., Delange, H. & Vansteenhoven, A. (2005). Tar Reduction through Partial Combustion of Fuel Gas. *Fuel*, 84(7-8), 817–824.

IPCC, I. P. O. C. C. (2007). Climate Change 2007: Synthesis Report (R. K. Pachauri and A. Reisinger, Eds.). *Assessment*, 21(September), 24–29.

Iversen, H. & Gøbel, B. (2005). Update on Gas Cleaning Technologies. *Handbook of biomass gasification. BTG Biomass*

Jeffery, S., Verheijen, F. G. A., van der Velde, M. & Bastos, A. C. (2011). A Quantitative Review of the Effects of Biochar Application to Soils on Crop Productivity Using Meta-Analysis. *Agriculture, Ecosystems & Environment*, 144(1), 175–187.

Jess, A. (1996). Mechanisms and Kinetics of Thermal Reactions of Aromatic Hydrocarbons from Pyrolysis of Solid Fuels. *Fuel*, 75(12), 1441–1448.

Kim, H. D., Rajesh, G., Setoguchi, T. & Matsuo, S. (2006). Optimization Study of a Coandă Ejector. *Journal of Thermal Science*, 15(4), 331–336.

Kirkels, A. F. & Verbong, G. P. J. (2011). Biomass Gasification : Still Promising ? A 30-Year Global Overview. *Renewable and Sustainable Energy Reviews*, 15, 471–481.

Klass, D. L. (1998). *Biomass for Renewable Energy, Fuels, and Chemicals*. California: Academic Press.

Kolb, T. (2011). Technical systems for biomass gasification – challenges and potential, in: *9th European Conference on Industrial Furnaces and Boilers*, (pp. 1–10).

Kumar, A., Jones, D. D. & Hanna, M. A. (2009). Thermochemical Biomass Gasification: A Review of the Current Status of the Technology. *Energies*, 2, 556–581.

Kurkela, E., Ståhlberg, P., Simell, P. & Leppälahti, J. (1989). Updraft Gasification of Peat and Biomass. *Biomass*, 19(1-2), 37–46.

Laird, D. A., Brown, R. C., Amonette, J. E. & Lehmann, J. (2009). Review of the Pyrolysis Platform for Coproducing Bio-Oil and Biochar. *Biofuels, Bioproducts and Biorefining*, 3(5), 547–562.

Larson, E. D. (1998). Small-Scale Gasification-Based Biomass Power Generation, in: *Biomass Workshop*. Changchun, Jilin Province, China.

Li, C. & Suzuki, K. (2009). Tar Property, Analysis, Reforming Mechanism and Model for Biomass gasification—An Overview. *Renewable and Sustainable Energy Reviews*, 13(3), 594–604.

Li, X. ., Grace, J. R., Lim, C. J., Watkinson, A. P., Chen, H. P. & Kim, J. R. (2004). Biomass Gasification in a Circulating Fluidized Bed. *Biomass and Bioenergy*, 26(2), 171–193.

Liu, Z., Zhang, F.-S. & Wu, J. (2010). Characterization and Application of Chars Produced from Pinewood Pyrolysis and Hydrothermal Treatment. *Fuel*, 89(2), 510–514.

Maniatis, K. & Beenackers, A. A. C. M. (2000). Tar Protocols. IEA Bioenergy Gasication Task. *Biomass and Bioenergy*, 18, 1–4.

Maniatis, K. & Millich, E. (1998). Energy from Biomass and Waste: The Contribution of Utility Scale Biomass Gasification Plants. *Biomass and Bioenergy*, 15(3), 195–200.

Maschio, G., Koufopanos, C., Lucchesi, A. (1992). Pyrolysis, a Promising Route for Biomass Utilization. *Bioresource Technoogy,* 42(3), 219-231.

Mayoral, M. C., Izquierdo, M. T., Andres, J. M. & Rubio, B. (2001). Different Approaches to Proximate Analysis by Thermogravimetry Analysis. *Thermochimica Acta*, 370, 91–97.

Milne, T. A., Evans, R. J. & Abatzoglous, N. (1998). Biomass Gasifier "Tars": Their Nature , Formation , and Conversion. *National Renewable Energy Laboratory*.

Miura, K., Kawase, M., Nakagawa, H., Ashida, R., Nakai, T. & Ishikawa, T. (2003). Conversion of Tar in Hot Coke Oven Gas by Pyrolysis and Steam Reforming. *Journal of chemical engineering of Japan*, 36(7), 735–741.

Mohan, D., Pittman, C. U. & Steele, P. H. (2006). Pyrolysis of Wood / Biomass for Bio-Oil : A Critical Review. *Energy*, 20, 848–889.

Morf, P., Hasler, P. & Nussbaumer, T. (2002). Mechanisms and Kinetics of Homogeneous Secondary Reactions of Tar from Continuous Pyrolysis of Wood Chips. *Fuel*, 81(7), 843–853.

Morrison, J. F. & Gregory-Smith, D. G. (1984). Calculation of an Axisymmetric Turbulent Wall Jet over a Surface of Convex Curvature. *International Journal of Heat and Fluid Flow*, 5(3), 139–148.

Muñoz-Guillena, M. J., Linares-Solano, A. & de Lecea, C. S.-M. (1992). Determination of Calorific Values of Coals by Differential Thermal Analysis. *Fuel*, 71(5), 579–583.

Nair, S. A., Yan, K., Pemen, A. J. M., van Heesch, E. J. M., Ptasinski, K. J. & Drinkenburg, A. A. H. (2004). Tar Removal from Biomass-Derived Fuel Gas by Pulsed Corona Discharges. A Chemical Kinetic Study. *Industrial & Engineering Chemistry Research*, 43(7), 1649–1658.

Neathery, J. K. (2010). Biomass Gasification. *RSC Energy and Environment Series: Thermochemical Conversion of Biomass to Liquid Fuels and Chemicals*, 1, 67–94.

Neves, D., Thunman, H., Matos, A., Tarelho, L. & Gómez-Barea, A. (2011). Characterization and Prediction of Biomass Pyrolysis Products. *Progress in Energy and Combustion Science*, 37, 611–630.

Norinaga, K., Sakurai, Y., Sato, R. & Hayashi, J. (2011). Numerical Simulation of Thermal Conversion of Aromatic Hydrocarbons in the Presence of Hydrogen and Steam Using a Detailed Chemical Kinetic Model. *Chemical Engineering Journal*, 178, 282–290.

O'Nions, P. (1997). *Low NOx Combustion Utilising a Coandă Ejector Burner*. PhD Thesis, the University of Sheffield.

Obernberger, I. & Thek, G. (2004). Physical Characterisation and Chemical Composition of Densified Biomass Fuels with Regard to Their Combustion Behaviour. *Biomass and Bioenergy*, 27(6), 653–669.

Obernberger, I. & Thek, G. (2010). *The Pellet Handbook: The Production and Thermal Utilisation of Pellets*. London: Earthscan.

Olgun, H., Ozdogan, S. & Yinesor, G. (2011). Results with a Bench Scale Downdraft Biomass Gasifier for Agricultural and Forestry Residues. *Biomass and Bioenergy*, 35(1), 572–580.

OPET Finland. (2002). Review of Finnish Biomass Gasification Technologies, in: *Organisations for the Promotion of Energy Technologies*. Technical Research Centre of Finland.

Orfão, J. J. M., Antunes, F. J. A. & Figueiredo, J. L. (1999). Pyrolysis Kinetics of Lignocellulosic Materials - Three Independent Reactions Model. *Fuel*, 78, 349–358.

Parr Instrument Company. (2010). 6200 Oxygen Bomb Calorimeter: Operating Instruction Manual. *Control*, (585), 89.

Phan, A. N., Ryu, C., Sharifi, V. N. & Swithenbank, J. (2008). Characterisation of Slow Pyrolysis Products from Segregated Wastes for Energy Production. *Journal of Analytical and Applied Pyrolysis*, 81(1), 65–71.

Plis, P. & Wilk, R. K. (2011). Theoretical and Experimental Investigation of Biomass Gasification Process in a Fixed Bed Gasifier. *Energy*, 36(6), 3838–3845.

Poe, R., Patel, A., Baukal, C. E. & Wright, D. (2007). Advanced Low NOx Burners for Cracking Furnaces. *Petroleum Technology Quarterly*.

Prior, D. S. (1977). *Pollutant Mimimisation by Blue Flame Staged Combustion*. PhD Thesis, the University of Sheffield.

PYREG. (2011). *PYREG 500 Carbonisation Plant*.

Quaak, P., Knoef, H. & Stassen, H. E. (1999). *Energy from Biomass: A Review of Combustion and Gasification Technologies, Volumes 23-422*. World Bank Publications.

Reed, T. B. & Das, A. (1988). *Handbook of Biomass Downdraft Gasifier Engine Systems*. Golden, Colorado: Solar Energy Research Institute.

Rezaiyan, J. & Cheremisinoff, N. P. (2005). *Gasification Technologies: A Primer for Engineers and Scientists*. CRC Press.

Ryu, C., Sharifi, V. N. & Swithenbank, J. (2007). Waste Pyrolysis and Generation of Storable Char. *International Journal of Energy Research*, 31, 177–191.

Sikkema, R., Steiner, M., Junginger, M., Hiegl, W., Hansen, M. T. & Faaij, A. (2011). The European Wood Pellet Markets: Current Status and Prospects for 2020. *Biofuels, Bioproducts and Biorefining*, 5(3), 250–278.

Stassen, H. E. (1995). Small-Scale Biomass Gasifiers for Heat and Power: A Global Review. *World Bank Technical Paper Number 296: Energy Series*.

Stassen, H. E. M. & Knoef, H. A. M. (1993). Small Scale Gasification Systems, in: *The Netherlands: Biomass Technology Group,* University of Twente.

Stiegel, G. J. & Maxwell, R. C. (2001). Gasification Technologies: The Path to Clean, Affordable Energy in the 21st Century. *Fuel Processing Technology*, 71(1-3), 79–97.

Su, Y., Luo, Y., Chen, Y., Wu, W. & Zhang, Y. (2011). Experimental and Numerical Investigation of Tar Destruction under Partial Oxidation Environment. *Fuel Processing Technology*, 92(8), 1513–1524.

Sutton, D., Kelleher, B. & Ross, J. R. H. (2001). Review of Literature on Catalysts for Biomass Gasification. *Fuel Processing Technology*, 73(3), 155–173.

Swithenbank, J., Sharifi, V. & Finney, K. (2012). *Waste Heat Recovery,* Nextgen Expo 2012, Presentation.

Taylor, G. (2008). Bioenergy for Heat and Electricity in the UK: A Research Atlas and Roadmap. *Energy Policy*, 36(12), 4383–4389.

Telmo, C., Lousada, J. & Moreira, N. (2010). Bioresource Technology Proximate Analysis , Backwards Stepwise Regression between Gross Calorific Value , Ultimate and Chemical Analysis of Wood. *Bioresource Technology*, 101, 3808–3815.

The Royal Society. (2010). *Climate Change: A Summary of the Science*. London.

U.S. DoE & NETL. (2010). Gasification 2010 Worldwide Database.

U.S. Energy Information Administration. (2013). *International Energy Outlook 2013*. Washington, DC.

Van der Hoeven, T. A. (2007). *Partial Product Gas Combustion for Tar Reduction*. PhD Thesis, Eindhoven University of Technology, The Netherlands.

Van der Hoeven, T. A., de Lange, H. C. & van Steenhoven, A. A. (2006). Analysis of Hydrogen-Influence on Tar Removal by Partial Oxidation. *Fuel*, 85(7-8), 1101–1110.

Venkat, C., Brezinsky, K. & Glassman, I. (1982). High Temperature Oxidation of Aromatic Hydrocarbons. *Symposium (International) on Combustion*, 19(1), 143–152.

Verheijen, F. G. A., Jeffery, S., Bastos, A. C., van der Velde, M. & Diafas, I. (2010). Biochar Application to Soils: A Critical Scientific Review of Effects on Soil Properties, Processes and Functions. *JRC Scientific and Technical Reports*, 149.

Verhoeven, L. (2011). *Radical Tar Removal; Numerical Modeling of Tar Conversion in a Partial Combustion Reactor*. PhD Thesis, Eindhoven University of Technology, The Netherlands.

Violi, A., D'Anna, A. & D'Alessio, A. (1999). Modeling of Particulate Formation in Combustion and Pyrolysis. *Chemical Engineering Science*, 54(15-16), 3433–3442.

Vreugdenhil, B. J. & Zwart, R. W. R. (2009). *Tar Formation in Pyrolysis and Gasification*. ECN Report, The Netherlands.

Wang, L., Weller, C. L., Jones, D. D. & Hanna, M. A. (2008). Contemporary Issues in Thermal Gasification of Biomass and Its Application to Electricity and Fuel Production. *Biomass and Bioenergy*, 32, 573–581.

Williams, P. T. & Besler, S. (1996). The Influence of Temperature and Heating Rate on the Slow Pyrolysis of Biomass. *Renewable Energy*, 1481(96), 233–250.

Wu, W., Luo, Y., Chen, Y., Su, Y., Zhang, Y., Zhao, S., et al. (2011). Experimental Investigation of Tar Conversion under Inert and Partial Oxidation Conditions in a Continuous Reactor. *Energy & Fuels*, 25(6), 2721–2729.

Xu, C. (Charles), Donald, J., Byambajav, E. & Ohtsuka, Y. (2010). Recent Advances in Catalysts for Hot-Gas Removal of Tar and NH3 from Biomass Gasification. *Fuel*, 89(8), 1784–1795.

Zainal, Z. ., Rifau, A., Quadir, G. . & Seetharamu, K. . (2002). Experimental Investigation of a Downdraft Biomass Gasifier. *Biomass and Bioenergy*, 23(4), 283–289.

Zhang, R., Brown, R. C., Suby, A. & Cummer, K. (2004). Catalytic Destruction of Tar in Biomass Derived Producer Gas. *Energy Conversion and Management*, 45(7-8), 995–1014.

Zhang, Y., Kajitani, S., Ashizawa, M. & Oki, Y. (2010). Tar Destruction and Coke Formation during Rapid Pyrolysis and Gasification of Biomass in a Drop-Tube Furnace. *Fuel*, 89(2), 302–309.

Zwart, R. (2009). *Gas Cleaning Downstream Biomass Gasification–status Report 2009*. ECN Report, The Netherlands.

Appendix I - TGA Example

Filename:	C:\Program Files\Pyris\Data\Wes...\pw-a.t6d	——————	PW-A: pw-a
Operator ID:	K Penny		Derivative Weight (mg/min) (Smoothed) : Steps: 1-7
Sample ID:	PW-A	················	PW-B: pw-b
Sample Weight:	43.078 mg		Derivative Weight (mg/min) (Smoothed) : Steps: 1-7
Comment:	run with 40C start temp	- - - - - - -	PW-C: pw-c
			Derivative Weight (mg/min) (Smoothed) : Steps: 1-7
		·–·–·–·–·–	PW-D: pw-d
			Derivative Weight (mg/min) (Smoothed) : Steps: 1-7

Pyrolysis Only Char Comparison
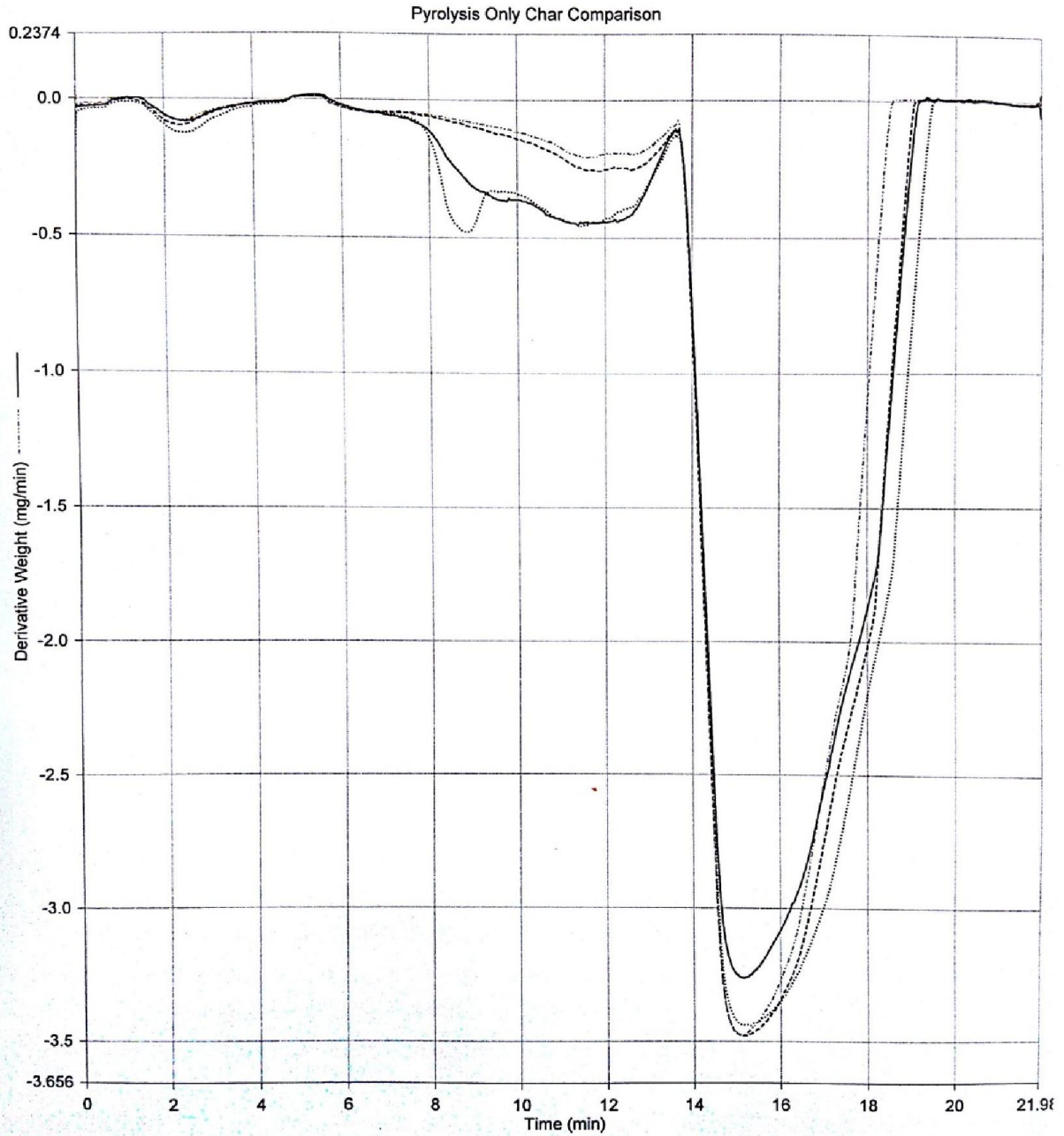
08/05/2013 15:15:25

1) Hold for 1.0 min at 40.00°C
2) Heat from 40.00°C to 110.00°C at 65.00°C/min
3) Hold for 3.0 min at 110.00°C
4) Heat from 110.00°C to 900.00°C at 100.00°C/min
5) Hold for 1.0 min at 900.00°C
6) Hold for 7.0 min at 900.00°C
7) Heat from 900.00°C to 950.00°C at 50.00°C/min

Appendix II – Tar Analysis

NICHOLLS COLTON
ANALYTICAL

Nicholls Colton Analytical
7 - 11 Harding Street
Leicester
LE1 4DH

Chemical & Biological Engineering
Gate 1
Sir Robert Hadfield Building
Portobello Street
Sheffield
S1 3JD

Analytical Test Report:	13707/SHU/001a

Your Project Reference:	**Tar Analysis**	Samples Received on:	25.04.2013
Your Order Number:	ZHO/4500483152	Testing Instruction Received:	25.04.2013
Report Issue Number:	1	Sample Tested :	25.04 to 07.05.2013
Samples Analysed	8 Solvents	Report issued:	13.05.2013

Signed

James Gane
Manager - Data Logistics
Nicholls Colton Analytical

Notes:

General

Please refer to Methodologies tab for details pertaining to the analytical methods undertaken.

Samples will be retained for 14 days after issue of this report unless otherwise requested.

Samples were supplied by customer.

Page 1 of 6

NICHOLLS COLTON
ANALYTICAL

13707/SHU/001a

Project Reference - Tar Analysis

Analytical Test Results - VOC

NCA Reference			13-9041	13-9042	13-9043	13-9044	13-9045	13-9046
Client Sample Reference			A500	A600	A700	A800	B500	B600
Sample Matrix			Solvent	Solvent	Solvent	Solvent	Solvent	Solvent
Determinant	Units	Accreditation						
Benzene	(µg/l)	None	363288	1726888	1286183	2412553	154873	148871
Toluene	(µg/l)	None	453612	1199022	481941	1099048	89574	58542
Ethylbenzene	(µg/l)	None	57699	98692	12857	35088	7476	3332
m&p Xylene	(µg/l)	None	133586	226155	60779	151720	17851	8769
o-Xylene	(µg/l)	None	55477	88737	20978	53364	6633	3146
Dichlorodifluoromethane	(µg/l)	None	<6.00	<6.00	<6.00	<6.00	<6.00	<6.00
Chloromethane	(µg/l)	None	<6.00	<6.00	<6.00	<6.00	<6.00	<6.00
Vinyl Chloride	(µg/l)	None	<6.00	<6.00	<6.00	<6.00	<6.00	<6.00
Bromomethane	(µg/l)	None	<6.00	<6.00	<6.00	<6.00	<6.00	<6.00
Chloroethane	(µg/l)	None	<6.00	<6.00	<6.00	<6.00	<6.00	<6.00
Trichlorofluoromethane	(µg/l)	None	<6.00	<6.00	<6.00	<6.00	<6.00	<6.00
1,1-Dichloroethylene	(µg/l)	None	<6.00	<6.00	<6.00	<6.00	<6.00	<6.00
Dichloromethane	(µg/l)	None	13112	23420	12697	11626	12105	13341
MTBE	(µg/l)	None	<6.00	<6.00	<6.00	<6.00	<6.00	<6.00
trans-1,2,-dichloroethylene	(µg/l)	None	<6.00	<6.00	<6.00	<6.00	<6.00	<6.00
1,1-Dichloroethane	(µg/l)	None	<6.00	<6.00	<6.00	<6.00	<6.00	<6.00
2,2-Dichloropropane	(µg/l)	None	<6.00	<6.00	<6.00	<6.00	<6.00	<6.00
cis--1,2,-dichloroethylene	(µg/l)	None	<6.00	<6.00	<6.00	<6.00	<6.00	<6.00
Bromochloromethane	(µg/l)	None	<6.00	<6.00	<6.00	<6.00	<6.00	<6.00
Chloroform	(µg/l)	None	4551	<6.00	<6.00	<6.00	<6.00	<6.00
1,1,1-Trichloroethane	(µg/l)	None	<6.00	<6.00	<6.00	<6.00	<6.00	<6.00
1,1-Dichloropropene	(µg/l)	None	<6.00	<6.00	<6.00	<6.00	<6.00	<6.00
Carbon Tetrachloride	(µg/l)	None	<6.00	<6.00	<6.00	<6.00	<6.00	<6.00
1,2-dichloroethane	(µg/l)	None	<6.00	<6.00	<6.00	<6.00	<6.00	<6.00
Trichloroethylene	(µg/l)	None	<6.00	<6.00	<6.00	<6.00	<6.00	<6.00
1,2-Dichloropropane	(µg/l)	None	<6.00	<6.00	<6.00	<6.00	<6.00	<6.00
Dibromomethane	(µg/l)	None	<6.00	<6.00	<6.00	<6.00	<6.00	<6.00
Bromodichloromethane	(µg/l)	None	<6.00	<6.00	<6.00	<6.00	<6.00	<6.00
cis-1,2-dichloropropylene	(µg/l)	None	<6.00	<6.00	<6.00	<6.00	<6.00	<6.00
trans-1,3-dichloropropylene	(µg/l)	None	<6.00	<6.00	<6.00	<6.00	<6.00	<6.00
1,1,2-Trichloroethane	(µg/l)	None	<6.00	<6.00	<6.00	<6.00	<6.00	<6.00
1,3-Dichloropropane	(µg/l)	None	<6.00	<6.00	<6.00	<6.00	<6.00	<6.00
Tetrachloroethylene	(µg/l)	None	<6.00	<6.00	<6.00	<6.00	<6.00	<6.00
Chlorodibromomethane	(µg/l)	None	<6.00	<6.00	<6.00	<6.00	<6.00	<6.00
1,2-Dibromoethane	(µg/l)	None	<6.00	<6.00	<6.00	<6.00	<6.00	<6.00
Chlorobenzene	(µg/l)	None	<6.00	<6.00	<6.00	<6.00	<6.00	<6.00
1,1,1,2-tetrachloroethane	(µg/l)	None	<6.00	<6.00	<6.00	<6.00	<6.00	<6.00
Styrene	(µg/l)	None	55278	257187	121977	305811	22683	11910
Isopropylbenzene	(µg/l)	None	5684	4741	<6.00	<6.00	<6.00	<6.00
Bromoform	(µg/l)	None	<6.00	<6.00	<6.00	<6.00	<6.00	<6.00
1,1,2,2-Tetrachloroethane	(µg/l)	None	<6.00	<6.00	<6.00	<6.00	<6.00	<6.00
1,2,3-Trichloropropane	(µg/l)	None	<6.00	<6.00	<6.00	<6.00	<6.00	<6.00
n-Propylbenzene	(µg/l)	None	5226	6100	<6.00	<6.00	<6.00	<6.00
Bromobenzene	(µg/l)	None	<6.00	<6.00	<6.00	<6.00	<6.00	<6.00
1,3,5-Trimethylbenzene	(µg/l)	None	4284	5862	<6.00	4637	<6.00	<6.00
2-chlorotoluene	(µg/l)	None	<6.00	<6.00	<6.00	<6.00	<6.00	<6.00
4-chlorotoluene	(µg/l)	None	1245	<6.00	<6.00	<6.00	<6.00	<6.00
tert-butylbenzene	(µg/l)	None	<6.00	<6.00	<6.00	<6.00	<6.00	<6.00
1,2,4-trimethylbenzene	(µg/l)	None	20804	24687	4298	11033	2312	1128
sec-Butylbenzene	(µg/l)	None	1039	18079	<6.00	<6.00	<6.00	<6.00
4-Isopropyltoluene (P-Cymene)	(µg/l)	None	<6.00	<6.00	<6.00	<6.00	<6.00	<6.00
1,3-Dichlorobenzene	(µg/l)	None	<6.00	<6.00	<6.00	<6.00	<6.00	<6.00
1,4-Dichlorobenzene	(µg/l)	None	<6.00	<6.00	<6.00	<6.00	<6.00	<6.00
n-Butylbenzene	(µg/l)	None	<6.00	<6.00	<6.00	<6.00	<6.00	<6.00
1,2-Dichlorobenzene	(µg/l)	None	<6.00	<6.00	<6.00	<6.00	<6.00	<6.00
1,2-Dibromo-3-chloropropane	(µg/l)	None	<6.00	<6.00	<6.00	<6.00	<6.00	<6.00
1,2,4-Trichlorobenzene	(µg/l)	None	<6.00	<6.00	<6.00	<6.00	<6.00	<6.00
Hexachlorobutadiene	(µg/l)	None	<6.00	<6.00	<6.00	<6.00	<6.00	<6.00
Naphthalene	(µg/l)	None	37708	440316	332671	823561	101717	55010
1,2,3-Trichlorobenzene	(µg/l)	None	<6.00	<6.00	<6.00	<6.00	<6.00	<6.00

NICHOLLS COLTON
ANALYTICAL

13707/SHU/001a

Project Reference - Tar Analysis

Analytical Test Results - VOC

NCA Reference			13-9047	13-9048
Client Sample Reference			B700	B800
Sample Matrix			Solvent	Solvent
Determinant	Units	Accreditation		
Benzene	(μg/l)	None	145861	44283
Toluene	(μg/l)	None	45965	16782
Ethylbenzene	(μg/l)	None	1451	675
m&p Xylene	(μg/l)	None	5776	2612
o-Xylene	(μg/l)	None	2007	891
Dichlorodifluoromethane	(μg/l)	None	<6.00	<6.00
Chloromethane	(μg/l)	None	<6.00	<6.00
Vinyl Chloride	(μg/l)	None	<6.00	<6.00
Bromomethane	(μg/l)	None	<6.00	<6.00
Chloroethane	(μg/l)	None	<6.00	<6.00
Trichlorofluoromethane	(μg/l)	None	<6.00	<6.00
1,1-Dichloroethylene	(μg/l)	None	<6.00	<6.00
Dichloromethane	(μg/l)	None	11747	11957
MTBE	(μg/l)	None	<6.00	<6.00
trans-1,2,-dichloroethylene	(μg/l)	None	<6.00	<6.00
1,1-Dichloroethane	(μg/l)	None	<6.00	<6.00
2,2-Dichloropropane	(μg/l)	None	<6.00	<6.00
cis--1,2,-dichloroethylene	(μg/l)	None	<6.00	<6.00
Bromochloromethane	(μg/l)	None	<6.00	<6.00
Chloroform	(μg/l)	None	<6.00	<6.00
1,1,1-Trichloroethane	(μg/l)	None	<6.00	<6.00
1,1-Dichloropropene	(μg/l)	None	<6.00	<6.00
Carbon Tetrachloride	(μg/l)	None	<6.00	<6.00
1,2-dichloroethane	(μg/l)	None	<6.00	<6.00
Trichloroethylene	(μg/l)	None	<6.00	<6.00
1,2-Dichloropropane	(μg/l)	None	<6.00	<6.00
Dibromomethane	(μg/l)	None	<6.00	<6.00
Bromodichloromethane	(μg/l)	None	<6.00	<6.00
cis-1,2-dichloropropylene	(μg/l)	None	<6.00	<6.00
trans-1,3-dichloropropylene	(μg/l)	None	<6.00	<6.00
1,1,2-Trichloroethane	(μg/l)	None	<6.00	<6.00
1,3-Dichloropropane	(μg/l)	None	<6.00	<6.00
Tetrachloroethylene	(μg/l)	None	<6.00	<6.00
Chlorodibromomethane	(μg/l)	None	<6.00	<6.00
1,2-Dibromoethane	(μg/l)	None	<6.00	<6.00
Chlorobenzene	(μg/l)	None	<6.00	<6.00
1,1,1,2-tetrachloroethane	(μg/l)	None	<6.00	<6.00
Styrene	(μg/l)	None	11437	4511
Isopropylbenzene	(μg/l)	None	<6.00	<6.00
Bromoform	(μg/l)	None	<6.00	<6.00
1,1,2,2-Tetrachloroethane	(μg/l)	None	<6.00	<6.00
1,2,3-Trichloropropane	(μg/l)	None	<6.00	<6.00
n-Propylbenzene	(μg/l)	None	<6.00	<6.00
Bromobenzene	(μg/l)	None	<6.00	<6.00
1,3,5-Trimethylbenzene	(μg/l)	None	<6.00	<6.00
2-chlorotoluene	(μg/l)	None	<6.00	<6.00
4-chlorotoluene	(μg/l)	None	<6.00	<6.00
tert-butylbenzene	(μg/l)	None	<6.00	<6.00
1,2,4-trimethylbenzene	(μg/l)	None	<6.00	<6.00
sec-Butylbenzene	(μg/l)	None	<6.00	<6.00
4-Isopropyltoluene (P-Cymene)	(μg/l)	None	<6.00	<6.00
1,3-Dichlorobenzene	(μg/l)	None	<6.00	<6.00
1,4-Dichlorobenzene	(μg/l)	None	<6.00	<6.00
n-Butylbenzene	(μg/l)	None	<6.00	<6.00
1,2-Dichlorobenzene	(μg/l)	None	<6.00	<6.00
1,2-Dibromo-3-chloropropane	(μg/l)	None	<6.00	<6.00
1,2,4-Trichlorobenzene	(μg/l)	None	<6.00	<6.00
Hexachlorobutadiene	(μg/l)	None	<6.00	<6.00
Naphthalene	(μg/l)	None	52700	<6.00
1,2,3-Trichlorobenzene	(μg/l)	None	<6.00	<6.00

NICHOLLS COLTON ANALYTICAL

13707/SHU/001a

Project Reference - Tar Analysis

Analytical Test Results - SVOC

NCA Reference			13-9041	13-9042	13-9043	13-9044	13-9045	13-9046	13-9047
Client Sample Reference			A500	A600	A700	A800	B500	B600	B700
Sample Matrix			Water	Water	Water	Water	Water	Water	Water
Determinant	Units	Accreditation							
1,2,4-trichlorobenzene	(µg/l)	none	<20	<20	<20	<20	<20	<20	<20
1,3,5-Cycloheptatriene	(µg/l)	none	<20	<20	<20	<20	<20	<20	<20
1,3-dichlorobenzene	(µg/l)	none	<20	<20	<20	<20	<20	<20	<20
1,4-dichlorobenzene	(µg/l)	none	<20	<20	<20	<20	<20	<20	<20
1-chloronaphthalene	(µg/l)	none	<20	<20	<20	<20	<20	<20	<20
2,3,4,6-tetrachlorophenol	(µg/l)	none	<20	<20	<20	<20	<20	<20	<20
2,4,5-trichlorophenol	(µg/l)	none	<20	<20	<20	<20	<20	<20	<20
2,4,6-trichlorophenol	(µg/l)	none	<20	<20	<20	<20	<20	<20	<20
2,4-Dichlorophenol	(µg/l)	none	<20	<20	<20	<20	<20	<20	<20
2,4-dimethylphenol	(µg/l)	none	477	607	47.6	115	<20	<20	<20
2,4-Dinitrophenol	(µg/l)	none	<20	<20	<20	<20	<20	<20	<20
2,6-Dichlorophenol	(µg/l)	none	<20	<20	<20	<20	<20	<20	<20
2,6-Dinitrotoluene	(µg/l)	none	<20	<20	<20	<20	<20	<20	<20
2-chlorophenol	(µg/l)	none	<20	<20	<20	<20	<20	<20	<20
2-Methylnaphthalene	(µg/l)	none	26.8	177	80.5	230	<20	<20	<20
2-methylphenol	(µg/l)	none	298	615	79.7	240	24.2	<20	<20
2-Nitroaniline	(µg/l)	none	<20	<20	<20	<20	<20	<20	<20
2-Nitrophenol	(µg/l)	none	<20	<20	<20	<20	<20	<20	<20
3,3-Dichlorobenzidine	(µg/l)	none	<20	<20	<20	<20	<20	<20	<20
3/4-methylphenol	(µg/l)	none	387	1043	142	412	40.6	27.0	<20
3-Nitroaniline	(µg/l)	none	<20	<20	<20	<20	<20	<20	<20
4 Chlorophenyl phenyl ether	(µg/l)	none	<20	<20	<20	<20	<20	<20	<20
4,6-Dinitro-2-methylphenol	(µg/l)	none	<20	<20	<20	<20	<20	<20	<20
4-bromophenyl phenyl ether	(µg/l)	none	<20	<20	<20	<20	<20	<20	<20
4-chloro-3-methylphenol	(µg/l)	none	<20	<20	<20	<20	<20	<20	<20
4-Chloroaniline	(µg/l)	none	<20	<20	<20	<20	<20	<20	<20
4-Nitroaniline	(µg/l)	none	<20	<20	<20	<20	<20	<20	<20
4-nitrophenol	(µg/l)	none	<20	<20	<20	<20	<20	<20	<20
Acenaphthene	(µg/l)	none	<20	22.1	<20	22.1	<20	<20	<20
Acenaphthylene	(µg/l)	none	<20	111	88.8	286	<20	<20	<20
Aniline	(µg/l)	none	<20	<20	<20	<20	<20	<20	<20
Anthracene	(µg/l)	none	<20	22.8	22.0	64.5	<20	<20	<20
Azobenzene	(µg/l)	none	<20	<20	<20	<20	<20	<20	<20
Benz[a]anthracene	(µg/l)	none	<20	<20	<20	23.5	<20	<20	<20
Benzene, 1,2-dichloro-	(µg/l)	none	<20	<20	<20	<20	<20	<20	<20
Benzidine	(µg/l)	none	<20	<20	<20	<20	<20	<20	<20
Benzo[ghi]perylene	(µg/l)	none	<20	<20	<20	<20	<20	<20	<20
Benzo[a]pyrene	(µg/l)	none	<20	<20	<20	<20	<20	<20	<20
Benzo[b]fluoranthene	(µg/l)	none	<20	<20	<20	<20	<20	<20	<20
Benzo[k]fluoranthene	(µg/l)	none	<20	<20	<20	<20	<20	<20	<20
Benzoic Acid	(µg/l)	none	<20	<20	<20	<20	<20	<20	<20
Benzyl Alcohol	(µg/l)	none	<20	<20	<20	<20	<20	<20	<20
Benzyl butyl phthalate	(µg/l)	none	<20	<20	<20	<20	<20	<20	<20
Bis(2-chloroethoxy)methane	(µg/l)	none	<20	<20	<20	<20	<20	<20	<20
Bis(2-chloroethyl)ether	(µg/l)	none	<20	<20	<20	<20	<20	<20	<20
Bis(2-chloroisopropyl)ether	(µg/l)	none	<20	<20	<20	<20	<20	<20	<20
Bis(2-ethylhexyl) phthalate	(µg/l)	none	<20	504	306	421	413	868	438
Chrysene	(µg/l)	none	<20	<20	<20	<20	<20	<20	<20
Dibenzo[a,h]anthracene	(µg/l)	none	<20	<20	<20	<20	<20	<20	<20
Dibenzofuran	(µg/l)	none	<20	27.3	<20	51.8	<20	<20	<20
Dibutyl phthalate	(µg/l)	none	<20	<20	<20	<20	<20	<20	<20
Diethyl Phthalate	(µg/l)	none	<20	<20	<20	<20	<20	<20	<20
Dimethyl phthalate	(µg/l)	none	<20	<20	<20	<20	<20	<20	<20
Di-n-octyl phthalate	(µg/l)	none	<20	<20	<20	<20	<20	<20	<20
Diphenylamine	(µg/l)	none	<20	<20	<20	<20	<20	<20	<20
Fluoranthene	(µg/l)	none	<20	<20	21.3	58.2	<20	<20	<20
Fluorene	(µg/l)	none	<20	45.5	33.7	101	<20	<20	<20
Hexachlorobenzene	(µg/l)	none	<20	<20	<20	<20	<20	<20	<20
Hexachlorobutadiene	(µg/l)	none	<20	<20	<20	<20	<20	<20	<20
Hexachlorocyclopentadiene	(µg/l)	none	<20	<20	<20	<20	<20	<20	<20
Hexachloroethane,	(µg/l)	none	<20	<20	<20	<20	<20	<20	<20
Indeno[1,2,3-cd]pyrene	(µg/l)	none	<20	<20	<20	<20	<20	<20	<20
Isophorone	(µg/l)	none	<20	<20	<20	<20	<20	<20	<20
Methyl Methanesulfonate	(µg/l)	none	<20	<20	<20	<20	<20	<20	<20
Naphthalene	(µg/l)	none	32.9	452	395	1014	27.2	52.9	34.1
NitroBenzene	(µg/l)	none	<20	<20	<20	<20	<20	<20	<20
N-Nitrosodimethylamine	(µg/l)	none	<20	<20	<20	<20	<20	<20	<20
Pentachlorophenol	(µg/l)	none	<20	<20	<20	<20	<20	<20	<20
Phenanthrene	(µg/l)	none	<20	57.0	53.0	156	<20	<20	<20
Phenol	(µg/l)	none	345	1150	359	1095	85.9	69.8	23.3
Pyrene	(µg/l)	none	<20	20.1	23.6	63.4	<20	<20	<20
Pyridine	(µg/l)	none	<20	<20	<20	<20	<20	<20	<20

13707/SHU/001a

Project Reference - Tar Analysis

Analytical Test Results - SVOC

NICHOLLS COLTON
ANALYTICAL

NCA Reference			13-9048
Client Sample Reference			B800
Sample Matrix			Water
Determinant	**Units**	**Accreditation**	
1,2,4-trichlorobenzene	(µg/l)	none	<20
1,3,5-Cycloheptatriene	(µg/l)	none	<20
1,3-dichlorobenzene	(µg/l)	none	<20
1,4-dichlorobenzene	(µg/l)	none	<20
1-chloronaphthalene	(µg/l)	none	<20
2,3,4,6-tetrachlorophenol	(µg/l)	none	<20
2,4,5-trichlorophenol	(µg/l)	none	<20
2,4,6-trichlorophenol	(µg/l)	none	<20
2,4-Dichorophenol	(µg/l)	none	<20
2,4-dimethyphenol	(µg/l)	none	<20
2,4-Dinitrophenol	(µg/l)	none	<20
2,6-Dichorophenol	(µg/l)	none	<20
2,6-Dinitrotoluene	(µg/l)	none	<20
2-chlorophenol	(µg/l)	none	<20
2-Methylnaphthalene	(µg/l)	none	<20
2-methylphenol	(µg/l)	none	<20
2-Nitroaniline	(µg/l)	none	<20
2-Nitrophenol	(µg/l)	none	<20
3,3-Dichlorobenzidine	(µg/l)	none	<20
3/4-methylphenol	(µg/l)	none	<20
3-Nitroaniline	(µg/l)	none	<20
4 Chlorophenyl phenyl ether	(µg/l)	none	<20
4,6-Dinitro-2-methylphenol	(µg/l)	none	<20
4-bromophenyl phenyl ether	(µg/l)	none	<20
4-chloro-3-methylphenol	(µg/l)	none	<20
4-Chloroaniline	(µg/l)	none	<20
4-Nitroaniline	(µg/l)	none	<20
4-nitrophenol	(µg/l)	none	<20
Acenaphthene	(µg/l)	none	<20
Acenaphthylene	(µg/l)	none	<20
Aniline	(µg/l)	none	<20
Anthracene	(µg/l)	none	<20
Azobenzene	(µg/l)	none	<20
Benz[a]anthracene	(µg/l)	none	<20
Benzene, 1,2-dichloro-	(µg/l)	none	<20
Benzidine	(µg/l)	none	<20
Benzo(ghi)perylene	(µg/l)	none	<20
Benzo[a]pyrene	(µg/l)	none	<20
Benzo[b]fluoranthene	(µg/l)	none	<20
Benzo[k]fluoranthene	(µg/l)	none	<20
Benzoic Acid	(µg/l)	none	<20
Benzyl Alcohol	(µg/l)	none	<20
Benzyl butyl phthalate	(µg/l)	none	<20
Bis(2-chloroethoxy)methane	(µg/l)	none	<20
Bis(2-chloroethyl)ether	(µg/l)	none	<20
Bis(2-chloroisopropyl)ether	(µg/l)	none	<20
Bis(2-ethylhexyl) phthalate	(µg/l)	none	155
Chrysene	(µg/l)	none	<20
Dibenzo(a,h)anthracene	(µg/l)	none	<20
Dibenzofuran	(µg/l)	none	<20
Dibutyl phthalate	(µg/l)	none	<20
Diethyl Phthalate	(µg/l)	none	<20
Dimethyl phthalate	(µg/l)	none	<20
Di-n-octyl phthalate	(µg/l)	none	<20
Diphenylamine	(µg/l)	none	<20
Fluoranthene	(µg/l)	none	<20
Fluorene	(µg/l)	none	<20
Hexachlorobenzene	(µg/l)	none	<20
Hexachlorobutadiene	(µg/l)	none	<20
Hexachlorocyclopentadiene	(µg/l)	none	<20
Hexachloroethane,	(µg/l)	none	<20
Indeno[1,2,3-cd]pyrene	(µg/l)	none	<20
Isophorone	(µg/l)	none	<20
Methyl Methanesulfonate	(µg/l)	none	<20
Naphthalene	(µg/l)	none	<20
NitroBenzene	(µg/l)	none	<20
N-Nitrosodimethylamine	(µg/l)	none	<20
Pentachlorophenol	(µg/l)	none	<20
Phenanthrene	(µg/l)	none	<20
Phenol	(µg/l)	none	<20
Pyrene	(µg/l)	none	<20
Pyridine	(µg/l)	none	<20

13707/SHU/001a

Project Reference - Tar Analysis

Analysis Methodologies

Matrix	Determinant	Sample condition for analysis	Test Method used
Solvent	SVOC	Air Dried	In house method statement - MS - CL - SVOC
Solvent	VOC	As Received	In house method statement - MS - CL - VOC and BTEX

Appendix III - Publications

Journal and Conference Papers

Peter M. Weston, Vida Sharifi, Jim Swithenbank., 2014, Destruction of Tar in a Novel Coandă Tar Cracking System. *Energy Fuels*, 28 (2), pp. 1059 – 1065.

Peter M. Weston, Vida Sharifi, Jim Swithenbank*., 2014, Design and development of a Coandă tar cracker to operate in a three-stage biomass gasifier. New Horizons in Gasification, IChemE 12th European Gasification Conference, March 2014.*

Conference Presentations and Posters

Design and development of a Coandă tar cracker to operate in a three-stage biomass gasifier. New Horizons in Gasification, IChemE 12th European Gasification Conference, March 2014, Oral presentation.

Design and Development of a Coandă Tar Cracker for Tar Destruction in Biomass Gasification *Postgraduate Research Conference*, May 2014, (University of Sheffield), Oral presentation.

Destruction of Tarry Residues in a Novel Dual Pyrolysis – Coandă Tar Cracking System. *Delivering Low Carbon Energy from Biomass Resources*, IChemE, London, May 2013, Poster presentation.

Destruction of Tarry Residues in a Novel Dual Pyrolysis – Coandă Tar Cracking System. *24 Month Poster* Presentation, November 2013, (University of Sheffield).

Destruction of Tarry Residues in a Novel Dual Pyrolysis – Coandă Tar Cracking System. *SUPERGEN Bioenergy Hub Assembly*, Leeds, November 2013, Poster presentation.

energy&fuels

Article

Destruction of Tar in a Novel Coandă Tar Cracking System

Peter M. Weston,* Vida Sharifi, and Jim Swithenbank

Energy and Environmental Research Group, Department of Chemical and Biological Engineering, The University of Sheffield, Mappin Street, Sheffield S1 3JD, United Kingdom

ABSTRACT: The main objective of this research program was to develop and test a small-scale system that used a novel Coandă burner for tar destruction through partial oxidation. An experimental rig consisting of a tar injector, in which wood pellets were pyrolyzed, and a Coandă tar cracking unit was designed, constructed, and operated to determine the effectiveness of the unit. The experimental program was divided into two phases, so that comparisons of the tar composition with and without treatment could be made. In the first phase, wood pellets were pyrolyzed at a range of temperatures between 500 and 800 °C and the pyrolysis products (gas, tar, and char) were analyzed. Increasing the temperature from 500 to 700 °C caused an increase in the production of hydrogen, methane, and carbon dioxide. As the pyrolysis temperature increased from 500 to 800 °C, there was a decrease in the yield of gravimetric tar in the sampled gas from 67.2 to 15.7 g/nm³. This reduction can be attributed to higher pyrolysis temperature, causing an increase in thermal cracking and depolymerization reactions, which, in turn, promotes production of permanent gas species. In the second phase, the gas produced in the first phase was treated in sub-stoichiometric conditions in the Coandă tar cracker. When the yield of tar species was set at 800 °C, benzene was reduced by 95%, toluene was reduced by 96%, naphthalene was reduced by 97.7%, and the gravimetric tar yield was reduced by 86.7%. The Coandă tar cracker was shown to be effective at significantly reducing the tar content in the product gas. The reduction can be attributed to the high flame temperature (>1000 °C) and the addition of oxygen, which leads to the formation of free radicals, causing tar destruction.

1. INTRODUCTION

The importance of biomass as a key source for the production of energy has intensified over the past decade. There have been strong endorsements globally and nationally to replace traditional fuels with sustainable and renewable alternatives. Supplies of oil, coal, and natural gas are expected to deplete over the next 100 years, thus strengthening the need for an alternative energy source. In addition, it is predicted that the global energy demand will soar over the next 30 years because of the population increase and continuing industrial expansion. The combination of decreasing fossil fuel supplies and increasing energy demand poses a challenging and complicated problem.

Biomass gasification is considered to be potential solution because of a number of technological advantages, as summarized by Rezaiyan and Cheremisinoff,[1] and could provide sustainable energy in both developed countries using advanced techniques and electrification in both developing countries for rural electrification.[2] The problems associated with the tar yield in the producer gas remains a limiting factor, hampering widespread installation and continued operation of biomass gasification plants. Tars are formed when biomass is heated, which causes molecular bonds within the biomass structure to break. Produced tar species then condense at lower temperatures, causing fouling, blocking, and plugging in downstream equipment, thus causing reliability issues with filters, engines, and turbines.[3-5]

Existing tar removal methods can be classified as either primary or secondary. Primary methods refer to operations within the thermal conversion unit, and secondary methods cover technologies that are external to the process. The key primary measures include selecting the most efficient operating

parameters, using bed additives or catalysts, and modifying the reactor design.[6] Secondary methods are downstream of the process and treat the produced gas; examples include mechanical methods [OLGA (the Dutch acronym for oil-based gas washer), filters, and scrubbers], catalysts cracking, thermal cracking, and partial oxidative treatment.[7] OLGA technology was developed by the Energy Research Center of the Netherlands (ECN). Multiple scrubbing towers are used and interact in a classical absorption and regeneration setup.[8] The final application of the producer gas influences the choice of the tar removal method. For gas engines and turbines, the tar content in the gas needs to be below 50 mg/nm³; for fuel cells, this is reduced to 1 mg/nm³; and for syngas and methanol production, this is decreased further to 0.5 mg/nm³.[9]

Thermal cracking and partial oxidation (POX) are considered to be two of the most attractive tar treatment options available. Thermal cracking is the breakdown of tar molecules into lighter gases caused by high temperatures. High temperatures influence internal tar stability, allowing for conversion into other species; however, the energy required to reach the required temperatures is a detriment to the overall efficiency. Increasing the temperature at which thermal cracking is performed results in an increase to the heating value of the gas, which is an important characteristic to consider when evaluating the overall energy efficiency of the process.[1] Anis and Zainal[8] determined that the temperate range for tar cracking is between 700 and 1250 °C. For effective decomposition, additional means are required, such as

---

Energy & Fuels

Article

increasing the gas residence time, directly contacting the gas with an independently heated surface, or adding oxygen or steam.

Partial oxidation offers tar reduction without waste or soot and the additional benefit of maintaining the heating value of the tars in the gas product, although at the loss of a proportion of the heating value of the treated gas, which is partially combusted.[10] There are a number of previous studies that have used two-staged systems to analyze the effectiveness of POX for tar reduction.[11-14] In these systems, biomass is pyrolyzed in the first stage and the resulting tarry gas is processed in a second stage, which uses high temperatures and/or the addition of oxygen.

The majority of these studies control the equivalence ratio (ER) in the partial oxidation stage; however, the addition of oxygen was not used for combustion. Instead, oxygen or air was supplied in a high-temperature second-stage unit and reacts with the pyrolysis vapors. Wu et al.[11] reported that gases produced from the slow pyrolysis of rice straw pellets at 500 °C were partially oxidized at ERs from 0.0 to 0.4 and at reactor temperatures between 700 and 1100 °C. Results from this study showed that increasing the ER led to an increase in tar destruction and an increase in the conversion of primary tars to permanent gaseous products, namely, carbon monoxide, methane, and hydrogen.

Houben[16] designed a microswirl burner to partially oxidize a model tar component, naphthalene. An artificial gas was treated with known quantities of a naphthalene-based model tar species. The excess air ratio, λ, was varied from 0.19 to 0.75. It was shown that, when not counting benzene as a tar component, the naphthalene in the artificial gas could be reduced to as much as 95% through either polymerization or cracking. Naphthalene was cracked when λ was less than 0.4 and the fuel hydrogen concentration was greater or equal to 20% by volume. When conditions were not within this remit, naphthalene was primarily converted into other larger species through polymerization.

Coandă burners have been proven to operate at ERs less than 1, as shown in previous studies by Prior[17] and O'Nions.[18] O'Nions[18] built a Coandă burner that combusted propane and methane to reduce NOx emissions. Coandă ejector devices can be modified for combustion by adding a combustible fuel and an ignition source to the system. The principle of operation for Coandă ejectors is shown in Figure 1. Coandă ejectors make use of the Coandă effect; the phenomenon in which a jet passed over a curved surface will attach to the wall. Pressurized air is supplied to the ejector and enters through an annular slit (1). As air flows through the annular slit, the velocity of the air

increases and the injected air attaches to the curved surface and continues along the length of the ejector (3).[19] The high-velocity injected flow passes momentum to the surrounding fluid, causing secondary or entrained flow (2). The increased contact between injected primary flow and induced secondary flow creates high mixing potential in Coandă devices, making them useful for fuel-rich, high-temperature, blue-flame combustion.

The primary aim for this study was to determine the suitability and effectiveness of a Coandă tar cracking (CTC) system for tar destruction. In the proposed two-stage system, wood pellets are pyrolyzed in the tar injection stage and then treated by the CTC. High-velocity air is supplied to the system through an annular slit, creating strong entrainment at the inlet of the burner; as a result, products from the flame are recycled. This promotes mixing between the fresh pyrolysis gases and the recycled flame products in a prechamber positioned before the ejector. The products of the prechamber react with the supplied oxidant in fuel-rich conditions, so that the local mixture is never stoichiometric.

2. EXPERIMENTAL SECTION

A two-stage setup was designed and constructed. In the first stage, wood pellets were pyrolyzed to generate a tarry gas product to be treated in the CTC. The design of the pyrolysis stage was simplified, so that it was straightforward to operate. The first stage is principally designed to supply a tarry gas for treatment in the second stage. The experimental program was divided into two phases to enable comparison and analysis into the suitability of the CTC for tar destruction. In the first phase, wood pellets were pyrolyzed at four different temperatures between 500 and 800 °C. In the second phase, the CTC system was used, where gases produced from the pyrolysis stage were combusted in sub-stoichiometric conditions in the CTC. The results are determined from the analysis from a single operation at each of the four pyrolysis temperatures for both experimental phases.

2.1. Biomass Material. Wood pellets were used as the biomass fuel in this study; the key properties of the pellets are shown in Table 1. The pellets are cylindrical in shape; the average diameter is 6 mm;

Table 1. Wood Pellet Properties as Received

gross calorific value (MJ/kg)	18.0
Proximate Analysis (wt %)	
moisture	8
volatile matter	74
fixed carbon	17
ash	>1
Ultimate Analysis (wt %)	
carbon	45.6
hydrogen	6.0
nitrogen	0.2

the length of the pellets range in size from 10 to 40 mm; and the average length is 15 mm. The raw material used to manufacture the pellets is predominantly chemically untreated deposits from the wood-processing industry. The pellets are robust and easy to handle. The pellets were analyzed using a Parr 6200 oxygen bomb calorimeter, a PerkinElmer thermogravimetric analyser (TGA) 4000, and a Thermo Scientific FLASH 2000 organic elemental analyzer. The proximate analysis results acquired from the TGA were determined by evaluating the weight reduction of the fuel sample against an increasing temperature and changes from inert to reactive environments. The fuel sample was loaded into the analyzer and heated from ambient to 35 °C, where it was held for 4 min. At the same time, the furnace is purged with nitrogen gas to create an inert atmosphere. The sample was first heated at a rate of 75 °C/min to 110 °C and held at this

Figure 1. Coandă ejector principle (adapted with permission from ref 20).

and combusted in the system before each experiment to preheat the components in the cracking zone. Gases were taken from sample port 2 (K). Tar species were collected, and permanent gases were analyzed in the tar and gas sampling unit.

The tar and gas sampling unit consisted of two 2 m long cylindrical tar traps (L) containing 150 mL each of isopropanol. The first trap in the sample line was cooled using a continuous flow of water through a surrounding water jacket. A pump (N) was used to drive the gases through the tar and gas sampling unit. A wet gas meter (M) was used to determine the total volume of gas sampled per experiment. Noncondensable gases, including CO, CO_2, H_2, N_2, CH_4, and O_2, were analyzed by a thermal conductivity detector by an ABB gas chromatograph (O), model PGC2000. The tar collected in isopropanol was analyzed using a Shimadzu GCMS-QP2010. Gravimetric tar yields were determined by taking 50 mL of isopropanol from the tar traps. The samples were left in a fume cupboard for 48 h, so that isopropanol could evaporate, leaving a tar residue, which was weighed. The total amount of tar was then determined from the total amount of isopropanol used in the tar traps and the total volume of gas sampled.

3. RESULTS AND DISCUSSION

3.1. Phase 1 Results. Figure 4 shows the average gas yield of H_2, CH_4, and CO contained in the pyrolysis gas. The
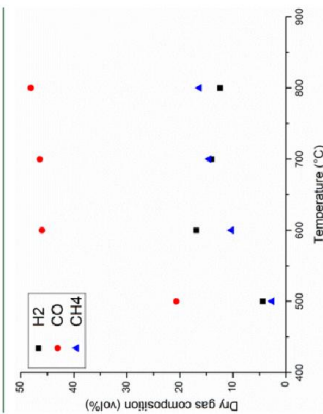
Figure 4. Gas composition versus pyrolysis temperature.

concentration of hydrogen in the pyrolysis gas increased steadily as the pyrolysis temperature increased from 500 to 700 °C, before reducing slightly at 800 °C. Methane and carbon monoxide compositions also follow the same pattern.

Fagbemi et al.[22] found that the concentration of methane reaches a maximum at 750 °C, which is in good agreement with the results obtained from this study. The concentration of methane, as shown in Figure 4, is also within a range of results from Fagbemi et al.,[22] who found that the methane concentration was between 13 and 15% at temperatures between 700 and 800 °C. The measured methane concentration in this study was around 12%. The increase in methane as the pyrolysis temperature increased can be attributed to the decomposition of methoxyl groups.[11] Hydrogen is generated by the dehydrogenation of char, tar, and hydrocarbons.

Table 2 shows the effect of the temperature on the key tar species present in the collected tar. The majority of the tar species found were one or two ringed species. Larger ringed polycyclic aromatic hydrocarbon (PAH) species, such as pyrene and fluoranthene, were present but only in negligible amounts

Table 2. Yield of Gravimetric Tar and a Selection of Key Tar Species Per Unit of Sampled Gas

temperature (°C)	500	600	700	800
	Tar Determinant (mg/nm³)			
benzene	1843	5495	10718	7385
toluene	2301	3815	4016	3364
ethylbenzene	293	314	107	107
m- and p-xylene	678	720	506	464
o-xylene	281	282	175	163
styrene	280	818	1016	936
isopropylbenzene	29	15	a	a
naphthalene	191	1401	2772	2521
phenol	1.8	3.7	3.0	3.4
gravimetric tar (g/nm³)	67.2	26.9	17.4	15.7

a The tar components were below the limit of detection.

and, hence, are not analyzed. Benzene, toluene, and naphthalene are the main tar species that appear in the highest concentrations. The quantities of these three tar species increase as the temperature of the pyrolyser increases from 500 to 700 °C. The decrease as the pyrolysis temperature rose to 800 °C. The data shown in Tables 2 and 4, which represent the individual tar concentrations, should not be considered absolute because of sampling and analysis errors; however, the trends for each species are reliable, which is what the discussion is based.

The gravimetric tar test results show that the total amount of tar collected per unit of gas sampled reduces as the temperature at which pyrolysis performed is increased. Table 2 indicates how the increase in the pyrolysis temperature led to a decrease of gravimetric tar. Because of the method used to determine the gravimetric tar yields, it is likely that the results contain errors because isopropanol used to collect tar will not have fully evaporated from the tested sample; therefore, the values for gravimetric tar are likely to have been overestimated. Because of the amount of solvent sample required for the component species analysis, the gravimetric tar yield results were determined from a single solvent sample. The reduction in tar from pyrolysis was also recorded by Fassinou et al.,[12] who pyrolyzed pine to determine the tar cracking behavior when changing a number of parameters. This change was attributed to an increase in thermal cracking, decarboxylation, and depolymerization reactions, thus promoting gas production. Lower temperatures support the production of char and liquid, whereas higher gas production is caused by higher temperatures.

Fagbemi et al.[22] reported that the quantity of tar reached a maximum at 500 °C and then dropped as the temperature increased. It is thought that, at a temperature above 600 °C, secondary reactions increase, which leads to the production of a larger amount of gas. Cracking of tar is one of the key reactions and causes an increase to the calorific value of gas as more energetic gases are produced. At higher temperatures, stable tar species, benzene, toluene, and naphthalene, are the most abundant. Further investigation into effect of the temperature and secondary tar reactions can be found in ref 23. In this study, there was prominent reduction in the tar yield of silver birch as the temperature of the reactor increased from 500 to 800 °C.

Table 3 shows that, as the pyrolysis temperature increased, the yield of char reduced. Fassinou et al.[12] researched how the temperature, biomass flow rate, and residence times influenced
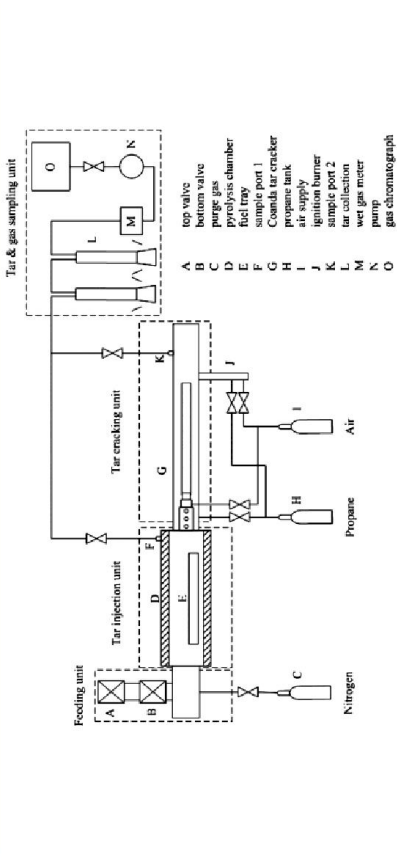
Figure 2. Schematic diagram of the experimental rig.

A top valve
B bottom valve
C pyrolysis chamber
D fuel tray
E sample port 1
F Coandă tar cracker
G propane tank
H air supply
I ignition burner
J sample port 2
K tar collection
L wet gas meter
M pump
N pump
O gas chromatograph
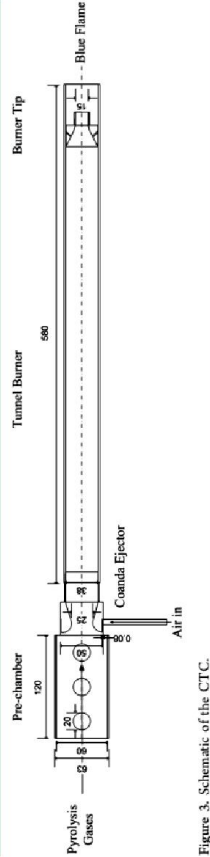
Figure 3. Schematic of the CTC.

temperature for 6 min, allowing for calculation of the moisture content. The sample was then heated at a rate of 80 °C/min to 900 °C and held for 1 min, prompting the release of volatile matter. The material was held at 900 °C for 4 min. Finally, the furnace was heated from 900 to 950 °C at a rate of 50 °C/min. Lastly, oxygen was added into the furnace, so that the remaining fixed carbon was burnt, leaving behind an ash residue.[21] This method of analysis is also used for analysis of the char product, as detailed in Table 3 in section 3.1.

2.2. Experimental Rig and Operating Procedure. The experimental rig consisted of four main units: (i) feeding, (ii) tar injection, (iii) tar cracking, and (iv) tar/gas sampling. A schematic diagram of the equipment is shown in Figure 2. A batch loading system was used to feed wood pellets into the tar injection unit. As previously mentioned, the design of the first stage is simplified because its central aim is to supply a tarry gas to the second stage; hence, the design of the feeding system was developed for uncomplicated operation. Pellets were loaded in 10 batches (100 g), making a total of 1 kg of wood pellets per experiment. The wood pellet feed rate was dependent upon the pyrolysis temperature and varied between 3 and 4.5 kg/h. The feeding system used a twin-valve lock hopper, which prevented (i) air from entering and (ii) gases from exiting the system. When loading the wood pellets, the top valve (A) was opened and the pellets were inserted and held in a position between the valves. The top valve was then closed, and the bottom valve (B) was opened, which allowed the pellets to drop into a loading vessel. The loading vessel was manually pushed and then rotated, depositing the pellets into a fuel tray (E), which was positioned in the pyrolysis chamber (D).

The tar injection stage consisted of a cylindrical tube placed horizontally and held in position by a supporting frame. The tube is

constructed from 316 stainless steel and is approximately 1300 mm long with an internal diameter of 200 mm. The chamber is heated by six helically wound semi-cylindrical ceramic heaters. The heaters are controlled by a control unit, which regulates the temperature within the chamber. Nitrogen was used as the cold purge gas (C), and the flow rate of nitrogen was controlled by a rotameter. The flow rate was set at 8 L/min (LPM) for each experiment. In the first phase of experiments, pyrolysis gases are taken from sample port 1 (F). The permanent gases and tar species are collected and analyzed in the tar and gas sampling unit described below.

For the second set of experiments, the CTC is used. The tar cracking zone consisted of three parts: a mixing vessel or prechamber, a Coandă ejector (G), and a tunnel burner. Figure 3 shows a schematic of the unit. The prechamber is a hollow cylindrical vessel and is manufactured from EN3A mild steel. The vessel is 120 mm in length, and its internal diameter is 60 mm. Six 20 mm diameter recirculation holes were drilled into the vessel. The ejector is a motorless and bladeless ejector, which is normally used to extract gases and other materials using a small volume of compressed air, and takes advantage of the Coandă effect to entrain large volumes of surrounding gases. The flow rate of air to the Coandă is controlled by a rotameter and can be set between 4 and 40 LPM. The total length of the ejector is 85 mm. The diameter at the inlet is 50 mm, and it is made from stainless-steel 304. The tube burner is made from EN3A mild steel and is 580 mm long with an internal diameter of 38 mm. One end of the burner is threaded to the outlet of the Coandă ejector; the combustion end has a tip that is used to stabilize the flame. The CTC system is enclosed in an outer casing; one K-type and five K-type thermocouples were used to monitor the temperature in this region. A propane ignition burner (J) was used to ignite the flame. Propane is also fed into the burner

Energy & Fuels

Article

recorded are high enough for thermal cracking of tar to take place. The temperature range for thermal cracking was reported to be between 700 and 1250 °C.[8]

The reduction of the gravimetric tar yield and the key tar species (benzene, toluene, and naphthalene) when compared to first phase of experiments can be attributed to a number of factors. The addition of oxygen is likely to promote the formation of a number of radicals, which promote the destruction of tar species. When oxygen is present in the mixture, hydrogen, oxygen, hydroxyl, and hydroperoxy radicals are formed.[10] These radicals accelerate the decomposition of hydrocarbon because of an increase in hydrogen-atom abstraction.

In each of the four cases, when the dual system was used, the value for ER was recorded to be between 0.77 and 0.90. This is relatively high when compared to other studies.[11,14,15] If the flow rate of air to the CTC was decreased, the flame would become unstable and extinguish. The flame stability issue would be improved if the supply of tarry gas to the CTC was at a constant rate. In the present setup, the wood pellets are pyrolyzed in a chamber, which acts as a tar injector to the second stage. The existing batch feeding system causes fluctuations in both the gas composition and volume. A continuous feeding system, most likely a screw feeder, would remedy this issue.

There was a significant decrease in the yields of some of the key tar species when tests were carried out using the CTC (Figure 5). When the temperature of the pyrolyser was 800 °C,
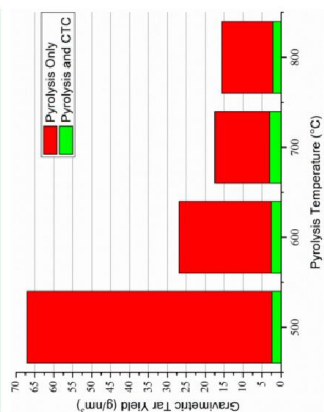
Figure 5. Comparison of the gravimetric tar yield with and without CTC treatment.

the benzene concentration was reduced by 95% when comparing the treated gas to the non-treated gas. The toluene content was reduced by 96%, and naphthalene was reduced by 98%. Gravimetric tar yields were also reduced at each pyrolysis condition. For example, at a pyrolysis temperature of 800 °C, there was an 86.7% clear reduction in the gravimetric tar yield. Figure 6 shows the clear reduction in the key tar species.

Although the CTC was shown to be efficient at tar destruction, the gas analyzed from after the treatment was of low quality. This is due to the flow rate of air required to maintain a stable flame in the CTC, which results in almost complete combustion of the gas. The issues with flame stability also affected the gas composition, but it is thought that these can be remedied with an improved design to the feeding system and further work on the design and operation of the CTC. The resulting gas after treatment with the CTC was found to have low concentrations of active ingredients, such as hydrogen (2–4 vol %) and carbon monoxide (1–6 vol %); as such, the calorific value of the treated gas was found to be less than 2 MJ/kg.

On the basis of the results obtained from this research study, it can be concluded that the novel design and operational features have been shown to be effective devices for tar destruction and char production. It is thought that there are two potential applications for the CTC. First, the existing system could be redesigned for char generation. As discussed, the biochar produced has a high energy content (>28 MJ/kg), which would allow for heat generation in systems that currently use pulverized coal; alternatively, the biochar could be used in soil remediation.[29] A redesign of the system would be required to recycle the high-temperature produced gas from the outlet of the CTC; this gas would then be used as the heat source for pyrolysis of wood pellets. Second, with an improved performance of the CTC, where a lower flow rate of air to the device would allow for the production of a product gas with a low heating value (2–5 MJ/kg), this gas could be used directly in a gas turbine for electricity production.[30,31]

4. CONCLUSION

The main conclusions from this study are as follow: (i) Tests showed that increasing the pyrolysis temperature from 500 to 700 °C caused an increase in the production of hydrogen, methane, and carbon dioxide. As the temperature of the pyrolyser increased to 800 °C, there was a decrease in the yield of gravimetric tar from 67.2 to 15.7 g/nm³. This reduction can be attributed to a higher pyrolysis temperature, causing an increase in thermal cracking and depolymerization reactions, which, in turn, promotes production of permanent gas species,

---

in the temperature reduce the amount of hydrogen and oxygen in the char because of the scission of weaker bonds in the structure of the biochar; thus, increasing the temperature increases the percentage of fixed carbon in the char. At 800 and 900 °C, the mass of fixed carbon is above 90%, making the char of high quality.

3.2. Phase 2 Results. The second series of tests were carried out using the CTC. The same pyrolysis temperatures were used in the first stage, and the produced gas at each condition was treated using the CTC. The ER was calculated by first working out the mass of air required to completely combust the wood pellets added to the system. It was calculated that, to combust 1 kg of wood pellets, 5.52 kg of air was required. From the previous pyrolysis only experiments, the yield of char at certain temperatures was known. The total amount of wood pellets minus the char was used as the basis for the calculations. The amount and feed rate of wood pellets being loaded into the pyrolyser were recorded. From this, it was possible to calculate the air required to fully combust the volatile portion of the wood pellets. The flow rate of air entering the burner was recorded throughout the experiment, and by knowing the pressure at which air is fed into the CTC, it is possible to calculate the mass flow of air in kilograms; this can then be divided by the stoichiometric value to work out the excess air ratio. The ER was calculated using eq 1. This is the same technique used by Ahrenfeldt et al.[14] to calculate the excess air ratio.

$$ ER = \frac{\dot{m}_{air,supplied}}{\dot{m}_{air,stoich}} \qquad (1)$$

The flow of air into the Coandă was not constant throughout each experiment because of issues with flame stability; however, the changes were noted, and it was then possible to work out an average value for the ER by taking the average value of air that was entered into the Coandă.

Table 4 shows the operating conditions of the CTC and the yield of analyzed tar. The thermocouple was positioned in the

Table 4. Yield of Gravimetric Tar and Key Tar Species

pyrolysis temperature (°C)	500	600	700	800
	CTC Operating Conditions			
average temperature (°C)	650	685	795	991
highest temperature (°C)	925	930	955	1290
ER	0.77	0.88	0.88	0.90
	Tar Determinant (mg/nm³)			
benzene	385	327	763	350
toluene	223	129	241	132
ethyl benzene	19	7	8	5
m- and p-xylene	44	19	30	21
o-xylene	16	7	11	7
styrene	56	26	60	36
naphthalene	253	121	276	a
phenol	0.2	0.2	0.1	a
gravimetric tar (g/nm³)	2.34	2.54	3.05	2.08

aThe tar components were below the limit of detection.

blue flame region of the burner. The highest temperature recorded exceeded 900 °C in all four cases. When the pyrolyser was run at 800 °C, the average temperature recorded in the flame zone of the CTC was slightly below 1000 °C and the highest temperature recorded was 1290 °C. The temperatures

---

Energy & Fuels

Article

Table 3. Wood Pellet Char Analysis

pyrolysis temperature (°C)	500	600	700	800
	Char Yield Analysis			
char weight (g)	293	228	159	156
char yield (%)	29.3	22.8	15.9	15.6
calorific value (MJ/kg)	31.2	28.9	31.1	31.1
	Proximate Analysis (wt %)			
moisture	>1	>1	1	1
volatile matter	14	13	7	6
fixed carbon	84	85	91	92
ash	>1	>1	>1	>1
	Ultimate Analysis (wt %)			
carbon	80.7	86.5	87.3	93.7
hydrogen	2.7	2.0	1.1	1.0
nitrogen	0.3	0.3	0.3	0.3

the products when pyrolyzing pine. The results from this study showed a clear decrease in the yield of char as the temperature of the reactor was increased. This can be explained by the increase in the temperature, promoting thermal cracking, depolymerization, and decarboxylation reactions, which causes an increase in the gas yield. Higher char yields are favored at lower temperatures, whereas a high pyrolysis temperature promotes gas formation. The char yield percentages also compare constructively to the results from Fassinou et al.[12]

The caloric values of the char samples collected are within 10% of each other. The calorific value is closely linked to the amount of fixed carbon contained within the structure of the char. The mass percentage of fixed carbon contained in the char increases as the pyrolysis temperature is increased; however, this does not appear to alter the calorific value in a uniform relationship. This could be because the analyzed chars have a high rate of fixed carbon (above 85%), and with the value of fixed carbon being within a small range (between 84 and 92%), the slight changes in fixed carbon do not result in significant changes to the calorific value.

Ryu et al.[24] batch pyrolyzed pinewood in a reactor at temperatures between 300 and 700 °C. The mass yield of char dropped steadily as the temperature was increased from 500 to 700 °C. At 700 °C, the char yield in this study is 15.89%, which is lower than that found by Ryu et al.,[24] where the char yield was 22%. This difference can be attributed to the fuels used in both experiments being different and also the setup and execution of the actual pyrolysis process. A temperature increase causing a reduction in the char yield was found in a number of other studies on the pyrolysis of biomass.[23−27]

The ash content in the char was below 1% (by mass) of the analyzed sample in this study. Fassinou et al.[12] established that the ash content in char from the pyrolysis of pine was below 2% and that the yield of ash increased gradually from 1 to 1.7% as the temperature increased from 450 to 750 °C.

An increase in the pyrolysis temperature leads to a decrease in the amount of volatile matter contained within the char sample. The volatile matter content dropped from 14 to 6% as the temperature was increased from 500 to 800 °C. This relationship was also found by a number of researchers, including refs 12, 22, 24, 27, and 28. Molecules within biomass crack when they are thermally treated, and lighter molecules crack more readily.[12] When the temperature at which pyrolysis is performed is increased, this phenomenon is intensified; therefore, the volatile matter content is reduced as the temperature is increased. Demirbas[27] determined that increases

Figure 6. (Left) Reduction in toluene, (center) reduction in benzene, and (right) reduction in naphthalene, at various pyrolysis conditions.

such as hydrogen, methane, and carbon monoxide. (ii) The use of CTC was proven to be effective at tar destruction. A significant reduction in the tar species concentration was observed when processing the gas through the combined CTC system. The benzene concentration was reduced by 95%; toluene was reduced by 96%; and naphthalene was reduced by 97.7%. (iii) The fixed carbon content in the char increased from 84 to 92% as the temperature increased. The biochar produced from the system has a high calorific value (>28 MJ/kg) and can be used as a valuable fuel in existing heat and power generation.

■ AUTHOR INFORMATION

Corresponding Author

*E-mail: peter.weston@sheffield.ac.uk.

Notes

The authors declare no competing financial interest.

■ ACKNOWLEDGMENTS

■ NOMENCLATURE

CTC = Coandă tar cracker
ER = equivalence ratio
PAH = polycyclic aromatic hydrocarbon
POX = partial oxidation
TGA = thermogravimetric analyser

■ REFERENCES

(1) Rezaiyan, J.; Cheremisinoff, N. P. *Gasification Technologies: A Primer for Engineers and Scientists*; Taylor and Francis Group: London, U.K., 2005.
(2) Kirkels, A. F.; Verbong, G. P. J. *Renewable Sustainable Energy Rev.* **2011**, *15*, 471–481.
(3) Han, J.; Kim, H. *Renewable Sustainable Energy Rev.* **2008**, *12*, 397–416.
(4) Li, C.; Suzuki, K. *Renewable Sustainable Energy Rev.* **2009**, *13*, 594–604.
(5) Houben, M.; Delange, H.; Vansteenhoven, A. *Fuel* **2005**, *84*, 817–824.
(6) Devi, L.; Ptasinski, K. J.; Janssen, F. J. J. G. *Biomass Bioenergy* **2003**, *24*, 125–140.
(7) Van der Hoeven, T. A.; de Lange, H. C.; van Steenhoven, A. A. *Fuel* **2006**, *85*, 1101–1110.
(8) Anis, S.; Zainal, Z. A. *Renewable Sustainable Energy Rev.* **2011**, *15*, 2355–2377.
(9) Knoef, H. A. M. *Handbook Biomass Gasification*; Biomass Technology Group (BTG): Enschede, Netherlands, 2005.
(10) Van der Hoeven, T. A. Partial product gas combustion for tar reduction. Ph.D. Thesis, Technical University Eindhoven, Eindhoven, Netherlands, 2007.
(11) Wu, W.; Luo, Y.; Chen, Y.; Su, Y.; Zhang, Y.; Zhao, S.; Wang, Y. *Energy Fuels* **2011**, *25*, 2721–2729.
(12) Fassinou, W. F.; Van de Steene, L.; Toure, S.; Volle, G.; Girard, P. *Fuel Process. Technol.* **2009**, *90*, 75–90.
(13) Chen, Y.; Luo, Y.; Wu, W.; Su, Y. *Energy Fuels* **2009**, *23*, 4659–4667.
(14) Ahrenfeldt, J.; Egsgaard, H.; Stelte, W.; Thomsen, T.; Henriksen, U. B. *Fuel* **2012**, *112*, 662–680.
(15) Su, Y.; Luo, Y.; Chen, Y.; Wu, W.; Zhang, Y. *Fuel Process. Technol.* **2011**, *92*, 1513–1524.
(16) Houben, M. P. Analysis of tar removal in a partial oxidation burner. Ph.D. Thesis, Technical University Eindhoven, Eindhoven, Netherlands, 2004.
(17) Prior, D. S. Pollutant minimisation by blue flame staged combustion. Ph.D. Thesis, The University of Sheffield, Sheffield, U.K., 1977.
(18) O'Nions, P. Low NO_x combustion utilising a Coandă ejector burner. Ph.D. Thesis, The University of Sheffield, Sheffield, U.K., 1997.
(19) Lien, T. K.; Davis, P. G. G. *CIRP Ann.* **2008**, *57*, 33–36.
(20) Beckair. *Ringjet Air Amplifiers Datasheet*; Beckair: Elstree, U.K., 2013; http://www.beck-air.com/Portals/0/docs/Ringjet Air Amplifiers.pdf (accessed Dec 12, 2013).
(21) Mayoral, M. C.; Izquierdo, M. T.; Andres, J. M.; Rubio, B. *Thermochim. Acta* **2001**, *370*, 91–97.
(22) Fagbemi, L.; Khezami, L.; Capart, R. *Appl. Energy* **2001**, *69*, 293–306.
(23) Stiles, H. N.; Kandiyoti, R. *Fuel* **1989**, *68*, 275–282.
(24) Ryu, C.; Sharifi, V. N.; Swithenbank, J.; Int. *J. Energy Res.* **2007**, *31*, 177–191.
(25) Neves, D.; Thunman, H.; Matos, A.; Tarelho, L.; Gómez-Barea, A. *Prog. Energy Combust. Sci.* **2011**, *37*, 611–630.
(26) Encinar, J. M.; Beltrán, F. J.; Bernalte, A.; Ramiro, A.; González, J. F. *Biomass Bioenergy* **1996**, *11*, 397–409.
(27) Demirbas, A. *J. Anal. Appl. Pyrolysis* **2004**, *72*, 243–248.
(28) Phan, A. N.; Ryu, C.; Sharifi, V. N.; Swithenbank, J. *J. Anal. Appl. Pyrolysis* **2008**, *81*, 65–71.
(29) Laird, D. A.; Brown, R. C.; Amonette, J. E.; Lehmann, J. *Biofuels, Bioprod. Biorefin.* **2009**, *3*, 547–562.
(30) Gupta, K. K.; Rehman, A.; Sarviya, R. M. *Renewable Sustainable Energy Rev.* **2010**, *14*, 2946–2955.
(31) Gökalp, I.; Lebas, E. *Appl. Therm. Eng.* **2004**, *24*, 1655–1663.

DESTRUCTION OF TARRY RESIDUES IN A NOVEL DUAL PYROLYSIS - COANDA TAR CRACKING SYSTEM

Energy and Environmental Engineering Research Group
Department of Chemical and Biological Engineering
University of Sheffield
Mappin Street
Sheffield
S1 3JD
United Kingdom

Peter Weston
Vida Sharifi & Jim Swithenbank

EPSRC
Engineering and Physical Sciences Research Council

Main Objective

• The main objective of this research was to develop a small-scale three stage biomass gasifier which employs a novel Coandă tar cracker to generate a tar-free synthetic gas.

Scientific Background

• Biomass gasification has the potential to provide clean, efficient and renewable energy.

• Tar yield in the producer gas is one of the major technical challenges hindering commercial progress.

• Tars condense at lower temperatures, blocking and fouling downstream equipment causing reliability issues.

• A two-stage system consisting of a pyrolyser and a Coandă tar cracking (CTC) unit was tested to determine its feasibility for tar destruction.
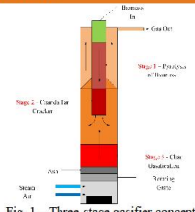
Fig. 1 – Three-stage gasifier concept

Experimental Rig & Procedure

Calorific Value (MJ/kg)	18.0
Proximate analysis (wt%)	
Moisture	7.7
Volatiles	73.8
Fixed Carbon	17.7
Ash	0.4
Ultimate Analysis (wt%)	
Carbon	45.6
Hydrogen	6.0
Nitrogen	0.2

Fuels and Feeding
• Wood Pellets are fed into the pyrolyser using a twin-valve lock feeding system
• Feed rate: 3 – 4.5 kg/hr
• Ten 100g batches were loaded
• Total of 1 kg of pellets pyrolysed

Fig. 2 – Wood pellets & wood pellet properties (as received)

Pyrolysis Chamber
• 316 stainless steel
• Internal diameter – 200 mm
• Length - 1300 mm
• Temperature range (500 – 800 °C)
• Purge gas : Nitrogen – 8 LPM

Fig. 4 – Pyrolyser and control unit

Fig. 3 – Twin-valve feeder

Coandă Tar Cracking
1) Pressurised air is supplied to the ejector and enters through an annular slit at high velocity.
2) The high velocity injected flow passes momentum to the surrounding fluid causing secondary or entrained flow.
3) Injected air attaches to the curved surface and continues along the length of the ejector.

Fig. 5 – Coandă ejector principle (Lien & Davis 2008)

• Air flow rate to ejector: 4 – 40 LPM
• 5 K-type and 1 R-type thermocouples
• Sub-stoichiometric, high temperature (> 1000 °C) blue flame combustion of pyrolysis gas

Fig. 6 - Outer case of the CTC

Tar & gas sampling unit

A	top valve
B	bottom valve
C	purge gas
D	pyrolysis chamber
E	fuel tray
F	sample port 1
G	Coanda tar cracker
H	propane tank
I	air supply
J	ignition burner
K	sample port 2
L	tar collection
M	wet gas meter
N	pump
O	gas chromatograph

Fig. 7 – Schematic of the two-stage system

Two-Stage Process

FEEDING UNIT Wood pellets are loaded into the pyrolyser using a twin-valve batch feeding system

PYROLYSIS UNIT Wood pellets are pyrolysed at 500 – 800 °C producing a tarry pyrolysis gas.

TAR CRACKING UNIT The tarry is gas is partially combusted in a sub-stoichiometric blue flame.

SAMPING UNIT Tars species contained in the gas are collected in tar traps and analysed.

CFD Modelling of the Coandă Ejector

Fig. 8   (a) Flow field in the ejector (b) High velocity region (c) Geometry

• High velocity at the inlets leads to a low pressure zone which causes recirculation.
• The high velocity air attaches to the curved surface.

Coanda gap, e, (mm)	0.08
Nozzle length, a, (mm)	1.2
Radius, R, (mm)	5
Nozzle Ratio, R/a	4.2
Diameter, D, (mm)	26.6
Air velocity at inlet, (m/s)	75
Pressure of air at inlet, (Barg)	6.6

Experimental Results & Discussion

Fig. 9 – Comparison of gravimetric tar yield

• The addition of oxygen is likely to promote the formation of a number of radicals which promote the destruction of tar species.
• Hydrogen, oxygen, hydroxyl and hydroperoxy radicals are formed. These radicals accelerate the decomposition of hydrocarbon due to an increase in H-atom abstraction.

Pyrolysis Temperature (°C)	500	600	700	800
Char Yield Analysis				
Char weight (g)	293.4	227.8	158.9	156.3
Char Yield (%)	29.34	22.78	15.89	15.63
Calorific Value (MJ/kg)	31.2	28.9	31.1	31.1
Proximate Analysis (wt%)				
Moisture	1.0	1.2	1.0	0.9
Volatiles	13.9	12.9	6.8	6.4
Fixed Carbon	85.7	85.4	91.3	92.7
Ash	0.0	0.3	0.6	0.0
Ultimate Analysis (wt%)				
Carbon	80.7	86.5	87.3	93.7
Hydrogen	2.7	2.0	1.1	1.0
Nitrogen	0.3	0.3	0.3	0.3

Fig. 10 – Wood pellet char analysis at a range of pyrolysis temperatures

Fig. 11 – (a) Benzene, (b) Toluene and (c) Naphthalene reduction at various pyrolysis temperatures

Conclusions

• At a pyrolysis temperature of 800 °C, the yield of gravimetric tar decreased from 67.2 to 15.7 g/nm³ when the producer gas was treated by the CTC.

• The benzene concentration was reduced by 95%, toluene by 96% and naphthalene by 97.7% when comparing the tar analysis from the pyrolysis only and the combined experiment.

• The fixed carbon content increased from 86% to 93% as the pyrolysis temperature increased.